DESARROLLO DE UNA HERRAMIENTA MATEMÁTICA DE MODELACIÓN HIDROGEOLÓGICA EN 3D QUE INCORPORE LA VARIABILIDAD DE LA DENSIDAD DEL FLUIDO

Madrid, 2006

MINISTERIO
DE EDUCACIÓN
Y CIENCIA

Instituto Geológico
y Minero de España

MINISTERIO
DE EDUCACIÓN
Y CIENCIA

Instituto Geológico
y Minero de España

63196

INFORME	Identificación: 6 Modelación 001/07
	Fecha: 26 de enero de 2007

TÍTULO

DESARROLLO DE UNA HERRAMIENTA MATEMÁTICA DE MODELACIÓN HIDROGEOLÓGICA EN 3D QUE INCORPORE LA VARIABILIDAD DE LA DENSIDAD DEL FLUIDO

PROYECTO

DESARROLLO DE UNA HERRAMIENTA MATEMÁTICA DE MODELACIÓN HIDROGEOLÓGICA EN 3D QUE INCORPORE LA VARIABILIDAD DE LA DENSIDAD DEL FLUIDO

RESUMEN

La intrusión marina es el principal problema de contaminación asociado a la explotación intensa de acuíferos costeros. El diseño de medidas para controlarla se ve dificultado por la complejidad del fenómeno. El agua dulce flota sobre la salada, que tiende a penetrar a favor de la zonas mas permeables y profundas. Es decir, el proceso está afectado por las diferencias de densidad, por la heterogeneidad y por la topografía del acuífero, además de por los factores habituales (explotación, recarga, etc). En este contexto, el Instituto Geológico y Minero de España (IGME), la Universidad Politécnica de Cataluña (UPC) y la Comunidad de Usuarios de Aguas del Delta del Llobregat (CUADLL) firmaron un Convenio de Colaboración para la investigación y desarrollo de una herramienta informática que modele la intrusión marina en los acuíferos costeros en 3D. Este documento contiene una síntesis de los trabajos realizados en el contexto de dicho convenio.

El objetivo concreto era el estudio de los acuíferos del Delta del Llobregat ya que son un sistema hidrogeológico representativo del litoral Mediterráneo y representan una reserva hídrica estratégica para el área metropolitana de Barcelona.

Revisión	**Autores:**
	José Manuel Murillo (IGME) Jesús Carrera (UPC) Enric Queralt (CUADLL) Enric Vázquez-Suñé (UPC) Elena Abarca (UPC) Juan Hidalgo (UPC) Desiré Gámez (UPC) María Poll (IGME-UPC)
Nombre: Juan Antonio López Geta **Unidad:** Hidrogeología y Aguas Subterráneas **Fecha:** 26-01-2007	**Responsable:** José Manuel Murillo

CORREO ELECTRÓNICO
igme@igme.es

RÍOS ROSAS, 23
28003-MADRID
TELÉFONO: 91 349 5700
FAX: 91 442 6216

El presente informe forma parte de los trabajos contemplados dentro del Convenio de Colaboración establecido entre el Instituto Geológico y Minero de España (IGME), el Departamento de Ingeniería del Terreno de la Universidad Politécnica de Cataluña y la Comunidad de Usuarios de Aguas del Delta del Llobregat, que lleva por título: "*DESARROLLO DE UNA HERRAMIENTA MATEMÁTICA DE MODELACIÓN HIDROGEOLÓGICA EN 3D QUE INCORPORE LA VARIABILIDAD DE LA DENSIDAD DEL FLUIDO*"

El equipo de trabajo ha sido el siguiente:

- José Manuel Murillo (IGME)
- Jesús Carrera (UPC)
- Enric Queralt (CUADLL)

Equipo técnico de realización:

- Enric Vázquez-Suñé (UPC)
- Elena Abarca (UPC)
- Juan Hidalgo (UPC)
- Desiré Gámez (UPC)
- María Poll (IGME-UPC)

RESUMEN EJECUTIVO

La intrusión marina es el principal problema de contaminación asociado a la explotación intensa de acuíferos costeros. El diseño de medidas para controlarla se ve dificultado por la complejidad del fenómeno. El agua dulce flota sobre la salada, que tiende a penetrar a favor de la zonas mas permeables y profundas. Es decir, el proceso está afectado por las diferencias de densidad, por la heterogeneidad y por la topografía del acuífero, además de por los factores habituales (explotación, recarga, etc). En este contexto, el Instituto Geológico y Minero de España (IGME), la Universidad Politécnica de Cataluña (UPC) y la Comunidad de Usuarios de Aguas del Delta del Llobregat (CUADLL) firmaron un Convenio de Colaboración para la investigación y desarrollo de una herramienta informática que modele la intrusión marina en los acuíferos costeros en 3D. Este documento contiene una síntesis de los trabajos realizados en el contexto de dicho convenio.

El objetivo concreto era el estudio de los acuíferos del Delta del Llobregat ya que son un sistema hidrogeológico representativo del litoral Mediterráneo y representan una reserva hídrica estratégica para el área metropolitana de Barcelona. Es por tanto un valor que conviene proteger y gestionar de forma correcta para su preservación futura. Una peculiaridad de estos acuíferos es que su espesor es pequeño en relación a su extensión, por lo que parecería innecesario modelarlos en tres dimensiones. Precisamente, uno de los objetivos subsidiarios es estudiar bajo qué condiciones puede modelarse el flujo con densidad variable en dos dimensiones. Con estas motivaciones (necesidad de tres dimensiones, modelación del Delta del Llobregat y desarrollo de una herramienta informática), los trabajos realizados son:

1. Desarrollo del programa TRANSDENS, que no solo simula el flujo con densidad variable en tres dimensiones, sino que también permite resolver el problema inverso. Se ha mostrado que, en caso de resolverse el problema inverso, resulta ventajoso hacerlo mediante el algoritmo de Newton Raphson.

2. Se ha estudiado la geología del Delta. Para ello se han empleado técnicas de sedimentología secuencial, que han conducido a un avance notable del conocimiento del acuífero principal. En particular, se han identificado un conjunto de paleocauces que actúan como vías preferentes de intrusión.

3. Respecto al estudio de la intrusión en tres dimensiones, se ha observado que, cuando el acuífero es delgado y el régimen estacionario, se produce una celda de convección subhorizontal. La importancia de esta celda depende de la pendiente lateral del acuífero.

Cuando ésta es baja, como en el Llobregat, apenas se produce. Cabe por tanto esperar que en condiciones naturales, sin bombeo, el acuífero profundo no tuviese salinidad.

4. La observación anterior, junto con la naturaleza confinada del acuífero principal del Delta del Llobregat han motivado un estudio específico para analizar bajo qué condiciones se puede estudiar la intrusión en dos dimensiones, sin tener en cuenta el efecto de la densidad. Se concluye que en general no es posible. Sin embargo, cuando la pendiente lateral es baja y, bajo condiciones de explotación, la simplificación es válida.

5. Por ello, los acuíferos del Delta se han simulado bajo la hipótesis de densidad constante. El modelo se calibró, con resultados muy buenos entre 1965 y 2001. Con el modelo así calibrado, se ha simulado el período 2001-04. Los resultados de la validación son aún mejores que los de la fase de calibración, lo que confirma la validez del modelo.

INDICE

1.- INTRODUCCIÓN

Hasta principios del Siglo XX, la intrusión marina estaba rodeada de un halo de misterio. Las observaciones de la Isla Cefalonia, en la que el agua de mar conducida por gravedad mediante un canal se infiltra en una sima, no solo confundieron a los griegos clásicos, sino que también condujeron a ideas erróneas sobre la intrusión marina mucho después de que se hubiera aclarado la verdadera naturaleza del Ciclo Hidrológico. Ghyben (1889) y Herzberg (1901) observaron una relación lineal entre la profundidad del agua salada y el nivel de agua dulce. Esta relación resulta de las diferencias de densidad, que provocan que el agua dulce en acuíferos costeros flote sobre el agua del mar. Suponiendo que ambos fluidos están en equilibrio y que el agua salada permanece estática, se puede demostrar que, efectivamente, la profundidad de la interfaz por debajo del nivel del mar es 40 veces el nivel de agua dulce sobre el nivel del mar.

En realidad, incluso en régimen estacionario, el agua de mar no permanece estática: los dos fluidos se mezclan. Esta mezcla se produce por difusión/dispersión y conlleva que parte de la sal sea arrastrada de nuevo hacia el mar por el agua dulce. Para suplir la sal que se ha lavado es necesario un flujo de sal tierra adentro. El resultado de este proceso es una celda de convección vertical en la que el agua salada penetra en el acuífero en profundidad hasta alcanzar la zona de mezcla donde se dispersa y es arrastrada por el agua dulce otra vez hacia el mar. Esta discusión indica que el movimiento de agua salada en los acuíferos costeros se debe a la combinación del flujo debido a variaciones de densidad y a la dispersión hidrodinámica. Este efecto fue descrito por primera vez por (Cooper 1964).

En la práctica, la situación es aún mas compleja, porque si la topografía del fondo es variable, el agua de mar penetrará preferentemente por las zonas más profundas. Si, además, se reconoce que los acuíferos son heterogéneos, se concluye que el fenómeno es complejo. Es esta complejidad lo que hace que la intrusión solo se haya estudiado de forma parcial. De hecho, hasta que no han aparecido programas fiables de simulación del flujo con densidad variable en tres dimensiones, no se ha podido proceder a un estudio serio del fenómeno. Precisamente, este era el objetivo de partida del Convenio de Colaboración firmado entre el Instituto Geológico y Minero de España (IGME), la Universidad Politécnica de Cataluña (UPC) y la Comunidad de Usuarios de Aguas del Delta del Llobregat (CUADLL) para la investigación y desarrollo de una herramienta informática que modele la intrusión marina en los acuíferos costeros en 3D.

La necesidad de un campo de trabajo, unido a las características de los acuíferos del Delta del Llobregat, aconsejó centrar los trabajos en los mismos. Los acuíferos del delta del Llobregat son un sistema hidrogeológico representativo del litoral Mediterráneo y representa una reserva hídrica estratégica de gran importancia que abastece el área

metropolitana de Barcelona. Es por tanto un valor que conviene proteger y gestionar de forma correcta para su preservación futura. Además, estos acuíferos se encuentran entre los mas estudiados de España y, posiblemente, del mundo. Por ello, representan un buen campo de prácticas para el estudio de la intrusión.

Este documento contiene una síntesis de los trabajos realizados en el contexto de dicho convenio. Se ha estructurado, de acuerdo con los trabajos realizados en los siguientes capítulos:

Capítulo 2: Contiene las ecuaciones de simulación del flujo con densidad variable. Estas ecuaciones han dado pie al desarrollo del programa TRANSDENS, que no solo simula el flujo con densidad variable en tres dimensiones, sino que también permite resolver el problema inverso.

Capítulo 3: Contiene el estudio de la Geología del Delta. Para ello se han empleado técnicas de sedimentología secuencial, que han conducido a un avance notable del conocimiento del acuífero principal. En particular, se han identificado un conjunto de paleocauces que actúan como vías preferentes de intrusión.

Capítulo 4: Contiene un estudio sobre las celdas de convección de agua salada en acuíferos de bajo espesor y gran extensión.

Capítulo 5: Contiene un análisis de las condiciones bajo las que se puede estudiar la intrusión en dos dimensiones, sin tener en cuenta el efecto de la densidad. Este trabajo surge como consecuencia de los resultados del Capítulo 4, junto con la naturaleza confinada del acuífero principal del Delta del Llobregat.

Capítulo 6: Contiene un resumen del modelo realizado en los acuíferos del Delta.

En los anejos se incluyen varias publicaciones surgidas del proyecto.

2.- MODELACIÓN INVERSA DE FLUJO CON DENSIDAD VARIABLE

Los medios con densidad variable son comunes en hidrogeología. Los cambios en las propiedades físicas del fluido pueden tener consecuencias significativas sobre el comportamiento de los sistemas hidrogeológicos y, algunas veces, una importancia vital para la describir de forma precisa la dinámica de los acuíferos. La densidad es depende de la temperatura, concentración y presión. En acuíferos costeros, la densidad del agua subterránea se ve afectada principalmente por la concentración pudiendo despreciarse el efecto de los cambios de presión y temperatura. Los cambios en la densidad del agua subterránea aparecen en el caso de intrusión marina en acuíferos costeros o en acuíferos afectados por disolución de sal proveniente de formaciones geológicas salinas.

La teoría general del flujo con densidad variable se describe en Bear (1972). Una gran cantidad de trabajo se ha desarrollado a partir de este estudio básico y las propuestas paras las ecuaciones de conservación de masa de fluido, es decir, agua más solutos disueltos, y masa de soluto es variada. Voss (1984) propone un balance de masa en términos de presiones mientras que Huyakorn et al. (1987) derivan las ecuaciones en términos de niveles equivalentes de agua dulce. El transporte de soluto puede expresarse en términos de concentración (Bear, 1979, Kinzelbach, 1986) o de fracción másica (Olivella et al., 1994). Una revisión más extensa de las formulaciones del flujo con densidad variable puede encontrase en Kolditz et al. (1998), Holzbecher (1998) y Diersch y Kolditz (2002).

Bajo condiciones de densidad variable el flujo y el transporte se convierten en dos fenómenos no lineales acoplados. La simulación, entonces, es una tarea compleja que puede sufrir problemas de convergencia y requerir un alto coste computacional. Existen muchos códigos disponibles para la simulación del flujo con densidad variable y el transporte de soluto como pueden ser SUTRA (Voss,1984), HYDRUS-2D (Simunek et al., 1998), ROCKFLOW (Kolditz et al., 2002), MOCDENSE (Sandford y Konikow, 1985), MOCDENS3D (Oude Essink, 1998) SALTFLOW (Molson y Frind, 1994), SEAWAT (Guo y Bennet, 1998). Todos ellos utilizan un proceso iterativo conocido como método de Picard para la resolución del acoplamiento entre las ecuaciones de flujo y transporte. Sin embargo, un algoritmo más robusto sería más adecuado en este caso, y más aún si se añade la calibración de parámetros como se verá más tarde. Los algoritmos basados en el método de Newton-Raphson son una alternativa viable que ha sido implementada en códigos como CODE_BRIGHT (Olivella et al., 1996), FEFLOW (Diersch, 2002) o d3f (Fein et al., 1998) para problemas de densidad variable. Putti y Paniconi (1995) desarrollaron un esquema de Newton parcial (despreciando las

contribuciones de los términos no diagonales) que demostró una eficiencia superior a la del método de Picard.

Durante el proceso de modelación una de las principales fuentes de incertidumbre es el valor de los parámetros hidráulicos implicados en el modelo (conductividad hidráulica, almacenamiento, porosidad, etc.). Los valores se eligen usualmente a partir de ensayos de campo, la caracterización geológica y el resto de información previa, que puede proceder de fuentes diversas. La experiencia ha demostrado que la calibración automática es una herramienta útil para reducir la incertidumbre. Los parámetros se calculan como aquellos valores que minimizan una cierta función objetivo, que mide la diferencia entre los valores simulados y observados de las variables de estado. Los resultados así obtenidos son más robustos y fiables que los provenientes de la calibración manual.

El proceso de calibración puede mejorarse en el caso del flujo con densidad variable. El acoplamiento entre el flujo y el transporte da la posibilidad de integrar globalmente los datos de concentración en el proceso de calibración. El movimiento de la interfaz agua dulce – agua salada puede verse como un ensayo de trazadores a escala de acuífero, el cual proporciona una enorme cantidad de información sobre los parámetros del acuífero. A pesar de que la calibración automática se ha aplicado durante años, existe muy poca experiencia cuando se trata de sistemas en los que existe variación de densidad. Iribar et al., 1996, realizaron una primera aproximación calibrando parámetros de un acuífero con intrusión marina con buenos resultados, pero despreciando los efectos de densidad. La identificación de parámetros en flujo con densidad variables ha sido también tratada por Piggott et. al (1993), quienes implementaron un algoritmo de inversión para SUTRA llamada SUTRA^{-1} (o SUTRAINV). El algoritmo se basa en el método de mínimos cuadrados generalizado. La función error se minimiza mediante un método *simplex downhill*. El código CALIF (Häfner et al., 1998) resuelve el problema inverso minimizando la función objetivo mediante una combinación de descenso máximo, los métodos de Gauss-Newton y Powell y Levenberg-Marquardt (Press et al. 1994). Johansenn et al. (2002), resuelven un problema de mínimos cuadrados aplicando el método de Newton. La matriz jacobiana se calcula por medio de cocientes incrementales. Existen otros algoritmos que pueden ser utilizados para calculado el jacobiano del sistema. PEST (basado en Vecchia et al., 1987) y UCODE (Poeter et al., 1998) son códigos genéricos para la minimización de una función objetivo de mínimos cuadrados que pueden acoplarse a cualquier otro código que resuelva los problemas de flujo y transporte. Ambos calculan la matriz jacobiana mediante cocientes incrementales, lo cual es computacionalmente caro e impreciso.

La calibración es un proceso iterativo (Figura 2.1). Independiente mente del método utilizado, cada vez que el conjunto de parámetros se perturba, debe hacerse una

simulación. Cuando se trata con problemas no lineales, el proceso de calibración puede volverse extremadamente costoso. El bucle de calibración puede verse interrumpido por dificultades en la convergencia durante la fase de simulación, siendo necesario comenzar de nuevo el proceso completo. Por esta razón, si se desea estimar los parámetros de un modelo, es necesario tener un algoritmo de calibración eficiente junto con un método robusto para la simulación.

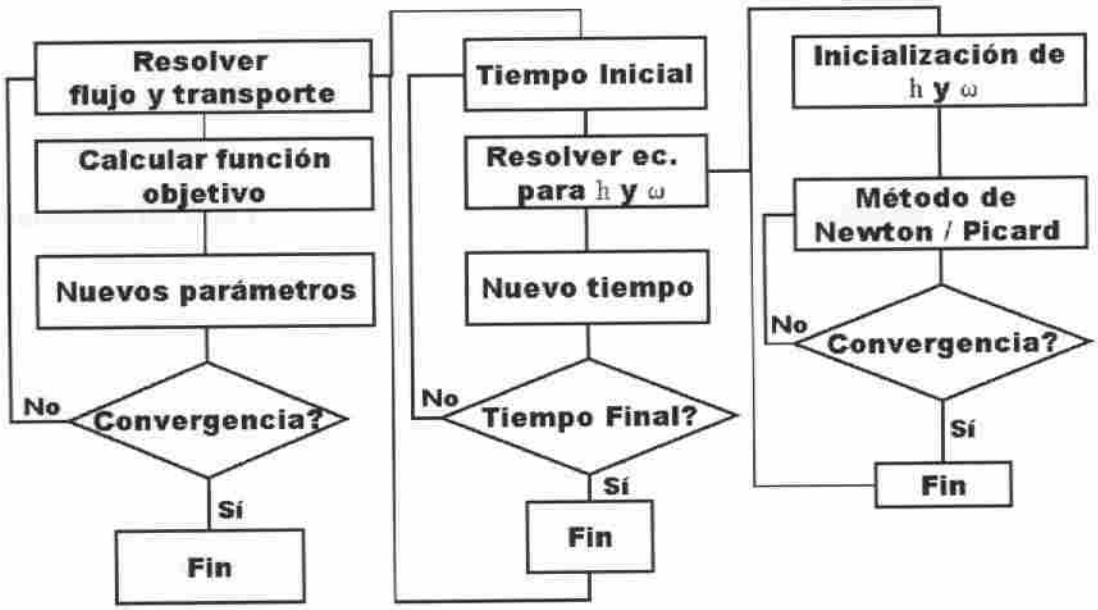

Figura 2.1.- Diferentes bucles iterativos en el proceso de calibración automática de parámetros.

2.1.- ECUACIONES DE FLUJO Y TRANSPORTE CON DENSIDAD VARIABLE

2.1.1.- Flujo

La ecuación de flujo puede expresarse en términos del nivel equivalente de agua dulce, que se define como

$$h_f = \frac{P}{\rho_f g} + z \qquad (1)$$

Donde P es la presión del fluido, ρ_f es la densidad del agua dulce, g el módulo del vector gravedad y z la elevación. Entendiéndose por elevación la dirección opuesta a la gravedad.

La densidad se considera sólo función de la variable de estado de transporte, es este caso la fracción másica ω. (kg. de soluto por kg. de fluido).

$$\rho = \rho_f e^{\beta_\omega(\omega-\omega_0)} \qquad (2)$$

Donde ω_0, es la fracción másica de referencia (aquella a la cuál $\rho = \rho_f$) y β_ω se define como

$$\beta_\omega = \frac{1}{\rho}\frac{\partial\rho}{\partial\omega} \qquad (3)$$

La ecuación de flujo en términos de niveles equivalentes de agua dulce es

$$\rho\frac{\partial\Theta}{\partial h_f}\frac{\partial h_f}{\partial t} + \rho\Theta\beta_\omega\frac{\partial\omega}{\partial t} = -\vec{\nabla}\cdot[\rho\mathbf{q}] + \rho^* q_r \qquad (4)$$

Donde Θ es contenido volumétrico de fluido (volumen de fluido por volumen de acuífero), q_r representa las fuentes y sumideros en el sistema, ρ^* es la densidad de dichas fuentes/sumideros y $\mathbf{q}$ es la velocidad de Darcy. La velocidad de Darcy viene dada por

$$\mathbf{q} = -\frac{\mu_f}{\mu}\mathbf{K}\left(\nabla h_f + \frac{\rho-\rho_f}{\rho_f}\nabla z\right) \qquad (5)$$

Donde μ y μ_f son la viscosidad del fluido y la viscosidad de referencia respectivamente, $\mathbf{K}$ es la conductividad hidráulica a ω_0 (lo cual hace necesario incluir explícitamente en la fórmula las variaciones de viscosidad).

2.1.2.- Transporte

De manera general, la ecuación de transporte se expresa en términos de la fracción másica de soluto.

$$\rho[\Theta+\alpha_s]\frac{\partial\omega}{\partial t} = -\rho\mathbf{q}\nabla\omega + \nabla(\rho\mathbf{D}\nabla\omega) - \rho\lambda[\Theta+\alpha_s]\omega + q_r(\rho^*\omega^* - \rho\omega) \qquad (6)$$

Donde α_s es el coeficiente de retardo, que representa los procesos de adsorción, **D** es el tensor de difusión-dispersión, λ es el coeficiente de desintegración de primer orden y ω^* es la fracción másica de las fuentes y sumideros del sistema. Normalmente, tanto el retardo como la desintegración serán nulos cuando se trate de transportar sal.

Si se utiliza el método de Newton-Raphson, el sistema de ecuaciones resultante se puede escribir como

$$\begin{pmatrix} \frac{\partial f_f}{\partial h_f} & \frac{\partial f_f}{\partial \omega} \\ \frac{\partial f_T}{\partial h_f} & \frac{\partial f_T}{\partial \omega} \end{pmatrix} \begin{pmatrix} \Delta h_f \\ \Delta \omega \end{pmatrix} = - \begin{pmatrix} f_f \\ f_T \end{pmatrix} \tag{7}$$

Donde f_f es la ecuación de flujo y f_T la ecuación de transporte.

2.2.- PROBLEMA INVERSO

Los parámetros óptimos son aquellos que minimizan un a función objetivo F dependiente de los parámetros y de las variables de estado.

$$F = F(\mathbf{p}, h_f, \omega) \tag{8}$$

La minimización de esta función objetivo implica resolver

$$\frac{dF}{d\mathbf{p}} = \frac{\partial F}{\partial h_f}\frac{\partial h_f}{\partial \mathbf{p}} + \frac{\partial F}{\partial \omega}\frac{\partial \omega}{\partial \mathbf{p}} + \frac{\partial F}{\partial \mathbf{p}} = 0 \tag{9}$$

Este cálculo requiere conocer las llamadas sensibilidades, es decir, las derivadas de las variables de estado respecto de los parámetros del sistema

El cálculo de las sensibilidades es una tarea computacionalmente cara en el problema inverso. Puede llevarse a cabo mediante perturbación y diferencias finitas de los resultados obtenidos o por derivación directa. La derivación directa de las ecuaciones de estado, llevan a

$$\begin{pmatrix} \frac{\partial f_f}{\partial h_f} & \frac{\partial f_f}{\partial \omega} \\ \frac{\partial f_T}{\partial h_f} & \frac{\partial f_T}{\partial \omega} \end{pmatrix} \begin{pmatrix} \frac{\partial h_f}{\partial p} \\ \frac{\partial \omega}{\partial p} \end{pmatrix} = \begin{pmatrix} \frac{\partial f_f}{\partial p} \\ \frac{\partial f_T}{\partial p} \end{pmatrix} \tag{10}$$

Como puede verse, la matriz del sistema es igual a la que parece cuando se resuelve el problema directo por el método de Newton-Raphson. Lo cual hace que este algoritmo sea el más adecuado cuando se quiere hacer estimación de parámetros, dado que ahorra el cálculo de la matriz del sistema.

3.- MODELO GEOLÓGICO DEL DELTA DEL LLOBREGAT

La geología delta del Llobregat se empezó a estudiar a finales del siglo XIX, pero los estudios se han intensificado desde los años 60. Esto ha promovido la recopilación de multitud de información de interés geológico e hidrogeológico. Sin embargo, apenas se han realizado estudios globales que integren toda la información y conocimientos existentes, ni se ha considerado el estudio detallado y la importancia de la calidad de las aguas subterráneas. Los primeros modelos, tampoco caracterizaban correctamente la intrusión marina, uno de los mayores problemas de contaminación descritos en el delta de Llobregat. En consecuencia, la necesidad de conocer con precisión el comportamiento hidráulico de los acuíferos y disponer de una metodología de cuantificación de los procesos hidrogeológicos se ha convertido en una prioridad para disponer de una herramienta eficaz de gestión y administración de los recursos hídricos.

Uno de los pasos previo e imprescindible para explicar el comportamiento hidrogeológico del sistema es la representación de los reservorios hídricos en 3D de una forma realista y a partir de herramientas geológicas. El delta del Llobregat se ha tomado como ejemplo para la comprobación y mejora de estas herramientas, pero su campo de aplicación es mucho más amplio y abarca cualquier sistema acuífero, en sentido amplio.

3.1.- MODELO GEOLÓGICO CONCEPTUAL

Marqués (1984) diferenció en el delta del Llobregat dos complejos detríticos, nombrados Complejo Detrítico Inferior (CDI), de edad Pleistocena, y Complejo Deltaico (posteriormente nombrado Complejo Detrítico Superior (CDS) por Simó et al, 2005), de edad Holocena. Posteriormente, Maldonado et al. (1986 y 1989) describieron, mediante sísmica de reflexión, cuatro unidades deltaicas en la plataforma marina del delta del Llobregat (nombrados Q1 a Q4), de edad Pleistocena a Holocena. De ellos, los tres más antiguos (Q1 a Q3) se corresponden con el CDI.

En el marco del estudio se ha revisado el modelo geológico realizado por Marqués (1984) de la parte emergida del delta y se está reinterpretando los perfiles sísmicos disponibles en la parte sumergida del delta (a partir de perfiles sísmicos obtenidos para la campaña de la realización de mapas geológicos de la Plataforma continental española 1:200.000, Maldonado et al., 1986 y 1989) reconstruyendo el modelo geológico conceptual y utilizando correlaciones basadas en estratigrafía secuencial. En el nuevo modelo geológico conceptual se enfatiza la conexión que existe entre la parte emergida y sumergida, ignorada hasta el momento pero esencial para conocer las vías preferentes de intrusión marina.

3.1.1.- Delta emergido

La nueva interpretación geológica se está realizando a partir de la revisión de 446 sondeos, de los cuales unos 150 traviesan toda la arquitectura cuaternaria deltaica.

La metodología seguida para la reconstrucción de los cuerpos sedimentarios ha sido la representación de las columnas estratigráficas (sondeos) en los cortes estrátigraficos (paralelos y perpendiculares a la línea de costa) e la interpretación (relleno) del espacio entre las mismas aplicando criterios de estratigrafía secuencial para identificar unidades deposicionales. También se han elaborado mapas de isopacas e isobatas de las distintas unidades deposicionales.

Como observaciones más relevantes realizadas en la geología del delta del Llobregat se puede destacar:

-Margen de la Zona Franca (Figura 3.1): se caracteriza por la baja acumulación de cuaternario y la estructuración, a partir de fallas y superficies de erosión, de 4 unidades zócalo de distinta permeablidad (Triásico, Mioceno Burdigaliense, Mioceno Serrevaliense y Plioceno)

- Zona central del delta y el margen del Garraf: se caracteriza por la gran acumulación de cuaternario. Lo mas característico es la identificación de tres secuencias granodecrecientes en el Complejo Detrítico Inferior que se interpretan como sistemas fluviales amalgamados y encajados durante los estadios de bajo nivel del mar durante el Pleistoceno (Simó et al., 2005, ver anejos).

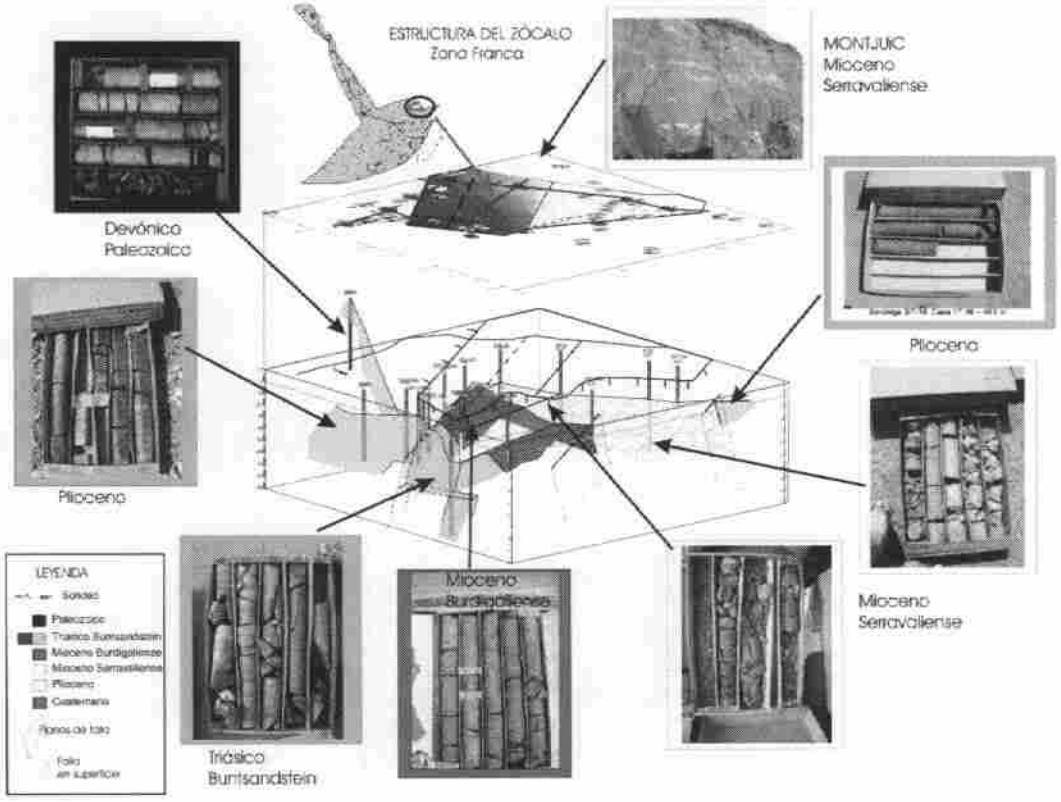

Figura 3.1.- *A partir de datos de afloramientos, datos petrográficos, dataciones y paleontología se reconstruyó la estructura del zócalo de la Zona Franca (margen izquierdo del delta del Llobregat). Esta estructura esta afectada por fallas y condiciona al depósito de los materiales cuaternarios. A nivel hidrogeológico se pueden distinguir unidades acuíferos de edad miocena serravaliense y unidades acuitardo de edad triásica, miocena burdigaliense y pliocena.*

3.1.2.- Delta sumergido

La conexión vertical entre los sistemas de paleocanales cartografiados en el delta emergido (3 sistemas fluviales) y su continuidad hacia la parte sumergida del delta (a facies deltaicas) son la clave para conocer las vías preferentes de intrusión marina.

En la parte emergida del delta los sistemas fluviales se encuentran amalgamados, el estudio de los perfiles sísmicos realizados a mar nos permitirá conocer:

- cuantos sistemas deltaicos pleistocenos existen.
- la continuidad hidráulica de los acuíferos (sistemas de paleocanales) reconocidos en la parte emergida del delta, hacia mar.

A partir de la colaboración con el IGME, trabajando con los perfiles sísmicos y aplicando los conceptos de estratigrafía secuencial se ha podido reconocer la arquitectura pleistocena del delta sumergido, con la repetición de ciclos de regresión-transgresión.

En los intervalos regresivos se han identificado clinoformas con un ángulo de inclinación que varia de la parte proximal a la distal, como indicador característico de la formación de deltas en estadios de regresiones forzadas (Figura 3.2).

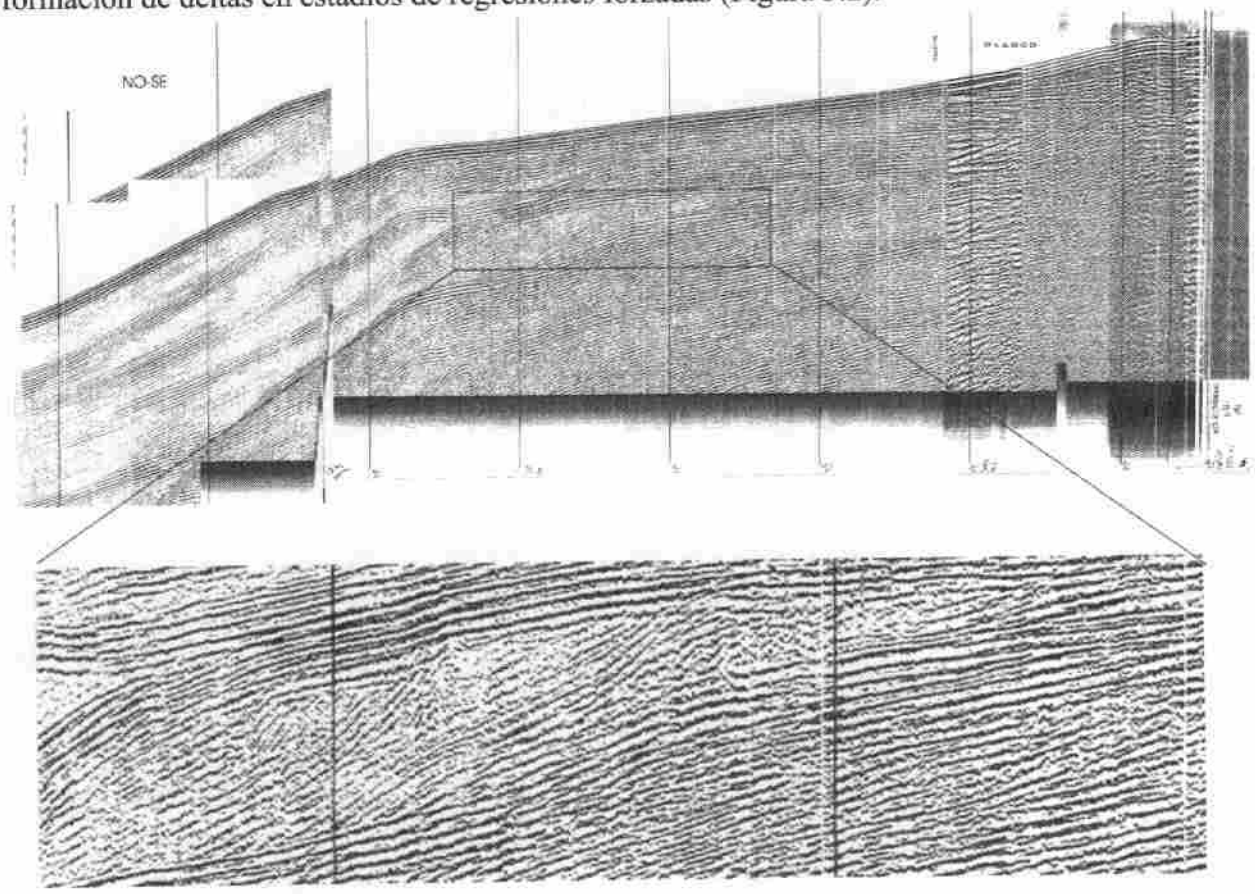

***Figura 3.2.**- Perfil sísmico perpendicular a la actual línea de costa realizado en la parte sumergida del delta del Llobregat. Muestra los diferentes ángulos de inclinación de las reflectores como característica indicativa de la formación del sistema deltaico durante un estadio de regresión forzada.*

Se puede destacar que se han identificado como mínimo 3 grandes deltas pleistocenos (Figura 3.3). Es de gran importancia destacar que la interpretación de los depósitos formados durante estadios de regresiones forzadas en las unidades deltaicas pleistocenas aporta un gran avance respecto:

a) Al conocimiento de los procesos que formaron el delta del Llobregat durante el Pleistoceno y compararlo con otros sistemas deltaicos mediterráneos.

b) La interpretación de los depósitos gruesos formados durante los estadios de las regresiones forzadas, son de gran interés desde un punto de vista hidrogeológico, ya que conectan con los sistemas de paleocanales cartografiados en el delta emergido. Por lo tanto, existen unos conductos de alta conductividad hidráulica desde tierra y hacia mar que permiten unas vías preferentes para la intrusión

marina.

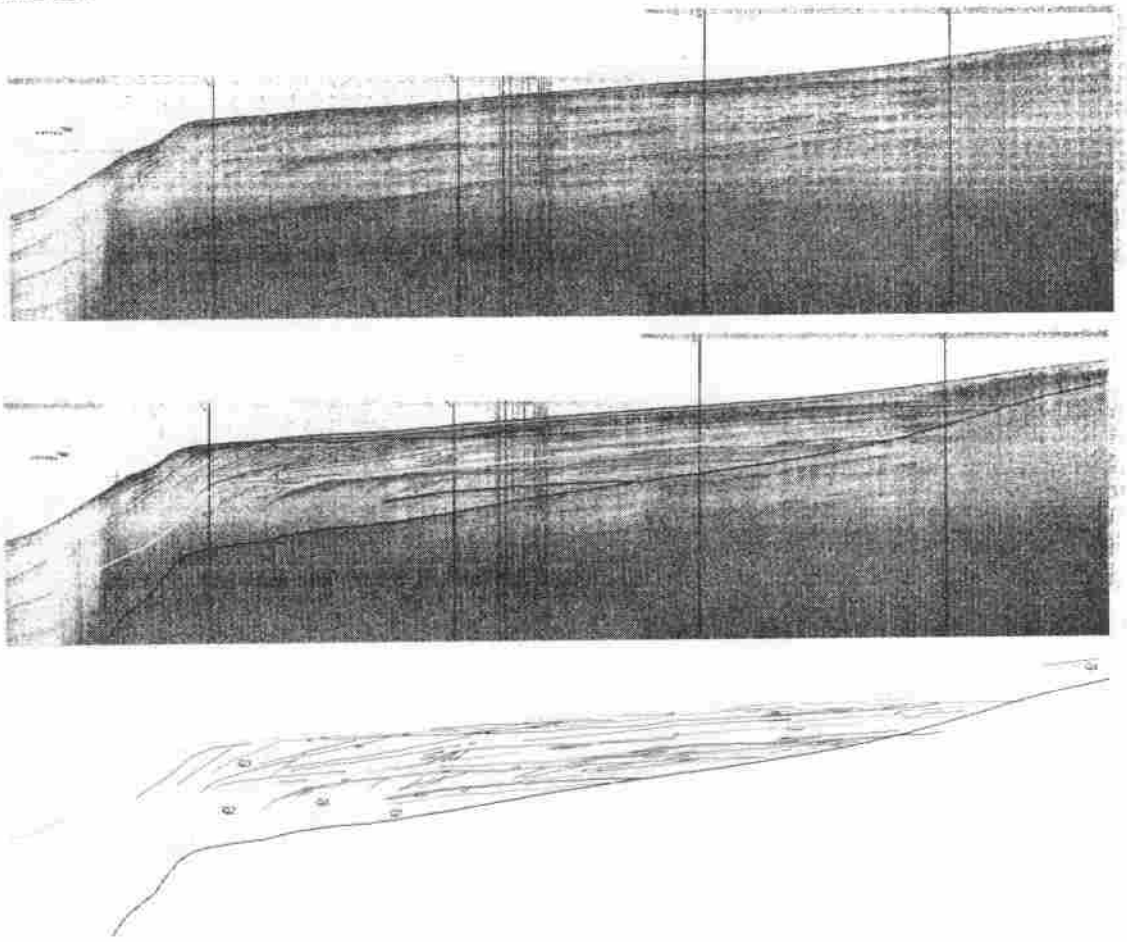

Figura 3.3.- *a) Perfil sísmico e interpretación de una línea perpendicular a la actual línea de costa del delta del Llobregat. b) En la interpretación del perfil sísmico se muestran las de 3 a 4 unidades deltaicas pleistocenas*

3.2.- MODELO NUMÉRICO GEOLÓGICO

3.2.1.- Reconstrucción de la geometría de los cuerpos geológicos

A partir de la reconstrucción del modelo conceptual de la parte emergida y sumergida del delta del Llobregat se han diferenciado distintas superficies que configuran la geometría de los cuerpos geológicos (Tabla 3.1). Estas superficies se han identificado para cada sondeo (446 sondeos) de tal manera que se incorporarán al modelo numérico geológico. Una vez se incorporen las superficies, se reconstruirán tridimensionalmente, mediante técnicas geoestadísticas que incorporen criterios geológicos.

El programa de visualización geológica utilizado será el software GoCad. En una primera fase, se han incorporado al programa, 159 (88 profundos) de los 446 totales, introduciendo las distintas superficies definidas en el modelo conceptual y que limitan las unidades deposicionales.

En la Figura 3.4 se observan las primeras visualizaciones realizadas con GoCad donde se representan los distintos sondeos con los *well-markers* que representan las superficies de cada unidad deposicional.

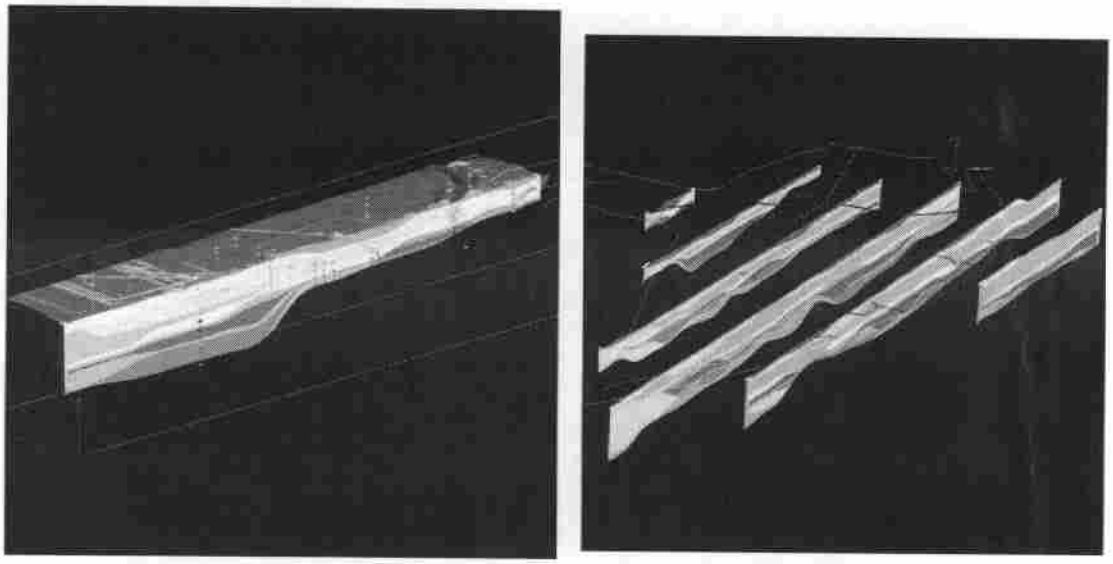

Figura 3.4.- *Visualizaciones extraídas del programa GoCad realizadas a partir de la incorporación de los 159 sondeos donde se definieron las bases de cada unidad deposicional definidas en el modelo conceptual.*

3.2.2.- Reconstrucción de los rellenos de los cuerpos geológicos

Una vez se tengan incorporados todas las superficies a partir de los datos de sondeos y la posterior interpolación geoestadística y construidos las geometrías de cada unidad deposicional, se procederá al relleno de los cuerpos geológicos. Para ello será necesario:
a) Incorporación de las facies interpretadas de los 446 sondeos.
b) Empleo de algoritmos geoestadísticos para el relleno de los cuerpos geológicos creados en el punto 3.2.1, condicionados por las interpretaciones de facies incorporadas en cada sondeo.

Tabla 3.1.- Descripción de las capas empleadas en el modelo geológico del Delta.

Delta	Sup.		Descripción	Zona identificada	Edad
1	1a		relleno antropico	Del.Emerg.	Holoceno
	1ll		llanura deltaica	Del.Emerg.	
	1		sin distinción de facies	Zona Franca y Garraf	
	1rc		conglomerados fluvial regresivo	Centro delta	
	1rf		frente progradante, **regresivo**	Centro delta	
	1p		**prodelta**	Centro delta y Del.Sumerg.	
	1t		frente retrogradante **transgresivo**	Todos y Del.Sumerg.	Pleistoceno-Holoceno
2	2z		sin distinción de facies	Zona Franca y Garraf	Pleistoceno
	2rc		conglomerados fluviales regresivo	Centro delta y Del.Sumerg.	
	2rf		frente progradante, regresivo	Del.Sumerg.	
	2p		prodelta	Del.Sumerg.	
	2t		frente retrogradante transgresivo	Del.Sumerg.	
3	3z		amalgacion de 3 +cuerpos inferiores	Garraf+centro del delta	
	3lp		finos llanura o prodeltaicos	Del.Emerg.	
	3rc		canales fluviales	Del.Emerg.	
	3.2	3.1rc	conglomerados fluviales regresivo	Del.Sumerg.	
		3.1rf	frente progradante, regresivo	Del.Sumerg.	
		3.1p	prodelta	Del.Sumerg.	
		3.1t	frente retrogradante transgresivo	Del.Sumerg.	
		3.2rc	conglomerados fluviales regresivo	Del.Sumerg.	
		3.2rf	frente progradante, regresivo	Del.Sumerg.	
	3.1	3.2p	prodelta	Del.Sumerg.	
		3.2t	frente retrogradante transgresivo	Del.Sumerg.	
4	4lp		finos llanura o prodeltaicos	Del.Emerg.	
	4rc		conglomerados fluviales regresivo	Del.Emerg. y sumerguido	
	4rf		frente progradante, regresivo	Del.Sumerg.	
	4p		prodelta	Del.Sumerg.	
	4t		frente retrogradante transgresivo	Del.Sumerg.	
OBSERVACIONES			**Del.Emerg.**: Delta emergido, margen de la Zona Franca+centro delta+margen del Garraf **Del.Sumerg.: Delta Sumergido**		

4.- EFECTO DE LA TRIDIMENSIONALIDAD DE LA INTRUSION MARINA

En este capítulo se presenta un resumen del trabajo realizado para el estudio de la formación de celdas de convección horizontal en intrusión marina, presentados en Abarca et al., 2005a.

Las diferencias de densidad provocan que el agua dulce en acuíferos costeros flote sobre el agua del mar. Este efecto fue descrito por primera vez por (Ghyben, 1889) y (Herzberg, 1901) quienes descubrieron, de forma empírica, que la profundidad del agua salada se correlaciona con el nivel de agua dulce. Asumiendo que ambos fluidos están en equilibrio y que el agua salada permanece estática, la profundidad a la que se encuentra la interfaz de agua dulce / agua salada, z, es $\alpha_s z = h$; donde h es el nivel de agua dulce, $\alpha_s = (\rho_s - \rho)/\rho_f$ donde ρ_s y ρ_f son las densidades del agua del mar y dulce, respectivamente. A esta fórmula se la conoce como la aproximación de Ghyben-Herzberg para intrusión marina. Como α_s es aproximadamente igual a 1/40, una regla frecuente es suponer que la profundidad de la interfaz por debajo del nivel del mar es 40 veces el nivel de agua dulce sobre el nivel del mar.

Un segundo efecto asociado con las diferencias de concentración es la mezcla entre los dos fluidos. Está mezcla se produce debido a los procesos de difusión/dispersión y conlleva que parte de la sal sea arrastrada de nuevo hacia el mar por el agua dulce. Para rellenar la sal que se ha lavado es necesario un flujo de sal tierra adentro. El resultado de este proceso es una celda de convección vertical en la que el agua salada penetra en el acuífero en profundidad hasta alcanzar la zona de mezcla donde se dispersa y es arrastrada por el agua dulce otra vez hacia el mar (Figura 4.1). La hipótesis de equilibrio de la aproximación de Ghyben-Herzberg no es válida porque el flujo de agua salada produce una pérdida de energía que se traduce en una menor penetración de la cuña de agua salina. Por lo tanto, la profundidad de la interfaz se subestima. Esta discusión indica que el movimiento de agua salada en los acuíferos costeros se debe a la combinación del flujo debido a variaciones de densidad y a la dispersión hidrodinámica. Este efecto fue descrito por primera vez por (Cooper, 1964).

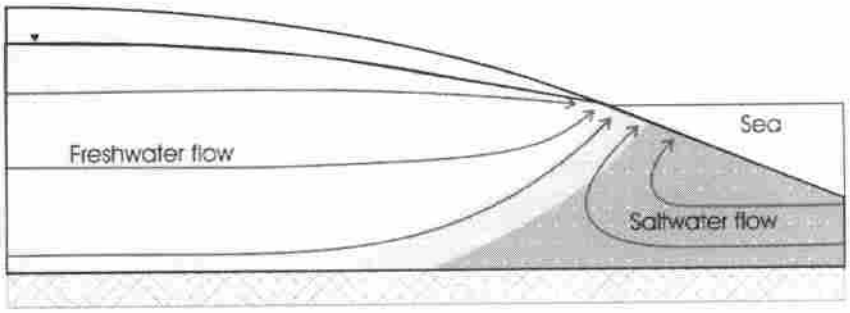

Figura 4.1.- *Clásica celda de convección vertical de agua salada inducida por la combinación de fuerzas de flotación y procesos de dispersión hidrodinámica*

La tridimensionalidad puede ser un factor crítico, y sin embargo, es a menudo olvidada a la hora de analizar los procesos de intrusión marina. Las distribuciones irregulares de salinidad pueden estar causadas por muchos factores como son, entre otros, las variaciones en el espesor del acuífero, la heterogeneidad y la variación en la profundidad de los límites del acuífero. En este capítulo analizaremos este último factor. El objetivo es evaluar si éste es un factor determinante a la hora de entender, analizar y modelar la intrusión marina en el caso del acuífero profundo del delta del Llobregat.

Cuando los acuíferos presentan una gran extensión lateral comparada con su espesor, las variaciones de éste pueden considerarse despreciables. En este caso, las variaciones en la topografía del fondo pueden convertirse en el factor crítico. El efecto de la gravedad viene dado, en estos casos, por la gravedad efectiva, proyección del vector gravedad sobre la superficie de contorno. Esta gravedad efectiva está controlada por la pendiente y forma de los contornos. Cuando la pendiente lateral es grande, el flujo vertical es de menor orden que los flujos laterales.

Algunos estudios geofísicos proporcionan pruebas de que el agua de mar penetra más tierra adentro en la parte más profunda de los acuíferos costeros ((Flores-Marquez et al., 1998; Rangel-Medina et al., 2003; Benkabbour et al., 2004). En la literatura hidrogeológica no se encuentran análisis cualitativos del efecto de la morfología del acuífero sobre la intrusión, aunque su importancia ha sido considerada en numerosos estudios de transporte de calor. (Dorgarten y Tsang, 1991; Bachu, 1995; Lahm, et al., 1998; Bachu y Karsten, 2002; Malkovsky y Pek, 2002; Assouline y Shavit 2004). La falta de análisis del efecto de la tridimensionalidad en la intrusión marina es, en parte, debida a falta de herramientas manejables tales como códigos 3D eficientes y computadores suficientemente potentes.

4.1.- NÚMEROS ADIMENSIONALES

Con el fin de analizar el efecto de la tridimensional del acuífero se definen dos números adimensionales. El primero de ellos, N_b, se define comparado los dos términos de la ley de Darcy escrita en términos de nivel de agua dulce equivalente. El primer término, flujo de agua dulce ($K\nabla h_f$), se aproxima por el flujo de agua dulce, q_b, que entra por el contorno interno. El segundo, término de flotación, se aproxima por la máxima pendiente del fondo del acuífero, *m*.

$$N_b = \frac{\alpha_s |K\nabla z|}{|K\nabla h_f|} \approx \frac{\alpha_s |Km|}{q_b} \qquad (1.11)$$

El segundo número compara la fuerza de arrastre hacia el mar (flujo de agua dulce) con la componente lateral de la flotación.

$$N_b = \frac{\alpha_s K \partial z / \partial y}{q_b} \qquad (1.12)$$

4.2.- METODOLOGÍA DE MODELACIÓN NUMÉRICA

La contribución de la profundidad del acuífero a las irregularidades en los patrones de intrusión se ha evaluado mediante una metodología numérica consistente en considerar distintas geometrías de un acuífero horizontal confinado y de espesor constante con un modelo 3D de tamaño 10000x50x50m3. La geometrías consideradas pueden agruparse en cuatro categorías: (1) horizontal, (2) inclinado hacia el mar, (3) en forma de V (con una sección central más profunda) y (4) alabeado (curvado con un punto más profundo situado en el centro del contorno de mar (Figura 4.2). Este último es el que podría representar la situación en el Llobregat. Todas las geometrías consideradas son simétricas por lo que sólo es necesario modelar la mitad del dominio (Figura 4.3.).

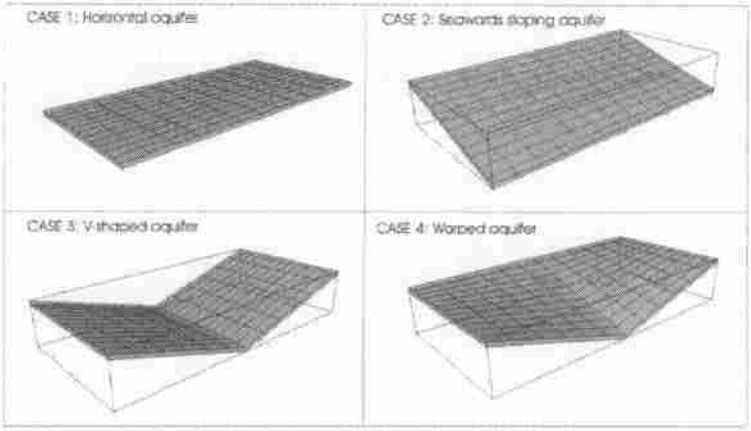

Figura 4.2.- *Esquema de las geometrías consideradas. El agua dulce fluye desde el fondo hacia el frente.*

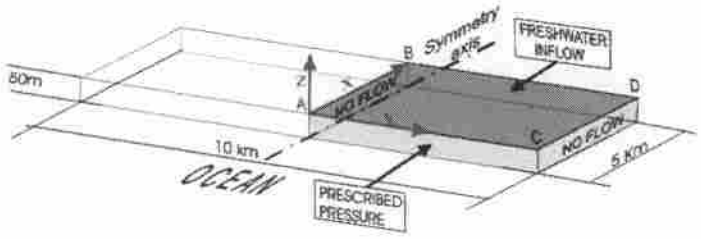

Figura 4.3.- *Acuífero y dominio del modelo (área en gris), incluyendo las diferentes condiciones de contorno impuestas*

Las condiciones de contorno utilizadas son:

1.- Flujo de agua dulce constante (1.18 hm^3/año) a través de todo el contorno interior (sección vertical BD en la Figura 4.3).

2.- Presión prescrita ($p=\rho_s\, g\, z$) a lo largo del contorno de mar (sección AC en Figura 4.3) con concentración igual al agua de mar para el flujo entrante e igual a la concentración residente para el saliente.

3.- Los contornos restantes (planos verticales AB y CD y las superficies superiores e inferiores de la Figura 4.3) son de flujo nulo.

Tanto el nivel del mar como el plano horizontal (ABCD en la Figura 4.3) están situados a cota cero ($z = 0$). Los parámetros de flujo y transporte utilizados en las simulaciones se especifican en la Tabla 4.1.

Tabla 4.1.- *Parámetros usados en la simulaciones.*

Parámetro	Valor	
ϕ	0.25	Porosidad
k	1.25e-11 m^2	Permeabilidad (isotropa)
$\alpha_{Lmax}=\alpha_{Lmed}$	20 m	Max. y min. dispersividad longitudinal
α_{Lmin}	2 m	Min. dispersividad longitudinal (para flujos verticales)
α_T	2 m	Dispersividad transversal
D_m	1.0e-9 m^2/s	Coeficiente de diffusion molecular
α	1.0e-8 $(kg/m\cdot s^2)^{-1}$	Compresibilidad de la matriz
β	4.4e-10 $(kg/m\cdot s^2)^{-1}$	Compresibilidad del fluido
μ	0.001 kg/m·s	Viscosidad del agua dulce

Tabla 4.2.- *Descripción de las diferentes simulaciones realizadas en el presente análisis (m_x y m_y son las componentes de la pendiente en la dirección perpendicular y paralela a la costa, respectivamente).*

Geometría	Max m_x	Max m_y	N_{by}
CASO 1: Horizontal	0	0	0
CASO 2: Pendiente hacia mar	0.01	0	0
CASO 2: Pendiente hacia mar	0.03	0	0
CASO 2: Pendiente hacia mar	0.1	0	0
CASO 3: Forma de V	0	0.01	0.25
CASO 3: Forma de V	0	0.03	0.6
CASO 3: Forma de V	0	0.1	2.5
CASO 4: Alabeado	0.01	0.01	0.25
CASO 4: Alabeado	0.03	0.03	0.6
CASO 4: Alabeado	0.1	0.1	2.5

Los casos simulados se clasifican según la forma y la pendiente de los contornos y el número N_{by}. Las simulaciones se realizado con SUTRA (Voss y Provost, 2002) sobre una malla de 36x73x11 nudos. Los resultados se analizan para un estado estacionario natural que se alcanza con seguridad tras una simulación transitoria de 1500 años. Las condiciones iniciales corresponden a las de un acuífero de agua dulce.

4.3.- RESULTADOS

Con el fin de comparar el comportamiento de la intrusión marina en los diferentes casos simulados, se ha elegido cómo parámetro de comparación la penetración de la isolínea de 50% de mezcla y, más particularmente, el *pie* de esta línea. Este *pie* se define como la distancia (medida a lo largo del eje x) entre el contorno de mar y el punto en el que la línea de 50% de mezcla interfecta el fondo del acuífero. A continuación se presenta un resumen de los resultados obtenidos según el acuífero tenga o no pendiente lateral ($m_y \neq 0$). Los resultados del acuífero horizontal (Caso 1) sirven como referencia. Primero analizaremos el comportamiento de la interfaz en la sección central del acuífero (AB en la Figura 4.3) en la que se alcanzar profundidades mayores en los casos con pendientes laterales.

4.3.1.- Acuíferos sin pendiente lateral

En la Figura 4.4 (izquierda) se presenta la posición de la interfaz para los acuíferos horizontal y con pendiente hacia el mar (es decir, aquellos cuyas pendientes laterales, m_y, son cero y por tanto el número N_{by}). Se observa que los acuíferos inclinados hacia el mar presentan un comportamiento muy similar al del acuífero horizontal. En otras palabras, la pendiente m_x no afecta a la geometría de la interfaz.

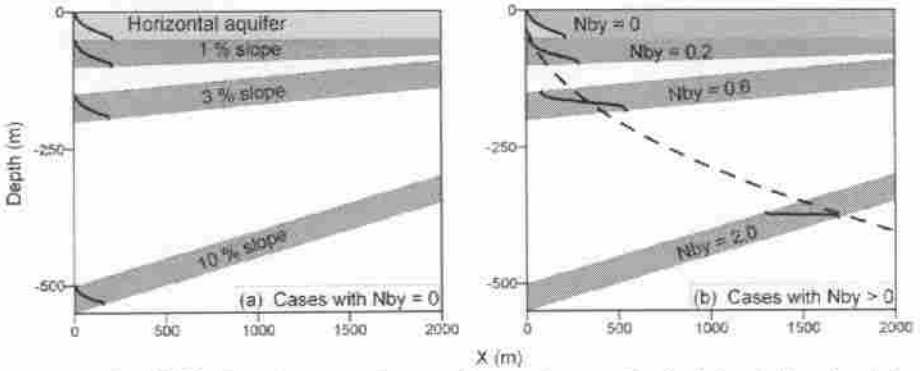

Figura 4.4.- *Posición de la interfaz para los acuíferos sin pendiente lateral (izquierda) y para los acuíferos alabeados (caso 4) en los que $m_x = m_y$. La línea discontinua representa la posición de la interrfaz de un acuífero de 550 m de espesor con la mismo flujo unitario de entrada de agua dulce por el contorno interior.*

4.3.2.- Acuíferos con pendiente lateral.

La posición de la interfaz se ve fuertemente alterada cuando se consideran acuíferos con pendientes laterales (con $N_{by} \neq 0$), como puede observarse en la gráfica derecha de la Figura 4.4. Al aumentar la pendiente lateral, es decir, N_{by}, aumenta la penetración de la interfaz en la sección central del acuífero. Es interesante observar que la posición de la interfaz coincide con la que tendría a esa altura un acuífero horizontal de espesor mayor (en este caso 550 m de espesor) pero con el mismo flujo específico de entrada de agua dulce (línea discontinua en Figura 4.4).

La mayor penetración en esta sección central puede entenderse mejor si se observan los vectores velocidad. En la Figura 4.5 se presentan los vectores velocidad para el acuífero inclinado hacia el mar con mayor pendiente. Los vectores muestran la típica celda de convección vertical ilustrada en la Figura 4.1. El agua dulce descarga hacia el mar y se forma una celda de convección de agua salada que entra en profundidad, se mezcla con el agua dulce y es arrastrada hacia el mar por esta. Sin embargo, en el acuífero los alabeado (Figura 4.6) la interfaz se encuentra tierra adentro, lejos del contacto con el mar. Por lo tanto el agua dulce que fluye en esta sección no puede descargar en el mar. ¿Hacia donde va esa agua dulce? ¿Toda ella se dispersa en la zona de mezcla? Los vectores velocidad parecen indicar que hay una celda de convección cerrada en esa zona. Sin embargo, si existe entrada constante tanto de agua dulce como de agua salada, tiene que existir una zona de salida.

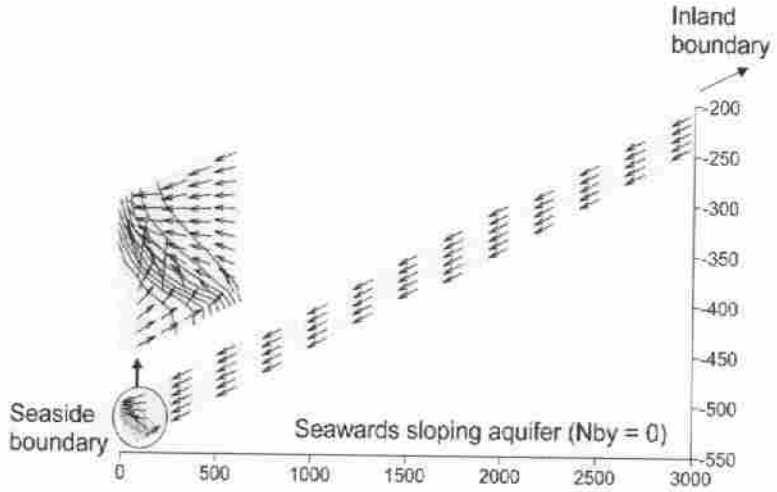

Figura 4.5.- *Proyección de los vectores velocidad en la sección central del acuífero inclinado hacia el mar con mayor pendiente m_x.*

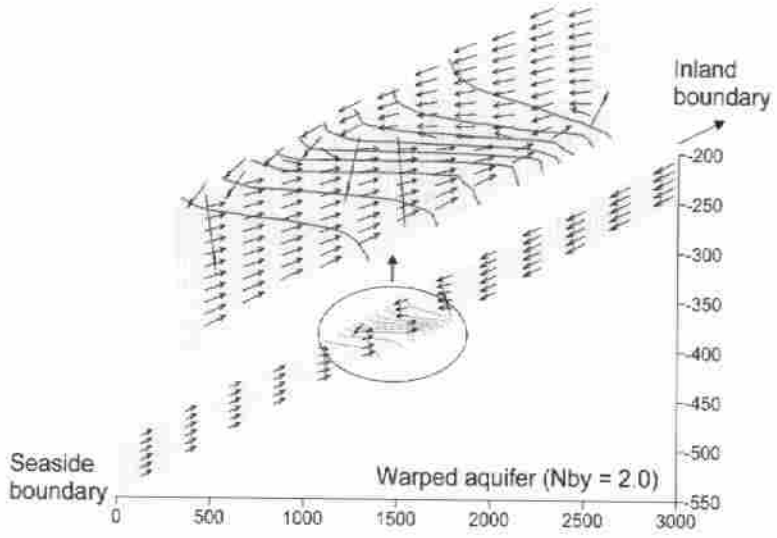

Figura 4.6.- *Proyección de los vectores velocidad en la sección central del acuífero alabeado con N_{by} =2.*

Estos resultados aparentemente poco realistas pueden entenderse mejor si se observa el flujo en el fondo del acuífero en los acuíferos con pendientes laterales (en forma de V y alabeados) tal como se presenta en la Figura 4.7. Está figura muestra hacia donde se mueve el agua que entra por la sección central, más profunda, una vez alcanza la zona de mezcla. El agua de mar es desviada lateralmente y pendiente arriba. Lo mismo le ocurre al agua dulce, que es empujada por el agua de mar y solamente puede descargar en las partes más someras de la costa. La pendiente lateral provoca, por lo tanto, que la celda de convección de la cuña de intrusión se desarrolle principalmente de forma lateral. Esto explica por qué el agua de mar penetra tan lejos tierra adentro en la parte más profunda del acuífero. Tanto la penetración del agua de mar cono la forma de la interfaz están condicionadas por el patrón tridimensional del flujo. Por tanto, se observa

diferente penetración en las secciones central y lateral en todos los ejemplos con $N_{by} \neq 0$.

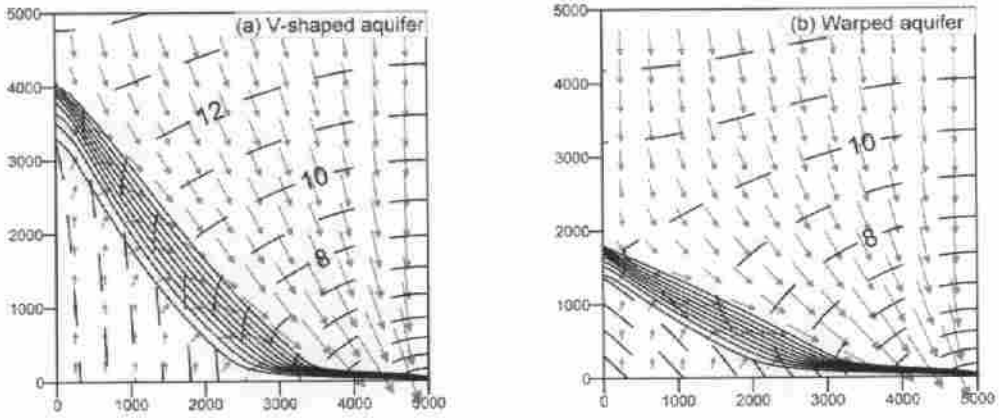

Figura 4.7.- *Vista en planta de los vectores velocidad en el fondo del acuífero, líneas de isoconcentración e isolíneas de nivel equivalente (líneas discontinuas) para el acuífero en forma de V (izquierda) y alabeado (derecha). Ambos tienen* N_{by} *=2.*

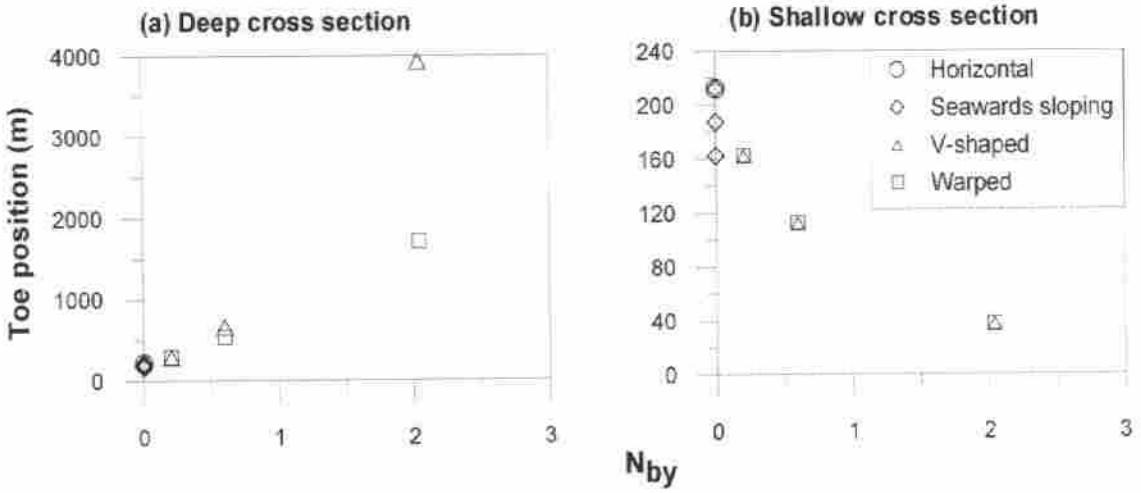

Figura 4.8.- *Posición del pie para las secciones central (a) y lateral (b) en función del número adimensional* N_{by}

La penetración del agua de mar en las sección más profunda aumenta conjuntamente con el valor del número N_{by} (*Figura 4.8 a*). Este efecto va acompañado de un retroceso del pie de la cuña de intrusión en las secciones más someras (Figura 4.8 b). Por tanto, se puede considerar N_{by} como un indicador de la magnitud de la celda de convección lateral horizontal.

Como consecuencia de esta tridimensionalidad del flujo, la cantidad de agua salada que entra en el acuífero a través del acuífero no esta uniformente distribuida a lo largo de la costa en los acuíferos con pendientes laterales (Figura 4.9). El flujo integrado

verticalmente es prácticamente 0 para acuíferos sin pendiente lateral como era de esperar dada la simetría del flujo. En los acuíferos con forma de V se pueden distinguir dos zonas a lo largo de la zona de costa, una dominada por el flujo entrante y otro por el saliente. El valor máximo de descarga de sal depende de la extensión de la celda horizontal de convección que se forma y por tanto de N_{by} .

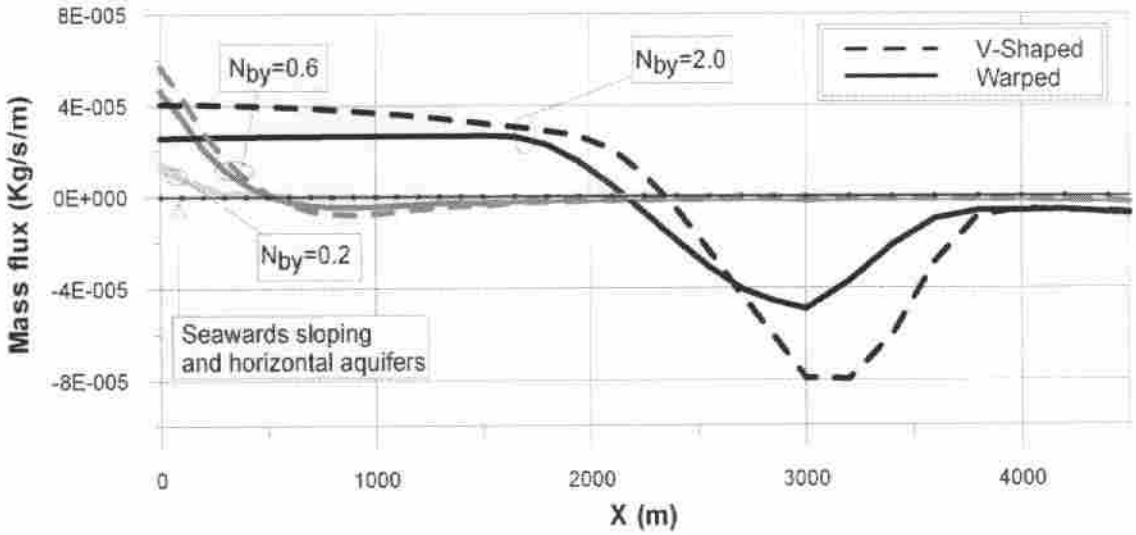

Figura 4.9.- *Flujo de sal integrado verticalmente por unidad de longitud de línea de costa (x). Los valores positivos indican flujo de sal entrante y los negativos, de descarga. El valor mínimo indica la situación del principal punto de descarga.*

4.4.- IMPLICACIONES PARA EL ACUÍFERO PROFUNDO DEL DELTA DEL LLOBREGAT

El acuífero profundo del delta del Llobregat, es como ya se ha comentado anteriormente un acuífero de gran extensión horizontal comparado con su espesor. De hecho, su forma es similar a la representada por el acuífero alabeado (caso 4) con una parte central, distal más profunda que los laterales. Por lo tanto, las conclusiones extraídas de este análisis son plenamente aplicables a este acuífero. El estudio del efecto de las pendientes laterales de los contornos en este tipo de acuíferos ha evidenciado que la tridimensionalidad del flujo puede llegar a ser crítica en algunos casos, cuando las pendientes laterales son importantes. Un indicador de la importancia de este efecto es, como ya hemos dicho, el número N_{by}. Valores de N_{by} menores de 0.5 indican que el efecto de las pendientes laterales es despreciable, sin embargo ha de tenerse en cuenta para valores mayores. En la situación previa a la explotación, el N_{by} del acuífero principal del delta del Llobregat puede considerarse claramente inferior a este umbral. Por tanto, el efecto de la tridimensionalidad del flujo puede considerarse poco importante para la definición de las condiciones iniciales.

5.- SIMULACIÓN DE INTRUSIÓN MARINA EN ACUÍFEROS CONFINADOS

5.1.- INTRODUCCIÓN

El objetivo de este capítulo es el análisis de los procesos de intrusión marina en acuíferos costeros confinados estudiando bajo qué condiciones se puede simplificar el problema a dos dimensiones y con densidad constante en el interior del dominio.

5.2.- METODOLOGÍA

Para cumplir dicho objetivo se ha modelado con el código de elementos finitos SUTRA un caso teórico en tres dimensiones tomando el problema acoplado y desacoplado, luego se ha modelado lo mismo en dos dimensiones, de esta manera se pueden cuantificar las diferencias existentes entre los casos anteriores para poder aclarar en qué casos se pueden aplicar estas simplificaciones.

Se ha tomado como caso base un acuífero confinado de dimensiones 5000x5000x50, homogéneo e isótropo, con una cierta pendiente (5%) paralela al mar.

Las condiciones de contorno impuestas son:

- Caudal de agua dulce preescrito del continente al mar (1.18 hm^3/año).

- Presión preescrita en el contorno del mar, siendo $P = -\rho_s g z$, de tal forma que si el acuífero descarga al mar tomará la concentración correspondiente al interior del acuífero, y si existe una entrada de fluido al acuífero la concentración será igual a la concentración de agua de mar.

- Flujo nulo en el contorno superior e inferior.

La discretización espacial supone dividir el dominio en una serie de elementos o celdas, el método de elementos finitos resuelve la ecuación de flujo y transporte en los vértices de los elementos. Se ha dividido el dominio en celdas rectangulares, refinando la malla en los lugares de mayor interés.

En la Figura 5.1 se muestran la geometría, la malla y los parámetros del acuífero.

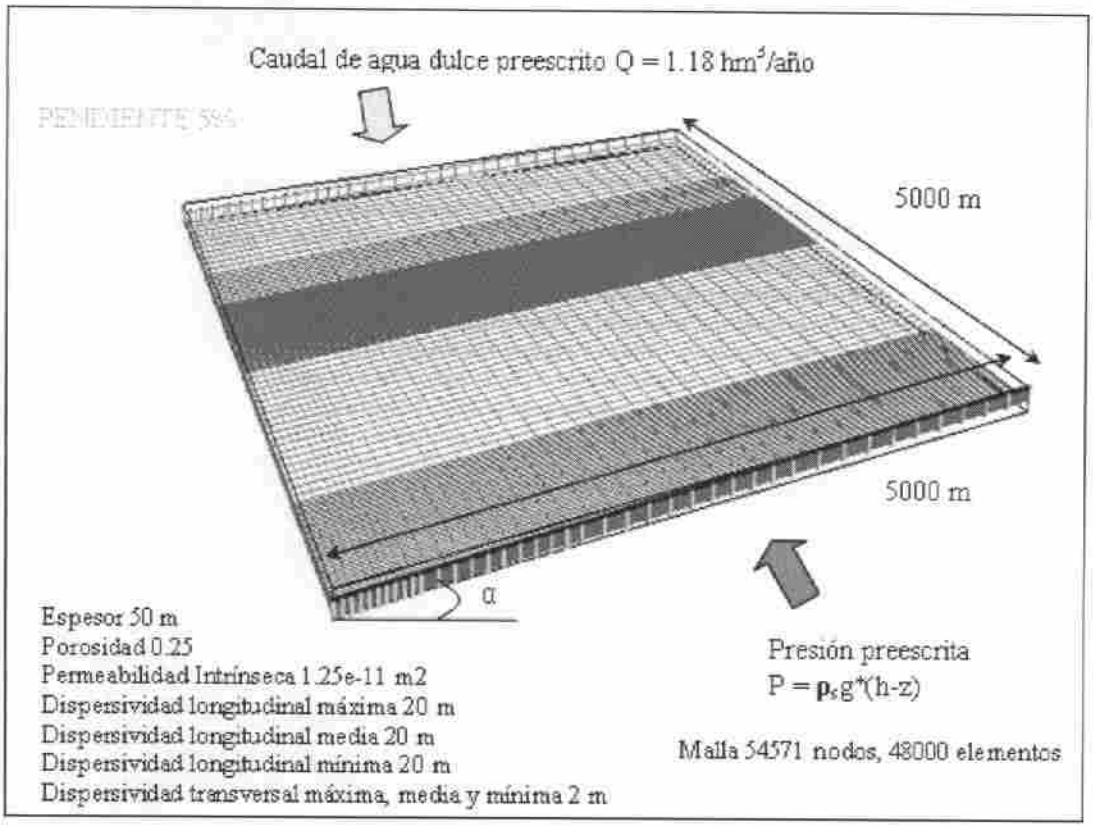

Figura 5.1.- *Dimensiones, malla y propiedades del modelo.*

Se han simulado los siguientes casos:

- Modelos 3D:

  -Problema desacoplado, que llamaremos con densidad constante, en el cual la densidad dentro del dominio es la del agua dulce, aunque en la condición de contorno del mar tome la densidad de agua salina.

  -Problema acoplado, que llamaremos problema con densidad variable, en el cual la densidad dentro del dominio es función de la concentración.
- Modelos 2D con densidad constante y variable.
- Análisis de sensibilidad al caudal de agua dulce.
- Análisis de sensibilidad a las dispersividades.
- Análisis de sensibilidad a las pendientes.
- Influencia de un bombeo, insertando un pozo de extracción (Figura 5.2.)

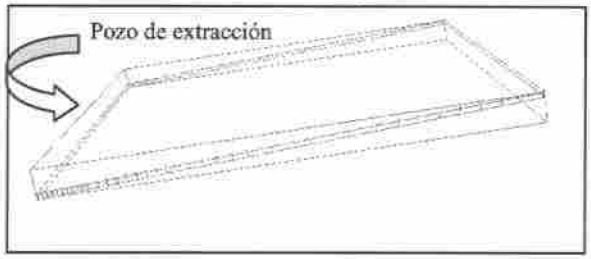

Figura 5.2.- *Situación del pozo de extracción.*

5.3.- RESULTADOS

5.3.1.- Modelos 3D

Se ha modelado el caso base en 3D con densidad constante y densidad variable hasta alcanzar un estado estacionario. En la Figura 5.3 se muestran las isoconcentraciones y los vectores de velocidad para los dos casos tomadas en el plano inferior del acuífero:

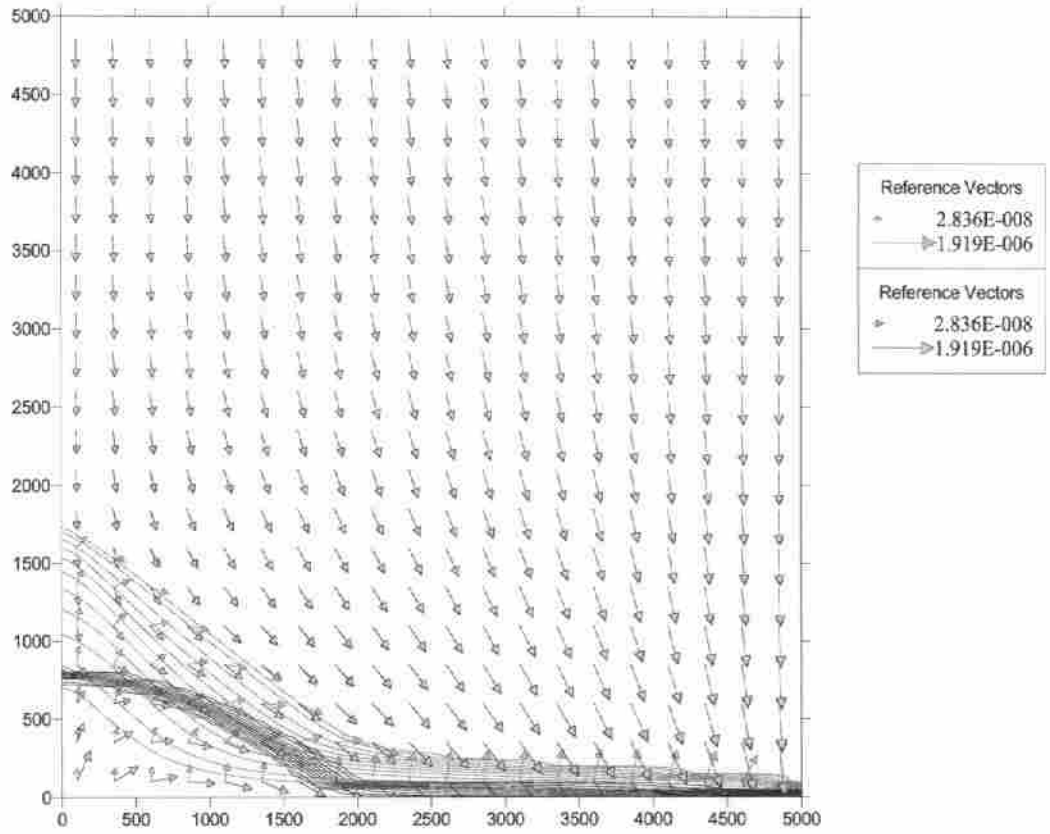

Figura 5.3.- *Caso base. Mapa en planta de isoconcentraciones y velocidades de flujo para los modelos 3D con densidad variable, color rojo, y densidad constante, color azul, tomando el plano inferior del acuífero.*

Como puede observarse la longitud del pie es mayor para el caso con densidad variable (diferencia de más de 900m), así como el ancho de la zona de mezcla (la forma de la interfaz es tendida en el caso de densidad variable y verticalizada en el caso de densidad constante). La velocidad de entrada es mayor en el modelo con densidad constante cerca del contorno del mar y disminuye progresivamente hacia el continente, en el caso de densidad variable la velocidad de entrada de agua salina es prácticamente constante.

En el modelo con densidad constante la componente vertical es muy importante mientras que en el modelo de densidad variable la componente principal es la

transversal. Existen diferencias en la zona de descarga, mientras que en los modelos con densidad constante la descarga se produce a lo largo de todo el acuífero, en los modelos con densidad variable la mayor descarga se produce en las zonas menos profundas. Es por esto por lo que se puede afirmar que la componente vertical en los modelos con densidad constante es muy importante.

Existe gran diferencia con respecto al balance de masas. En el modelo con densidad constante para el caudal de agua dulce tomado entra mayor caudal de agua salina, 315.88 kg/sg con respecto a 21.62 kg/sg que entra en el modelo 3D con densidad variable; esto es porque el gradiente de presión es mayor en el modelo con densidad constante (en el contorno está fijada la presión con respecto a la densidad de agua salina y en el interior del acuífero la densidad no es función de la concentración, es decir, la densidad es la del agua dulce).

5.3.2.- Modelos 2D

Se ha modelado el caso base en 2D con densidad constante y densidad variable, como en el apartado anterior, hasta alcanzar un estado estacionario. Para los modelos 2D ocurre lo mismo que para los modelos 3D, la longitud del pie es mayor en los modelos con densidad variable. El ancho de la zona de mezcla es mucho menor en los modelos 2D que en los modelos 3D y la interfaz es más vertical.

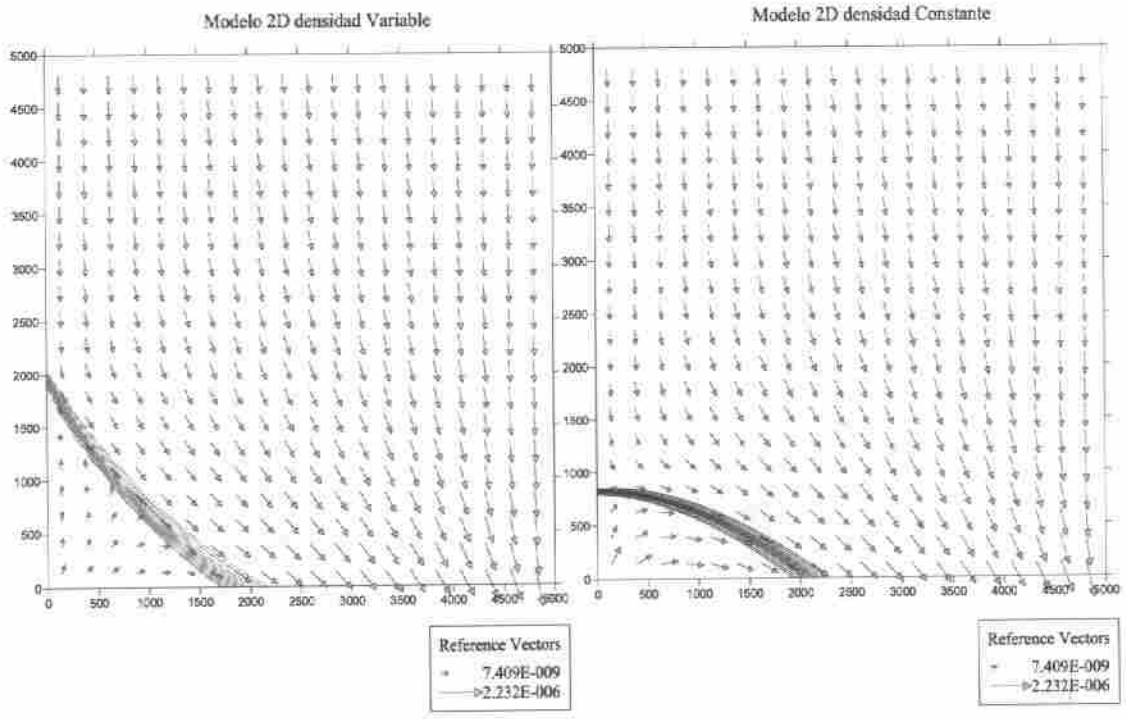

Figura 5.4.- *Caso base. Mapa en planta de isoconcentraciones y velocidades de flujo para los modelos 2D con densidad variable y densidad constante.*

Al igual que en los modelos 3D las velocidades difieren, de modo que para el modelo 2D con densidad constante la velocidad de entrada en el contorno es elevada y va disminuyendo de forma progresiva hacia el continente, en el modelo 2D con densidad variable la velocidad de entrada es prácticamente constante.

Como en el caso anterior existe gran diferencia con respecto al balance de masas. En el modelo 2D con densidad constante entra mayor caudal de agua salina, 8.61 kg/sg con respecto a 0.57 kg/sg que entra en el modelo 2D con densidad variable; esto es porque el gradiente de presión es mayor en el modelo con densidad constante. Estos resultados son muy diferentes con respecto a los modelos 3D.

5.3.3.- Análisis de sensibilidad al caudal de agua dulce

Al modelar el mismo problema tanto en 3D como en 2D imponiendo otros caudales de agua dulce prescritos (el doble y la mitad del inicial) se ha observado que al aumentar el caudal de agua dulce la forma de la interfaz y el ancho de zona de mezcla son similares en todos los casos, pero las velocidades de entrada, y los balances difieren mucho.

Al aumentar el gradiente en los modelos 3D con densidad variable las velocidades aumentan, mientras que en el caso 3D con densidad constante disminuyen. En los modelos 2D las velocidades permanecen prácticamente igual.

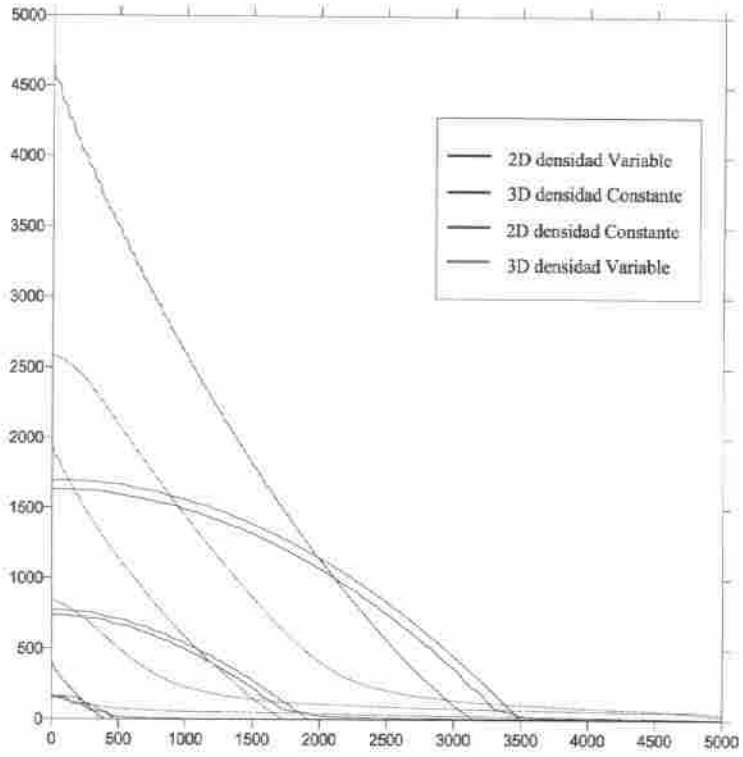

***Figura 5.5.**- Caso base. Mapa en planta para los modelos 2D y 3D con densidad variable y densidad constante, tomando unos caudales de 0.6 hm^3/año, 1.18 hm^3/año y 2.36 hm^3/año. La línea marca el 90% de concentración.*

Como se observa en la figura la longitud del pie para el modelo 2D con densidad variable tomando un caudal de agua dulce de 0.6 hm^3/año es mucho mayor que para los modelos 3D (diferencia con respecto al modelo 3D con densidad variable de 2000 metros y con respecto al modelo 3D con densidad constante más de 3000 metros), al aumentar el gradiente tomando un caudal de agua dulce de 2.36 hm^3/año estas diferencias disminuyen notablemente, la isolínea del 90% de concentración coincide siendo el modelo 2D con densidad variable el que presenta diferencia con respecto a los otros.

Con respecto a los balances de masas al aumentar el caudal de agua dulce en el modelo 3D con densidad variable, la cuña de intrusión se retira pero entra mayor cantidad de agua salada (aumenta el gradiente de presión y aumenta el coeficiente de dispersión, por lo que para equilibrar el sistema ha de entrar mayor cantidad de agua). Esto en el resto de modelos no queda reflejado.

Los balances de masas de los modelos 2D también son diferentes al compararlos con los modelos 3D, la entrada de agua salina es bastante menor que en los modelos 3D con

densidad variable (sobretodo al comparar 2D con densidad variable), y al aumentar el gradiente la entrada de agua salina no aumenta.

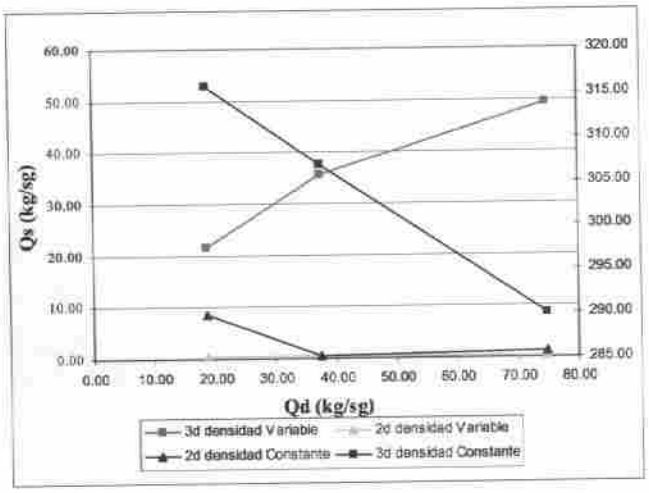

Presión en este punto, tomando la densidad variable, aumenta algo por aumento de caudal, pero disminuye mucho porque tiene menor cantidad de agua salada encima.

Con densidad constante no ocurre esto, sino que la presión aumenta por el aumento del caudal (menor gradiente y menor flujo), y no se ve modificado por el traslado de la cuña ya que la concentración no afecta en la presión.

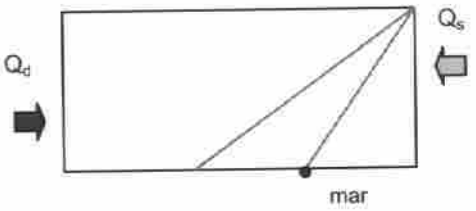

Figura 5.6.- *Caso base modificando el caudal de agua dulce. Relación entre el caudal de entrada de agua salina y el caudal impuesto de agua dulce para los modelos 2D y 3D con densidad constante y densidad variable.*

En los modelos 3D con densidad variable al aumentar el caudal de entrada al acuífero, aumenta el caudal de entrada de mar. En los modelos 3D con densidad constante disminuye, y esta disminución es lineal. En la Tabla 5.1 se muestran los balances de masas de los modelos 3D y 2D con densidad variable y densidad constante.

Tabla 5.1- *Caso base. Balances de masas de los modelos 3D con densidad variable y densidad constante al aumentar el caudal de entrada de agua dulce.*

MODELOS 2D	Q= 0.6 hm^3/año		Q= 1.18 hm^3/año		Q= 2.36 hm^3/año	
	ρ Variable	**ρ Constante**	**ρ Variable**	**ρ Constante**	**ρ Variable**	**ρ Constante**
flujo salida (kg/sg)	18.75	18.75	37.50	37.50	74.75	75.00
flujo entra por contorno de Presión (kg/sg)	0.57	8.61	0.375	4.445	0.18	1.15
flujo sale por contorno de Presión (kg/sg)	-19.31	-27.36	-37.874	-41.940	-75.18	-76.14
concentración (kg soluto/sg)	0.02	0.33	0.01	0.17	0.01	0.04
MODELOS 3D	**ρ Variable**	**ρ Constante**	**ρ Variable**	**ρ Constante**	**ρ Variable**	**ρ Constante**
flujo salida (kg/sg)	18.75	18.75	37.50	37.50	74.75	74.75
flujo entra por contorno de Presión (kg/sg)	21.62	315.88	35.688	306.994	49.32	290.00
flujo sale por contorno de Presión (kg/sg)	-40.36	-334.58	-73.166	-344.494	-124.06	-364.75
concentración (kg soluto/sg)	0.83	12.19	1.38	11.85	1.90	11.19

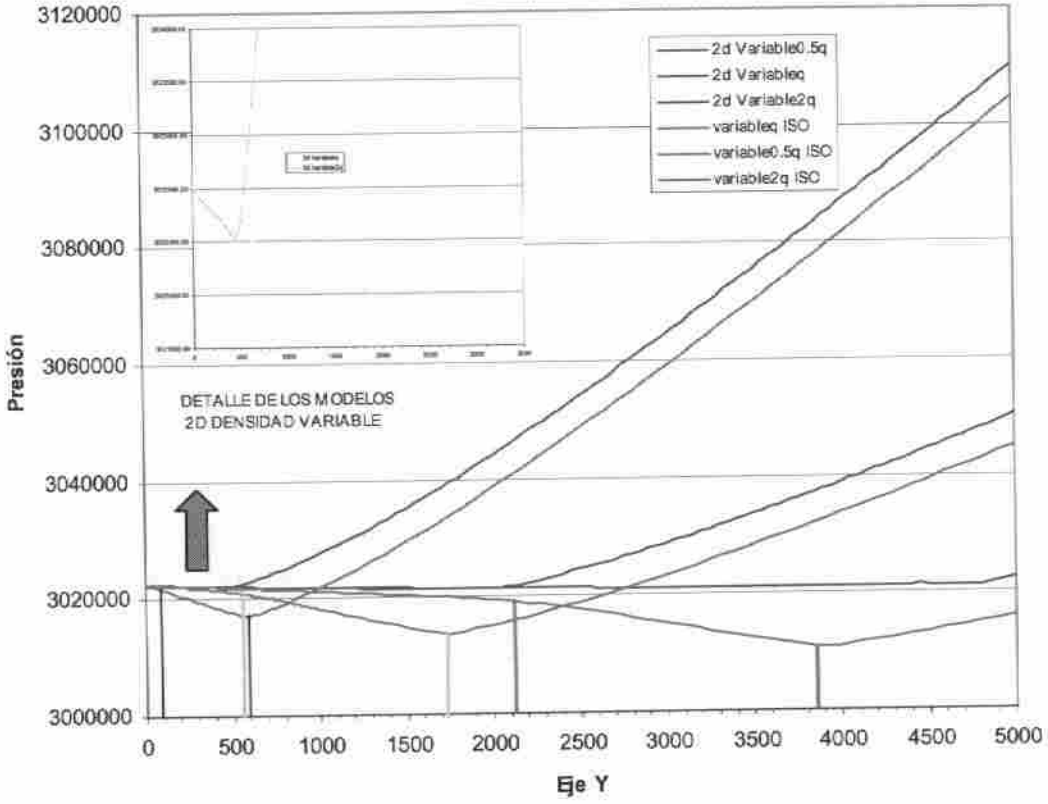

Figura 5.7.- *Perfiles de presión para los modelos 3D (color rojo) y 2D (color verde) con densidad variable, tomando unos caudales de 0.6 hm^3/año, 1.18 hm^3/año y 2.36 hm^3/año. Las líneas verticales muestran el cambio de pendiente en los modelos 3D con densidad variable*

Si comparamos los resultados obtenidos de los modelos 3D y 2D todas estas diferencias se reflejan en los gradientes de presión en Y para X = 0 tomando en los modelos 3D el plano inferior (Figura 5.7). En los modelos 3D con densidad variable la presión comienza con una pequeña pendiente, todos los puntos tienen la concentración máxima, a partir de un cierto punto las concentraciones empiezan a disminuir, mayor gradiente de presión y por tanto mayor pendiente, hasta que la concentración es nula, nuevo cambio de pendiente (pendiente positiva). En 2D los puntos tienen la máxima concentración, por lo que las presiones son prácticamente iguales, el gradiente es muy pequeño (pendiente pequeña), el ancho de la zona de mezcla es pequeño, por lo que la pendiente cambia bruscamente a una pendiente mayor hasta el momento en el que la concentración es nula, pendiente positiva.

En los modelos 3D y 2D con densidad constante la curva es cóncava y el cambio de pendiente coincide aproximadamente con la isolínea de 70% de concentración.

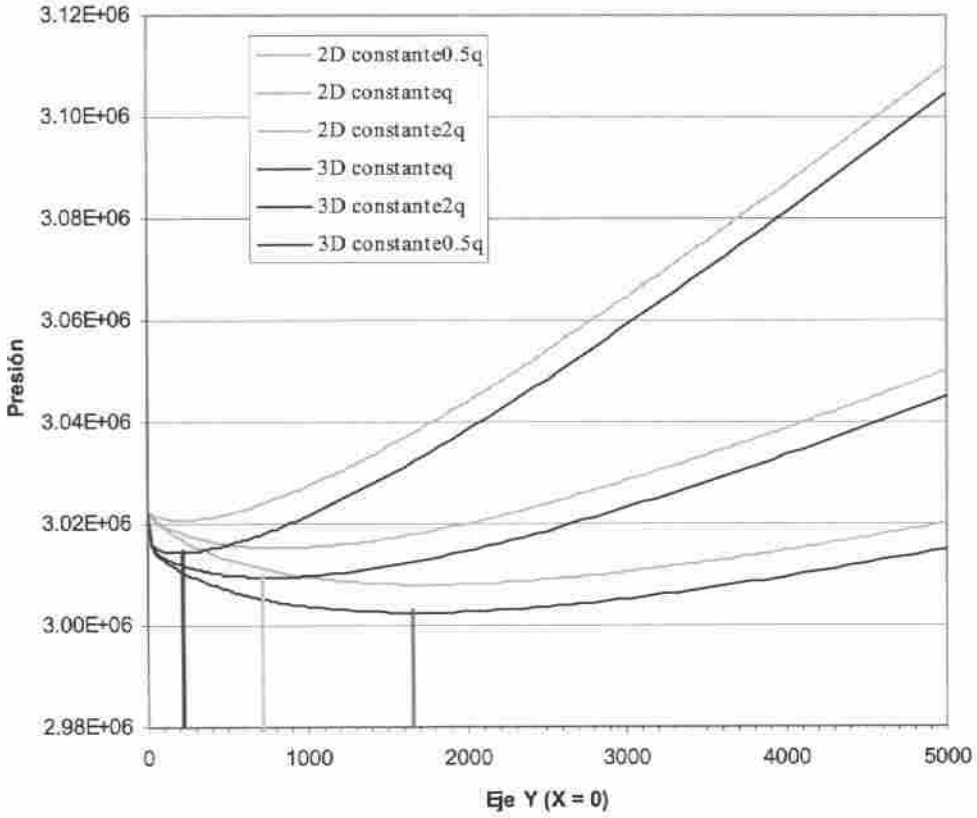

Figura 5.8.- *Perfiles de presión para los modelos 3D (y 2D con densidad constante, tomando unos caudales de 0.6 hm^3/año, 1.18 hm^3/año y 2.36 hm^3/año.*

El modelo más coherente con respecto al modelo 3D con densidad variable es el modelo 2D con densidad constante, existiendo diferencias en la longitud del pie, la forma de la interfaz, el ancho de la zona de mezcla y los balances de masas, pero siendo estas diferencias menores que en los modelos 3D con densidad constante y 2D con densidad variable.

5.3.4.- Análisis de sensibilidad a la dispersividad

Para intentar ajustar la longitud del pie y el ancho de la zona de mezcla en el modelo 2D con densidad variable con respecto al modelo 3D con densidad variable, se ha aumentado el valor de las dispersividades, tanto longitudinal como transversal, en el modelo 2D.

Los valores de las dispersividades con las que se consigue un mejor ajuste son: dispersividad longitudinal 280m y dispersividad transversal 60m.
Con estas dispersividades la interfaz deja de ser vertical, ancho de la zona de mezcla mayor, sin embargo el balance de masas no se ajusta, entrando en el modelo 2D con

densidad variable menor cantidad de agua salina que en el modelo 3D con densidad variable.

Se ha comparado el modelo 2D con el modelo 3D promediado en la vertical, del mejor ajuste se muestra en la siguiente figura:

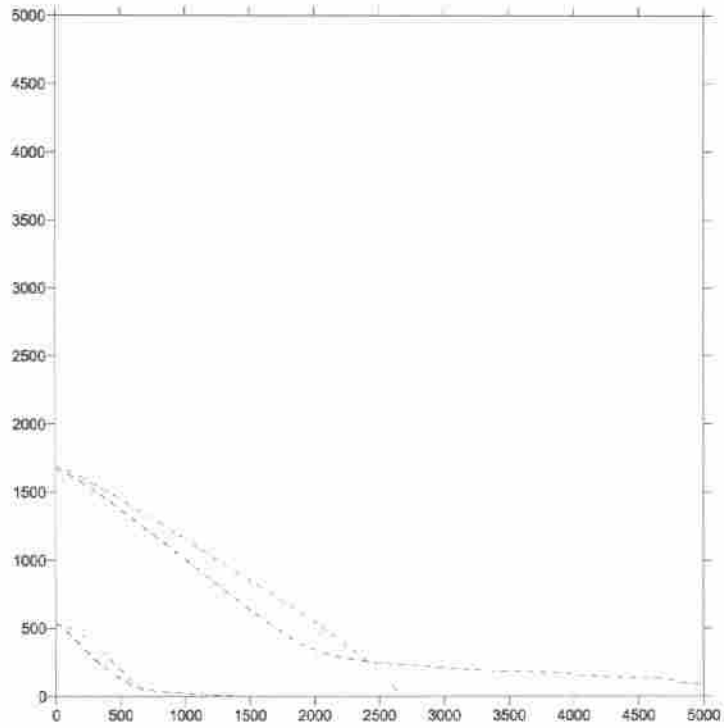

Figura 5.9.- *Caso base. Mapa en planta de líneas de isoconcentración del 90% para los modelos 3D promediado en la vertical (línea discontinua azul) y el modelo 2D con densidad variable (línea discontinua roja) aumentando el valor de las dispersividades longitudinal de 20m inicialmente a 280m y transversal de 2m a 60m.*

En la siguiente figura se muestra la forma de la interfaz en el eje Y siendo X = 0, de todos los ajustes. Como puede observarse los valores que mejor se ajustan al promedio en la vertical del modelo 3D con densidad variable son los anteriormente descritos.

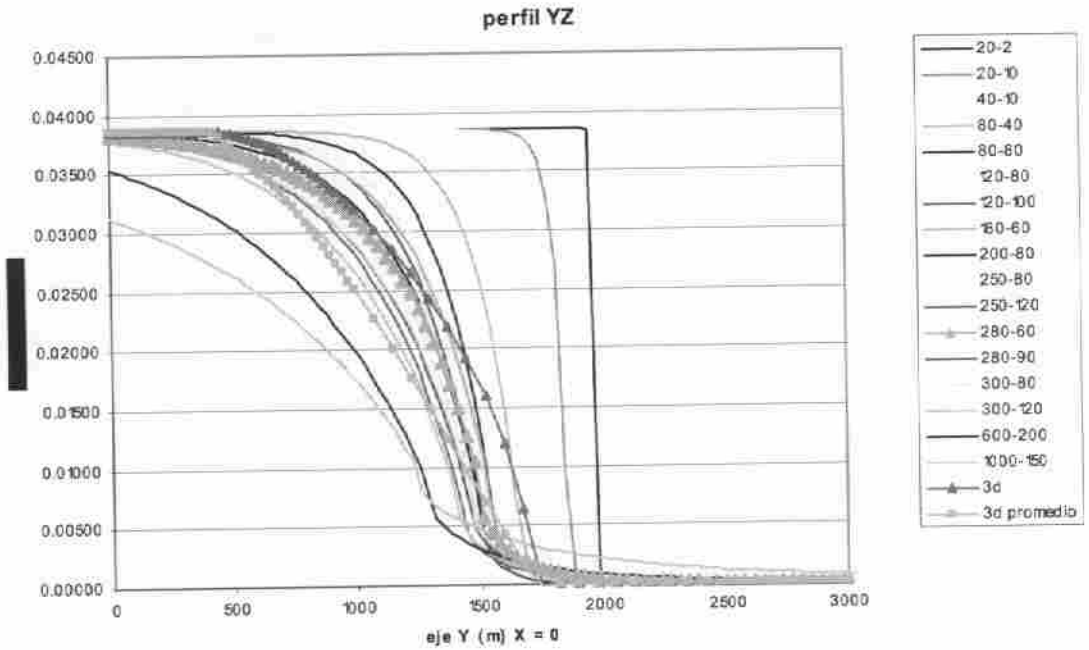

Figura 5.10.- *Forma de la interfaz en el eje Y para X = 0 el modelo 3D promediado en la vertical y el modelo 2D con densidad variable al modificar el valor de las dispersividades.*

Al aumentar los valores de las dispersividades la entrada de agua salina al acuífero aumenta, pero no lo suficiente como para alcanzar los valores resultantes del modelo 3D con densidad variable. Así si para el modelo 3D con densidad variable una vez alcanzado el estado estacionario y para un caudal de agua dulce de 1.18hm^3/año entra un caudal de agua salina de 35.6 Kg/s, para el caso del modelo 2D con densidad variable aumentando las dispersividades entra 1.29 kg/sg (valor bastante mayor que tomando las dispersividades iniciales, 20m la longitudinal y 2m la transversal, siendo este valor igual a 0.37 kg/sg).

5.3.5.- Análisis de sensibilidad a la pendiente

Para evaluar la influencia de la geometría del acuífero se ha modificado la pendiente manteniendo el resto de parámetros igual. Se ha modelado tanto en 3D como en 2D, tomando unas pendientes del 10% y 1%.

5.3.5.1.- Pendiente del 1%

En este caso se han tomado varios caudales de agua dulce debido a que si tomamos el caudal de agua dulce del caso base (1.18 hm^3/año), en los modelos 2D no entraba agua salina al acuífero, no se daba intrusión marina, por lo que se ha disminuido tomando unos caudales de 0.6 hm3/año, 0.295 hm3/año y 0.1475 hm3/año. Las diferencias existentes entre los modelos 3D y 2D con densidad constante son menores al disminuir la pendiente, la longitud del pie y el ancho de la zona de mezcla y las velocidades de entrada prácticamente coinciden, sin embargo siguen existiendo diferencias notables en los balances de masas. Con respecto a los modelos 2D y 3D con densidad variable, al disminuir la pendiente aumentan las diferencias de la longitud del pie y el ancho de la zona de mezcla.

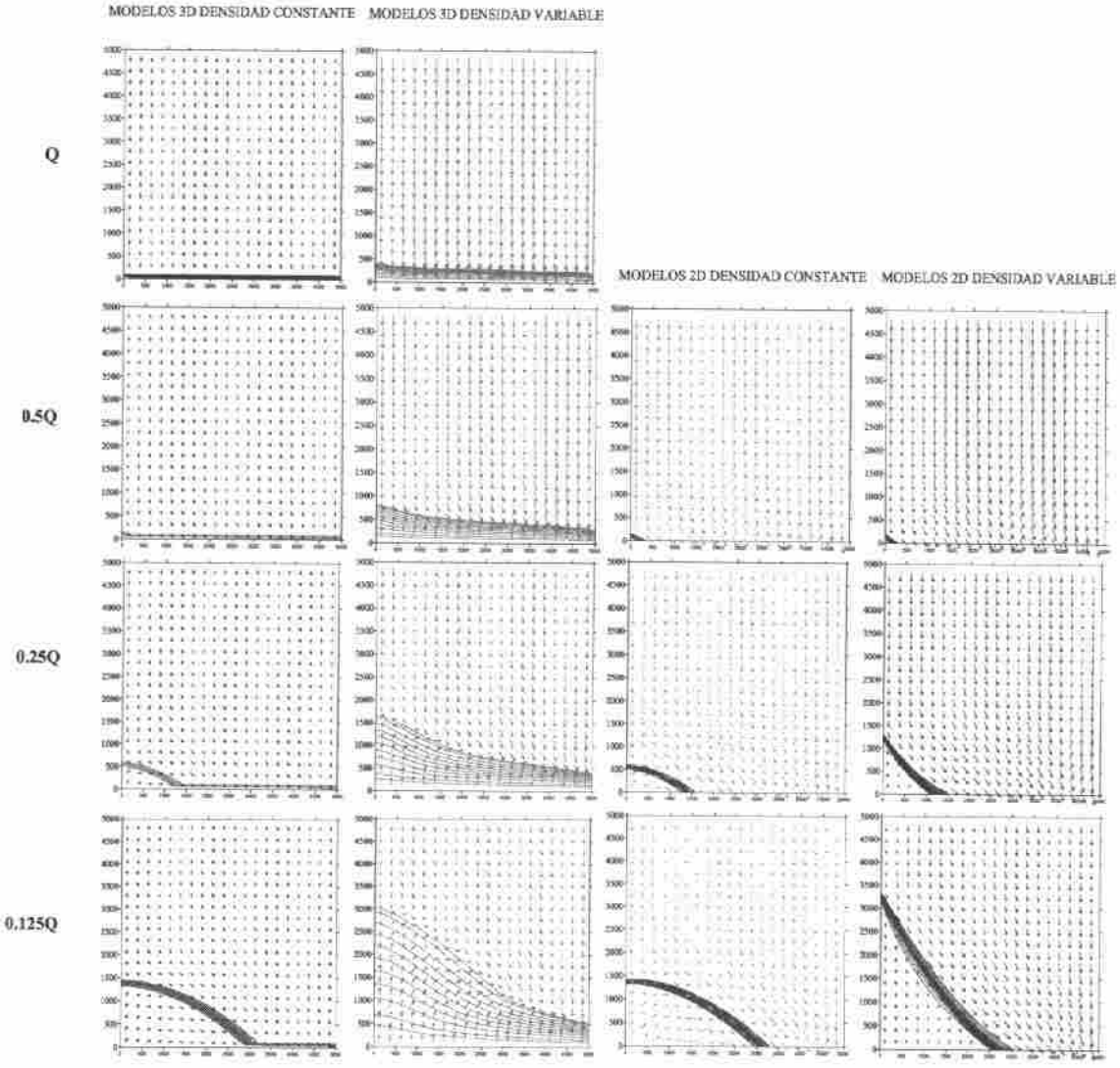

Figura 5.11.- *Pendiente 1%. Mapa en planta de líneas de isoconcentración y velocidades para los modelos 2D y 3D con densidad variable y densidad constante, tomando unos caudales de 0.1475 hm3/año, 0.295 hm3/año, 0.6 hm^3/año y 1.18 hm^3/año.*

Como ocurría en el caso base, pendiente del 5%, En el modelo 3D con densidad variable al aumentar el caudal de agua dulce aumenta la entrada de agua salina, en los modelos 2D la entrada es mucho menor, y al aumentar el caudal de agua dulce disminuye la entrada de agua salina de forma exponencial, en el modelo 3D con densidad constante la entrada de agua salina para una caudal de agua dulce dado es mucho mayor que en los otros casos (eje de la derecha), pero al aumentar el caudal de agua dulce disminuye esta entrada de forma prácticamente lineal.

Debido a que se ha tomado un rango mayor de caudales de extracción que en el caso base, las diferencias del balance entre los cuatro casos, 2D y 3D con densidad constante y variable, son más evidentes, como se puede observar en la siguiente figura.

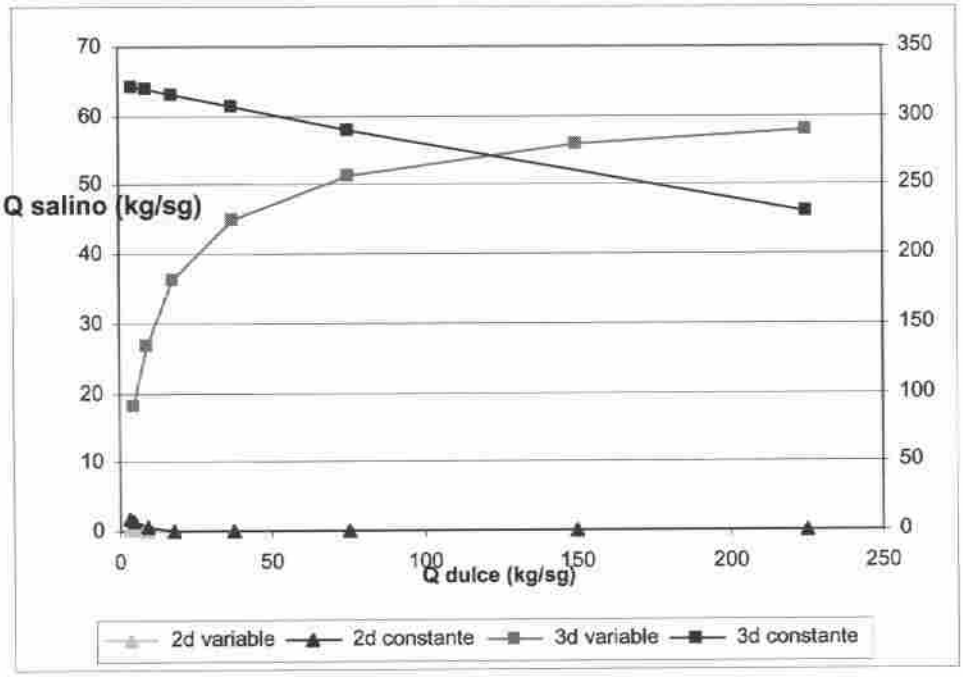

Figura 5.12.- *Pendiente del 1% modificando el caudal de agua dulce. Relación entre el caudal de entrada de agua salina y el caudal impuesto de agua dulce para los modelos 2D y 3D con densidad constante y densidad variable (el modelo 3D con densidad constante queda representado en el eje vertical derecho).*

5.3.5.2.- Pendiente del 10%

En este caso se han tomado además del caudal de agua dulce del caso base (1.18 hm^3/año) el doble y cuatro veces el mismo, ya que con caudales menores la interfaz quedaba influenciada, por cercanía, por la condición de contorno. Se confirma lo que se comentaba en el caso de pendiente del 1%, es decir, las diferencias existentes entre los modelos 3D y 2D con densidad constante aumentan al aumentar la pendiente, la

longitud del pie y el ancho de la zona de mezcla y las velocidades de entrada prácticamente.

Con respecto a los modelos 2D y 3D con densidad variable, al aumentar la pendiente disminuyen las diferencias de la longitud del pie y el ancho de la zona de mezcla.Todo esto se puede observar en la figura 5.13, en la que muestra en planta la línea del 90% de concentración de todos los casos modelados con las distintas pendientes.

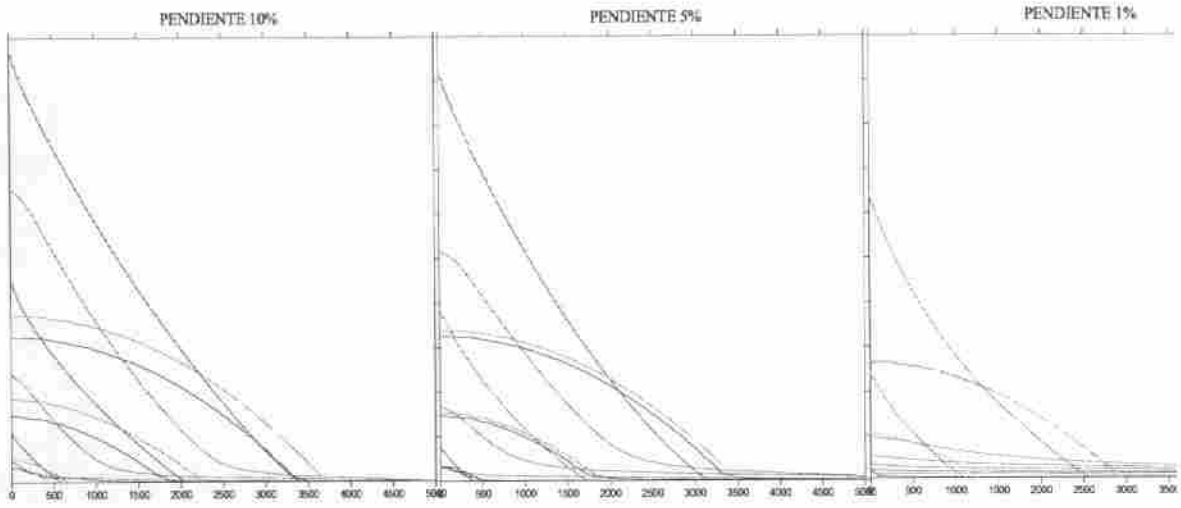

Figura 5.13.- *Mapa en planta de línea de isoconcentración del 90% de los modelos 3D con densidad variable (rojo), 3D con densidad constante (azul), 2D con densidad variable (verde) y 2D con densidad constante (morado) al modificar la pendiente, tomando unos caudales de 1.18 hm^3/año, 2.36 hm^3/año y 4.72 hm^3/año para el caso del 10% de pendiente, caudales de 0.6 hm^3/año, 1.18 hm^3/año y 2.36 hm^3/año para el caso del 5% de pendiente (caso base) y caudales de 0.1475 hm3/año, 0.295 hm3/año, 0.6 hm^3/año y 1.18 hm^3/año para el caso del 1% de pendiente.*

Las diferencias existentes en el balance de masas con respecto al modelo 3D con densidad variable tomando una pendiente del 10% son grandes, sobre todo al compararlo con el modelo 3D con densidad constante. Si tomamos el caudal inicial del caso base (1.18 hm^3/año) el modelo más parecido al 3D con densidad variable es el modelo 2D con densidad constante, entrando prácticamente la misma cantidad de agua salina, sin embargo al aumentar el caudal de agua dulce en el modelo 2D no aumenta dicha entrada, cosa que sí ocurre en el modelo 3D.

Tabla 5.2.- *Pendiente del 10%. Balances de masas de los modelos 3D con densidad variable y densidad constante al aumentar el caudal de entrada de agua dulce.*

MODELOS 2D	Q= 1.18 hm^3/año		Q= 2.36 hm^3/año		Q= 4.72 hm^3/año	
	ρ Variable	**ρ Constante**	**ρ Variable**	**ρ Constante**	**ρ Variable**	**ρ Constante**
flujo salida (kg/sg)	37.50	37.50	74.75	74.75	149.50	149.50
flujo entra por contorno de Presión (kg/sg)	3.66	21.03	2.22	11.75	0.78	3.56
flujo sale por contorno de Presión (kg/sg)	-41.16	-58.45	-76.97	-86.50	-150.28	-153.06
concentración (kg soluto/sg)	0.14	0.81	0.09	0.45	0.03	0.14
MODELOS 3D	**ρ Variable**	**ρ Constante**	**ρ Variable**	**ρ Constante**	**ρ Variable**	**ρ Constante**
flujo salida (kg/sg)	37.50	37.50	74.75	74.75	149.50	149.50
flujo entra por contorno de Presión (kg/sg)	23.51	307.58	39.27	290.42	53.81	258.63
flujo sale por contorno de Presión (kg/sg)	-61.01	-345.08	-114.02	-365.17	-203.31	-408.13
concentración (kg soluto/sg)	0.91	11.87	1.52	11.21	2.08	9.98

5.3.5.3.- Influencia de un bombeo.

Para observar el efecto de un bombeo, se ha modelado el caso base con pozo totalmente penetrante con un caudal de extracción de 4 hm^3/año durante un período de tiempo de 92 años.

Al final de este tiempo de simulación, la forma de la interfaz, así como la longitud del pie y el ancho de la zona de mezcla es muy similar para todos los casos: 2D y 3D con densidad constante y variable.

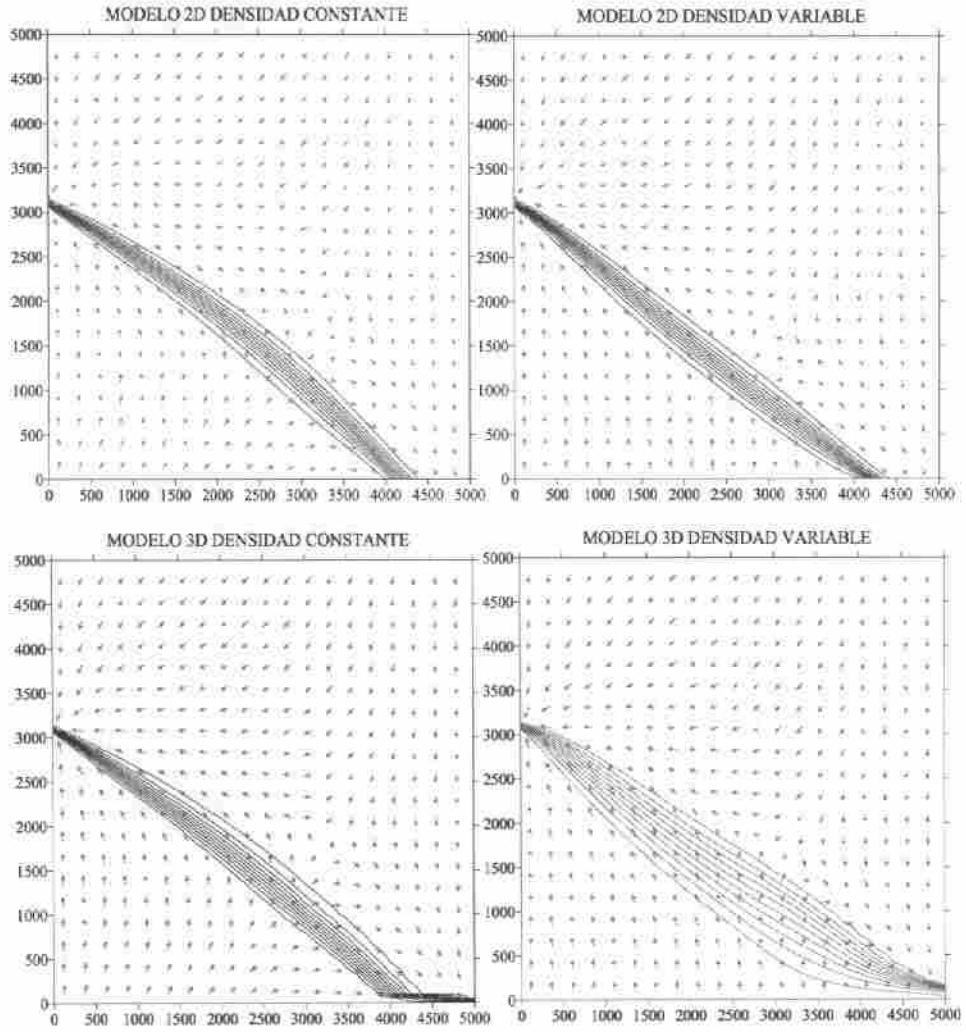

Figura 5.14.- *Mapa en planta de líneas de isoconcentración para los modelos 3D y 2D con densidad constante y variable, al insertar un pozo con un caudal de extracción de 4 hm^3/año.*

Con respecto a las concentraciones alcanzadas en el pozo se han comparado los modelos 2D con el promedio en toda la longitud del pozo en los modelos 3D. La concentración máxima se alcanza en el modelo 2D con densidad variable, la concentración alcanzada en el modelo 3D con densidad variable es muy similar al alcanzado en el modelo 2D con densidad constante, siendo algo menor dicha concentración en el modelo 3D con densidad constante.

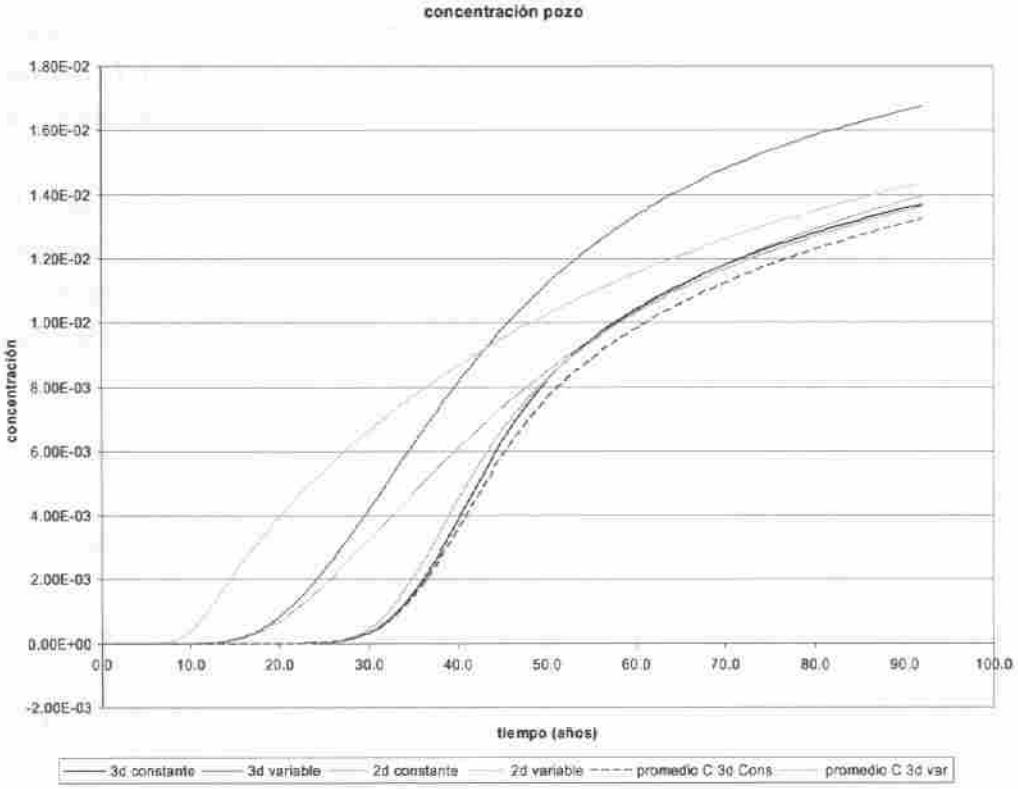

Figura 5.15.- *Concentración alcanzada en el pozo después de 92 años de simulación para los modelos 3D y 2D con densidad constante y variable, tomando un caudal de extracción de 4 hm^3/año.*

El descenso calculado es muy similar en todos los casos: 2D densidad constante descenso de 26.23m, 2D densidad variable descenso de 25.47m, 3D densidad constante 25.95m y 3D densidad variable descenso de 25.22m. La máxima velocidad se alcanza en el modelo 2D con densidad variable (≈130 m/año), y la mínima en el modelo 3D con densidad constante (≈80 m/año, muy similar a la velocidad alcanzada en el modelo 2D con densidad constante). Los balances de masas son muy parecidos en todos los casos excepto en el caso del modelo 3D con densidad constante, en el cual la entrada de agua salina es del orden de 8 veces mayor que en el resto de los casos.

Tabla 5.3.- *Caso base. Balances de masas de los modelos 3D y 2D con densidad variable después de 92 años de simulación al insertar un pozo con un caudal de extracción de 4 hm^3/año*

92 años de simulación	POZO Q 3D		POZO Q 2D	
	V.I.	**C.I.**	**Variable**	**Constante**
Bombeo (kg/sg)	-63.42	-63.42	-63.42	-63.42
flujo salida (kg/sg)	37.50	37.50	37.50	37.50
flujo entra por contorno de Presión (kg/sg)	41.51	338.69	33.77	37.13
flujo sale por contorno de Presión (kg/sg)	-15.32	-313.01	-7.58	-11.25
concentración (kg soluto/sg)	1.60	13.07	1.30	1.43
Concentración alcanzada en el pozo	1.67E-02	1.37E-02	1.44E-02	1.36E-02

Cuando existe un gradiente importante hacia el continente, el modelo más coherente con respecto al modelo 3D con densidad variable es el modelos 2D con densidad constante. La concentración alcanzada en el pozo es prácticamente la misma, y el balance de masas se ajusta bien, sin embargo el ancho de la zona de mezcla es menor en el caso del 2D. Las diferencias de presión en el pozo son muy parecidas en todos los casos (sin embargo si observamos la evolución de la presión en el pozo con respecto al tiempo en los modelos con densidad variable, la presión disminuye hasta que llega la concentración al pozo, dándose un pequeño aumento por aumento de la densidad).

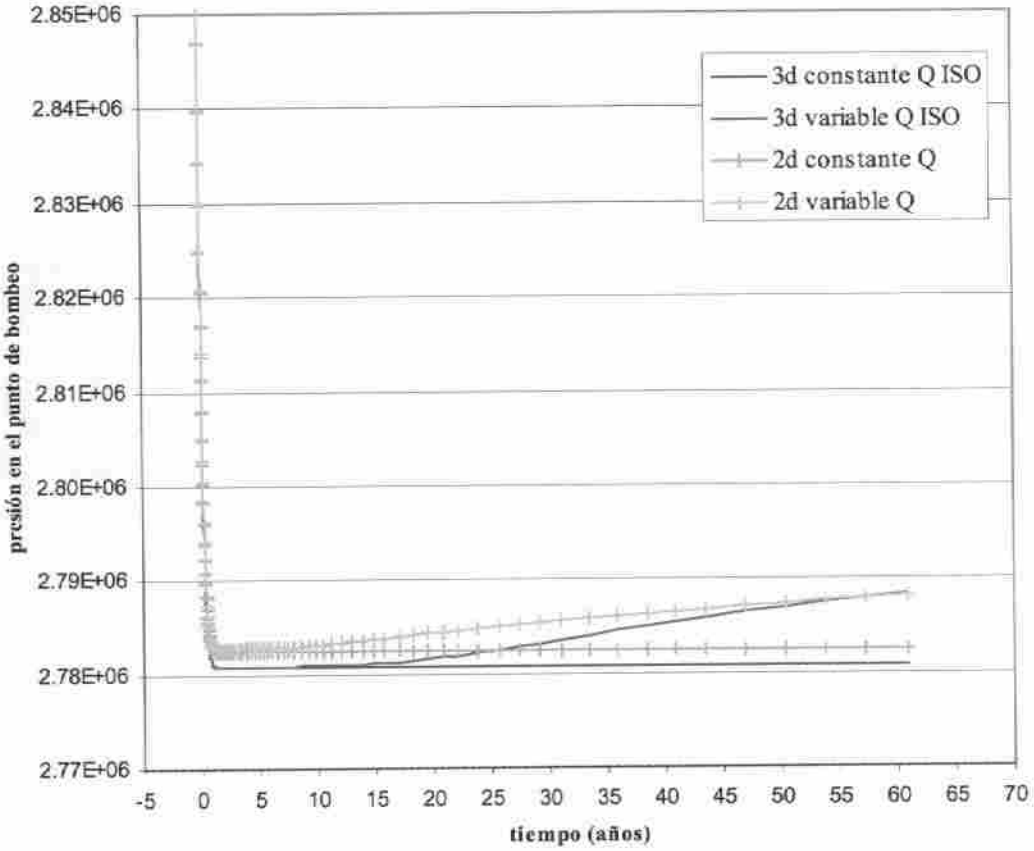

Figura 5.16. *Caso base. Presiones alcanzadas en el pozo de extracción (4hm^3/año) tras 92 años de simulación.*

Sin embargo todos estos resultados han de tomarse con cautela debido a que en ninguno de los casos anteriores se ha alcanzado el estado estacionario.

5.4.- CONCLUSIONES

De este estudio se pueden extraer las siguientes conclusiones:

- Longitud del pie es mayor en los modelos con densidad variable que con densidad constante, siendo mayor para el caso 2D (esta diferencia disminuye al aumentar el gradiente).

- La forma de la interfaz es tendida en los modelos 3D con densidad variable, siendo muy verticalizada para el resto de los casos.

- Balance. En los modelos 3D con densidad constante, para un Qd fijo, entra mayor cantidad de agua salada que en los modelos 3D con densidad variable, porque el gradiente de presión es mayor. En los modelos 2D la entrada de agua salina es mucho menor que en los modelos 3D.

- En los modelos 3D con densidad constante la componente vertical es importante, debido también a la gran diferencia de presión, en los modelos 3D con densidad variable la componente principal es la transversal.

- Al aumentar el caudal de agua dulce llega un momento que el gradiente es tan elevado que la forma de la interfaz y el ancho de zona de mezcla son similares en todos los casos, sin embargo las velocidades de entrada, y los balances difieren mucho.

- Al aumentar el caudal de agua dulce de entrada al acuífero aumentan las velocidades en los modelos 3D con densidad variable, en los modelos 3D con densidad constante sucede lo contrario. En los modelos 2D al aumentar el caudal de entrada las velocidades prácticamente no varían.

- Al aumentar el caudal de agua dulce, la cuña de intrusión marina se retira pero entra mayor cantidad de agua para los modelos 3D con densidad variable. Esto en los modelos 2D y en el modelo 3D con densidad constante no queda reflejado.

- Al aumentar los valores de las dispersividades en los modelos 2D con densidad variable se ajusta la forma de la interfaz (deja de ser verticalizada) y el ancho de la zona de mezcla, la entrada de agua salina al acuífero aumenta, pero no lo suficiente como para alcanzar los valores resultantes del modelo 3D con densidad variable.

- Las diferencias existentes entre los modelos 3D y 2D con densidad constante aumentan al aumentar la pendiente, la longitud del pie y el ancho de la zona de mezcla y las velocidades de entrada prácticamente. Con respecto a los modelos

2D y 3D con densidad variable, al aumentar la pendiente disminuyen las diferencias de la longitud del pie y el ancho de la zona de mezcla.

- Al introducir un pozo de extracción tanto en los modelos 3D como en los modelos 2D la forma de la interfaz, el descenso, las concentraciones alcanzadas en el pozo y los balances de masas son muy similares en todos los casos, excepto en el caso del modelo 3D con densidad constante, en el cual la entrada de agua salina es del orden de 8 veces mayor que en el resto de los casos.

- Cuando existe un gradiente importante hacia el continente, el modelo más coherente con respecto al modelo 3D con densidad variable es el modelos 2D con densidad constante. La concentración alcanzada en el pozo es prácticamente la misma, y el balance de masas se ajusta bien, sin embargo el ancho de la zona de mezcla es menor en el caso del 2D. Sin embargo estos resultados han de tomarse con cautela debido a que en ninguno de los casos se ha alcanzado el estado estacionario.

6.- MODELACIÓN DE LA HIDROGEOLOGÍA

Para el estudio de la hidrogeología se han realizado los siguientes trabajos:

Recopilación de datos piezométricos. Procedentes de los archivos del ACA y de otros (CUADLL, datos de la UPC, etc.). Todos estos datos han sido objeto de una revisión crítica y depuración. En la Figura 6.1 se muestran las ubicaciones de los pozos de medida considerados. Para el periodo 1-Ene-1966 a 31-Dic-2004 se dispone de unos 30.000 datos de nivel piezométrico repartidos en 325 pozos o piezómetros.

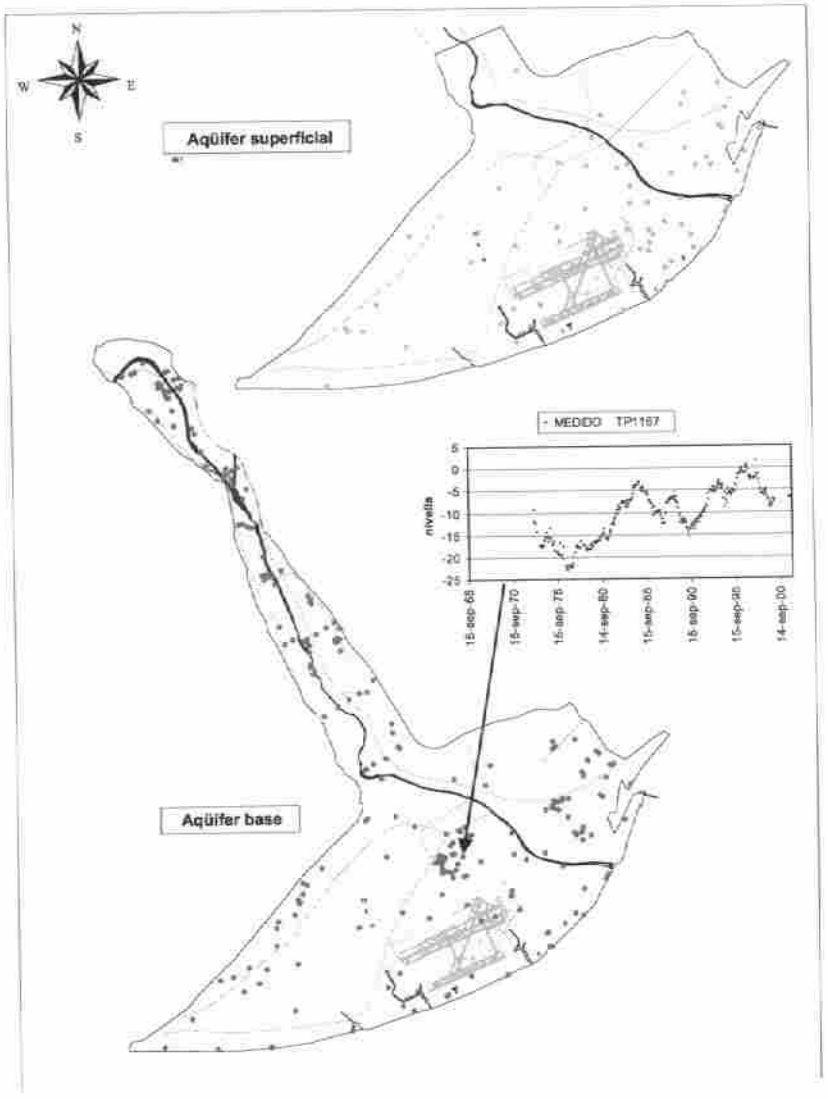

Figura 6.1.- *Ubicación de los puntos donde se dispone de medidas de nivel. Se muestra también un hidrograma típico de la evolución de niveles en el acuífero Principal durante el periodo de estudio. Como se puede observar, los niveles fueron muy bajos durante los años 70 y se han ido recuperando con periodos de sobreexplotación.*

Estudio de las explotaciones históricas. Los datos de bombeos proceden del ACA y de la CUADLL. Los datos son muy desiguales y se han tenido que completar con información complementaria de índole cualitativa (datos de cierre de empresas o similares) aportados por la CUADLL. En la Figura 6.2 se muestra la evolución de los caudales explotados integrados por zonas durante el periodo de estudio considerado.

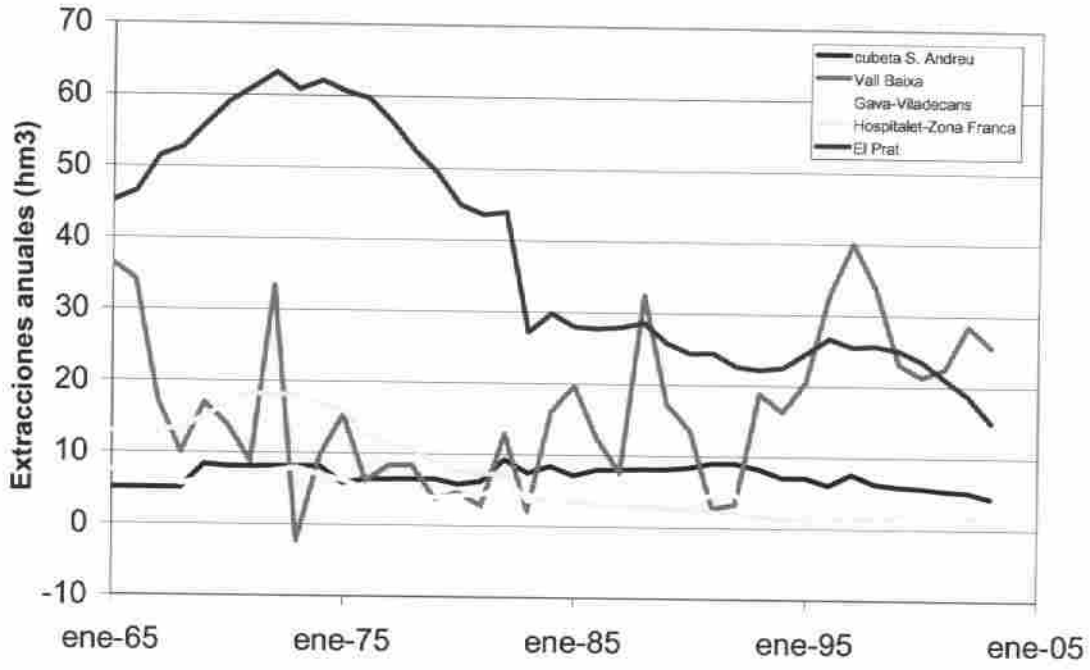

Figura 6.2.- *Evolución de los caudales bombeados en lo acuíferos del Baix Llobregat*

Parámetros químicos. Se han recopilado datos de parámetros de calidad: iones básicos y minoritarios y contaminantes específicos. Se ha hecho especial hincapié en la recopilación y estudio de los datos de cloruros que reflejan tanto la salinización por intrusión marina como las variaciones de calidad en el río como consecuencia de las operaciones de las minas de sal y de la puesta en marcha del colector de salmueras. De todos estos datos se han seleccionado las concentraciones en Cloruros disponibles y fiables en 477 pozos o piezómetros con un total de 2711 medidas. En la Figura 6.3 se muestran los datos de cloruros medios en el periodo 1996-2004.

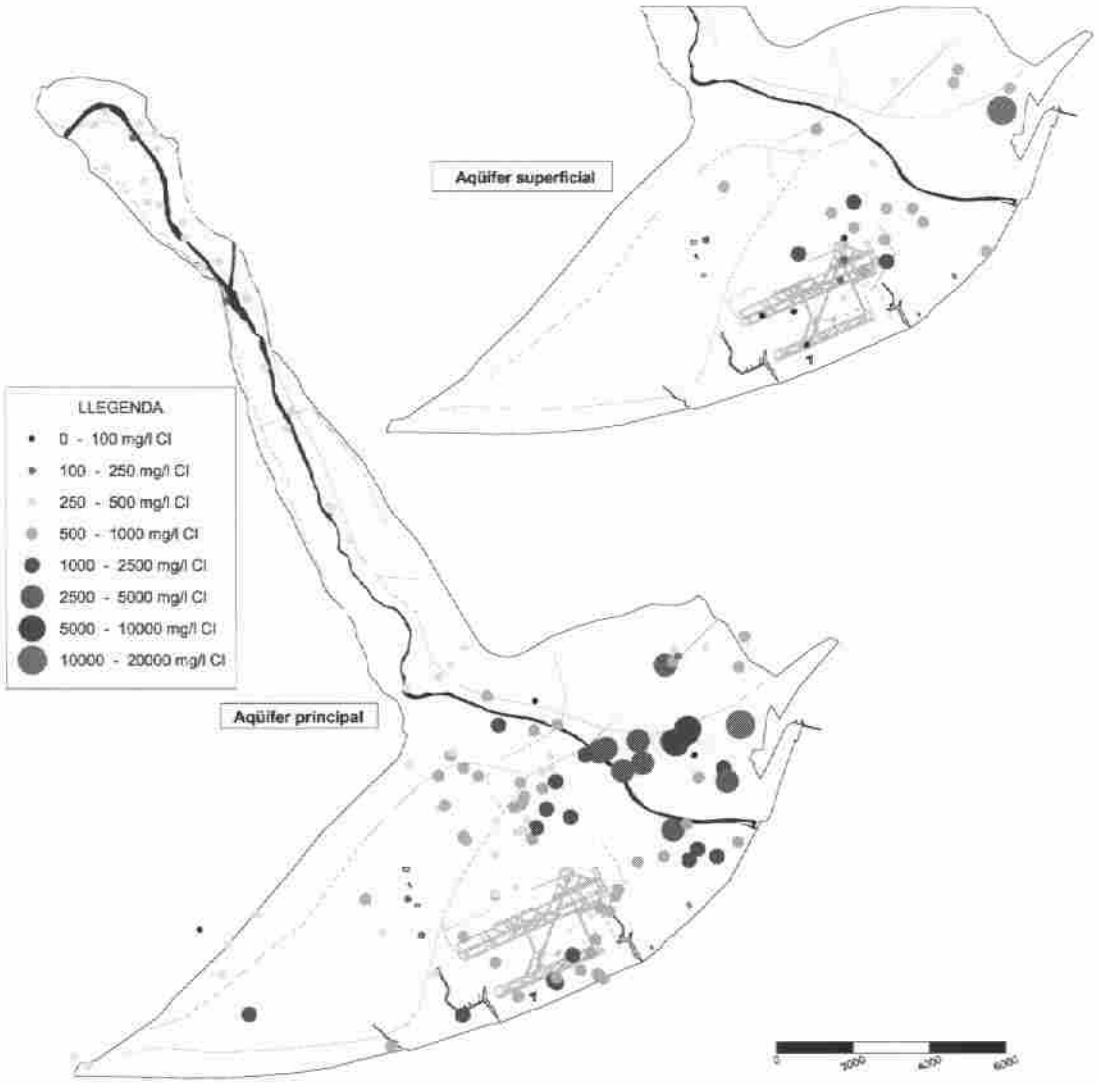

Figura 6.3.- *Datos de cloruros medios en el periodo 1996-2004 en el acuífero principal. Se puede observar la fuerte intrusión en todo el lado derecho del acuífero principal*

Evaluación de los parámetros hidráulicos. Se han recopilado datos de transmisividad y caudal específico (Figura 6.4). Con estos datos, juntamente con el modelo geológico del Capítulo 3, se ha elaborado un mapa con la distribución espacial de transmisividades. Para el coeficiente de almacenamiento se han adoptado los diversos valores para el acuífero principal (en parte confinado y en parte libre) y para el superficial (libre).

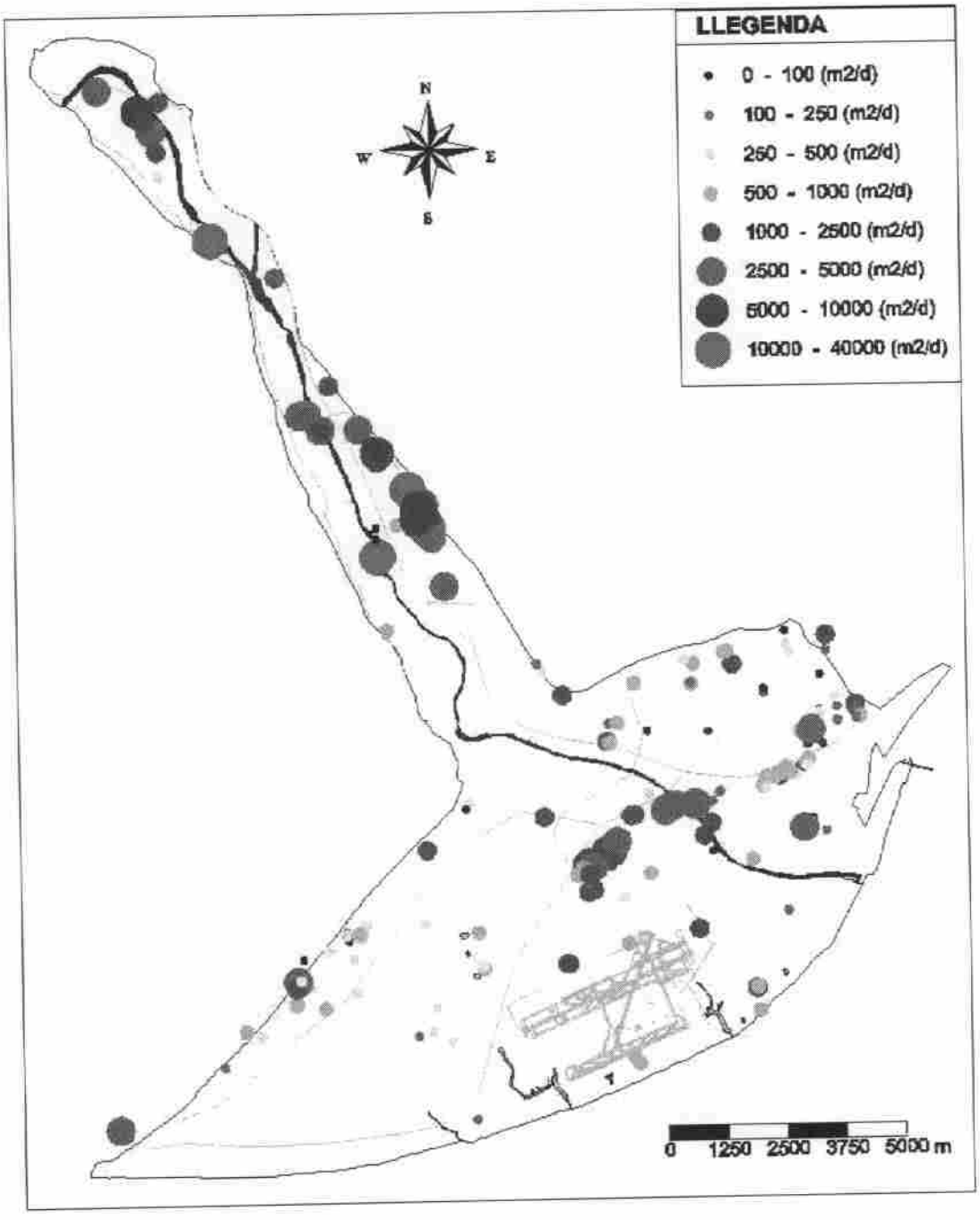

Figura 6.4.- *Datos de transmisividad deducidos a partir de los datos de caudal especifico recopilados para este estudio.*

Entradas/salidas de agua. Las entradas en el acuífero proceden de las siguientes fuentes:

Entradas laterales: Las entradas laterales (procedentes de las Sierras del Garraf y Collserola, de las rieras adyacentes y del Llano de Barcelona) se han evaluado a partir de estudios específicos en estas zonas, que han permitido evaluar las entradas medias. La distribución temporal se ha deducido por convolución con la lluvia, con un tiempo de respuesta de medio año.

Recarga. Las entradas por recarga se han evaluado mediante balance de masas en el suelo, aún considerando la lluvia, la evapotranspiración, el escorrentía y, si cabe, el riego. En las zonas urbana se ha extrapolado la recarga deducida para Barcelona. En resumen, entonces, la recarga se ha evaluado en función del uso del suelo (Figura 6.5).

Interacción con los ríos. La interacción con los ríos, singularmente el Llobregat, pero también La Riera de Rubí ha sido objeto de un tratamiento muy cuidado. En la parte alta (aguas arriba de Cornellá) el río está descolgado del acuífero y se ha supuesto que la entrada tiene dos componentes: una más o menos constante y una otra proporcional al caudal en el río en avenidas. En la parte baja (Delta), se ha supuesto que se puede aplicar una condición "mixta", es decir, que se produce una cierta conexión hidráulica (el río recarga o descarga en función de la diferencia de nivel en relación con el acuífero). También se ha supuesto esta misma condición en otras entradas en los acuíferos (canales, drenajes, etc.).

Mar. En el mar también se ha supuesto una condición mixta con un nivel igual al del agua dulce equivalente. Esto implica que cuando el nivel del acuífero es más bajo que el del mar, entra agua de mar y, cuando es más alto, se sale. El que a priori no se conoce son los caudales de entrada o salida (variante espacial y temporalmente).

Con todos estos datos se ha confirmado en líneas generales el modelo conceptual de funcionamiento de los acuíferos, que se ha acabado de perfilar con el modelo numérico. Hace falta decir, pero, que se ha concluido que la interacción con el mar es mucho más compleja de lo que se había previsto. En muchos sitios, el agua salada entra por la parte de arriba. Esto sugiere que la entrada se produce a través de la capa de limos (en contra de la hipótesis habitual) o bien que los niveles pleistocenos (acuíferos profundos por debajo del superficial) aportan agua dulce. Se ha adoptado el criterio de integrarlos en el acuífero principal, dado que no se dispone de suficientes datos para caracterizarlos.

Figura 6.5.- *Mapa de usos del suelo en los acuíferos del Baix Llobregat en el año 2001 (CREAF, 2001)*

6.4.- MODELO NUMÉRICO. FUNCIONAMIENTO DE LOS ACUÍFEROS.

A partir del modelo conceptual, descrito anteriormente, se ha realizado el modelo numérico de los acuíferos. Los objetivos de la modelación son diversos. En primer lugar, integrar todos los datos disponibles sobre el sistema, segundo, dar coherencia al modelo conceptual, y en tercer lugar, convertirse en una posible herramienta para la gestión de los acuíferos considerados. (Vàzquez-Suñé et al, 2005a; Abarca et al., 2005b).

La estructura del modelo se ha considerado bicapa (la capa superior representa el acuífero Superficial y la capa inferior el Principal (todo integrando, a nivel de parámetros, los inferiores). Se ha representado mediante elementos finitos (Figura 6.6). Sobre esta red se ha superpuesto todos los datos disponibles, esto quiere decir, límites y condiciones de contorno del dominio, parámetros hidráulicos de los acuíferos como transmisividades, coeficiente de almacenamiento, etc., los datos de recarga y de extracciones en los acuíferos y los datos de niveles y concentraciones necesarias para la calibración. El periodo de modelación cubre desde el año 1965 al 2001, los dos incluidos.

En la calibración de este modelo se ha utilizado el problema inverso. Es decir, se introducen todos los datos que se han ido recopilando y el programa devuelve los parámetros hidráulicos que, siendo coherentes con la información previa disponible, conducen al mejor ajuste con los niveles y concentraciones medidos.

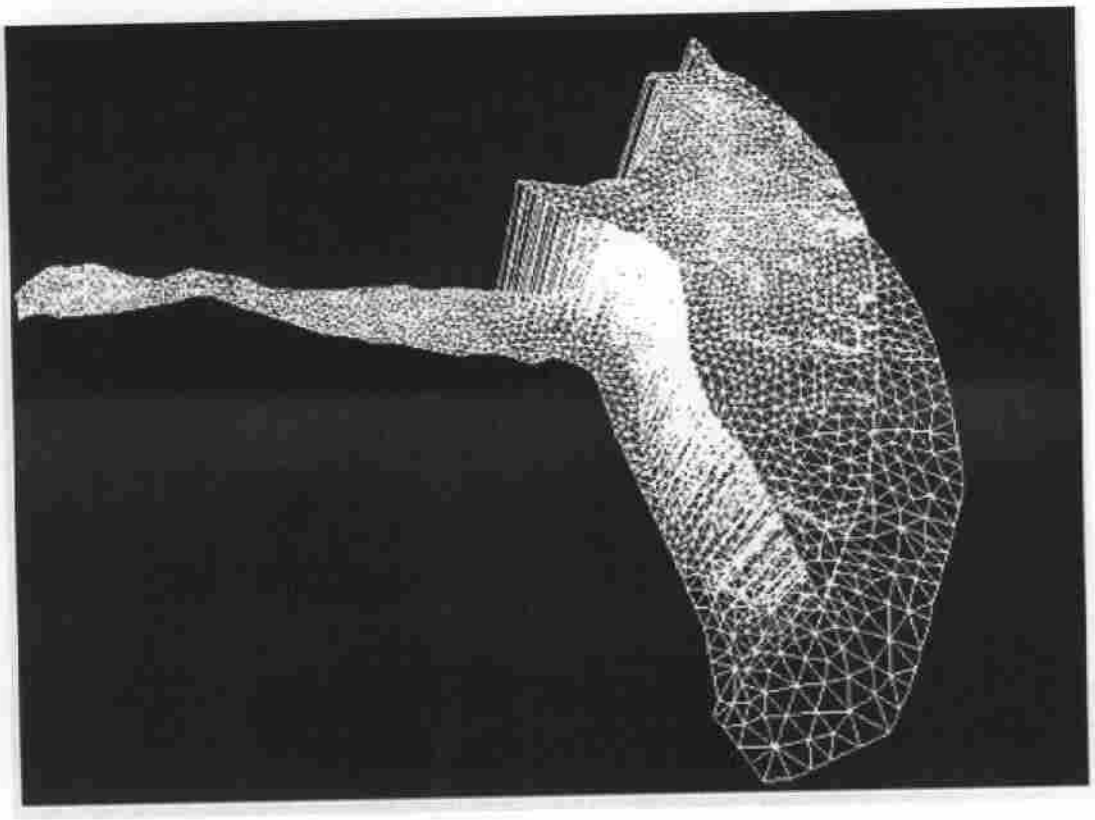

Figura 6.6.- *Red de elementos finitos de las dos capas del modelo. Donde las capas se superponen, se disponen elementos unidimensionales representando la capa de limos*

Los resultados y calidad del modelo se pueden analizar de diversas maneras. Primero, para un buen ajuste entre medidas (niveles y concentraciones) con las que calcula el modelo, segundo, por la coherencia entre los parámetros hidráulicos que definen el modelo conceptual y los parámetros que calibra el modelo, y tercero por la coherencia entre el resultado del balance de masas y los cálculos previos según el modelo conceptual. Además se ha contado con un periodo de validación que va de los años 2002 a 2004 ambos incluidos. Los ajustes obtenidos en el periodo de validación son excelentes, lo que da una idea de la robustez del modelo.

Sobre el ajuste, en las Figures 6.7 y 6.8 se muestran los mapas de errores medio de niveles y concentraciones calculadas, junto con el ajuste obtenido en algunos pozos. En general los ajustes se consideran bastante precisos.

Sobre el conjunto de los parámetros hidráulicos calibrados, los resultados han sido bastante satisfactorios y los valores obtenidos se ajustan, en líneas generales, muy bien a la información previa correspondiente al modelo conceptual. No se ha de olvidar que se trata de un modelo de características regionales, donde se toman los valores medios característicos generales de las unidades o zonas definidas. Con todo esto, se ha de destacar que la distribución de zonas de transmisividad, o de otros parámetros, su número y densidad obedece de forma muy ajustada a los datos previos. Sin perder de

vista el objetivo de servir de marco los modelos de detalle, en las zonas de interés el valor de estos parámetros es muy satisfactorio.

Como ejemplo de esto se puede hacer referencia a las transmisividades. En la Figura 6.9 se muestra en el mapa zonas de transmisividades. Las transmisividades tienden a ser más altas en las zonas donde el acuífero es más grosero y donde, presumiblemente, hay los paleocanales.

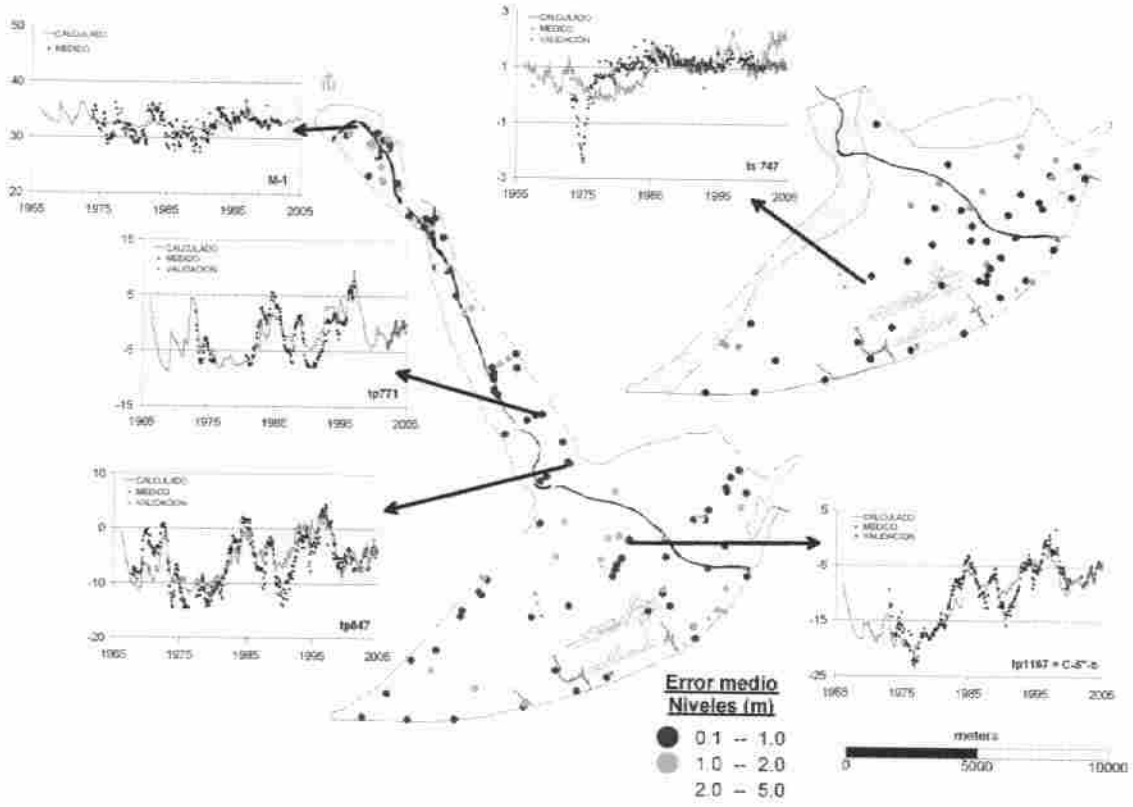

Figura 6.7.- *Mapa del error medio entre los niveles medidos y calculados junto con los hidrogramas calculados y medidos en algunos pozos.*

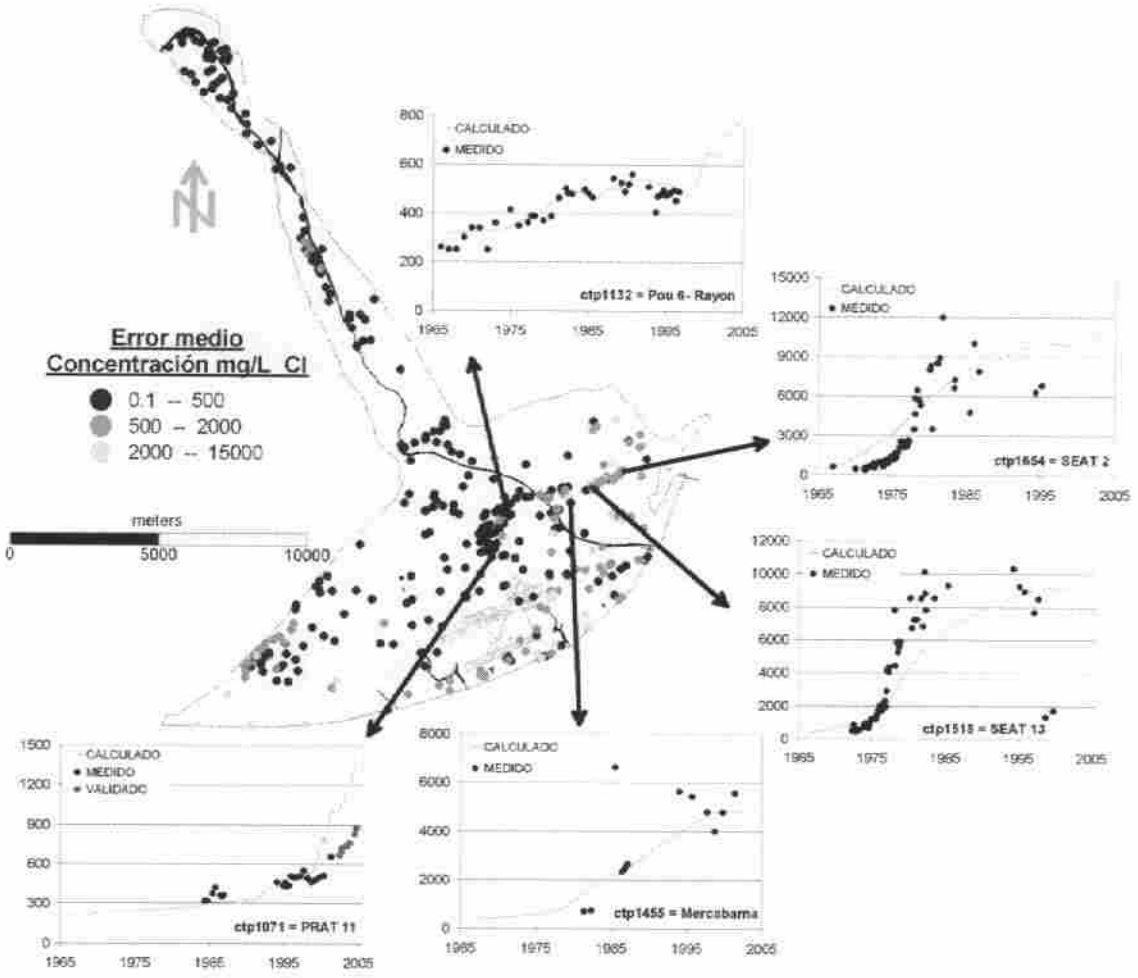

Figura 6.8.- *Mapa del error medio entre las concentraciones medida y calculadas junto con las evoluciones calculadas y medidas en algunos pozos.*

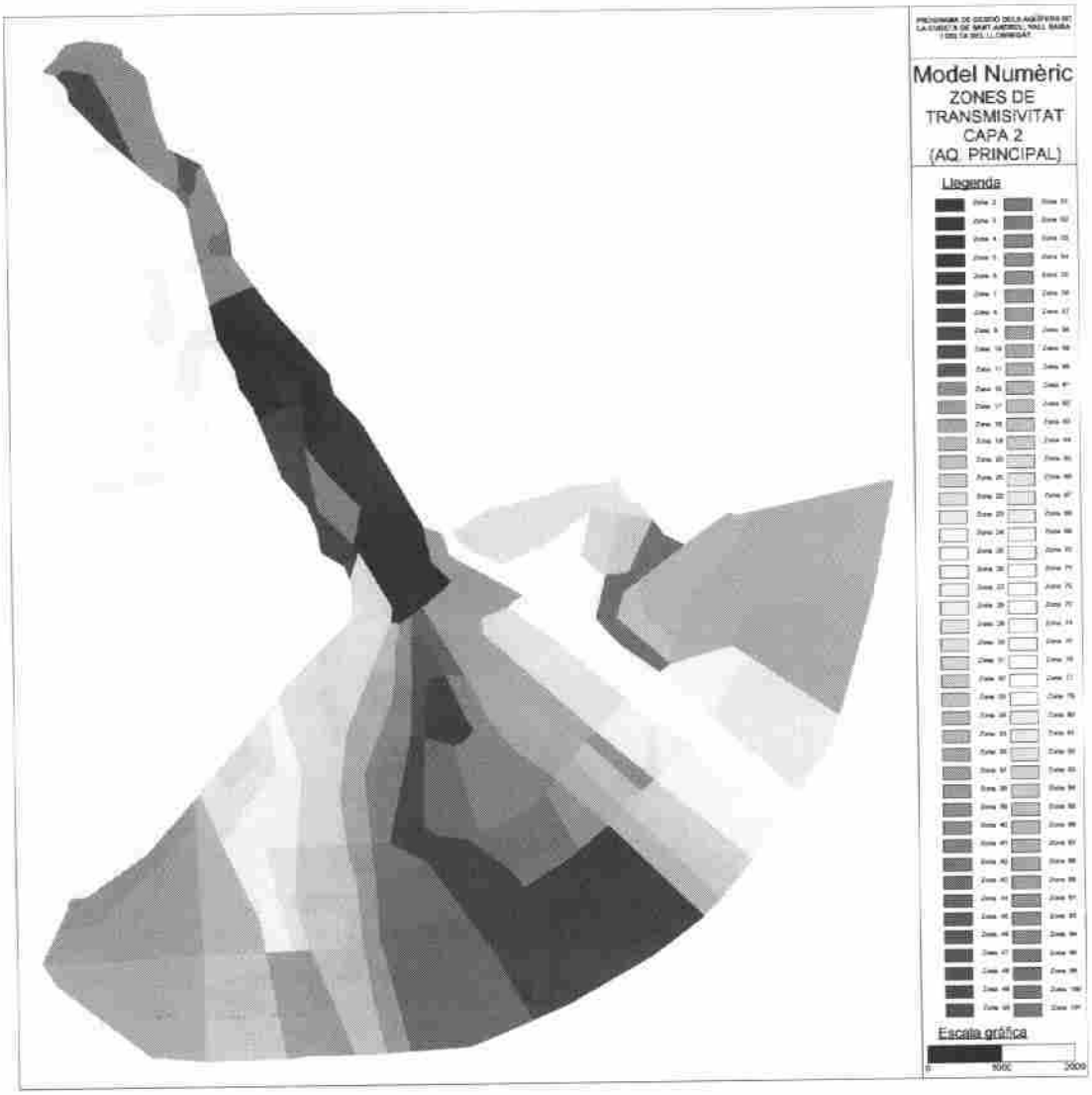

Figura 6.9.- *Mapa de zonas de transmisividad en el acuífero Principal.*

Otro de los aspectos importantes de la calibración es la coherencia en el balance de masas, es decir el balance de las entradas y salidas de agua en el conjunto del sistema y su variabilidad temporal.

En la Figura 6.10 se esquematiza el balance global obtenido por acuíferos con el caudal medio anual el periodo de estudio (1965 – 2004). De este balance se destacan las entradas por recarga, unos 15 hm^3/a sólo en el acuífero superficial, y las entradas desde el río Llobregat en épocas de avenidas, unos 14 hm^3/a entre la Cubeta de S. Andreu y la Vall Baixa. (Vàzquez-Suñé et al, 2005b). Como salidas destacan las extracciones que se han realizado en todo el acuífero principal, unos 75 hm^3/a de media. En gran medida la variación de almacenamiento de los acuíferos está muy condicionada a estos dos términos del balance.

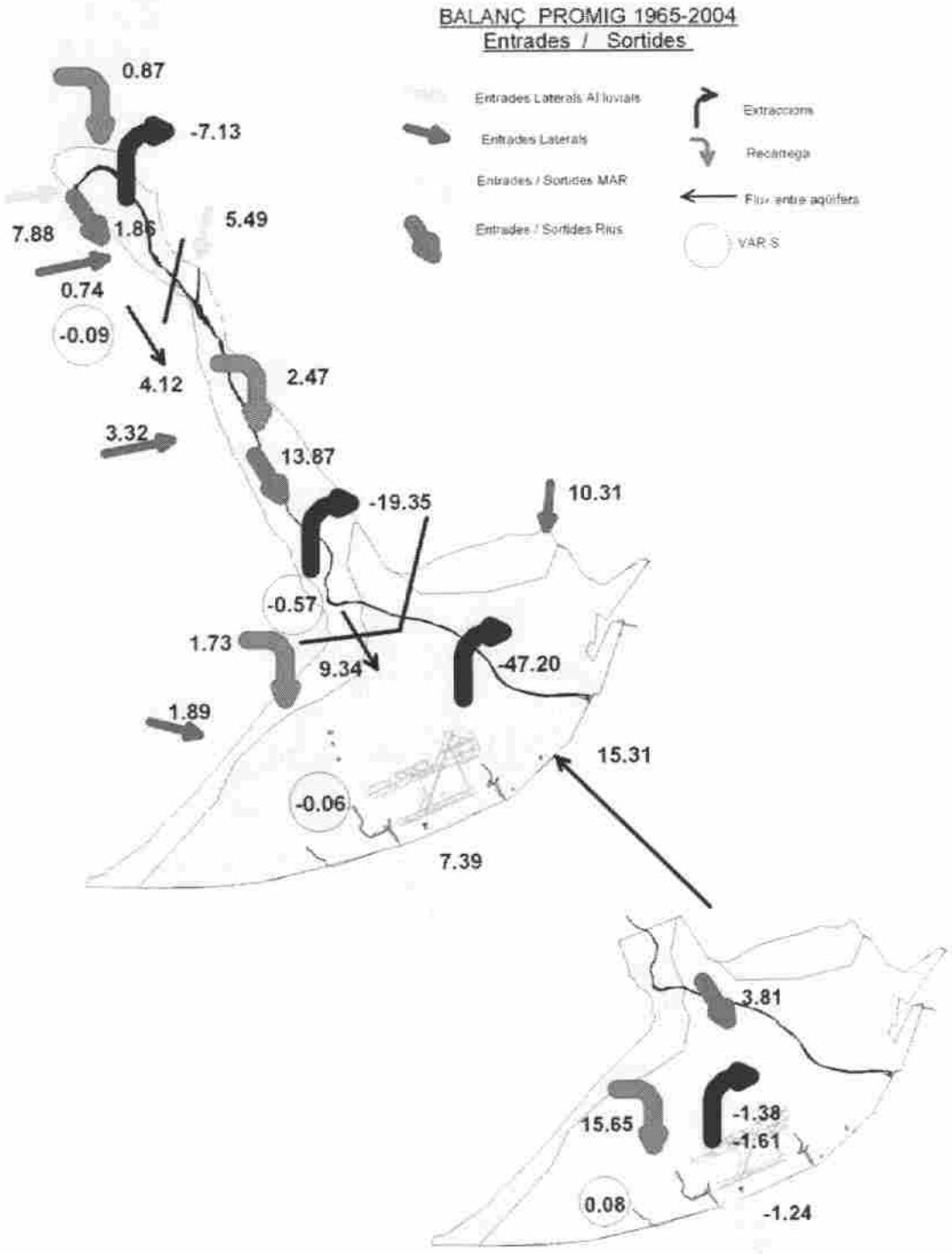

Figura 6.10.- *Esquema del balance de masas global.*

Normalmente entre la Vall Baixa y el Delta se produce un traspaso de agua en sentido Delta. Ha habido muchos periodos en los que el flujo se ha invertido debido a las extracciones de Vall Baixa i Delta. En el acuífero superficial del Delta las principales entradas de agua corresponden a la recarga superficial. Se establece un flujo desde el acuífero superficial al principal dadas sus diferencies hidráulicas. El acuífero superficial

siempre muestra una salida neta hacia el mar. En el Principal siempre hay entrada de agua de mar, más o menos intensa en función de la depresión piezométrica.

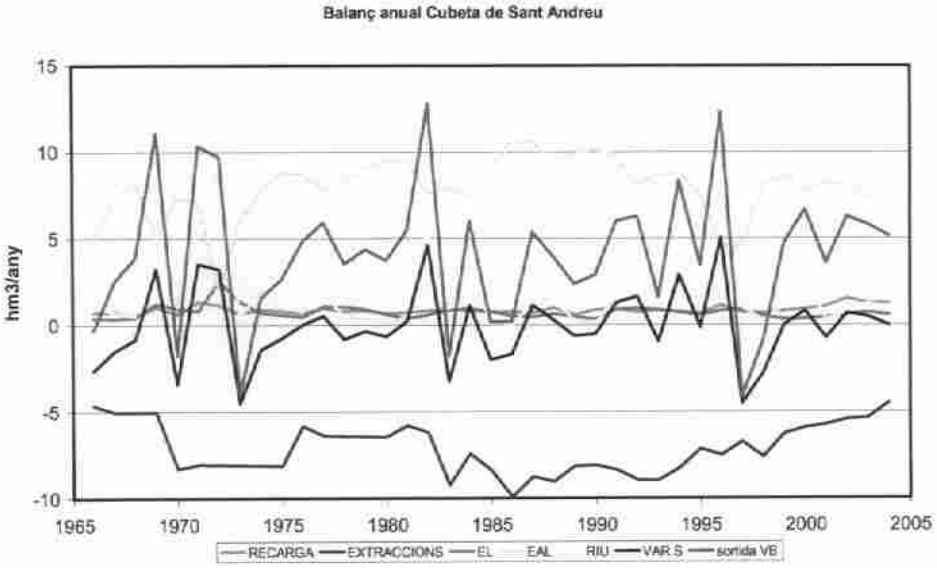

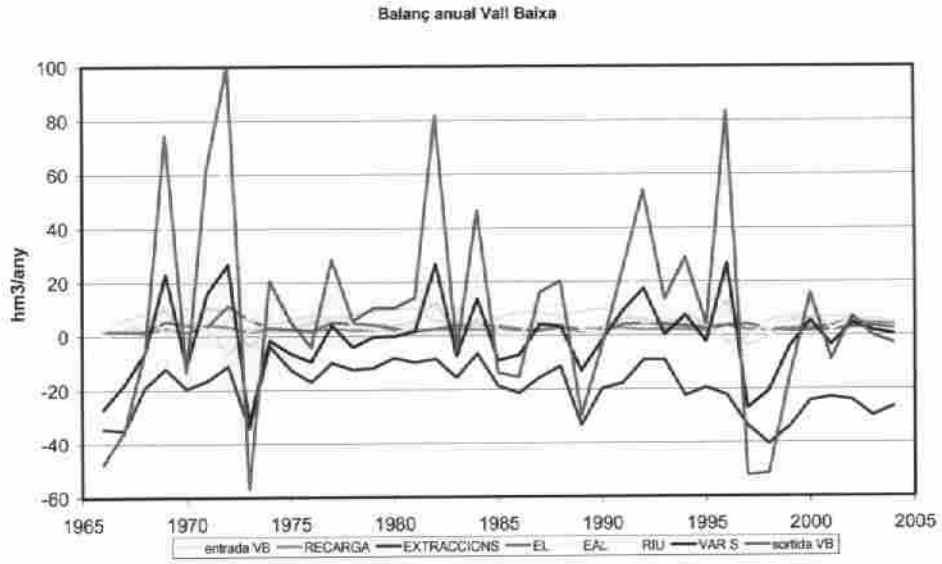

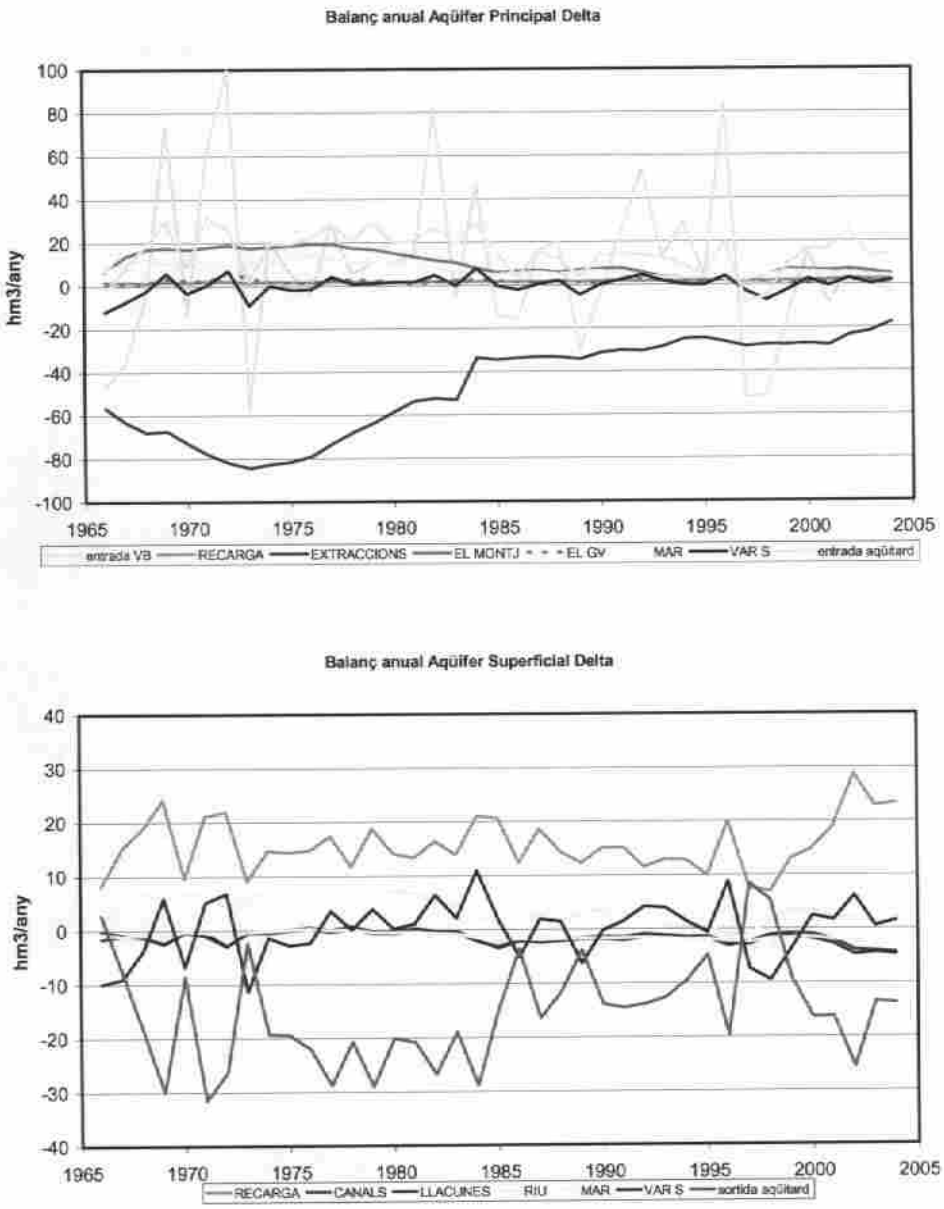

Figura 6.11 a, b, c y d.- *Evolución temporal balance de masas global en el acuífero Principal. Un valor negativo indica salidas del sistema, mientras que un valor positivo indica entradas*

Resulta de gran interés analizar la evolución temporal del sistema. En la Figura 6.11 se muestra la evolución temporal de los términos del balance en el acuífero principal donde se ve que las extracciones han sido muy importantes y han condicionado la evolución de los otros términos del balance, especialmente la variación en el almacenamiento (ΔS). Aún así la variación en el almacenamiento (ΔS) se ve en grande medida controlada por las aportaciones del río Llobregat en las épocas de avenidas.

Como consecuencia, estas avenidas representan unos de los términos más significativos de la recarga en este acuífero y viene a ser el contrapunto al efecto de las extracciones.
De hecho se puede determinar el efecto que las diversas avenidas han tenido sobre la recarga en los acuíferos. En la Figura 6.12 se han comparado los caudales de avenidas del río y el valor de la recarga que ha generado. Se compara el caudal diario máximo que se ha producido a lo largo de un mes (1 mes es la unidad temporal utilizada en la modelación) con la recarga generada. En la Figura 6.12 se ve esta relación donde, por ejemplo, los meses en que se han producido avenidas diarias del orden de 200 m^3/s la recarga producida es de unos 5 hm^3 y por avenidas diarias de unos 600 m^3/s la recarga producida es de entre 15 a 20 hm^3.
Si utilizamos como variable el caudal medio diario a lo largo de un mes (hay una buena correlación entre el caudal máximo diario y el caudal medio diario, a lo largo de un mes) también se puede establecerse cual será la recarga que comportará. Por ejemplo por un caudal medio diario de 40 m^3/s, a lo largo de un mes, se produce una recarga de 5 hm^3 y por un caudal medio diario de 120 m^3/s la recarga producida es de unos 17 hm^3.
Hará falta hacer un estudio más preciso (con tiempo de cálculo más pequeños) para acabar de establecerse de forma más precisa cual es la relación entre las avenidas y la recarga inducida que producen. Lo importante, pero, es reconocer este efecto y cuantificarlo.

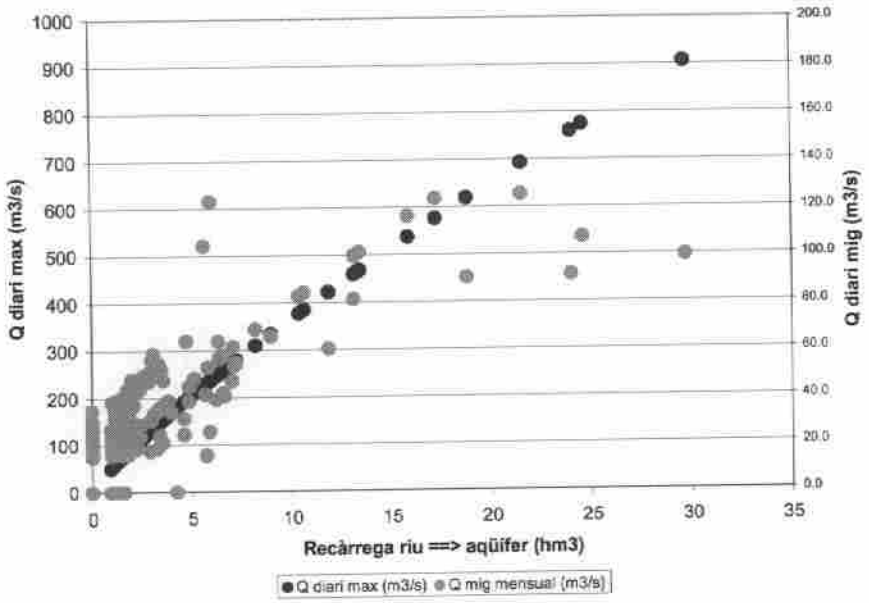

Figura 6.12.- *Relación entre el efecto de las diversas avenidas sobre la recarga inducida en los acuíferos. Como se puede ver, la recarga estimada durante el mes de la avenida correlaciona con el caudal máximo (expresado como media durante el día de avenida). Esto refleja tanto el aumento de la superficie de infiltración (debido a la inundación) como el aumento de la permeabilidad en el lecho del río.*

7.- RESUMEN Y CONCLUSIONES

De los trabajos presentados en los capítulos anteriores pueden resumirse las siguientes conclusiones:

Respecto a la modelación inversa. Se han presentado las ecuaciones para la simulación de flujo acoplado con densidad variable. Se ha mostrado que, en caso de resolverse el problema inverso, resulta ventajoso hacerlo mediante el algoritmo de Newton Raphson. Esté método se programado en un código, no presentado aquí, que está en fase de verificación.

Respecto a la geología del Delta, Se han empleado técnicas de sedimentología secuencial, que han conducido a un avance notable del conocimiento del acuífero principal, En particular, se han identificado un conjunto de paleocauces que actúan como vías preferentes de intrusión.

Respecto al estudio de la intrusión en tres dimensiones, se ha observado que, cuando el acuífero es delgado y el régimen estacionario, se produce una celda de convección subhorizontal. La importancia de esta celda depende de la pendiente lateral del acuífero. Cuando esta es baja, como en el Llobregat, apenas se produce. Cabe por tanto esperar que en condiciones naturales, sin bombeo, el acuífero profundo no tuviese salinidad.

La observación anterior, junto con la naturaleza confinada del acuífero principal del Delta del Llobregat han motivado un estudio específico para analizar bajo qué condiciones se puede estudiar la intrusión en dos dimensiones, sin tener en cuenta el efecto de la densidad. Se concluye que en general no es posible. Sin embargo, cuando la pendiente lateral es baja y, bajo condiciones de explotación, la simplificación es válida.

Por ello, los acuíferos del Delta se han simulado bajo la hipótesis de densidad constante. El modelo se calibró, con resultados muy buenos entre 1965 y 2001. Con el modelo así calibrado, se ha simulado el período 2001-04. Los resultados de la validación son aún mejores que los de la fase de calibración, lo que confirma la validez del modelo.

8.- REFERENCIAS

Abarca, E., J. Carrera, X. Sánchez-Vila (2005a), Quasi-horizontal circulation cells in seawater intrusión, *Water Resources Research* (enviado)

Abarca, E., E., Vázquez-Suñé, J. Carrera, B. Capino, D. Gámez, F. Batlle (2005b). Optimal design of measures to correct seawater intrusion. *Water Resources Research* (aceptado)

Assouline, S. y U. Shavit (2004). Effects of managemen policies, including artificial recharge, on salinization in a sloping aquifer: The Israeli Coastal Aquifer case, *Water Resources Research* 40: W04101, doi:10.1029/2003WR002290.

Bachu, S. (1995). Flow of variable density formation water in deep sloping aquifers: review of methods of representation with case studies, *Journal of Hydrology* 164: 19--38.

Bachu, S. y M. Karsten (2002). Flow of variable-density formation water in deep sloping aquifers: minimizing the error in representation and analysis when using hydraulic-head distributions, *Journal of Hydrology* 259: 49--65.

Bear, J. (1972), *Dynamics of Fluids in Porous Media*, 764 pp., Elsevier, New York.

Bear, J (1979), *Hydraulics of Groundwater*, 559 pp., McGraw-Hill, New York.

Benkabbour, B., E. A. Toto, et al. (2004). Using DC resistivity method to characterize the geometry and the salinity of the Plioquaternary consolidated coastal aquifer of the Mamora plain, Morocco, *Environ. Geol.* 45: 518--526, doi:10.1007/s00254-003-0906-y.

Cooper, H. H., Jr. (1964). A hypothesis concerning the dynamic balance of fresh water and salt water in a coastal aquifer, U.S. Geological Survey.

Diersch H.-J.G., (2002) FEFLOW finite element subsurface flow and transport simulation system - User's Manual/ Reference Manual/ White Paper. Release 5.0. WASY Ltd, Berlin.

Diersch, H.-J.G. y Kolditz, O.,(2002) Variable-density flow and transport in porous media: approaches and challenges, *Adv. Water Res.* 25, 899-944.

Dorgarten, H. W. and C. f. Tsang (1991). Modelling the density-driven flow movement of liquid wastes in deep sloping aquifers, *Groundwater* 29(5): 655--662.

Fein E. y Schneider A., (1999) d3f - Ein Programmpaket zur Modellierung von Dichteströmungen. Gesellschaft für Anlagen - und Reaktorsicherheit (GRS) mbH, Braunschweig.

Flores-Marquez, E. L., J. O. Campos-Enriquez, et al. (1998).. Saltwater intrusion of the Costa de Hermosillo aquifer, Sonora, Mexico: A numerical simulation. *Geofisica~Internacional* 37(3): 131--151.

Ghyben, B. W. (1889). Nota in verband met de voorgenomen put boring nabij Amsterdam, The Hague. K. Inst. Ing. Tydschrift, pp 8--22.

Gorelick, S. M., C. I. Voss, et al. (1984). Aquifer reclamation design - The use of contaminant transport simulation combined with nonlinear-programming, *Water Resources Research* 20(4): 415--427.

Herzberg, A. (1901). Die Wasserversorgung einiger Nordseebader, *Jour Gasbeleuchtung und Wasserversorgung* 44: 815--819, 842--844.

Lahm, T. D., E. S. Bair, et al. (1998). The role of salinity-derived variable-density fluid flow in the displacement of brine from shallow, regionally extensive aquifers, *Water Resources Research* 34(6): 1469--1480.

Maldonado et al., (1986). Memoria y hoja 41-42 (Tortosa-Tarragona) del Mapa geológico de la Plataforma Continental española y zonas adyacentes, Madrid.

Maldonado et al., (1989). Memoria y hoja 35-42I (Barcelona) del Mapa geológico de la Plataforma Continental española y zonas adyacentes. Madrid.

Malkovsky, V.I., Pek, A.A. y Tsang, C.F. (2002). Dynamic stabilization of heat-generating liquid waste plume in a sloping aquifer, *Journal of Hydrology*, 258, 69-82

Marqués, M.A. (1984). Les formacions quaternàries del delta del Llobregat. Institut d'Estudis Catalans, Barcelona. Tesis doctoral.

Rangel-Medina, M., R. Monreal-Saavedra, et al. (2003). Caracterizacion geoqu}mica e isotopica del agua subterranea y determinacion de la migracion de la intrusion marina en el acu}fero de la Costa de Hermosillo, Sonora, Mexico. Tecnología de la intrusión de agua de mar en acuíferos costeros: Países mediterráneos, Madrid, IGME.

Simó, J.A., D. Gàmez, J.M. Salvany, E. Vàzquez-Suñé, J. Carrera, A. Barnolas y F.J. Alcalà, 2005. Arquitectura de facies de los deltas cuaternarios del río Llobregat, Barcelona, España. *Geogaceta*, 38 pp 171-174

Vàzquez-Suñé, E., E. Abarca, J. Carrera, B. Capino, D. Gámez, M. Pool, J.A., Simó, F. Batlle, J.M., Niñerola, J. Ibáñez (2005a). Groundwater modelling as a tool for the European water framework directive (WFD) application: The Llobregat case. *Physics and Chemistry of the Earth* (aceptado)

Vàzquez-Suñé, E., B. Capino, E. Abarca, J. Carrera (2005b). Estimation of floods recharge in disconnected stream-aquifer systems. Application to the Baix Llobregat aquifers, Barcelona, Spain. *Groundwater* (enviado).

Voss, C. I. y A. M. Provost (2002). SUTRA, A model for saturated-unsaturated variable-density ground-water flow with solute or energy transport, U.S. Geological Survey.

ANEJOS

Avances en la simulación de la intrusión marina. Efectos y necesidad de la tridimensionalidad. Aplicación al Delta del Llobregat.

Informe final del Convenio IGME-CUADLL-UPC

PUBLICACIONES

- Simó, J.A., D. Gámez, J.M. Salvany, E. Vàzquez-Suñé, J. Carrera, A. Barnolas, F.J. Alcalá (2005) "Arquitectura de facies de los deltas cuaternarios del río Llobregat, Barcelona, España", *Geogaceta* 38, 2005

- Abarca, E., J. Carrera, X. Sánchez-Vila (2005a). "Quasi-horizontal circulation cells in seawater intrusión", *Water Resources Research* (enviado)

- Vàzquez-Suñé, E., E. Abarca, J. Carrera, B. Capino, D. Gámez, M. Pool, J.A., Simó, F. Batlle, J.M., Niñerola, J. Ibáñez (2005a). Groundwater modelling as a tool for the European water framework directive (WFD) application: The Llobregat case. *Physics and Chemistry of the Earth* (aceptado)

- Abarca, E., E. Vàzquez-Suñé, J. Carrera, B. Capino, D. Gámez, F. Batlle (2005b). "Optimal design of measures to correct seawater intrusion", *Water Resources Research* (aceptado)

- Vàzquez-Suñé, E., B. Capino, E. Abarca, J. Carrera (2005b). Estimation of floods recharge in disconnected stream-aquifer systems. Application to the Baix Llobregat aquifers, Barcelona, Spain, *Groundwater* (enviado).

Arquitectura de facies de los deltas cuaternarios del río Llobregat, Barcelona, España

Facies Architecture of the Llobregat River Quaternary Deltas, Barcelona, Spain

J.A. Simó [1], D. Gàmez [2], J.M. Salvany [2], E. Vàzquez-Suñé [2], J. Carrera [2], A. Barnolas [3] y F.J. Alcalà [4]

[1] ICREA, Geomodels-Departament d'Enginyeria del Terreny, Cartogràfica i Geofísica, UPC, 08034, Barcelona y Department of Geology and Geophysics, University of Wisconsin, Madison, 53706. simo@geology.wisc.edu
[2] Geomodels-Departament d'Enginyeria del Terreny, Cartogràfica i Geofísica, UPC, 08034, Barcelona
[3] Dirección de Geología y Geofísica, IGME, Ríos Rosas 23, 28003- Madrid
[4] Agencia Catalana de l'Aigua, Departament de Medi Ambient i Habitatge, 08008 Barcelona

ABSTRACT

The Llobregat River has accumulated multiple deltas through Quaternary eustatic cycles. The rapid rises and step-wise, relatively slower falls in sea level have produced a bias towards preserving forced regressive system tracks and eroding the high-stand system tracks with the exception of the Holocene delta. Subsurface data indicates that the Quaternary deltas were feed by the Llobregat river and «rieras» derived from Garraf and Collserola, but the sediment was probably redistributed by long-shore currents to form a unique delta front. The Holocene Llobregat River high-stand delta progrades over older fluvial, flood-plain and shoreline deposits equivalent to the older deltas now preserved at the continental margin. A number of paleo-flow channels feeding the older Quaternary deltas illustrate the complexity for the exploitation and protection of groundwater found in these deposits.

Key words: *Pleistocene delta, Llobregat River, Facies analysis, delta evolution*

Geogaceta, 38 (2005), 171-174
ISSN: 0213683X

Introducción

El delta del río Llobregat, al sur de la ciudad de Barcelona, es un ejemplo de delta mediterráneo iniciado en la época postglacial, que prograda sobre una plataforma marina estrecha, y que está encajado entre relieves montañosos. El delta moderno es parte de un complejo de deltas sumergidos, de edad pleistocena, que hoy en día tienen sus frentes deltaicos situados a profundidades de mas de 80 m y a una distancia de la línea de costa actual de, al menos, 12 km. El delta holoceno prograda sobre las facies más someras de los deltas sumergidos.

Una revisión de 288 sondeos antiguos y de otros 74 nuevos, con testigo continuo, procedentes de la zona emergida del delta y de las obras de ampliación del puerto de Barcelona, ha permitido establecer una distribución vertical y lateral de facies del delta holoceno y los pleistocenos. La estratigrafía de la parte emergida del delta se ha comparado con la estratigrafía sísmica del delta sumergido. La correlación de cortes y la reconstrucción de mapas paleogeográficos ha permitido subdividir el registro estratigráfico en se-

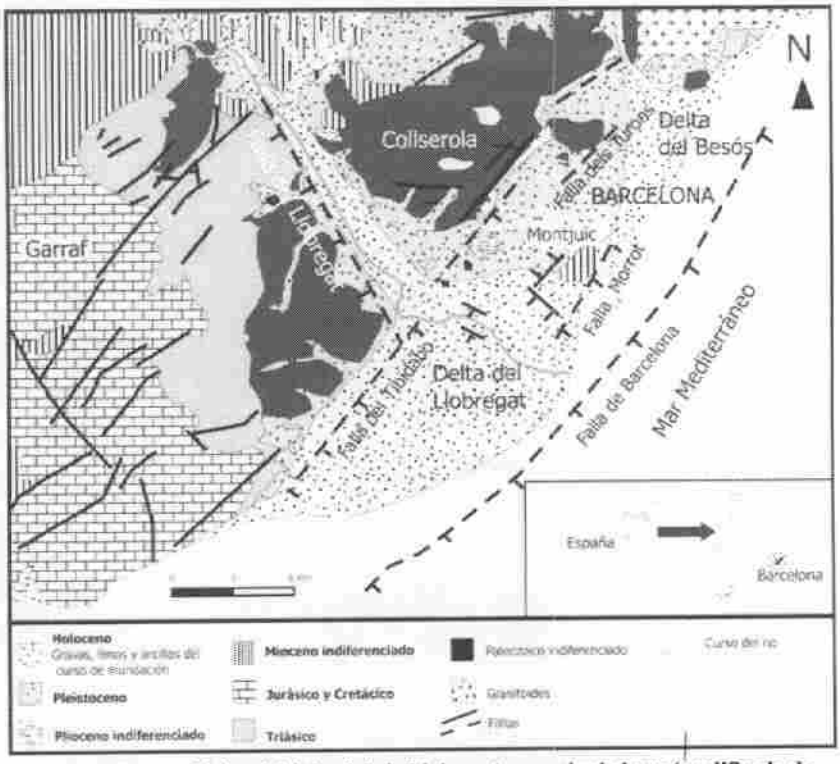

Fig. 1.- Mapa geológico del delta del río Llobregat y sus alrededores (modificado de Almera, 1891).

Fig. 1.- Geologic map of the Llobregat delta region (after Almera, 1891).

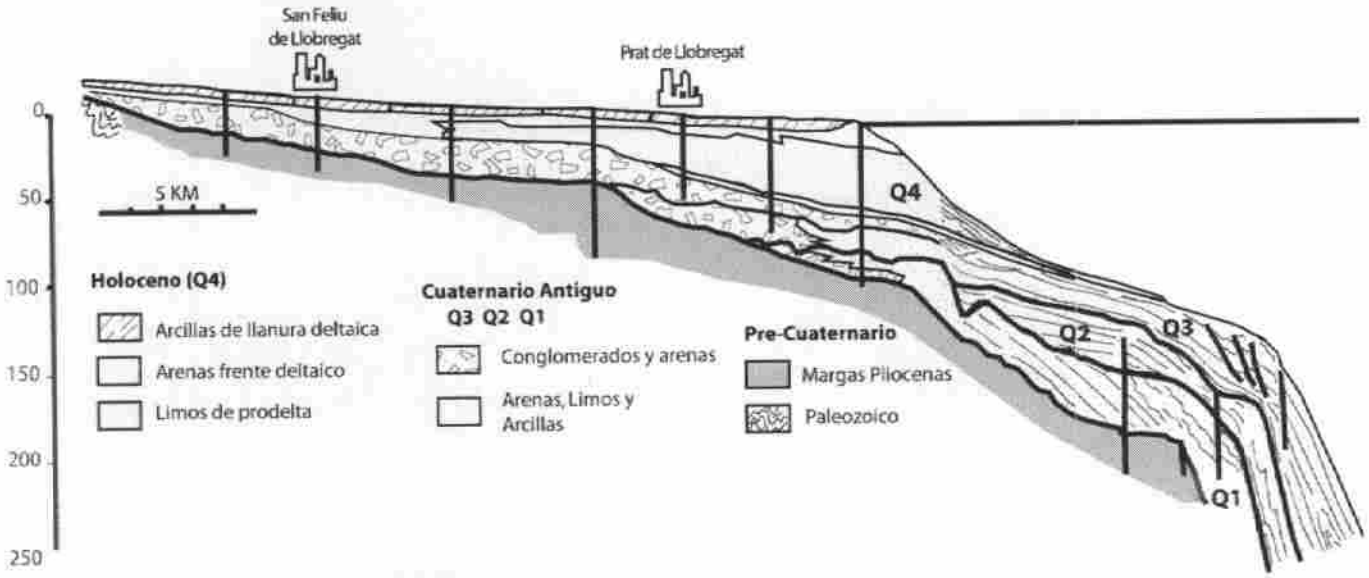

Fig. 2.- Corte geológico del delta emergido y sumergido con datos de MOP (1966) y del Maldonado et al. (1986). Los deltas del Cuaternario antiguo (Q1-Q3) corresponden en parte al Complejo Detrítico Inferior y el delta holoceno representa el Complejo Detrítico Superior (Q4).

Fig. 2.- Geologic cross section of the emerged and submerged parts of theLlobregat deltas (base on MOP, 1966; and Maldonado et al. 1986). The lower Quaternary deltas (Q1-3) correlate with the «Complejo Detrítico Inferior» and the Holocene delta (Q4) to the «Complejo Detrítico Superior».

cuencias deposicionales que reflejan los cambios eustáticos, en las direcciones de aportes sedimentarios, y tectónicos. El modelo conceptual que se presenta refleja un sistema dinámico con implicaciones a nivel hidroestratigráfico y de recursos naturales de la zona.

Geología Regional

La geología superficial del delta se conoce bien desde los trabajos de Almera (1891), Llopis (1942, 1946), y Solé-Sabarís (1957, 1963). La geología del subsuelo fue establecida por el MOP (1966), Custodio *et al.* (1976), Bayó *et al.* (1976 y 1977), Marqués (1984), Manzano (1986 y 1991), y Alcalá (2003). La geología de la plataforma marina fue cartografiada por Maldonado *et al.* (1986, 1989).

El delta del río Llobregat está limitado por numerosas fallas (Fig. 1). La falla del Llobregat condicionó la dirección del río para cruzar la Cordillera Litoral Catalana. El río, una vez cruzada la falla del Tibidabo, da lugar al Delta del Llobregat, con una amplia llanura litoral encajada en terrazas de edad pleistocena, que están limitadas en parte hacia el NE por un sistema de fallas que ponen en contacto el Holoceno y Pleistoceno con el Mioceno (Montjuic) y Plioceno. Otras fallas sin expresión geomorfológica afectan al Holoceno y Pleistoceno en profundidad así como al margen de la plataforma (Fig. 1).

El río Llobregat, cuya cabecera se sitúa en el Pirineo, tiene una longitud de 156,5 km y una cuenca de drenaje de 4948.4 km^2. Es de tipo mediterráneo con poco caudal (las aportaciones anuales entre 1912-1971 oscilan entre 1347,5 hm^3 y 270 hm^3), un marcado estiaje, fuertes crecidas y elevada irregularidad (Marqués, 1984). Numerosas rieras provenientes de Garraf y de Collserola desembocan en la llanura deltaica y están reflejadas por zonas inundadas y marismas. El delta del Llobregat está altamente modificado por procesos costeros como la deriva litoral hacia el SW, con corrientes de unos 30 cm/s (Font *et al.* 1987; Chiocci *et al.*, 1997), que redistribuyen estos sedimentos hacia el SW y traen sedimentos procedentes de la costa del norte de Barcelona. En menor medida el oleaje (de baja energía) y la marea (de pocos centímetros) contribuyen a la redistribución del sedimento. En el prodelta y talud hay numerosas fallas sinsedimentarias y cañones que redistribuyen el sedimento gravitacionalmente (Maldonado *et al.*, 1986). Probablemente, los mismos procesos fueron activos durante el Pleistoceno.

Sobreimpuestos a los procesos sedimentarios deltaicos, costeros y del margen de la plataforma continental se han de añadir la variación temporal del aporte de sedimento y los cambios eustáticos cuaternarios que afectaron a la distribución vertical y lateral de facies. El resultado de los cambios eustáticos es una amalgamación de deltas, ahora sumergidos, separados por múltiples superficies de erosión. No existe una geocronología de los deltas sumergidos y en este trabajo se presenta una primera correlación de la parte del delta emergido y sumergido.

Arquitectura del delta

El Cuaternario del delta del Llobregat está encajado en materiales que van del Plioceno al Paleozoico. Internamente existen muchas discontinuidades intracuaternarias; por ejemplo, en los márgenes del delta el Holoceno está encajado en el Pleistoceno y en los perfiles sísmicos se observan múltiples erosiones intra-pleistocenas. Por simplificar, el Cuaternario de la zona emergida se divide en el Complejo Detrítico Superior (CDS) o delta moderno, de edad holocena y el Complejo Detrítico Inferior (CDI) de edad pleistocena (Marqués, 1984). El CDI esta bien definido cuando, sobre él, existen las facies del prodelta holoceno; pero está poco definido en los márgenes del delta, cuando las facies de prodelta holoceno han sido remplazadas por facies costeras holocenas. El CDI corresponde a sedimentos fluviales, de pie de monte, de marisma y lagunares, caracterizados por litologías muy variadas de conglomerados (con o sin matriz arcillosa) a arenas y limos, así como antiguos suelos (Marqués, 1984). Hacia mar (Fig. 2), en la zona sumergida, el CDI se correlaciona con complejos deltaicos pleistocenos sumergidos que, asimismo, pueden contener subunidades separadas por truncaciones (Maldonado *et al.*, 1986).

En la plataforma marina se han identificado cuatro deltas pleistocenos (Maldonado *et al.*, 1986, 1989) pero una revisión preliminar de la sísmica del mar sugiere un sistema más complejo y posiblemente con un número mayor de deltas

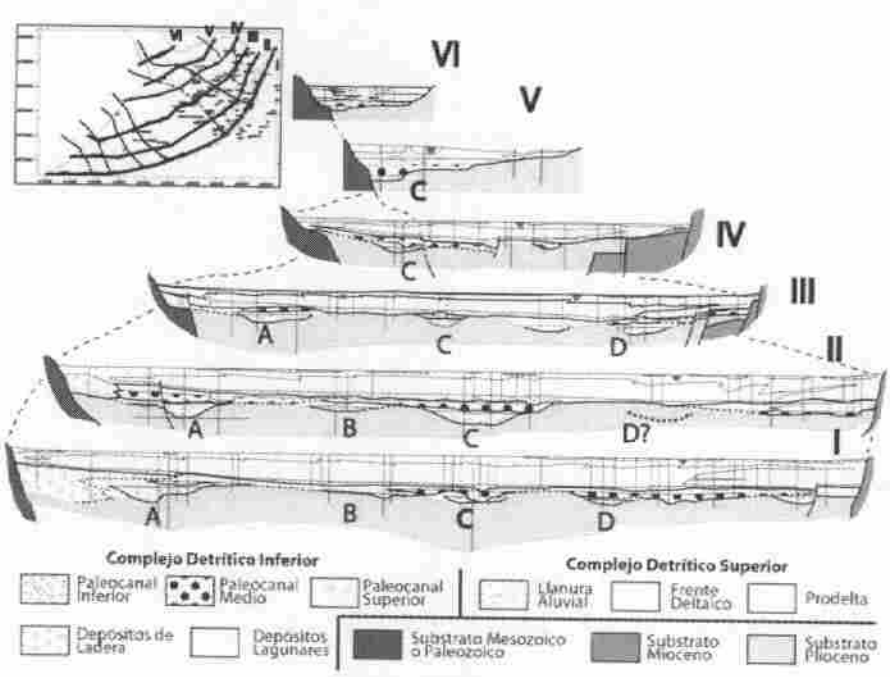

Fig. 3.- Modelo conceptual de los sistemas encajados del Complejo Detrítico Inferior en el delta emergido y distribución de facies del Complejo Detrítico Superior e Inferior. Los cortes (I-VI) son paralelos a la línea de costa (ver diagrama arriba a la izquierda). Las letras A-D se refieren a los paleocauces citados en el texto.

Fig. 3.- Conceptual model and facies distribution for the emerged part of the Llobregat delta. The cross sections (I-VI) are parallel to the shoreline (insert map). A-D corresponds to paleochannels.

sumergidos. De forma resumida se puede concluir que, durante el Pleistoceno, el río Llobregat construyó un sistema de deltas que progradaron y retrogradaron sobre una plataforma marina estrecha y un talud controlado por fallas normales y con cañones encajados. La figura 2 muestra la correlación entre el delta emergido y sumergido. Como se puede apreciar, el CDI corresponde a la parte proximal de los deltas sumergidos y refleja la complejidad interna de los sistemas encadenados de deltas formados cuando el nivel de mar bajaba.

La revisión de lo datos del delta emergido ha permitido identificar en el CDI tres unidades litoestratigráficas granodecrecientes con bases erosivas rellenas de conglomerados y gravas, que pasan hacia techo a arcillas (algunas con fauna salobre y marina) con niveles de arenas y algún canto. Las figuras 3 y 4 muestran, en corte y planta, que el CDI esta formado por una serie de conductos de sedimentos o paleovalles de granulometría gruesa interpretados como paleocanales en los que se amalgaman sucesivamente sistemas fluviales encajados durante los estadios de nivel del mar bajo del Pleistoceno. Estos materiales evolucionan verticalmente a sedimentos más finos, depositados cuando el nivel del mar subía, pero están mal preservados al ser erosionados durante las bajadas del nivel del mar.

En las figuras 3 y 4 se puede apreciar la importancia de las rieras procedentes de Garraf y de Collserola (Fig. 1). Los paleocanales de gravas A, B y D parecen estar asociados a descargas fluviales con granulometría gruesa que contribuyen a la arquitectura de facies del CDI pero no es clara su contribución con sedimentos finos a los deltas pleistocenos. La extensión lateral, especialmente hacia los márgenes del delta, de los depósitos del CDI es compleja debido a la presencia de fallas que rompen su continuidad y, posiblemente, condicionaron la posición de los paleocanales. Por ejemplo, el paleocanal C parece seguir la trayectoria de la falla del Llobregat (Figs. 1 y 4) y, en el margen de Montjuic, se observa como el bloque mioceno, limitado por fallas, condiciona la distribución y potencia del CDI (Fig. 3).

El delta holoceno corresponde a un conjunto de arcilla rojas, arenas y gravas progradantes sobre limos y arcillas gris-oscuras. En su conjunto, estas unidades están genéticamente relacionadas (llanura deltaica, frente deltaico y prodelta) y fueron depositadas cuando el nivel del mar empezó a estabilizarse y los sedimentos transportados por el Llobregat empezaron a acumularse en su desembocadura y migrar hacia mar sobre los depósitos del CDI (ver trabajo de Gàmez *et al.*, este volumen). Hacia los márgenes, el delta holoceno esta encajado en glacis de gravas de edad pleistocena y ocasionalmente descansa directamente en el Plioceno, Mioceno, o Mesozoico. La facies de prodelta cambia lateralmente, hacia el NE, a arenas gruesas de playa, que se interpretan como una flecha de arenas producida por la deriva litoral (Fig. 1). Facies de pie de monte se han observado en los laterales del delta holoceno, cerca del Macizo de Garraf. En algunos cortes de detalle se ha observado

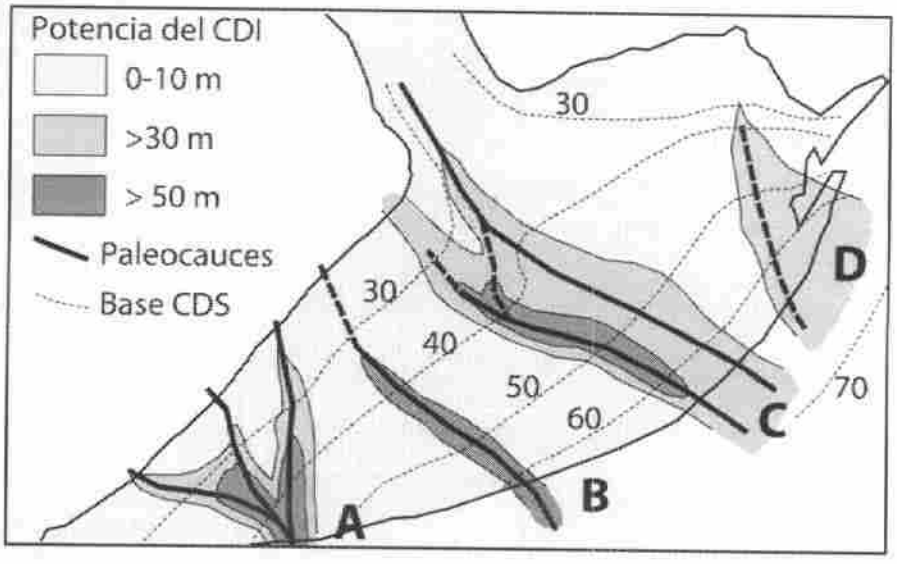

Fig. 4.- Mapa de la distribución y potencia de los sistemas encajados del Complejo Detrítico Inferior. Se observan cuatro paleocanales (A-D) donde se han acumulado gravas y arenas durante varios cambios eustáticos (Figura 3). La potencia indicada es acumulativa de todos los canales identificados en el CDI. Por referencia se da la profundidad, por debajo del nivel del mar, de la base del Complejo Detrítico Superior.

Fig. 4.- Facies distribution and thicknesses of the «Complejo Detrítico Inferior». For reference is given the base of the «Complejo Detrítico Superior» and the thickness is cumulative of all the coarse grained deposits.

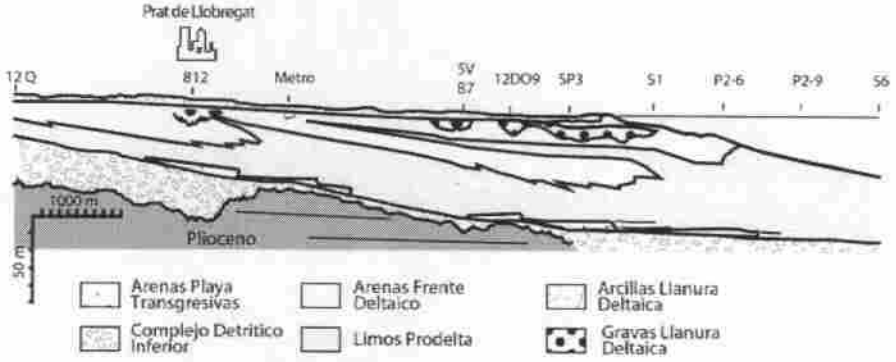

Fig.- 5 Corte geológico del delta holoceno en la zona de la depuradora mostrando la complejidad estratigráfica de las unidades progradantes.

Fig.- 5 Geologic cross section of the Holocene Delta showing sandstone wedges separated by prodelta deposits suggesting progradation pulses.

que la progradación ha sido en pulsos con periodos de rápida progradación seguida de retrogradación (Fig. 5) posiblemente debido a cambios en la tasa de sedimentación (ver Gàmez *et al.*, este volumen).

Conclusiones

El río Llobregat y sus depósitos deltaicos cuaternarios, han respondido a cambios eustáticos con subidas rápidas seguidas de bajadas escalonadas del nivel del mar. El delta holoceno (Q4, CDS) representa el mejor ejemplo de un sistema encadenado del nivel del mar alto con pulsos de sedimentación representados por cuñas de progradación. Por el contrario, los deltas pleistocenos (Q3-1) preservan de forma espectacular un sistema encadenado de deltas formados cuando el nivel de mar bajaba; a medida que el nivel de mar bajaba, el río canalizaba el sistema encadenado de alto nivel del mar y construía un delta a una cota mas baja. El resultado es una preservación selectiva de los sistemas encadenados regresivos y la erosión de los sistemas encadenados de nivel del mar alto. Se han reconocido un mínimo de cuatro secuencias deposicionales que, asimismo, se pueden subdividir en subunidades. Estas responden a la dinámica de subidas y bajadas escalonadas del nivel del mar y de variaciones del aporte de sedimentos.

Los deltas sumergidos parecen haber sido alimentados por el río Llobregat y también por las rieras procedentes del Macizo de Garraf y de la Sierra de Collserola que contribuyeron de forma significativa a la estratigrafía del CDI. No está clara la contribución de estas rieras con sedimentos finos a los deltas sumergidos. Es posible que la deriva litoral suavizase la presencia de múltiples lóbulos deltaicos. Los paleocanales de gravas, reconocidos en el CDI, posiblemente representan paleocauces excavados durante las bajadas del nivel del mar y rellenados durante las transgresiones. Numerosas fallas afectan el CDI pero están fosilizadas por los sedimentos prodeltaicos holocenos.

La complejidad de las geometrías deposicionales y la presencia de fallas hacen que la continuidad lateral de los cuerpos sedimentarios del CDI, en todas las direcciones, sea discontinua. El uso del CDI como acuífero se ha de plantear como un sistema de cuerpos potencialmente con baja conectividad y con transmisividades variables.

El delta holoceno contiene una base transgresiva, discontinua y poco potente, que representa condensación de tiempo durante una subida rápida y escalonada del nivel del mar. El techo regresivo es potente y responde a la progradación deltaica con pulsos de alta y baja sedimentación debido a la disminución relativa en la subida del nivel del mar (Gàmez *et al.*, este volumen).

Agradecimientos

Se agradece la contribución económica de la Agència Catalana de l'Aigua. Departament de Medi Ambient i Habitatge. Generalitat de Catalunya, AENA, Gestió d'Infraestrucutures S.A. Generalitat de Catalunya, y SALTRANS: Methods for assessing salt intrusion and transport in heterogeneous and fractured aquifers (UE-EVK1-2000-00692) así como el acceso a cajas de sondeos de la Depuradora de Aguas del Prat de Llobregat.

Referencias

Alcalá-García F.J., Miró, J., Rodríguez, P., Rojas-Martín I. y Martín-Martín M. (2003). *Geo-Temas*. 5; 23-26.

Almera, J. (1891). *Mapa geológico-topográfico de la provincia de Barcelona. Región I o de contornos de la capital, con la explicación somera en la misma hoja.* 1:40.000. 1ª ed., Barcelona.

Bayó, A., Batista, E. y Custodio E. (1976). *II Asamblea Nacional de Geodesia y Geofísica. Barcelona. Instituto Geográfico y Catastral. Madrid. 2103-2129.*

Bayó, A., Batista, E. y Custodio E. (1977). *General Assembly IAH.* Birmingham. Vol. XIII.1, F.1-14.

Chiocci F.L., Ercilla G. y Torres J. (1997). *Sedimentary Geology*, 112, 195-217.

Custodio, E., Cacho, F. y Peláez, M.D. (1976). *Actas de la II Asamblea Nacional de Geodesia y Geofísica.* Instituto Geográfico y Catastral. Madrid, 2069-2101.

Font, J., Julia, A.; Rovira, J.; Salat, J. y Sanchez-Pardo, J. (1987). *Acta Geologica Hispanica*, 21-22, 483-489.

Gàmez, D., J.A. Simó, E. Vàzquez-Suñé, J.M. Salvany, J. Carrera. (este volumen).

Llopis Llado, N. (1942). *Estudios Geográficos*, 321-383.

Llopis Llado, N. (1946). *Estudios Geológicos*, II, 181-236.

Maldonado, A., Alonso, B., Diaz, J.I., Ferran, M., Vazquez, A, Saonz-Amor, E. (1986). *Memoria y hoja 41-42 (Tortosa-Tarragona) del Mapa geológico de la Plataforma Continental española y zonas adyacentes.* Madrid.

Maldonado, A., Diaz, J.I., Escutia, C., Ferran, M., Giro, S., Serra, M. (1989). *Memoria y hoja 35-421 (Barcelona) del Mapa geológico de la Plataforma Continental española y zonas adyacentes.* Madrid.

Manzano, M. (1986). *Estudio sedimentológico del prodelta holoceno del Llobregat.* Tesis de Licenciatura, Univ. de Barcelona, 82 p.

Manzano, M. (1991). *CIHS. Hidrogeología, Estado Actual y Prospectiva. Centro Internacional de Métodos Numéricos en Ingeniería.* Barcelona (inédita).

Marqués, M.A. (1984). *Les formacions quaternàries del delta del Llobregat.* Institut d'Estudis Catalans, Barcelona. 208 p.

MOP (1966). *Estudio de los recursos hidráulicos totales de las cuencas de los ríos Besós y Bajo Llobregat.* CAPO-SGOP. 4 vol., Barcelona.

Solé Sabaris, L., Virgili, C. y Zamarreno I. (1957). *Livret guide d'excursions: Environs de Barcelone et Montserrat.* V Congress Inter. INQUA, 38 p. Barcelona.

Solé Sabaris, L. (1963). *Miscelania Barcilonensia*, II, 7-54.

WATER RESOURCES RESEARCH, VOL. ???, XXXX, DOI:10.1029/,

Quasi-horizontal circulation cells in seawater intrusion

Elena Abarca, Jesús Carrera and Xavier Sanchez-Vila

Dept. of Geotechnical Engineering & Geoscience, Technical University of Catalonia, Spain

Clifford Voss

U.S. Geological Survey, USA

Elena Abarca, Jesús Carrera and Xavier Sanchez-Vila, Hydrogeology Group, Dept. of Geotechnical Engineering and Geoscience, School of Civil Engineering, Technical University of Catalonia, Build. D-2, Campus Nord, 08034 Barcelona, Spain (elena.abarca@upc.es)

Clifford Voss, U.S. Geological Survey, 431 National Center, Reston, Virginia 20192 USA

Abstract.

The seawater intrusion process is characterized by the difference in fresh water and sea water density causing freshwater to float on seawater. Many confined aquifers have a large horizontal extent compared to the thickness, which itself can be considered uniform. In these cases, while buoyancy acts in the vertical direction, flow is confined between the upper and bottom boundaries and the effect of gravity is controlled by variations of aquifer elevation. Therefore, the effective gravity is controlled by the slope and shape of the aquifer boundaries. Variability in the topography of the aquifer boundaries is one case where three-dimensional analysis is necessary. In this work density dependent flow processes caused by the three-dimensionality of the aquifer geometry are studied numerically specifically considering a lateral slope of the aquifer boundaries. Subhorizontal circulation cells are formed in the salt water that enters the aquifer. The penetration of the saltwater (50% mixing line) can be quantified by a dimensionless buoyancy number that measures the lateral slope of the aquifer relative to freshwater flux. This slope controls seawater wedge's penetration more than do aquifer thickness and dispersivity. When the lateral slope is large, it must be taken into account to properly evaluate seawater penetration.

1. Introduction

Intrusion of seawater into coastal aquifers is a widespread contamination phenomenon that increasingly causes groundwater salinization problems worldwide. Seawater intrusion is especially severe in semiarid regions where high-pumping extraction rates are coupled with low freshwater recharge. What makes saltwater intrusion different and more complex than other solute transport problems is that variation of concentration causes water density to vary in space and time. Density differences cause freshwater to float over seawater. This effect was first addressed by *Ghyben* [1889] and *Herzberg* [1901] who empirically found that the depth to saltwater correlates with freshwater head. Assuming equilibrium between the two fluids and that saltwater remains static, the depth of the freshwater/saltwater interface, z, is $\alpha_s z = h$; where h is the freshwater head, $\alpha_s = (\rho_s - \rho_f)/\rho_f$ where ρ_s and ρ_f are the seawater and freshwater densities, respectively. This is called the Ghyben-Herzberg approximation for seawater intrusion. Since α_s is approximately equal to 1/40, a frequent rule-of-thumb is to assume that the depth to seawater below sea level is 40 times the freshwater head above sea level.

A second effect associated with concentration differences is the mixing between the two fluids. Mixing is caused by diffusion/dispersion processes and results in some of the salt to be driven seawards by freshwater. Replenishment of this salt requires an inland flow of seawater. The result is a vertical convection cell formed by seawater that flows landwards at depth and disperses into the freshwater flowing zone, where salt is flushed out by the discharging freshwater flow (Figure 1). The equilibrium assumption of Ghyben-Herzberg

is not valid because seawater flux causes an energy (head) loss. Therefore, the depth of the seawater wedge is underestimated. The above discussion indicates that seawater movement in coastal aquifers is caused by the combination of density driven flow and hydrodynamic dispersion. This effect was first discussed by *Cooper* [1964]. When taking into account density effects, the groundwater flow and solute transport are coupled by the presence of the density in the gravity (buoyancy) term in the momentum balance equation of fluid.

Three-dimensionality may be a critical factor that has often been ignored when analyzing seawater intrusion processes. Irregular patterns of salinity be caused by many factors such as variable thickness formations , heterogeneity and variations in the depth of the aquifer boundaries, among others. The latter is the object of the present work. In homogeneous aquifers where the horizontal extent is large compared to the constant thickness, aquifer topography may become critical. The impact of gravity is clearly controlled by the aquifer boundaries and the effective component of the gravity vector is its projection on the boundary plane. Therefore, the effective gravity is controlled by the boundaries slope and shape. When the lateral slope is large vertical flow can become of lesser order compared to the lateral flow.

Some geophysical studies provide evidence that seawater penetrates further inland at the deepest portion of coastal aquifers . *Flores-Márquez et al.* [1998] and more recently *Rangel-Medina et al.* [2003] compared the three-dimensional shape of the basement of the Costa de Hermosillo aquifer (Mexico) with geochemical and geophysical data. The crystalline basement presents a structure of alternating horsts and grabens and the integration of all available data indicates that preferential pathways for seawater intrusion correspond

to the lineation of basement depressions (grabens). Yet, only two-dimensional density dependent flow cross sections of the aquifer were modelled. Thus, the three dimensionality of the flux due to the irregularity of aquifer bottom was not considered. *Benkabbour et al.* [2004] determined, by the Direct Current method, the depth of the bottom of the coastal aquifer of Mamora Plain, Morocco and the lateral and vertical distribution of salinity. Seawater penetrates further inland in the area of the Sebou River, where the substratum is deeper. This fact was attributed to the higher thickness and the proportionality of the seawater penetration with the square of the aquifer thickness inferred from Ghyben-Herzberg approximation as shown in Figure ??. However, this assumption assumes that the total freshwater flow in each vertical section is constant. Buoyancy effects due to density differences were not taken into account.

The hydrogeological literature contains no qualitative analysis of the effect of aquifer morphology on seawater intrusion, although its importance has been considered in several heat transport studies. In those studies, variable density is taken into account and the effect of aquifer slope in the heat plume movement and velocity is addressed. *Bachu* [1995]; *Bachu and Karsten* [2002] studied density driven flow in sloping aquifers, applying results to two sedimentary basins: Alberta (Canada) and Los Llanos (Colombia). *Malkovsky and Pek* [2002] showed the importance of natural convection in a heat-generating liquid waste plume in a sloping aquifer, which could cause acceleration as well as slowing down of the plume depending on the system parameters. The role of aquifer's slope has also been addressed in brine movement in continental basins. a *Lahm et al.* [1998] studied the role of salinity, derived variable, density flow in the displacement of brine from a shallow, regionally extensive aquifer and argued that density dependent flow causes a decrease in

groundwater velocities and a reorientation of local flow directions of the aquifer within the mixing zone, but their model was 2D. *Assouline and Shavit* [2004] studied the effects of management policies, including artificial recharge, on salinization in a sloping aquifer in Israel. Although seawater intrusion processes were not taken into account, the importance of the thickness variations in the sloping aquifer in the salinization process was addressed.

Three-dimensional modeling of density dependent flow and solute transport is a useful tool to assess the effect of aquifer morphology in seawater intrusion. Until recently, 3D models were not practical due to high computer time requirements. As a result, most seawater modeling studies consisted of 2D cross section models or sharp interface models. However, three-dimensional density dependent flow models have been developed in the last decade, resulting in better ways to model advective and dispersive mechanisms with fluid density and viscosity effects. Nowadays, many codes are available: FEFLOW [*Diersch and Kolditz*, 1998], ROCKFLOW [*Kolditz et al.*, 1998], HST3D [*Kipp*, 1986], TVDT3D [*Ackerer et al.*, 1999], METROPOL [*Sauter et al.*, 1993], MVAEM [*Strack*, 1995], MOCDENSE3D [*Oude Essink*, 1998], SWICHA [*Huyakorn et al.*, 1987], SWIFT [*Ward*, 1991], CODESA [*Gambolati and Paniconi*, 1999], SUTRA [*Voss and Provost*, 2002], SEAWAT [*Guo and Langevin*, 2002] and d^3f [*Fein and Schneider*, 1999]. A recent 'state-of-the-art' of density-dependent flow modelling in porous media can be found in *Diersch and Kolditz* [2002]. Improvements in computer speed make increasingly feasible to build sufficiently refined grids to reduce problems of numerical dispersion, which explains the emergence of 3D benchmark problems [*Johannsen et al.*, 2002; *Oswald and Kinzelbach*, 2004] for density dependent codes. Variable density 3D models of real cases

are also becoming increasingly frequent [*Oude Essink*, 2001; *Xue et al.*, 1995; *Barrocu et al.*, 1994; *Gambolati and Paniconi*, 1999; *Bear et al.*, 2001; *Paniconi et al.*, 2001; *Gingerich and Voss*, 2002; *Milnes and Renard*, 2004]. Complex geometries are included in these real cases but no reference to the effect of the boundaries shape is made in the analysis of the results, either because it is not remarkable or because it has not been considered.

In summary, emphasis has been never been placed on analyzing the effect of aquifer topography on seawater intrusion, particularly the effect of lateral variations in aquifer depth. The objective of this paper is precisely to test the conjecture that aquifer bottom topography may significantly affect seawater intrusion patterns in coastal aquifers. First, the governing equations and some dimensionless numbers that can be used to characterize the effects upon groundwater flow patterns of aquifer bottom topography are presented. Then, a suite of numerical simulations including a sensitivity analysis is used to show the potential importance of this phenomenon in real coastal aquifers.

2. Governing equations and dimensionless numbers

Modelling seawater intrusion requires simulating the flow of variable density water and the transport of salt. These two equations are coupled through water density, which enters in the flow equation and is a function of concentration. The result is a set of two coupled non-linear equations. Nonlinearity further causes the density dependent flow to be very sensitive boundary conditions and variability in the permeability field. Nonlinearity causes fingering and rotational flow with closed streamlines when the initial configuration of the system is not stable. This calls for a proper description of the 3D problem. Equations governing these phenomena are presented in this section.

2.1. Flow equation

Flow of any fluid is governed by mass and momentum conservation. Mass conservation can be written as:

$$\frac{\partial \rho \phi}{\partial t} = -\nabla (\rho \boldsymbol{q}) + \rho^* Q_h \tag{1}$$

where ρ is the fluid density (kg/m^3), ϕ is porosity (volume of voids per unit volume of aquifer), $\boldsymbol{q}$ is fluid flux ($m^3/s/m^2$), and Q_h is the sink/source term (m^3/s of fluid per unit volume of aquifer), ρ^* is the density of the incoming water through the source terms.

Dependence of density on solute mass fraction is frequently described by a linear or an exponential law [*Kolditz et al.*, 1998]. A linear equation would read:

$$\rho(\omega) = \rho_f + \beta_\omega (\omega - \omega_f) \tag{2}$$

where ω is the solute mass fraction (kg of salt/kg of fluid), β_ω is the constant relation between the density and the salt mass fraction variation, ω_f is the freshwater salt mass fraction and ρ_f is the density of freshwater.

The flow equation can be written in terms of either pressure p (Pa) or equivalent freshwater head h_f (m). The freshwater equivalent head is defined as:

$$h_f = \frac{p}{\rho_f g} + z \tag{3}$$

Momentum conservation in flow through porous media is expressed by Darcy's law

$$\boldsymbol{q} = -\frac{\boldsymbol{k}\rho_f g}{\mu} [\nabla h_f + \alpha \nabla z] \tag{4}$$

where $\boldsymbol{k}$ is the intrinsic permeability tensor (m^2), μ is the fluid viscosity (kg/ms), $\alpha = \rho - \rho_f/\rho_f$ and ∇z, in 3D, represents a unit vector opposite to gravity. This explains

why the second term in 4 represents bouyancy. In relatively thin aquifers, where flow is confined to take place within the aquifer plane, $\boldsymbol{\nabla} z$ can be approximated by the aquifer slope. It is common to write (4) in terms of the hydraulic conductivity of freshwater $\boldsymbol{K} = \boldsymbol{k}\rho_f g/\mu$.

Finally, expanding (1) and using (4), the mass balance equation for general saturated problems is:

$$\rho S_s \frac{\partial h_f}{\partial t} + \rho\phi\beta_\omega \frac{\partial \omega}{\partial t} - \boldsymbol{\nabla}\Big(\boldsymbol{K}\Big(\boldsymbol{\nabla} h_f + \alpha \boldsymbol{\nabla} z\Big)\Big) - \rho^* Q_h = 0 \tag{5}$$

where S_s is the specific storage coefficient.

2.2. Transport equation

The mass balance of solutes is expressed in terms of solute mass fluxes, $\boldsymbol{j}$ (advective, diffusive and dispersive), as:

$$\frac{\partial (\rho\phi\omega)}{\partial t} = -\boldsymbol{\nabla}\left(\boldsymbol{j}_{adv} + \boldsymbol{j}_{diff}\right) + \rho^* Q_h \omega^* \tag{6}$$

The advective mass flux is equal to $\boldsymbol{j}_{adv} = \rho \boldsymbol{q}\omega$. The dispersive and diffusive fluxes are treated together as $\boldsymbol{j}_{diff} = -\rho \boldsymbol{D}\boldsymbol{\nabla}\omega$ where $\boldsymbol{D}$ is the hydrodynamic dispersion tensor.

2.3. Dimensionless Numbers

The motivation of this analysis comes from Darcy's law expressed in equivalent freshwater head (4). The first term is essentially directed towards the sea in unpumped aquifers. However, in aquifers with irregular bottoms, the second term may not. In fact, if the aquifer's slope is large, this term may become prevalent. For example, if $\alpha_s = 1/40$ and the aquifer slope, $\partial z/\partial y = 4\%$ (y being the coordinate parallel to the coast), then the second term becomes 0.1%, which is a sizable value in comparison with $\boldsymbol{\nabla} h_f$. In such a case,

buoyancy would cause a lateral flux, leading to the development of a lateral convection cell.

In order to analyze the effect of aquifer bottom topography, two dimensionless numbers are defined. The first one, N_b, is defined by comparing the two terms in equation (4). The first term, the freshwater head driven flow ($\boldsymbol{K}\boldsymbol{\nabla}h_f$), is approximated by the boundary freshwater influx, q_b. In the second one (buoyancy term), the gradient of altitude is approximated by the maximum slope of the aquifer bottom, m; this is applicable when the aquifer thickness is small compared to horizontal extent. Therefore, an "aquifer bottom buoyancy" dimensionless number may be defined:

$$N_b = \frac{\alpha_s / \boldsymbol{K}\boldsymbol{\nabla}z /}{/\boldsymbol{K}\boldsymbol{\nabla}h_f /} \approx \frac{\alpha_s / \boldsymbol{K}m /}{q_b} \tag{7}$$

However, for the purposes of this work it is more appropriate to consider a "lateral buoyancy" dimensionless number, N_{by}, by comparing the seawards driving force to the lateral component of buoyancy (y coordinate, parallel to coast):

$$N_{by} = \frac{\alpha \boldsymbol{K} \partial z / \partial y}{q_b} \tag{8}$$

The dimensionless number defined in (7) resembles the Driving Forces Ratio (DFR) proposed by *Bachu* [1995] and *Bear* [1972] to define free and forced convection in vertical flow.

$$DFR = \frac{\alpha}{\boldsymbol{\nabla}h_f} \tag{9}$$

The numbers defined here, N_b and N_{by}, are preferable to DFR, because the fresh water flux is usually better defined than $\boldsymbol{\nabla}h_f$. Moreover, these numbers explicitly take into account the aquifer slope, which induces an important driving force in geometrically confined aquifers. This has been recognized by *Dorgarten and Tsang* [1991] who proposed an

expression for DFR essentially identical to (7), although motivated by heat transport. Yet, N_{by} is preferred because it is the lateral slope ($\partial z/\partial y$) that causes flow to depart from the vertical plane.

3. Numerical modelling methodology

A numerical methodology is employed to evaluate the extent to which aquifer depth variation can contribute to irregularities in saltwater intrusion patterns. A 3D model of a confined aquifer of constant thickness is considered. An aquifer size of 10000 x 5000 x 50 m^3 is chosen resembling typical dimensions of coastal aquifers. In order to save computation time, the numerical analysis was carried out modelling only half of the symmetric aquifer (see Figure 2).

Several aquifer geometries of a horizontally large confined aquifer of constant thickness, as presented in Figure 3, were studied. They can be grouped into four cases: (1) "horizontal", (2) "sloping" (towards the sea), (3) "V-shaped" (with a central deeper section) and (4) a "warped" aquifer (curved with a deeper point located in the middle of the seaside boundary). All geometries are symmetric, in order to take advantage of the numerical simplification described in Figure 2.

Boundary conditions used are:

1. Constant freshwater ($\omega = 0$) inflow from inland (1.18 $hm^3/year$ across the whole boundary) at the vertical BD section in Figure 2.

2. Specified pressure along the seaside boundary ($p = \rho_s gz$) with solute concentration equal to seawater concentration for inflowing portions and resident concentration for outflowing boundaries at the vertical plane passing through AC in Figure 2.

3. The remaining boundaries (vertical planes passing through AB and CD in Figure 2 and top and bottom surfaces) are closed to flow and solute transport.

Both sea level and the horizontal plane (ABCD in Figure 2) are set at $z = 0$. Flow and transport parameters used for the simulation are specified in Table 1. The simulated cases are depicted according to the boundary planes' shape and slope and the N_{by} parameters in Table 2. The lateral slopes chosen for the test cases are 1%, 3% and 10%. Therefore, there are three simulations with $N_{by} = 0.2$, 0.6 and 2.04, respectively.

Computer simulations were performed with SUTRA [*Voss and Provost*, 2002]. The numerical technique used is the Galerkin finite element method with hexahedral elements. Implicit finite differences are used for time integration. The iterative methods chosen to solve the linear system of equations are the conjugate gradient method for the flow equation and GMRES for the transport equation. The Picard method is used to solve to the non-linear system. The mesh consists of 36 x 73 x 11 nodes and 25200 hexahedral elements. A fine discretization in the vertical direction is required to achive good resolution of the interface shape as well as to avoid numerical dispersion in the vertical direction. Horizontal discretization is finer near the seaside boundary as well as in the boundary representing the symmetry axis (AB in Figure 2) with a resolution of 25 m.

Results are analyzed for natural steady state. The simulations are the result of a transient run of 1500 years, starting from the initial concentration and pressure conditions that describe a completely fresh-water aquifer. The steady-state position of the saltwater-

freshwater interface is reached in all cases. Simulations with geometries without lateral slope need less than 100 years to reach steady-state. However, the required time increases when increasing N_{by} , needing as much as 1500 years for the simulations with largest N_{by} values.

The dispersion tensor used in the SUTRA code comes from an anisotropic-media dispersion model [*Voss and Provost*, 2002] that allows dispersion to vary depending on flow direction. This implementation is important to characterize transport in highly heterogeneous media, for instance, layered aquifers. Also large horizontal extent aquifers with reduced aquifer thickness need this kind of dispersion model to represent vertical transport (as in seawater intrusion process) because of the different scales in the horizontal and vertical directions.

4. Results

In order to compare similar values in all the simulations, the 50% isoline is selected as a representative value in the analysis of saline intrusion. A particular but most important point in this line is the "toe" position, defined as the distance (measured along the x axis direction) between the seaside boundary and the point in which the 50% isoline intersects the aquifer bottom. Results are presented as a function of the slope (m_x or m_y) and they are compared to the horizontal aquifer results which are taken as a reference.

4.1. Aquifers without lateral slope

The interface positions for the horizontal (case 1) and seawards sloping (case 2) aquifers with 1, 3 and 10% slope are shown in Figure 4a. When the slope is directed towards the sea (Figure 4a), intrusion patterns are very similar to those of horizontal aquifers. In other words, the interface geometry is not significantly affected by this slope. As the slope increases, the interface is slightly displaced seawards. The toe is somewhat displaced seawards both because of the no flow (nor transport) bottom boundary condition and because although the interface shape is the same, as the slope increases, the intersection of the interface with the aquifer bottom occurs closer to the seaside boundary.

4.2. Lateral sloping aquifers

The saltwater intrusion pattern discussed above is strongly modified in aquifers with a nonzero lateral slope (N_{by} greater than 0). This is illustrated in Figure 4b which displays interface positions at a central cross section for warped aquifers with 1, 3 and 10% lateral slopes. It is clear that increasing N_{by} value leads to a broader seawater penetration in the central section of the aquifer. It is interesting to notice that the interface for these aquifers coincides approximately with that of a horizontal 550 m thick aquifer with the same unit flux and dispersivity (dashed line in Figure 5b). This thickness (550 m) is the maximum difference in elevation between the top and the bottom boundaries of the warped aquifer with highest slope.

Enhanced seawater intrusion in the deepest portion of the warped aquifer can be properly illustrated by comparing the velocity vectors in a seawards sloping aquifer and a warped aquifer with equal seawards slope at the central section. Velocity fields and interfaces for case 2 and 4 (both with $m_x = 10\%$) in the central cross section of the aquifer are shown

in Figure 5. Vectors show the expected local flow directions in the sloping aquifer (Fig. 5a). Freshwater discharges to the sea, and a vertical convective cell is formed by saltwater entering from the seaside. However, the interface is far from the sea boundary in the warped aquifer (Fig. 5b). There is no discharge of freshwater at the shown cross-section and the velocity vectors might suggest that seawater flows inland and disappears, together with the freshwater along the interface area. This apparent unrealistic result becomes clear when the problem is analyzed in three dimensions. Figure 6 displays the velocity vector field, the isoconcentration lines and the equivalent freshwater head isolines on the aquifer bottom for the V-shaped and warped cases with N_{by} equal to 2.0. It is clear that the lateral slope causes the convection cell in the saltwater wedge to develop sideways. This explains why seawater entering the deepest portion of the aquifer penetrates so far inland. It also explains why seawater velocities are reduced near the interface in 5. Seawater is actually deflected sideways and upslope. The same happens to freshwater, which is pushed by the entering seawater and can only discharge in the shallower portions of the shore.

Both saltwater penetration and interface shape are conditioned by the three dimensional pattern of the flow field. Therefore, a different penetration between the central and the seaside cross-sections are observed in all the examples considered with N_{by} different from 0. The relationship between seawater penetration (toe position) in a central cross section and N_{by} is represented in Figure 7a for all simulated cases. Toe penetration increases significantly with the lateral slope at the aquifer central section (Figure 7a). This effect is accompanied by an opposite one in the shallowest end section (in this case the lateral boundary section, given by a vertical plane trough CD in Figure 2) as shown in Figure 7b. The interface penetration decreases in this section as the N_{by} number increases due to

the higher amount of freshwater that is diverted to the shallowest portions of the aquifer.

As a consequence of the three-dimensionality of flow the salt mass flux that comes into the aquifer through the seaside boundary is not equally distributed along the coast for aquifers with a lateral slope as shown in Figure 8. Vertically integrated flow is virtually equal to 0 for aquifers without lateral slope as expected because of the symmetry of the flow field. Two zones can be distinguished along the coast line in warped and V shaped aquifers: an inflow and an outflow dominated zones. The maximum salt outflow value depends on the extent of the horizontal convection cell formed and observed in Figure 6, and therefore, on the N_{by} number. When N_{by} equals 2.0, salt enters the aquifer through the deepest half of the seaside boundary. Salt discharge takes place upslope, with a maximum about 3000 meters away from the central and deepest part of the aquifer. These values become 500 m (salt inflow zone) and 900 m (maximum salt discharge) for N_{by} equal to 0.6.

Three dimensionality of the flow also implies that the generally used estimation of the saltwater wedge toe position via the Ghyben-Herzberg approximation is not valid when the aquifer has a lateral slope. The assumption of constant horizontal freshwater flow perpendicular to the coast is not met. Still, in Appendix A, an approximation is derived for the case of laterally sloping aquifers based on the Ghyben-Herzberg assumptions (sharp interface and immobile saltwater). Figure 9 shows the comparison between the model results (50% mixing line) and the toe position calculated with the tilted Gyben-Herzberg approximation (Appendix A). Two different interface position have been calculated. The first assuming that the interface intersects the coast line in the shallowest point, which is the standard in 2D vertical models and it is known to overestimate seawater penetration.

The second one is based on supposing that the interface intersects the coast line at the main salt discharge point (Figure 8). The second approximation fits the model results accurately, however, the main discharge point is not an easy parameter to know in advance. Toe penetration is slightly overestimated by the first approximation. Still, it can be considered as good approximation to the solution of the interface position as it is in vertical cross sections.

5. Sensitivity analysis

Other parameters may affect the behaviour of saltwater intrusion in aquifers with variable depth. In order to determine whether this effect is well characterized by the N_{by} number, the sensitivity of toe position to dispersivity coefficients, freshwater incoming flux (q_b) and aquifer thickness (b) is studied.

5.1. Dispersivity

Results of the sensitivity analysis with respect to dispersivity are shown in Figure 10. As explained in previous sections, the dispersivity tensor used can deal with three different values of the longitudinal dispersion coefficient (α_L). α_L values are the same for horizontal flow directions but ten times larger than α_L for vertical flow. To simplify, the transverse dispersivity coefficient (α_T) is the same for all flow directions. The toe penetration in a central cross section shows the expected behaviour. As dispersivity coefficients are increased, the toe penetration decreases. Toe penetration is more sensitive to transversal than to the longitudinal dispersivity. However, in both cases, sensitivity is low and does not affect the behaviour discussed above.

5.2. Freshwater boundary inflow

Freshwater inflow (q_b) is one of the parameters that appears in the N_{by} expression. Several simulations were carried out to assess the effect of this factor in the seawater intrusion behaviour in lateral sloping aquifers. The toe positions obtained for different values of the freshwater inflow are shown in Figure 11 for some of the geometries considered. The larger the freshwater inflow is, the smaller the saltwater penetration is. However the observed different behaviour for the aquifers with $N_{by} > 0$ is still observed for higher values of the freshwater boundary inflow.

5.3. Aquifer Thickness

As stated before, saltwater penetration depends on aquifer thickness provided the remaining parameters are kept constant. Moreover, the effect of the geometry of the aquifer boundaries should be smaller for increasing aquifer thickness, because of the less confinement of the buoyancy term. Therefore, aquifer thickness is one of the parameters that can have the greatest impact on seawater intrusion behaviour. In Figure 12, the results for different simulations with different values of the aquifer thickness are presented. The higher seawater penetration in the deepest aquifer cross sections for the warped and V-shaped aquifers is still present for all values of aquifer thickness.

6. Conclusions

Analysis of seawater intrusion problems is often carried out in vertical cross-sections perpendicular to the sea or areal 2D models using either simplified analytical solutions (based on Ghyben-Herzberg approximation) or sophisticated numerical codes. However, the seawater intrusion patterns in horizontally extensive aquifers are heavily dependent

on the shape of their boundaries. Intrusion patterns in aquifers with laterally varying bottom elevation are qualitatively different. The main differences stem from a lateral, essentially horizontal convection cell that develops along the ocean side of the aquifer in aquifers with valley-shaped bottoms. This is due to the slope in the impermeable aquifer bottom in the direction parallel to the coast. Lateral convection cells cause the seawater wedge to penetrate much further inland in the deepest portion of the aquifer.

These effects can be quantified by means of a lateral buoyancy dimensionless number. Lateral convection cells are completely developed with N_{by} numbers higher than approximately 0.4. Modelling such effects requires a full knowledge of the three-dimensional geometry of the bottom aquifer and can only be solved using 3D density-dependent groundwater flow and transport codes. Still, reliable approximations of saltwater penetration can be obtained using the tilted Ghyben-Herzberg approximation of Appendix A.

Appendix A: Tilted Ghyben-Herzberg Approximation

An approximate position of the saltwater wedge in coastal aquifers is usually calculated based on the Ghyben-Herzberg approximation in a cross section perpendicular to the coast. In aquifers with lateral slope this equation cannot be applied. Three-dimensionality of the flow field implies that freshwater flow is not perpendicular to the coast. However, a new approximation for thin laterally sloping aquifers can be used to obtain the tilted interface position. Two cases are considered here: (1) V-shaped aquifers and (2) Warped aquifers. The general domain is shown in Figure 13. Adopting the Dupuit-Forchheimer assumption, flow across the A-A' section, is given by Darcy's Law:

$$Q_x = TW(x)\frac{\partial h}{\partial x} \tag{A1}$$

where Q_x is the freshwater flowing through the AA' section; T the aquifer transmissivity; $W(x) = (y_L - y)$ the aquifer width in which freshwater flows; y the interface position in y direction. Ghyben-Herzberg assumptions of immobile saltwater and sharp interface (there is no mixing zone),imply:

$$h(x,y) = -\alpha z \tag{A2}$$

where $z(x,y)$ is the elevation of the interface.

Expressing W in terms of the equation of the aquifer surface, imposing that the interface must satisfy A2 and integrating in x yields the equation for the interface as shown below.

A1. V–shaped Aquifers

In aquifers described as V-shaped and shown as Case 3 in Figure 3, the geometry of the boundary planes have the following expression:

$$z - z_L = m(y - y_L) = mW \tag{A3}$$

where m is the plane's slope. Solving (A3) for W, substituting z by means of (A2) and integrating along the flow direction(x) leads to:

$$m\int_0^x Q_x dx' = T\int_{h_0}^{h}\left(\frac{h'(x)}{\alpha} + z_L\right)dh' \tag{A4}$$

$$mQ_x x = T\left[\frac{h^2 - h_0^2}{2\alpha} + (h - h_0)z_L\right] \tag{A5}$$

where h_0 is the freshwater head ($z_0\alpha$) at the point where the interface intersects the seaside boundary. Q_x is assumed to be constant (i.e. there is no areal recharge). Again using A2 for h and A3 for z yields the areal equation of the interface

$$x = \frac{Tm\alpha}{2Q}\left[(y - y_L)^2 - (y_0 - y_L)^2\right] \tag{A6}$$

where y_0 is the y value at the interface intersection with the coast line. A priori, one does no know y_0 and several approximations need to be made:

1. If the interface intersects the coast line in y_L, then

$$x = \frac{Tm\alpha}{2Q}(y - y_L)^2 \tag{A7}$$

2. If the interface intersects the coast line somewhere between $y = 0$ and y_L, A6 must be applied.

A2. Warped Aquifers

In Warped aquifers shown as Case 4 in Figure 3, the geometry of the boundary surfaces has the following expression:

$$z - z_L = -\frac{m}{L}(y_L - y)(x_L - x) \tag{A8}$$

where m is the slope in x and y direction and L the model domain length.

Following the same procedure as above, the final expression for the interface equation for warped aquifers is:

$$x = x_L \left(1 - \sqrt{\frac{LQ + T\alpha m(y_L - y_0)^2}{LQ + T\alpha m(y_L - y)^2}}\right) \tag{A9}$$

As above, two different approximations for y_0 can be adopted. First, assume that the interface intersects the coast line in y_L, in which case the interface equation simplifies to

$$x = x_L \left(1 - \sqrt{\frac{LQ}{LQ + T\alpha m(y_L - y)^2}}\right) \tag{A10}$$

Second, assume that the interface intersects the coast line somewhere between $y = 0$ and y_L, in which case A9 must be used.

Acknowledgments. This work was funded by the European Commission (SALTRANS project, contract EVK1-CT-2000-00062), the Catalonian Water Agency (ACA) and the

Spanish Geological Survey (IGME). The first author was supported by the Catalonia Government with a FI doctoral scholarship and by the Technical University of Catalonia (UPC) with a scholarship to finish the PhD thesis.

References

Ackerer, P., A. Younès, and R. Mosé (1999), Modeling variable density flow and solute transport in porous medium:.i numerical model and verification, *Transport Porous Med.*, *35*, 345–373.

Assouline, S., and U. Shavit (2004), Effects of managemen policies, including artificial recharge, on salinization in a sloping aquifer: The israeli coastal aquifer case, *Water Resour. Res.*, *40*, W04,101, doi:10.1029/2003WR002,290.

Bachu, S. (1995), Flow of variable density formation water in deep sloping aquifers: review of methods of representation with case studies, *J. of Hydrol.*, *164*, 19–38.

Bachu, S., and M. Karsten (2002), Flow of variable-density formation water in deep sloping aquifers: minimizing the error in representation and analysis when using hydraulic-head distributions, *J. of Hydrol.*, *259*, 49–65.

Barrocu, G., M. Sciabica, and C. Paniconi (1994), Three-dimensional model of salt water intrusion in the capoterra coastal aquifer system (sardinia), in *Proc. 13th SWIM*, edited by I. Torchio, p. ??, Cagliari.

Bear, J. (1972), *Dynamics of Fluids in Porous Media*, 764 pp., Elsevier, Amsterdam.

Bear, J., Q. Zhou, and J. Bensabat (2001), Three dimensional simulation of seawater intrusion in heterogeneous aquifers: application to the coastal aquifer of israel, in *Proceedings of the First International Conference on Saltwater Intrusion and Coastal Aquifers-Monitoring, Modeling, and Management.*

Benkabbour, B., E. Toto, and Y. Fakir (2004), Using dc resistivity method to characterize the geometry and the salinity of the plioquaternary consolidated coastal aquifer of the mamora plain, morocco, *Environ. Geol.*, *45*, 518–526, doi:10.1007/s00,254–003–0906–y.

Cooper, J., H.H. (1964), A hypothesis concerning the dynamic balance of fresh water and salt water in a coastal aquifer, *Water-Supply Paper 1613-C*, U.S. Geological Survey.

Diersch, H.-J. G., and O. Kolditz (1998), Coupled groundwater flow and transport: 2.thermohaline and 3d convection systems, *Adv. Water Resour.*, *21*(5), 401–425.

Diersch, H.-J. G., and O. Kolditz (2002), Variable-density flow and transport in porous media: approaches and challenges, *Adv. Water Resour.*, *25*(8–12), 899–944.

Dorgarten, H.-W., and C.-f. Tsang (1991), Modelling the density-driven flow movement of liquid wastes in deep sloping aquifers, *Ground Water*, *29*(5), 655–662.

Fein, E., and A. Schneider (1999), Ein programmpaket zur modellierung von dichteströmungen., *Tech. Rep. 139*, Gesellschaft für Anlagen - und Reaktorsicherheit (GRS) mbH, Braunschweig, Germany.

Flores-Márquez, E., J. Campos-Enríquez, R. Chávez-Segura, and J. Castro-García (1998), Saltwater intrusion of the costa de hermosillo aquifer, sonora, mexico: A numerical simulation, *Geofísica Internacional*, *37*(3), 131–151.

Gambolati, M. P., G., and C. Paniconi (1999), *Seawater Intrusion in Coastal Aquifers: Concepts, Methods, and Practices*, chap. Three-dimensional model of coupled density-dependent flow and miscible salt transport in groundwater, p. ??, Kluwer Academic, Dordrecht, Netherlands.

Ghyben, B. W. (1889), Nota in verband met de voorgenomen put boring nabij amsterdam, The Hague. K. Inst. Ing. Tydschrift, pp 8–22.

Gingerich, S., and C. Voss (2002), Three-dimensional variable-density flow simulation of a coastal aquifer in southern oahu, hawaii, usa, in *Proceedings SWIM17 Delft 2002*, edited by R. e. a. Boekelman, pp. 93–103, Delft University of Technology, Delft.

Guo, W., and C. Langevin (2002), *SEAWAT - User's guide to SEAWAT: A computer program for simulation of three-dimensional varible-density ground-water flow*, chap. A, p. 77, no. 6 in Techniques of Water Resources Investigations, USGS, Tallahassee, Florida.

Herzberg, A. (1901), Die wasserversorgung einiger nordseebäder, *Jour. Gasbeleuchtung und Wasserversorgung*, *44*, 815–819, 842–844.

Huyakorn, P., P. F. Andersen, J. Mercer, and H. White (1987), Saltwater intrusion in aquifers: Development and testing of a three-dimensional finite element model, *Water Resour. Res.*, *2*(23), 293–312.

Johannsen, K., W. Kinzelbach, S. Oswald, and G. Wittum (2002), The saltpool benchmark problem - numerical simulation of saltwater upconing in a porous medium, *Adv. Water Resour.*, *25*(3), 335–348.

Kipp, K. J. (1986), Hst3d. a computer code for simulation of heat and solute transport in three-dimensional groundwater flow systems, *Water-Resources Investigations 86–4095*, IGWMC, International Ground Water Modelling Center. USGS.

Kolditz, O., A. Habbar, R. Kaiser, Schulze-Ruhfus, M., and C. Thorenz (1998), *ROCKFLOW - Theory and Users Manual. Release 3.2*, Institut für Strömungsmechanik und Elektronisches Rechnen im Bauwesen, Universität Hannover.

Lahm, T., E. Bair, and J. VanderKwaak (1998), The role of salinity-derived variable-density fluid flow in the displacement of brine from shallow, regionally extensive aquifers,

Water Resour. Res., *34*(6), 1469–1480.

Malkovsky, V., and C. Pek, A.A.and Tsang (2002), Dynamic stabilization of heat-generating liquid waste plume in a sloping aquifer, *J. of Hydrol.*, *258*, 69–82.

Milnes, E., and P. Renard (2004), The problem of salt recycling and seawater intrusion in coastal irrigated plains: an example from the kiti aquifer (southern cyprus), *J. of Hydrol.*, *288*(3–4), 327–343.

Oswald, S., and W. Kinzelbach (2004), Three-dimensional physical benchmark experiments to test variable-density flow models, *J. of Hydrol.*, *290*(1–2), 22–42.

Oude Essink, G. (1998), Simulating density dependent groundwater flow: the adapted moc3d, in *Proc. 15th Salt Water Intrusion Meeting*, pp. 69–79, Ghent, Belgium.

Oude Essink, G. (2001), Salt water intrusion in a three-dimensional groundwater system in the netherlands: A numerical study, *Transport Porous Med.*, *43*(1), 137–158.

Paniconi, C., I. Khlaifi, G. Lecca, A. Giacomelli, and J. Tarhouni (2001), A modelling study of seawater intrusion in the korba coastal plain, tunisia, *Phys. Chem. Earth (B)*, *26*(4), 345–351.

Rangel-Medina, M., R. Monreal-Saavedra, M. Morales-Montaño, and J. Castillo-Gurrola (2003), Caracterización geoquímica e isotópica del agua subterránea y determinación de la migración de la inrusión marina en el acuífero de la costa de hermosillo, son., mexico, in *Tecnología de la intrusión de agua de mar en acuíferos costeros: Países mediterráneos*, IGME, Madrid.

Sauter, F., A. Leijnse, and A. Beusen (1993), Metropol. user's guide, *Tech. Rep. 725205.003*, National Institute of Public Health and Environmental Protection, Bilthoven, the Netherlands.

Strack, O. (1995), A dupuit-forcheimer model for three-dimensional flow with variable density, *Water Resour. Res.*, *31*(12), 3007–3017.

Voss, C. I., and A. Provost (2002), Sutra, a model for saturated-unsaturated variable-density ground-water flow with solute or energy transport, *Water-Resources Investigations 02–4231*, U.S. Geological Survey.

Ward, D. (1991), Data input for swift/386, version 2.50, *Technical report*, Geotrans, Sterling, Va.

Xue, Y., C. Xie, J. Wu, P. Lie, J. Wang, and Q. Jiang (1995), A 3-dimensional miscible transport model for seawater intrusion in china, *Water Resour. Res.*, *31*(4), 903–912.

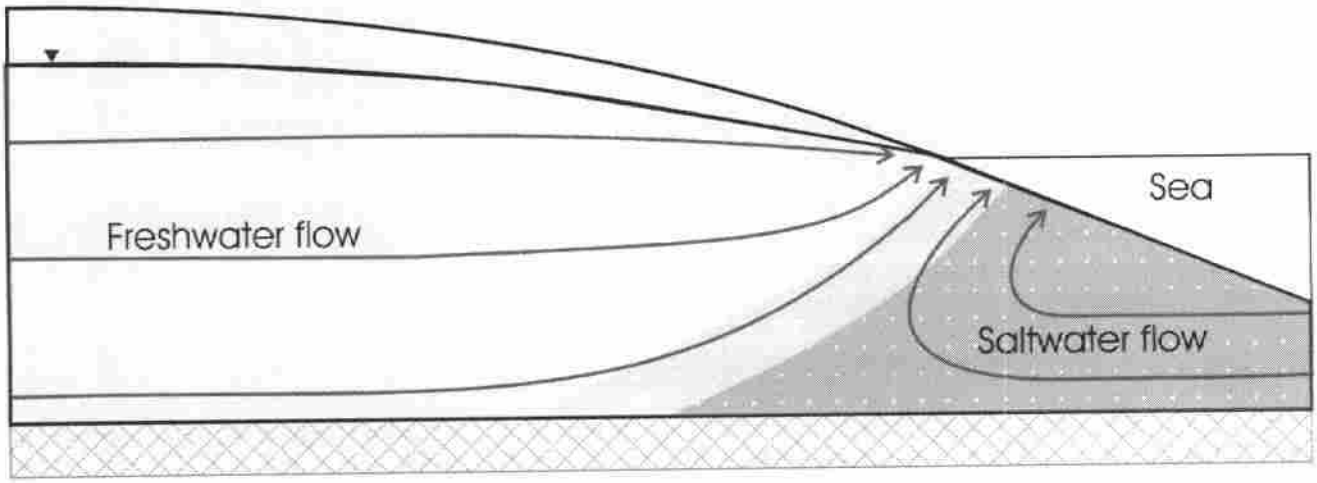

Figure 1. Classical vertical saltwater circulation cell induced by the combination of buoyancy forces and hydrodynamic dispersion processes.

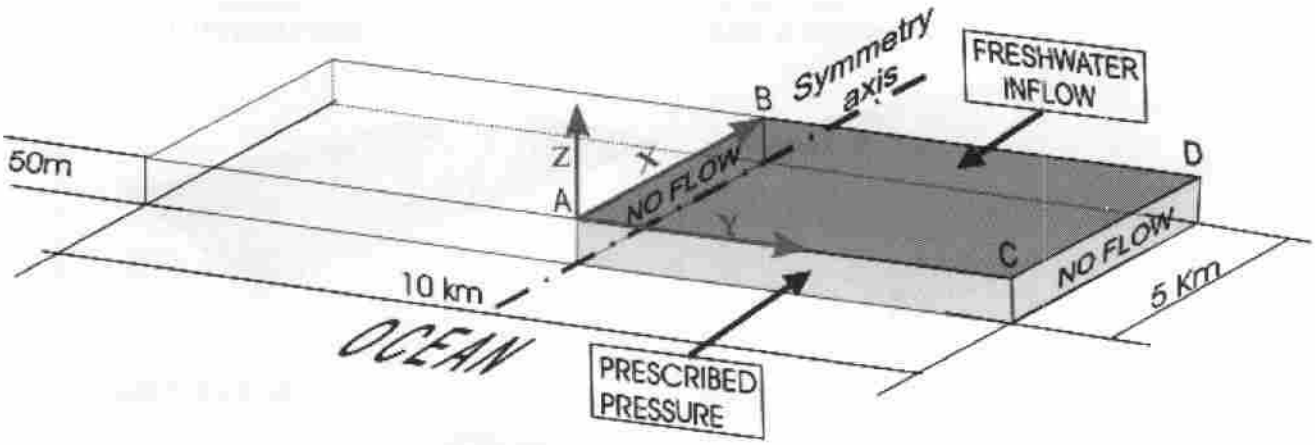

Figure 2. Geometry of the aquifer and model domain (grey area), including boundary conditions: freshwater inflow inland and specified pressure in the seaside boundary.

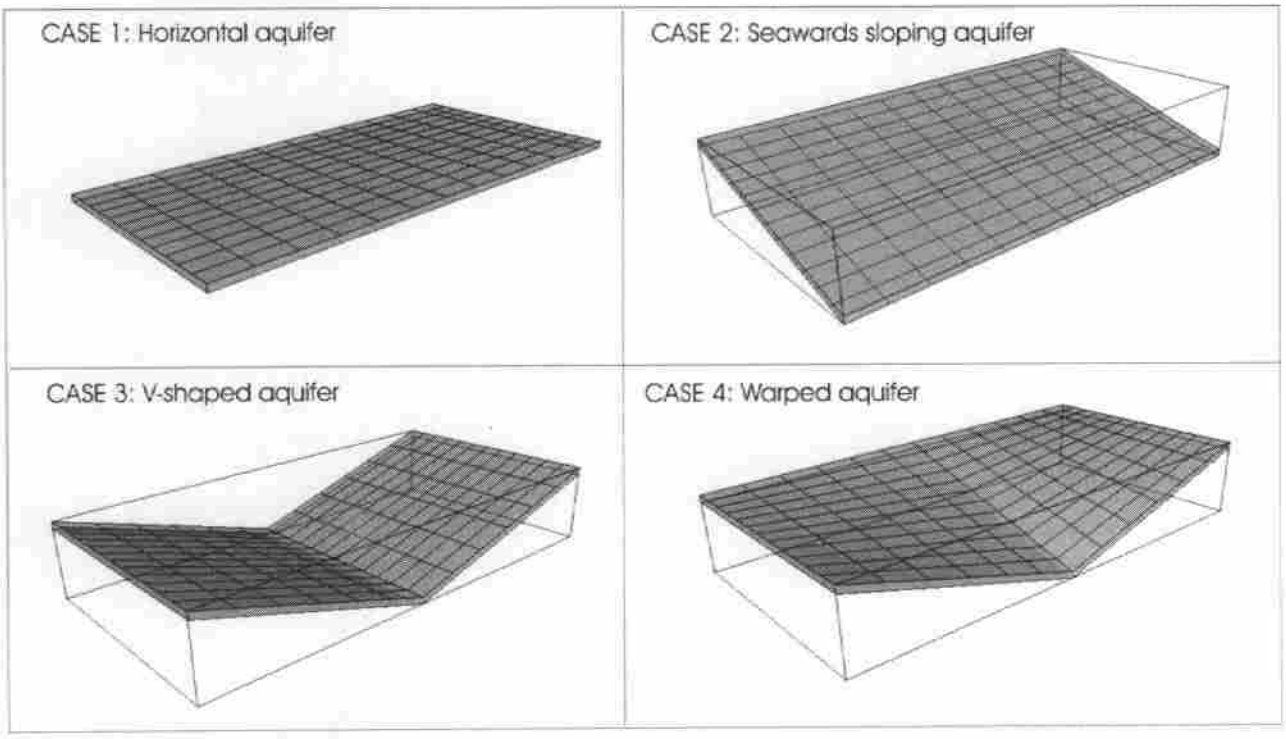

Figure 3. Schematic description of the test cases geometries: (1) horizontal, (2) seawards sloping, (3) V-shaped and (4) warped. Freshwater flows from the background (inland) towards the foreground (seaside).

Table 1. Parameters used in the simulations

Parameter	Value	
ϕ	0.2	Porosity
k	1.25e-11 m^2	[1]Permeability (isotropic)
$\alpha_{Lmax} = \alpha_{Lmed}$	20 m	Max. and med. longitudinal dispersivity
α_{Lmin}	2 m	Min. longitudinal dispersivity
α_T	2 m	Transverse dispersivity
D_m	1.0e-9 m^2/s	Molecular diffusion coefficient
α	1.0e-8 $(kg/ms^2)^{-1}$	Matrix compressibility
β	4.4e-10 $(kg/ms^2)^{-1}$	Fluid compressibility
μ	0.001 g/ms	Freshwater viscosity

[1] *This permeability is equivalent to a freshwater hydraulic conductivity of 1.225e-4 m/s*

Table 2. Description of simulations considered in the analysis (m_x and m_y are the components of the slope perpendicular and parallel to the sea coast, respectively)

Test case	Max m_x	Max m_y	N_{by}
1: Horizontal	0	0	0
2: Seawards sloping	0.01	0	0
2: Seawards sloping	0.03	0	0
2: Seawards sloping	0.1	0	0
3: V-shaped	0	0.01	0.2
3: V-shaped	0	0.03	0.6
3: V-shaped	0	0.1	2.04
4: Warped	0.01	0.01	0.2
4: Warped	0.03	0.03	0.6
4: Warped	0.1	0.1	2.0

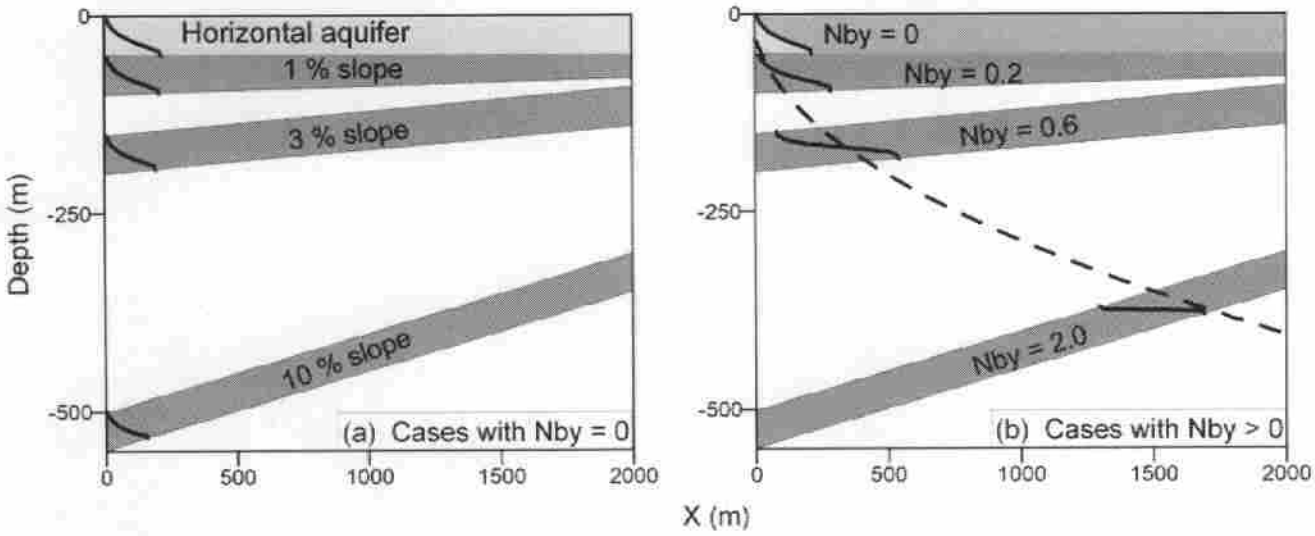

Figure 4. (a) Interface position in case 1 (horizontal) and 2 (seawards sloping) in the central cross section (vertical plane through BA in Figure 2); (b) Interface position in horizontal and warped aquifers. the dashed line represents the interface for a horizontal 550 m thick aquifer with the same inland unit flux. Horizontal axis is distance to the sea boundary (in meters); the vertical axis shows the depth (meters).

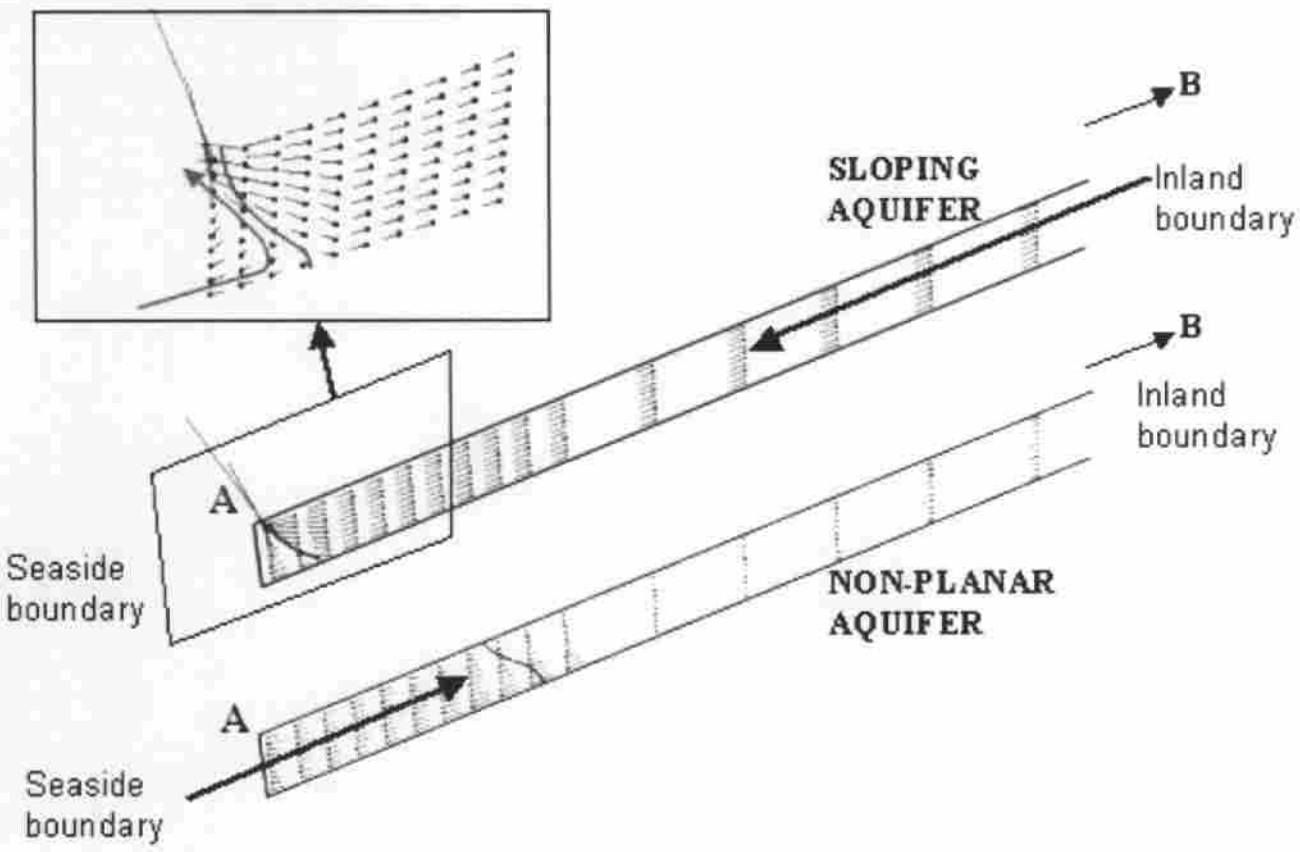

Figure 5. Projection of the velocity vectors on the aquifer central cross section (AB vertical section in Figure 2): (a) Cross section of a seawards sloping aquifer with a 10% slope. Notice the typical vertical convection cell, with seawater entering in the lowest part of the aquifer and exiting in the upper part. (b) Cross section of a warped aquifer with N_{by}=2.0. Notice that in this section, seawater enters through the whole aquifer thickness. Vector lengths indicate the magnitude of the velocity in each element.

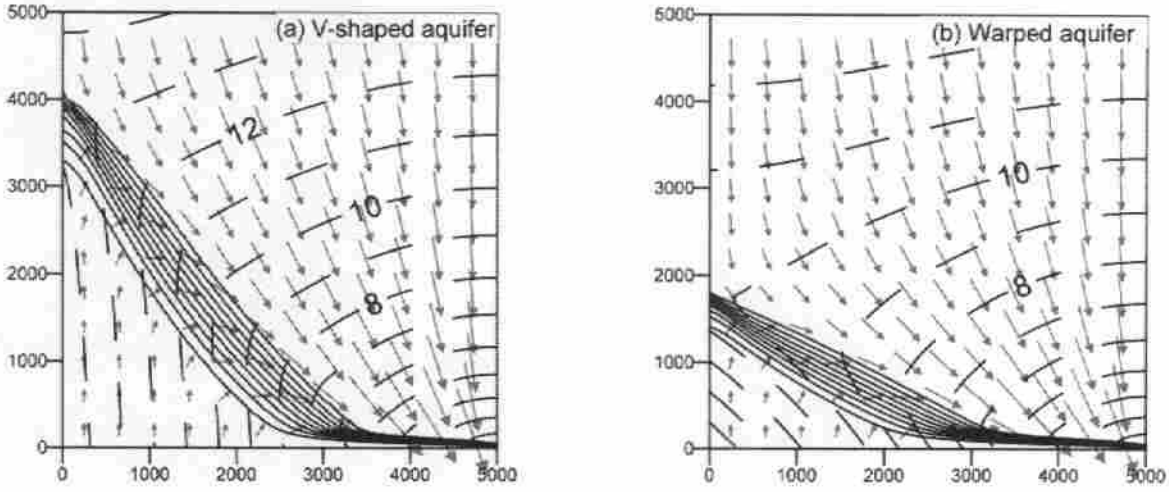

Figure 6. XY plan view of the velocity vectors, isoconcentration lines and equivalent freshwater head isolines (dashed lines) at the bottom of the aquifer in a V-shaped (a) and warped (b) aquifer with N_{by}=2.0. Notice that water entering the aquifer through its lowest point tends to exit at the much higher right hand corner, thus leading to an essentially horizontal convention cell. The lines (10% to 90% mixing lines) show the position and width of the mixing zone at the aquifer bottom. Notice that both fresh and salt waters are deflected sideways towards the high end of the outflowing boundary

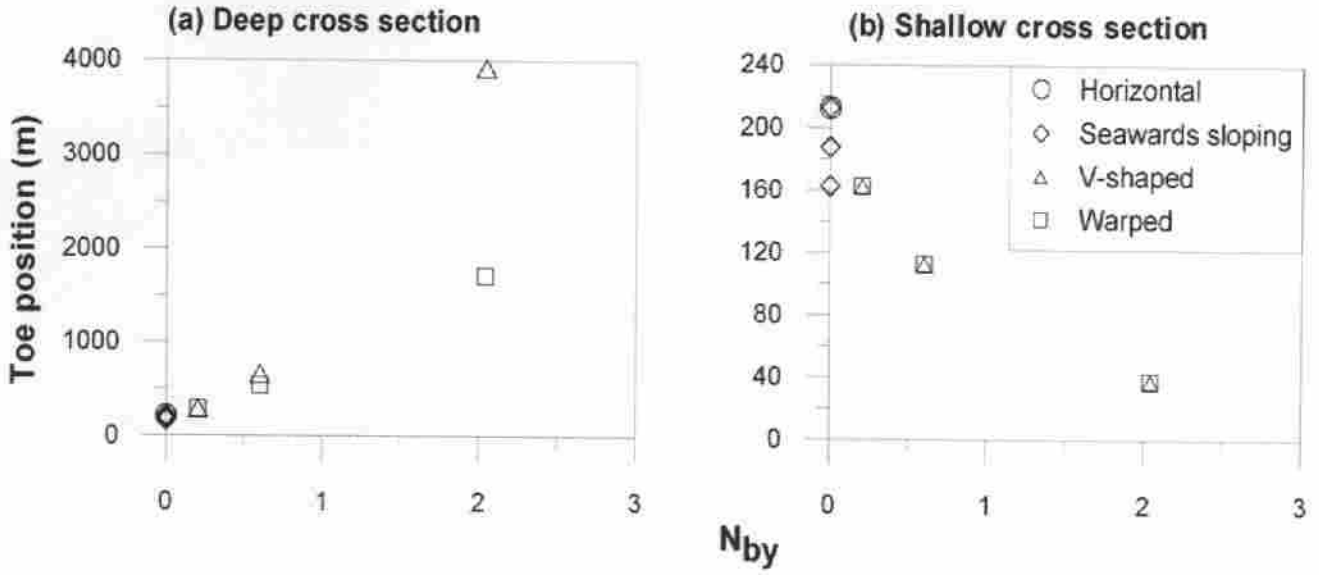

Figure 7. Toe position for the central cross section (a) and the lateral cross section (b). Notice the relation between the Nby number and the increase of the salt penetration in the central section. This effect is also accompanied by a decrease of toe penetration at the lateral boundary, which is caused by the convergence of freshwater outflow at the upslope portion of the aquifer.

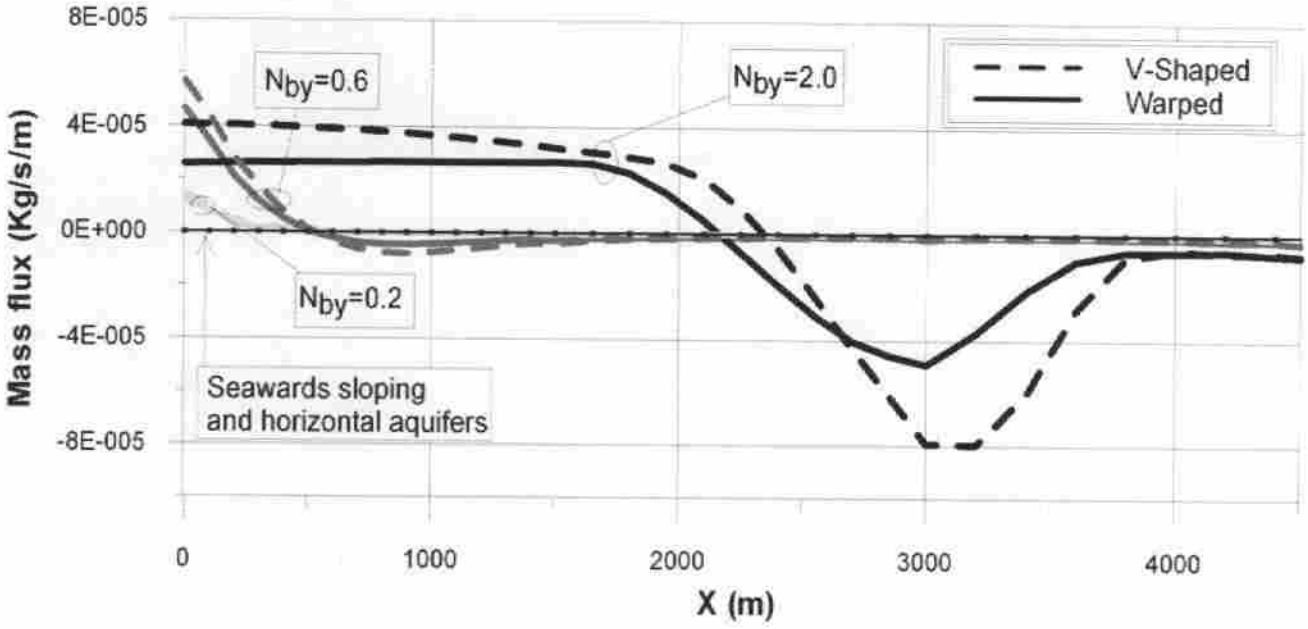

Figure 8. Vertically integrated salt flux per unit length of coastline. Positive values indicate salt inflow and negative values, outflow. The minimum salt flux in each case indicates the location of the main salt discharge point. Notice that the mass flux is 0 along the whole boundary in both horizontal and seawards dipping aquifers. However, seawater enters inland at the deepest portions of the aquifer and exits at swallower portions, though not at the shallowest, in aquifers with lateral slope

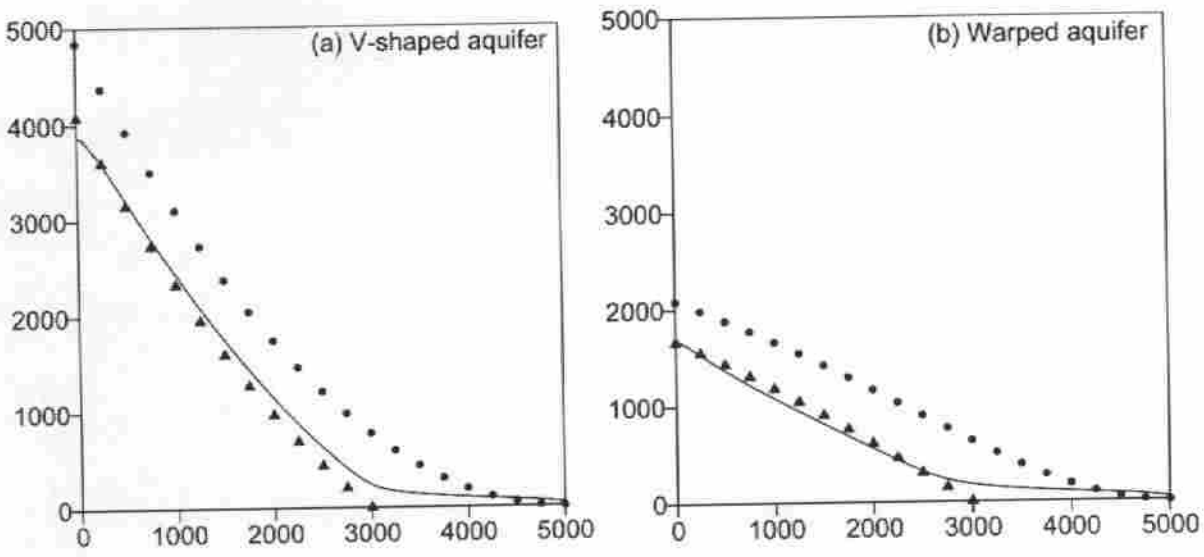

Figure 9. Model results (50% mixing is shown as a continuous line) at the bottom of the V-shaped (a) and warped (b) aquifers with $N_{by} = 2.0$. Also shown is the location (dots) of the interface derived from the Ghyben-Herzberg approximation of Appendix A for areal two dimensional aquifers with the same elevation. The tilted interface position calculated assuming that it intersects the coastline at the shallowest point is shown by circles. Triangles represent the solution assuming that the interface intersects the boundary at $y = 3000m$, the main salt discharge point as shown in Figure 8.

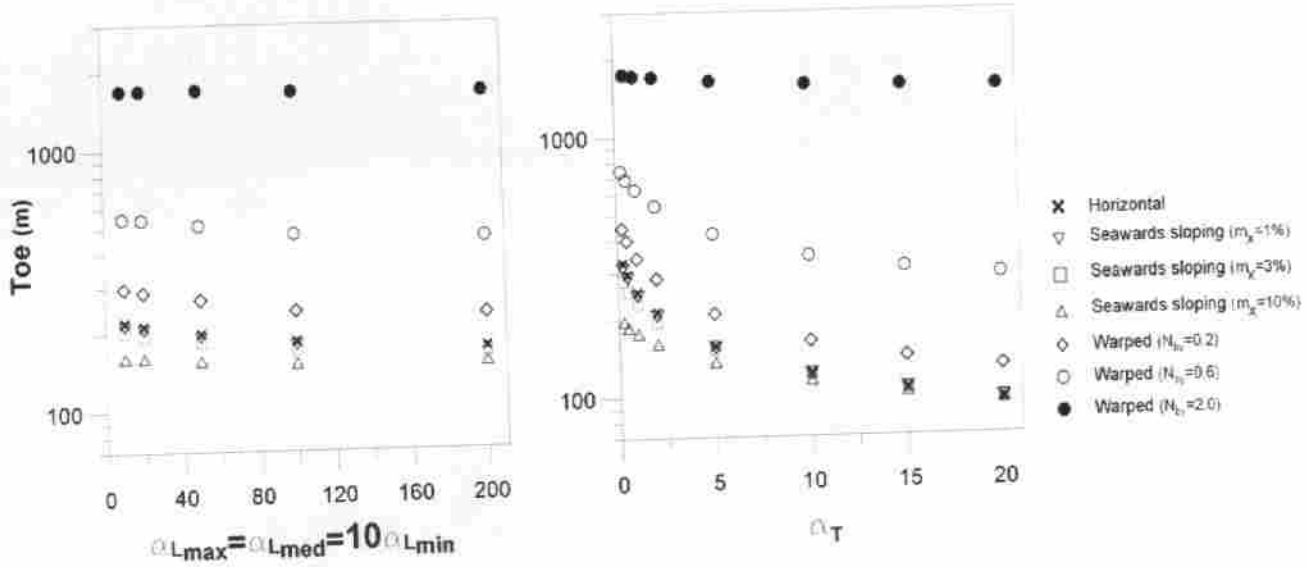

Figure 10. Sensitivity of toe penetration in the aquifer central cross section to the longitudinal (left) and transversal (right) dispersivity values for different aquifer geometries.

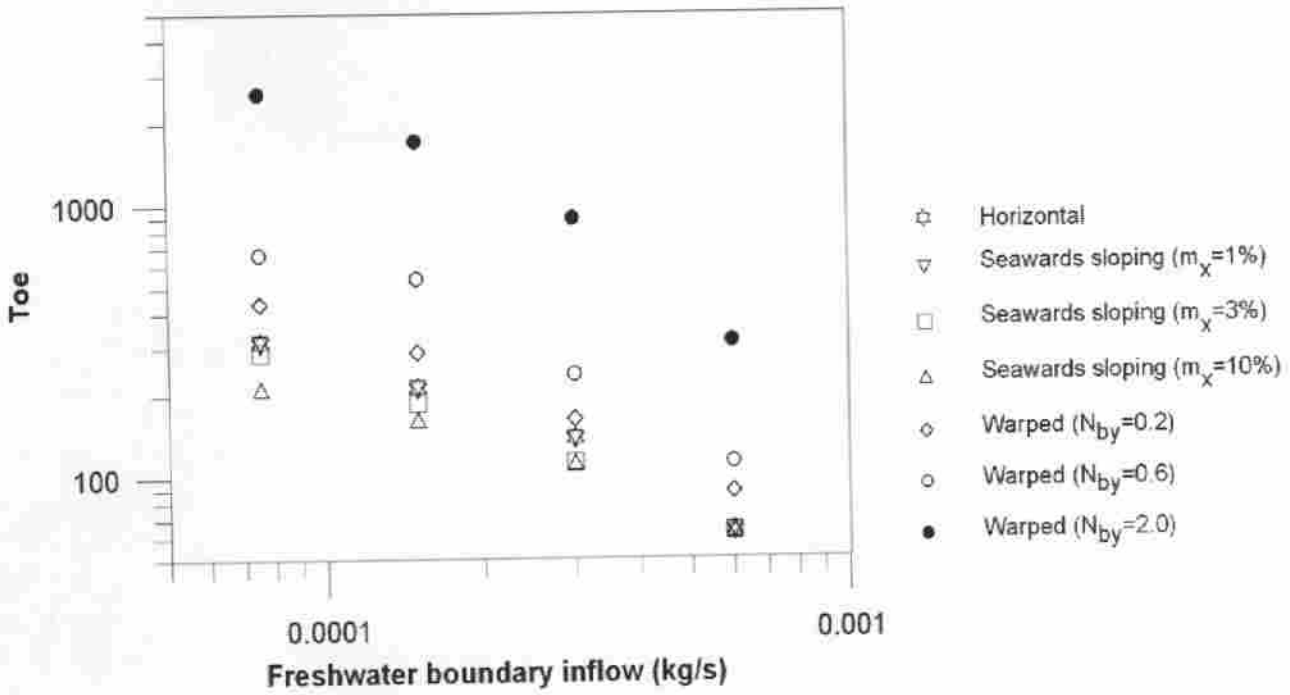

Figure 11. Sensitivity of toe penetration in the aquifer central cross section to the freshwater inflow through the inland boundary for different aquifer geometries.

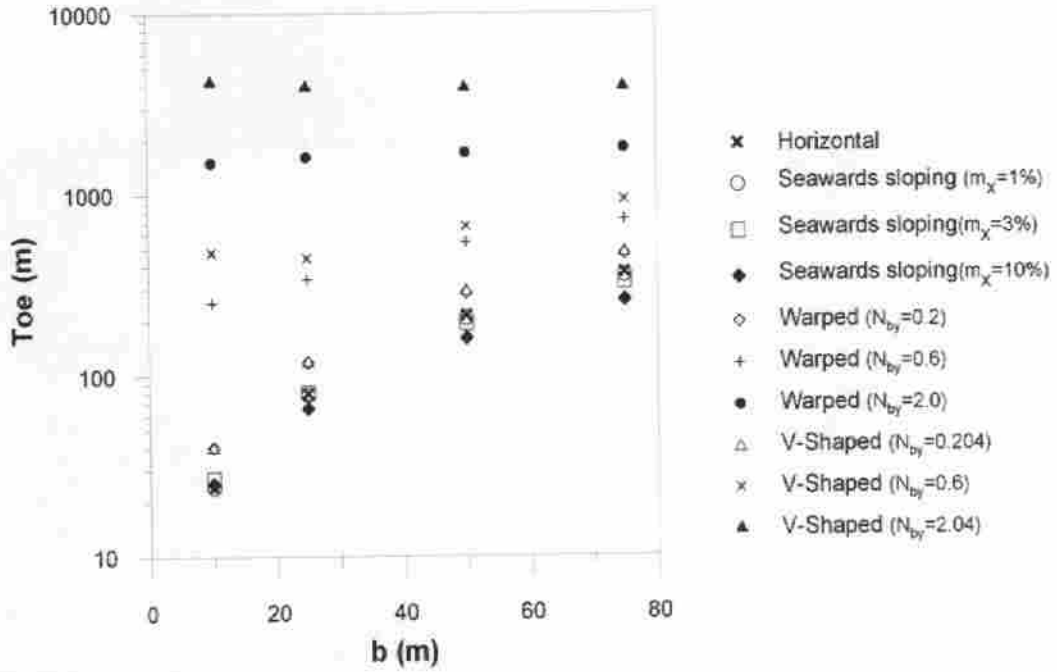

Figure 12. Sensitivity of toe penetration in the aquifer central cross section to different aquifer thickness for the different considered aquifer geometries.

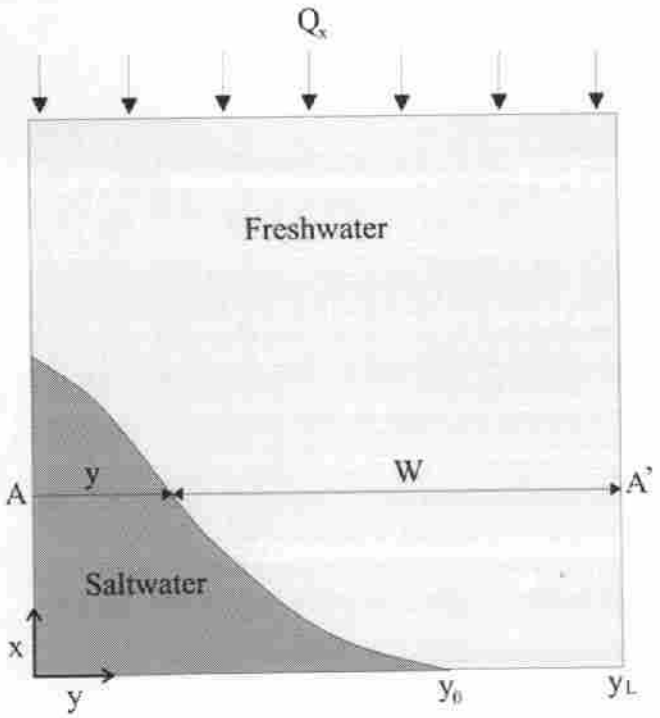

Figure 13. Plan view of the aquifer domain and some of the variables that appear in the calculations

GROUNDWATER MODELLING AS A TOOL FOR THE EUROPEAN WATER FRAMEWORK DIRECTIVE (WFD) APPLICATION: THE LLOBREGAT CASE.

E. Vázquez-Suñé (1), E. Abarca (1), J. Carrera (1), B. Capino (1), D. Gámez (1), M. Pool (1), T. Simó (1), F. Batlle (1), J.M. Niñerola (2), X. Ibáñez (2)

(1) Hydrogeology Group, GEOMODELS, Dept. of Geotechnical Engineering Geosciences, School of Civil Engineering, Technical University of Catalonia, Barcelona, Spain
(2) Agència Catalana de l'aigua, Barcelona, Spain

Corresponding author: Enric.vazquez-sune@upc.edu, Fax: 34 934017251, Phone : +34 934011859

Key words: WFD, management, groundwater modelling, Llobregat aquifers, optimization

ABSTRACT

The European Water Framework Directive (WFD, 2000) establishes the basis for Community action in the field of water policy. Water authorities in Catalonia (Agència Catalana de l'Aigua), together with users (CUADLL) are designing a management program to improve groundwater status and to assess the impact of infrastructures and city-planning activities on the aquifers and their associated natural systems. The objective is to describe the role of groundwater modelling in addressing the issues raised by the WFD, and its application to the Llobregat Delta, Barcelona, Spain. In this case modelling was used to address WFD in the following: (1) Characterization of aquifers and the status of groundwater by integration of existing knowledge and new hydrogeological information. Inverse modelling allowed us to reach an accurate description of the paths and mechanisms for the evolution of seawater intrusion; (2) Quantification of groundwater budget (mass balance). This is especially relevant for those terms that are difficult to asses, such as recharge from river infiltration during floods, which we have found to be very important; (3) Evaluation of groundwater related environmental needs in aquatic ecosystems. The model allows quantifying groundwater input under natural conditions, which can be used as a reference level for stressed conditions; (4) Evaluation of possible impacts of territory planning (Llobregat river course modification, new railway tunnels, airport and docks enlargement, etc.); (5) Definition of management areas; and (6) The assessment of possible future scenarios combined with optimization processes to quantify sustainable pumping rates and design measures to control seawater intrusion.
The resulting model has been coupled to a user friendly interface to allow water managers to design and address corrective measures in an agile and effective way.

1.- INTRODUCTION

The Water Framework Directive (WFD, 2000) establishes a framework to regulate the water and environmental resources of the European Community with the purpose of conserving, protecting and improving their quality and the sustainable use. Most of the obligations under the WFD are aimed at reaching good status of water bodies (in this case applied to groundwater) by 2015, both in a qualitative and in a quantitative sense.

The WFD establishes these objectives, the execution terms and the obligation to apply a specific control to verify its accomplishment. It basically makes it compulsory to:

- protect, improve and restore water bodies in order to reach a good status by 2015;
- adopt measures to prevent the deterioration of the good status (quality and quantity) of groundwater;
- adopt measures to prevent and limit the entrance of pollutants in groundwater;
- adopt measures to reverse negative trends (i.e. increase of contaminants in groundwater);
- ensure the protection of water bodies used for human consumption.

In addition to the above, other obligations are specified:

- Delineation of water bodies.
- Water body characterisation and potential impact assessment.
- Evaluation of quantitative status.
- Evaluation of qualitative status.
- Listing of protected areas (e.g. water bodies used for human consumption).
- Definition of management programme.
- Water body control / Assessment of the benefits of management programme implementation.

Moreover, Article 17 of the WFD requires adopting specific measures to prevent and control groundwater pollution by defining common criteria on good chemical status and quality trends. The proposal for a Groundwater Daughter Directive (COM, 2003) meets that requirement. Anyway, the proposed Directive is still not very specific, and there is a lot of ambiguity on how to apply it. For instance, concerning the prevention and restriction of the entrance of pollutants, there are no simple relationships between

preventive and corrective measures and their effects. Moreover, the relationship between abstractions and available resources is not clear and is debatable. For example, this relationship depends on the status of aquifer groundwater levels. The actual application of the Directive leaves a lot of room on how to apply it to real cases. This is useful, as it would be ludicrous to specify details of water management principles for all Europe. In practice, what the directive requires is a good understanding of the aquifer, of the implications of alternatives management strategies and thorough evaluations. We argue that these objectives can be achieved through groundwater modelling.

The objective of this paper is to describe the role of groundwater modelling in addressing the issues raised by the WFD, and its application to the Llobregat Delta, Barcelona, Spain. The methodology used to define an aquifer management programme according to the WFD is largely equivalent to groundwater modelling. In fact, modelling is normally one of the best ways to manage, integrate, validate and quantify hydrogeological information. An example of this methodology can be found in the Baix Llobregat aquifers. These aquifers are strategically relevant for the Barcelona urban area and surroundings, where one of the main issues is to have the basic management tools to define the best hydraulic policies for the short term. Defining a management programme makes it possible to evaluate the groundwater dynamics ahead of several planned territorial actions. This includes impact assessment of aquatic ecosystems (rivers, lakes, wetlands, etc.) and seawater intrusion into aquifers.

2. MANAGEMENT PROGRAM IMPLEMENTATION

A management program is a procedure for the execution and accomplishment of the WFD (Art. 13). One of its main themes is the need to define the set of measures needed to reach environmental objectives and other WFD requirements to be achieved.

Some basic features of the measures to adopt are:

- To ensure a reasonable equilibrium between groundwater abstractions and recharge rates.
- Groundwater levels should be compatible with the good status of water bodies and associated ecosystems.
- Reduce the effects of salt intrusion.
- To protect those groundwater bodies used, or potentially used, for human consumption.

- Those specific for water bodies with a longer term for the attainment of a good status.
- Those specific for water bodies with less rigorously defined environmental objectives.

In order to define a useful management programme, it is necessary to characterise the groundwater bodies and to define the management program criteria according to the WFD. Here, we present a methodology that has been successfully applied to the Baix Llobregat aquifers. The basic steps are:

Groundwater characterisation

- Characterisation of aquifers and the status of groundwater.
- Quantification of groundwater budget (mass balance).

Management criteria

- Evaluation of groundwater-related environmental needs in aquatic ecosystems.
- Evaluation of the possible impacts of territory planning.
- Definition of management areas.
- Assessment of possible future scenarios.
- Design of corrective measures.

3. GROUNDWATER CHARACTERISATION

3.1.- DEFINITION OF THE AQUIFERS AND THE STATUS OF GROUNDWATER.

Characterisation and analysis of pressures or impacts first requires the definition of the water body in order to optimise and simplify the adopted measures. The WFD is somewhat ambiguous in defining water bodies, leaving room for managers to decide in each case. The WFD simply recommends using the following criteria:

- The ability to achieve a water balance to evaluate its qualitative status
- A connection with superficial waters.
- The possibility of accurate management.
- The size of the water body must allow management beginning with the biggest size (for example corresponding to a Hydrogeological Unit) and subdividing it if necessary.
- Subdivision of water bodies on the basis of several criteria such as vulnerability, potential human activity impacts, the risk of not achieving a good status, etc.

- This can modify the meaning of "water body" if necessary.

The meaning of groundwater body does not necessarily coincide with other concepts or terms such as aquifer, aquifer system or hydrogeological unit. The aquifer is the "structure" where groundwater is stored. Aquifers can be defined on the basis of how much water can flow into them and the ability to extract significant quantities from them. Groundwater bodies constitute the "basic units" where it is possible to asses the water status.

In order to define groundwater bodies, it is necessary firsts to conduct a geological and hydrogeological review and data recollection defining the geometry, hydraulic parameters and other properties of aquifers.

An example of this can be seen in the Baix Llobregat aquifer application summarised below. In these aquifers, the integration of existing knowledge and new hydrogeological information, together with inverse modelling has allowed us to achieve a satisfactory description of the hydrogeological conceptual model (e.g. the paths and mechanisms for the evolution of seawater intrusion). We argue that calibration is needed in any model. However, inverse modelling is particularly advisable in regional large scale models for two reasons. First, significant head variations are usually observed, so that head data are very informative about the model parameters. Second, severe conceptual uncertainties are often present, so that automatic inversion allows modellers to concentrate on conceptual issues by freeing them of tedious manual calibration (Carrera et al, 2005).

GROUNDWATER CHARACTERIZATION

The Llobregat Delta is located at the SW end of the densely populated area of Barcelona City, in the NE of Spain. This area, formerly devoted to agriculture, now supports important industrial settlements and city suburbs. The high water demand brings about an intense and continuous exploitation of surface and groundwater resources. Intensive groundwater exploitation until the late 1970's caused a significant advance of the saline intrusion interface. Saline intrusion still affects large areas of the delta. At present, the Catalonian Water Agency (Agència Catalana de l'Aigua, ACA) together with users (CUADLL) are trying to correct the current situation and are developing a groundwater management programme to recover groundwater quality and quantity while trying to guarantee sustainable pumping rates.

It has been necessary to first carry out a groundwater review of previous works along with data collection and integration and an exhaustive geology review. The current delta is a medium-size quaternary formation. Some archaeological findings have shown that, in Roman times, the shore line was almost 2 km inland and that, in the Middle Ages, Barcelona harbour was sheltered by the western side of Montjuich Mountain, some 1.5 km inland from the present shore line.

For the Llobregat Delta geology general guidelines were established by Almera (1891), Llopis (1942, 1946), Solé-Sabaris et al. (1957) and Solé-Sabaris (1963). For hydrogeological purposes, the cross-sections proposed in the late 1960's and early 1970's in the framework of an important management project (MOP, 1966), and some other reports published at that time (Llamas and Molist, 1967), are still used today. Since then, civil works have provided additional geological information that has helped define a more accurate geological model. The motivation for reviewing the model stems from the need to account for medium-scale heterogeneities that would control the contamination transport processes that take place in the Llobregat Delta aquifers. This is especially true as there is a need to account for mass transport studies and even as remediation measures are to be designed or planned. A thorough sedimentological study was carried out to define the three-dimensional geological structure in detail. For example, well logs have been reviewed under a sedimentological point of view and it has been possible to redefine aquifer units, their geometries, and lateral connections both between units and the sea. The final geological model is presented in Figure 1a and 1b. All collected data were compiled in a GIS-compatible database.

(Figure 1a and 1b)

The Llobregat Delta is a well known case in classical hydrology and seawater intrusion studies. Numerous groundwater studies have been carried out in this area since the 1960's. Among others, the hydrogeological synthesis works by MOP (1966), PHPO (1985) and, more recently, Iribar and Custodio (1992) are worth noting. In the late 1970's, when salinisation problems became increasingly worrying, hydrochemistry works increased our knowledge of the aquifer systems and the mechanisms that cause seawater intrusion in the Llobregat Delta aquifers (Custodio et al., 1976; Custodio, 1981; Manzano et al., 1992; Bayó et al., 1977; Domenech et al., 1983, etc.).

It is possible to define the Main and the Upper aquifers from geological information. The Main Aquifer corresponds to alluvial sediments of Llobregat River and has

hydraulic continuity with lower permeable sediments of the Delta. The Upper Aquifer is present in the upper part of the delta. These two aquifers are separated by an aquitard constituted by silty clay sediments. In addition the main aquifer is divided in three management administrations, Cubeta de Sant Andreu in the northern, Vall Baixa in the centre, and the Delta (Figure 2).

In order to achieve a detailed characterisation, it is necessary to recover all the information used to define the conceptual model. One of the most difficult variables to obtain is recharge, which depends on soil use and varies with time, and groundwater extraction. Groundwater pumping was largest in the 1970's, when it reached values above than 130 hm^3/y. As a result heads dropped below 25 m.b.s.l. in the central part of the delta, Figure 3.

(Figure 2)

(Figure 3)

Due to this groundwater level decrease and some anthropic modifications to the medium (inland dock enlargement), sea water intrusion quickly progressed around the 1980's towards the central part of the delta, where some of the main pumping areas were located. Figure 4 shows the evolution of chloride concentration with time in some selected measurement points, to illustrate how seawater intrusion evolved in the main aquifer of the Llobregat Delta.

(Figure 4)

MODELLING

Groundwater modelling is needed to integrate and validate the conceptual model and to obtain a management tool. A variety of scenarios are simulated to allow managers to quantify the effects of different future policies on these aquifers. Groundwater flow models had been already developed for the Main Aquifer, referred to as Lower Aquifer in previous works (Custodio et al., 1971; Cuena and Custodio, 1971; PHPO, 1985; Iribar et al., 1997) and, more recently, for the main aquifer (UPC, 1997) and also for the upper aquifer (UPC, 1998).

A two-layer 2D flow and transport model of the system was built. The top layer represents the upper aquifer and the bottom layer represents the main aquifer. The numerical model does not take into account variable density effects because vertical

fluxes can be neglected in aquifers with small thickness as it is the case with the Llobregat delta aquifers. Moreover, lateral fluxes, which can be important when the lateral slope exceeds 3% (Abarca et al., 2005a) can be neglected here. The only important effect is boundary heads, which were taken into account by defining seaside boundary condition in terms of equivalent heads freshwater.

Visual Transin (UPC, 2003) is a graphical user-friendly interface for Transin (Medina and Carrera, 1996; Medina and Carrera, 2003)) which allows simulation and calibration of flow and transport parameters. This code has been used for automatically calibrating the numerical model against both head and chloride data. Spatial discretisation (Figure 5) is refined, near the main pumping areas, and the mesh is adapted to the main hydrogeological features. The average size per element is about 200 m. Calibration time steps are set monthly from 1965 to 2001. The model is validated for the extended period from 2001 to 2004.

(Figure 5)

Model's parameters were based on data integration and geological review. For example, it was possible to define 101 transmissivity zones conditioned by aquifer thickness, lithofacies description and hydraulic test values. The transmisivity zone map is shown in Figure 6, which also shows aquifer thickness isolines above it.

(Figure 6)

Three main points need to be taken into account when calibrating the model. First, we must try to ensure consistence between prior information and calibrated parameters; second, we must ensure a good fit between measured and computed data, in terms of both piezometric heads and concentrations (Figures 7 and 8) and, third, the water and chloride mass balances should be consistent with the conceptual model and previous calculations. One of the most significant contributions of the model is its ability to simulate the evolution of seawater intrusion and define a path for it.

(Figure 7)

(Figure 8)

3.2.- QUANTIFICATION OF GROUNDWATER BUDGET (MASS BALANCE)

In order to define and manage water bodies and to show understanding of the system, it is necessary to quantify the groundwater mass balance. This is especially relevant for

those terms that are difficult to assess. Mass balance is a natural output of the model. A summary of the water mass balance obtained for Baix Llobregat aquifers is show in Figure 9.

(Figure 9)

Several relevant aspects arise from Figure 9. Recharge from the river during floods is one of the most important contribution to aquifer recharge at the main aquifer. Pumping is the main term in aquifer discharge. Water storage variations are mainly conditioned by these two terms.

There is usually a net flow from the Vall Baixa to the Delta. However, this flow is sometimes reversed when intensive abstractions in the Vall Baixa area are performed.

Seawater intrudes the main aquifer through the whole simulation period. As expected, seawater intrusion is higher when groundwater heads are more depleted.

Infiltration from rain and irrigation excess are the main water input for the upper aquifer. In this aquifer the main output corresponds to the discharge to the sea and the vertical flow from the upper to the main aquifer through the aquitard (Figure 1).

4.- MANAGEMENT CRITERIA

4.1.- EVALUATION OF GROUNDWATER RELATED ENVIRONMENTAL NEEDS

Previous aquifer characterisation and modelling must give us guidelines to identify if aquifer is stressed and how difficult is it to correct this situation. It is necessary to define the environmental objectives that define whether the aquifer is in a good status or not. For Baix Llobregat aquifers these environmental objectives are:

Main Aquifer (Cubeta, Vall Baixa and Delta)

- Ensure the sustainability of those aquifers used, first, for human consumption and, second, for other complementary uses (industries, agriculture).
- Recovering the natural relationship between the river and the aquifer would make it possible to recover related aquatic ecosystems. However, this would imply flooding ancient landfills. Therefore, as long as those landfills are not cleaned up, it is preferred to keep heads below the landfill bottom.

Upper aquifer

- Guarantee environmental uses related to protected areas, specially the wetlands.
- Avoid seawater intrusion or any other contamination problems that may affect water quality equilibrium of wetlands.
- Avoid significant variation of groundwater heads due to the development of urban areas and the construction of infrastructures.

Most of the above criteria could be defined in terms of groundwater heads. Heads allow us to compute water transfer between aquifers and other water bodies, aquifer storage, contaminant rate transfers, etc. In the case of the Baix Llobregat aquifers, quantitative indicators must guarantee minimum strategic water storage, good yield for abstraction wells, water transfers to aquatic ecosystems, prevent sea water intrusion and the capture of other contaminants, prevent soil consolidation and other geotechnical problems, etc. On the other hand, groundwater heads need to be low enough to prevent the flushing of buried landfills or soil salinisation by evaporating subsurface groundwater and prevent groundwater drainage by underground structures.

Taking all these considerations into account, the range of groundwater heads that allows a good quantitative status of the aquifer, has been defined. Heads out of this range are deemed indicators of an unacceptable status. Figure 10 shows the location of the control points and their correspondent maximum and minimum reference groundwater head values.

(Figure 10)

Good management could be considered for Baix Llobregat aquifers when reversal trends will be shown in the evolution of qualitative indicators. The main quality problem of Baix Llobregat aquifers is seawater intrusion. In this case, chloride concentration or even, electrical conductivity are the best indicators for groundwater quality. We defined the ideal best qualitative status for main aquifer could be defined when groundwater concentrations are below 1000 mg/L Cl^- next to the coast, that is near natural conditions. The worse qualitative status corresponds to the current situation when the maximum contaminated area is allowed. A more realistic situation is one that represents the minimum contaminated area allowed at the beginning of the period of maximum abstraction (1965 to 2001). A good status could be defined as when chloride concentrations begin to be reduced, but a long term good status objective is to reach a seawater intrusion situation is similar to 1965, Figure 11.

(Figure 11)

4.2.- EVALUATION OF POSSIBLE IMPACTS OF NEW CONSTRUCTIONS.

To ensure the good status of groundwater and to define the best corrective measures it is necessary to assess the possible impact of territorial management and to consider all possible scenarios affecting the hydrogeological cycle.

In the Baix Llobregat aquifers the more important projected infrastructures are the Llobregat river final course modification, several new railway underground tunnels, the enlargement of the docks, the enlargement of the airport and associated drainage systems, changes in land uses, etc.

Most of these actions may affect the upper aquifer. Predictable impacts are related to, first, groundwater level drawdown due to the potential drainage effect over aquifer by airport drainage channels, tunnel seepage, and river drainage, and second, a rise in groundwater level caused by the reduction of the flow aquifer section (barrier effect). All this groundwater level movements may produce some of the negative impacts described before, that avoid groundwater good status.

Projected new hydraulic parameter modifications, and computed impacts based on them, are very uncertain. Additional monitoring network will be necessary to assess the possible impacts during construction and implementation phases.

4.3.- DEFINITION OF MANAGEMENT AREAS.

The meaning of "water body" in WFD context was described in section 3.1. One important issue is the possibility of dividing water bodies to facilitate management. The methodology consists of zoning several variables and then crossing all related variables, obtaining different management areas with homogeneous properties. The same quantitative and qualitative indicators must be applied to each one. As a result, it is possible to apply the same management criteria for the whole area. Keeping a small number of areas is recommended in order to simplify management.

Criteria considered here for defining management areas include groundwater pumping, aquifer recharge areas (land cover, soil uses, river interaction, etc), administrative limits and aquifer qualitative (concentrations) and quantitative (heads) indicators. Seven polygons or management areas were defined (Figure 12); six in the main aquifer, and

one corresponding to the upper aquifer. Pumping rates will be reduced in the same proportion for all pumping well in each management area.

(Figure 12)

4.4.- THE ASSESSMENT OF POSSIBLE FUTURE SCENARIOS.

Once an aquifer is satisfactorily represented by a model, this model is a useful tool to test different assumptions on how the system may develop in the future. Since the future is uncertain, some assumptions about the evolution of the main source/sink terms need to be made resulting in different future scenarios. The complete set of scenarios provides a wide insight the sustainability at long term of existing pumping rates under different considerations. Furthermore, they provide information about where and which additional corrective measures are needed.

In the Baix Llobregat aquifers a set of these simulations were carried out. The simulation period was defined from 2002 to 2036. One of these scenarios was chosen as the reference scenario to compare results against. This scenario assumes that:

- The meteorological series for the simulation/optimization period (2002-2036) is equal to that observed during the period 1965-2001. It includes long dry periods as well as long wet periods taking into account extreme possible cases. Global climate change has not been considered.
- The pumping history assumed for future years is the average of the last five years (1997-2001) for all wells, except for the main pumping area whose temporal variability for the last five years have been repeated along the simulation period.
- Current abstraction locations are maintained.
- Projected infrastructures to be built at short term are included into the simulation model (the Llobregat river course modification, the new railway and subway tunnels, the airport and the docks enlargement, the urban area expansion, etc.).

Alternative scenarios consider an increase or decrease of current pumping rates or the inland migration of the pumping areas caused by water salinization.

All proposed scenarios showed that current abstractions are not sustainable at long term. Seawater intrusion will progress if the current situation is not corrected in an immediate future. A strong reduction in pumping is needed to achieve a good quantitative and qualitative status unless additional corrective measures are implemented.

4.5.- DESIGN OF CORRECTIVE MEASURES

Many corrective measures can be considered to recover groundwater status. Basically, they can be grouped in: reduction of groundwater pumping; increase of recharge; relocation of pumping wells; and in the case of coastal aquifers, additional engineering solutions to restore groundwater quality (e.g. hydraulic barriers).

For Baix Llobregat aquifers potential corrective measures include:

1. To reduce groundwater abstraction.
2. Positive Recharge Seawater Intrusion Barriers with regenerated waters, between abstraction areas and seawater intrusion paths.
3. Artificial Recharge by:
    - Wells
    - Surface ponds
    - River bank and urban runoff infiltration
    - Induced recharge from controlled river floods

Once the alternatives are identified, the decision of the final management policy depends on the defined goals, the impact of the alternatives, their feasibility (costs, social agreement, etc.) and preferences of the decision makers. Finally three corrective measures were considered:

- Reducing the pumping rates in each management area.
- A seawater intrusion barrier (SWI). A freshwater injection barrier, divided in four sections according to the different transmissivity zones defined in the numerical model, was proposed in the eastern part of the coast. The optimization problem enables the optimal distribution of the total amount of water injected into the four segments. This total projected injection rate is 3.65 hm^3/y. The barrier is accompanied by two pumping wells, active only

during the first ten years, to clean the saltwater trapped inland of the seawater barrier.

- Recharging ponds to artificially increase the recharge. Two recharge ponds (11 ha) were proposed on the alluvial part of the main aquifer (Figure 13). Projected infiltration rate was 0.25 m/d resulting in a total projected recharge of 11 hm^3/y.

(Figure 13.)

After selecting some possible measures, optimization is a powerful tool to evaluate the best alternative to groundwater management in an aquifer subject to some environmental constraints. In the Baix Llobregat aquifers, two different simulation/optimization methods were applied. The objective was to asses the feasibility of the above three different measures and to quantify their effectiveness to recover an aquifer affected by seawater intrusion (Abarca et al., 2005b). Both optimization methods were aimed at maximizing total pumping.

In the first one, head constraints were imposed to warrant a seawards gradient along the coast line. This leads to a linear optimization problem. In the second, chloride concentration is constrained to represent the qualitative good status. The resulting problem is non-linear.

Both optimization processes were applied to the management areas defined previously (Figure 12) according to management criteria commented above. Moreover, the equity principle was applied to the pumping wells located in the same management area, so that, if necessary, pumping rates can be reduced by the same proportion.

The results in Table 1 compare the present to the optimal abstractions rates computed with both optimization methods for every management area.

The head constrained optimization method showed that the reduction to be applied in the main pumping areas (Zones 2 and 4 in Figure 12) is about 50%. This reduction was decreased to 25% when the recharge ponds and the seawater intrusion barrier are added. However, head constraints were not strict enough to achieve a good qualitative status after the optimization period (2002-2036). Linear optimization methods yield additional information as are the shadow prices of the constraints. In this case the shadow prices correspond with the hydraulic efficiency of corrective measures. The hydraulic

efficiency for the ponds is around 0.7 while for the seawater intrusion barrier is about 1.5. That is, 1 m^3 recharged in an inland pond allows increasing total pumping in 0.7 m^3. On the other hand, 1 m^3 of freshwater injected in the coastal barrier allows increasing pumping by 1.5 m^3. This contradicts the widely extended belief that injected water is lost to the sea. As it turns out, not only is most water actually used, but also its protection effect allows increased drawdown (and pumping) inland.

To ensure the recovery of groundwater quality, the second optimization method, with constrained chloride concentrations, was used. Table 1 shows that current abstraction can be maintained while reversing the qualitative status only if the recharge/injection projected in the recharge ponds and de SWI barrier is increased by 50% and 300% respectively. This method offers a good estimation of the injection rate to design efficient corrective measures. The resulting chloride distribution at the end of the optimization period is presented in Figure 14 (right).

(Table 1)

(Figure 14)

5.- CONCLUSIONS

The WFD indeed establishes a frame for the assessment and maintenance of the good status of water bodies. This objective relates to both qualitative and quantitative status.

We have shown that, at least groundwater bodies, the requirements established by the WFD can be naturally achieved through modelling. Groundwater modelling helps in integrating and validating the hydrogeological conceptual model. Groundwater modelling makes it possible to evaluate the groundwater dynamics ahead of alternative planned territorial actions. It also facilitates evaluating their impact and designing corrective measures.

This methodology has been applied to the Baix Llobregat aquifers. The application suggests that groundwater modelling is helpful in the following issues:

1. It helps in meeting the objective of aquifer characterization and groundwater status assessment by integrating existing knowledge and the new hydrogeological information. Inverse modelling allowed us to reach an accurate description of the paths and mechanisms for the evolution of seawater intrusion.

2. It helps in quantifying the groundwater mass balance. This is especially relevant for those terms that are difficult to asses, such as recharge from river infiltration during floods, which we have found to be one of the most important terms.
3. It helps in evaluating groundwater related environmental needs. The model allows quantifying groundwater input under natural conditions, which can be used as a reference level for stressed conditions. Modelling leads naturally to guidelines to identify if aquifer are stressed and if it is difficult to address this situation.
4. Modelling allows evaluating and quantifying possible impacts of territorial management. Possible impacts of any territorial planned actions and all possible changes on hydrogeological cycle must be taken into account in order to ensure the good status of groundwater and define the best corrective measures. In the Baix Llobregat aquifers, all of the scenarios proposed showed that current pumping rates are not sustainable in the long term. Therefore corrective actions are needed.
5. Finally, modelling is needed for designing corrective measures. In the Baix Llobregat aquifers corrective measures consist in the reduction in the pumping rates in each management area, recharge ponds to artificially increase the recharge, and a seawater intrusion barrier. Optimization processes were applied to management areas previously defined and to quantify how much water should be artificially recharged to maintain the total current pumping as well as its current distribution to guarantee the recovery of groundwater quality.

As an afterthought, we wish to add that the WFD does not require a formal evaluation of uncertainty. While modeling helps in integrating different kinds of data and available knowledge in a consistent description, it is not free of subjectivity and errors. Therefore, model predictions are uncertain. To large extent, this uncertainty can be evaluated and taken into account in the decision-making process. In general, this is desirable, but was not addressed in our work.

ACKNOWLEDGMENTS

This work has been done in the framework of project funded and supported by the Catalonian Water Agency (Agència Catalana de l'Aigua); Comunitat d'Usuaris d'Aigües del Llobregat (CUADLL) and Spanish Geological Survey (IGME). We would like to thanks two anonymous reviewers and editor for their comments on the manuscript that have helped improve the revised version of the paper.

REFERENCES

Abarca, E., Carrera, J., Sanchez-Vila, X. and Voss, C.I. (2005a). Quasi-horizontal circulation cells in seawater intrusion. (Submitted)

Abarca, E., E. Vázquez-Suñé, J. Carrera, B. Capino, D. Gámez and F. Batlle (2005b). Optimal design of mesures to correct seawater intrusion. Accepted for publication in Water Resour. Res.

Almera, J. (1891). Mapa geológico-topográfico de la provincia de Barcelona. Región 1 o contornos de la capital. Escala 1:40000. Barcelona.

Bayó, A, E. Batista, E. Custodio (1977). Sea water encroachment in Catalonia coastal aquifers. General Assembly IAH. Birmingham 1977. Vol. XIII.l pp. F.1-14.

Carrera, J., A. Alcolea, A. Medina, J. Hidalgo and L.J. Slooten (2005). Inverse problem in hydrogeology. Hydrogeology Journal 13:206-222.

COM (2003). COM (2003) 550, 2003/0210 (COD) Proposal for a directive of the European Parliament and of the Council on the protection of groundwater against pollution.

Cuena, S. and Custodio, E. (1971). Construction and adjustment of a two layer mathematical model of the Llobregat Delta, Barcelona, Spain. Mathematical Models in Hydrology. Studies and Reports in Hydrology. 15. UNESCO. Paris. II: 960-964.

Custodio, E., Cuena, J. and Bayó, A. (1971). Planteamiento, ejecución y utilización de un modelo matemático de dos capas para los acuíferos del río Llobregat, Barcelona. Memorias, 1er Congreso Hispano-Luso Americano de Geología Económica. Madrid-Lisboa. III, 1: 171-198.

Custodio, E., Cacho, F. and Peláez, M.D. (1976). Problemática de la intrusión marina en los acuíferos del Delta del Llobregat. Segunda Asamblea Nacional de Geodesia y Geofísica, Barcelona. Instituto Geofísico y Catastral Madrid. pp. 2069-2101.

Custodio, E. (1981). Sea water encroachment in the Llobregat delta and Besos areas, near Barcelona (Catalonia, Spain). Sea Water Intrusion Meeting: Intruded and Fosil Groundwater of Marine Origin. Uppsala Sveriges Geologiska Undersökning. Rep 27, pp., 120-152.

Doménech, J., E. Batista, A. Bayo, E. Custodio (1983). Some aspects of sea water intrusion in Catalonia (Spain). 8th SWIM. Bari. Instituto di Geologia Appicata e Geotecnia. Bari. 15 pp.

Iribar, V. and Custodio, E. (1992). Advancement of seawater intrusion in the Llobregat delta aquifer. In: E. Custodio and Galofre (Editors), SWIM Study and Modeling of Saltwater Intrusion into Aquifers. CIMNE-UPC, Barcelona, pp. 35-50.

Iribar, V., Carrera, J., Custodio, E. and Medina, A. (1997). Inverse modeling of sea water intrusion in the Llobregat delta deep aquifer. Journal of Hydrology, 198 (1-4) pp. 226-244.

Llamas, M.R., J. Molist (1967). Hidrologia de los deltas de los ríos Besós y Llobregat. Documentos de Investigación Hidrológica, n° 2. Centro de Estudios, Aplicaciones e Investigaciones del Agua. Barcelona.

Llopis i Lladó, Noel (1942). Los Terrenos cuaternarios del llano de Barcelona. Publ. Inst. Geol. Dip. Prov. de Barcelona, VI, 52 pp. 8 figs.

Llopis i Lladó, Noel (1946). Los movimientos corticales intracuaternarios del NE. de España. Estudios Geológicos (Madrid). 3; 181-236.

Manzano, M., Custodio, E. and Carrera, J. (1992). Fresh and salt water in the Llobregat delta aquifer: application of ion chromatography to the field data. In: E. Custodio and Galofre (Editors), SWIM Study and Modeling of Saltwater Intrusion into Aquifers. CIMNE-UPC, Barcelona, pp. 207-228.

Medina, A. and Carrera J. (1996). Coupled estimation of flow and solute transport parameters, Water Resour. Res., 32(10), 3036-3076.

Medina, A. and Carrera J. (2003) Geostatistical inversion of coupled problems: dealing with computational burden and different types of data. J. Hidrol. 281:251-264.

MOP (1966). Estudio de los recursos hidráulicos totales de las cuencas de los ríos Besós y Bajo Llobregat. CAPO-SGOP. 4 vol. Barcelona.

PHPO (1985). Modelo de simulación de los acuíferos del delta del Bajo Llobregat. Plan Hidrológico Nacional. Confederación Hidrográfica del Pirineo Oriental – Comisaría de Aguas del Pirineo Oriental. Realizado por E. Custodio, L. López, V. Iribar.

Solé-Sabaris, L., C. Virgili, I. Zamarreno (1957). "Livret guide d'excursions: Environs de Barcelona et Montserrat". V Congress. Inter.

Solé-Sabaris, L (1963). Ensayo de interpretación del Cuaternario Barcelonés. Miscelánea Barcinonensia, t. II, pp. 7-58, 8 figs., Barcelona.

UPC (1997) Estudi i modelació de l'evolució de nivells d'aigua subterrània a l'area Metropolitana de Barcelona. UPC – EMSHTR. Barcelona.

UPC (1998) Evaluación del impacto hidrogeológico de las obras de encauzamiento del río Llobregat. Departament d'Enginyeria del Terreny. UPC. Barcelona.

UPC (2003) Visual Transin Code. Departament d'Enginyeria del Terreny. UPC. Barcelona.

WFD (2000). Directive 2000/60/EC of the European Parliament and of the Council of 23 October 2000 establishing a framework for Community action in the field of water policy.

LIST OF FIGURES

Figure 9. Water mass balance scheme for the Llobregat delta aquifers expressed in hm^3/y. The mass balance for the main aquifer is on the left side and for the upper aquifer on the right. The black parallel arrows show the flux from the upper to the main aquifer.

Figure 10. Location of the control points and their correspondent maximum and minimum reference groundwater head values.

Figure 11. Main and upper aquifers chloride concentrations in 1965.

Figure 12. Management areas defined in main and upper aquifers.

Figure 13. Location of the pumping wells and their average pumping rate in the period from 1997 to 2001 and location of the proposed corrective measures those are included in the optimization process.

Figure 14. Left: simulation of the future evolution of salinity in the main aquifer of the delta (year 2036) if the pumping wells move inland as a consequence of salinity making the pumped water undrinkable. Right: Hypothetical situation in year 2037 if the current situation is remediate with some additional measures such as an injection barrier and recharge ponds.

LIST OF TABLES

TABLE 1.

Management Zones	*Present average 1997-2001*	*Head constraints (Q)*	*Head constraints (Q, ponds, barrier)*	*Concentration constraints*
Zone 1	5.29	5.28	5.28	5.29
Zone 2	30.23	21.92	21.92	28.62
Zone 3	1.77	1.83	1.83	1.98
Zone 4	24.59	4.64	18.49	23.38
Zone 5	0.00	1.83	1.83	4.16
Zone 6	2.14	0.00	0.0	--
Recharge ponds			-10.96	-16.45
Injection Barrier 1			-3.65	-2.68
Injection Barrier 2			0.00	-2.84
Injection Barrier 3			0.00	-1.27
Injection Barrier 4			0.00	-4.50
Total	64.02	35.48	49.35	63.41

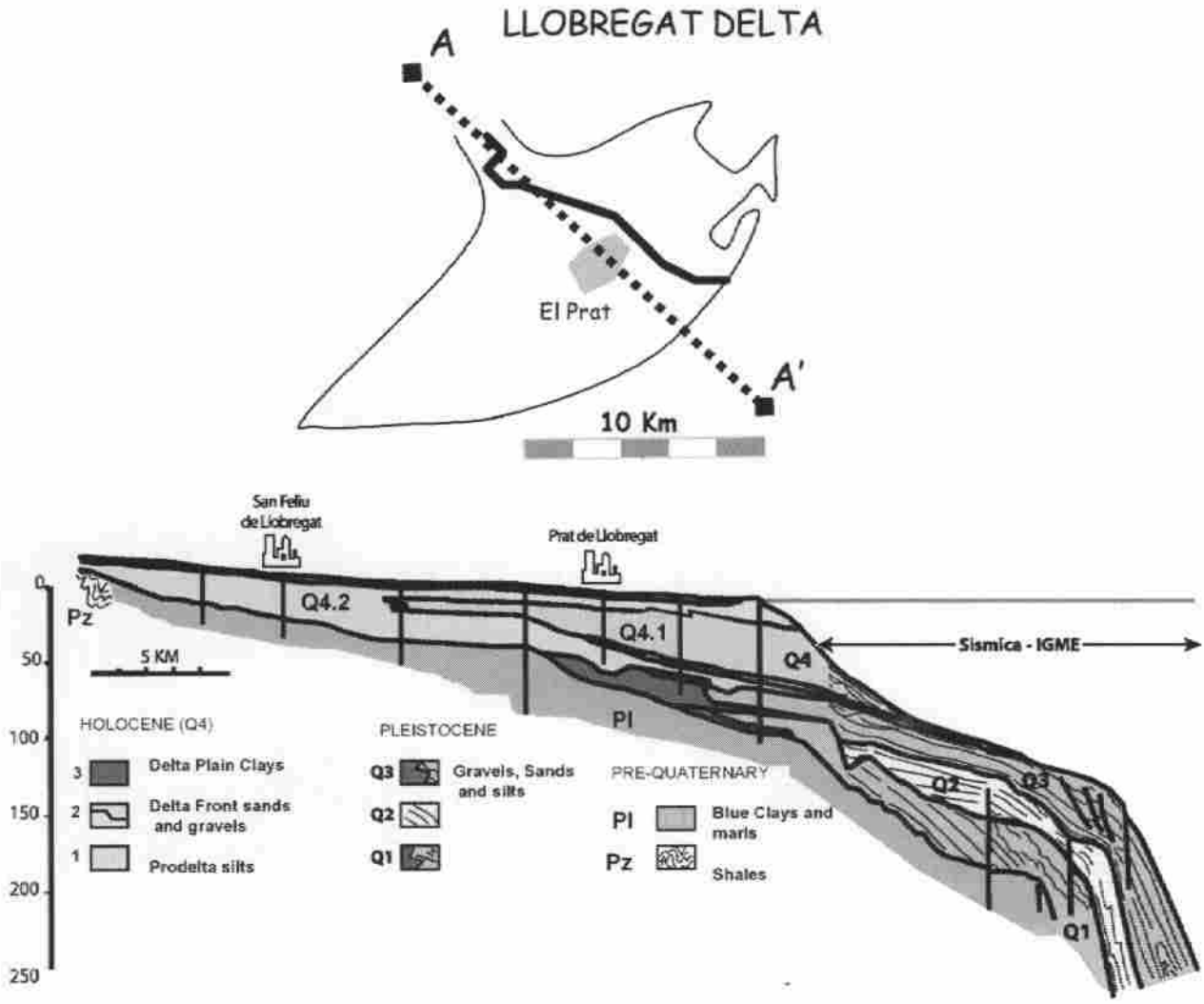
LLOBREGAT DELTA
A
A'
El Prat
10 Km
San Feliu de Llobregat
Prat de Llobregat
Pz
Q4.2
Q4.1
Q4
Pl
Q3
Q2
Q1
5 KM
Sismica - IGME
0
50
100
150
200
250
HOLOCENE (Q4)
3 Delta Plain Clays
2 Delta Front sands and gravels
1 Prodelta silts
PLEISTOCENE
Q3 Gravels, Sands and silts
Q2
Q1
PRE-QUATERNARY
Pl Blue Clays and marls
Pz Shales

Figure 1a.

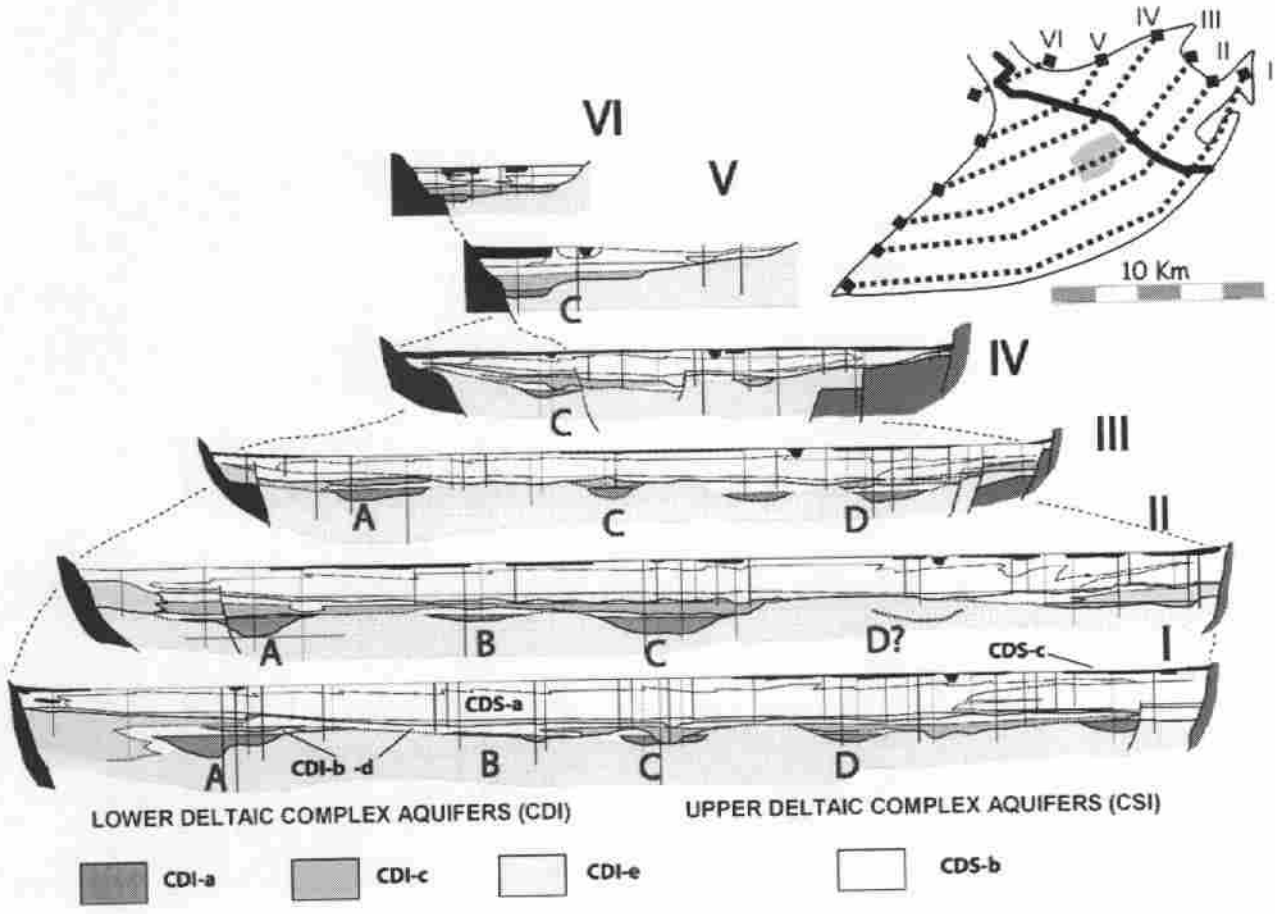
VI
V
IV
III
II
I
10 Km
C
C
A
C
D
A
B
C
D?
CDS-c
CDS-a
A
CDI-b -d
B
C
D
LOWER DELTAIC COMPLEX AQUIFERS (CDI)
UPPER DELTAIC COMPLEX AQUIFERS (CSI)
CDI-a
CDI-c
CDI-e
CDS-b

Figure 1b.

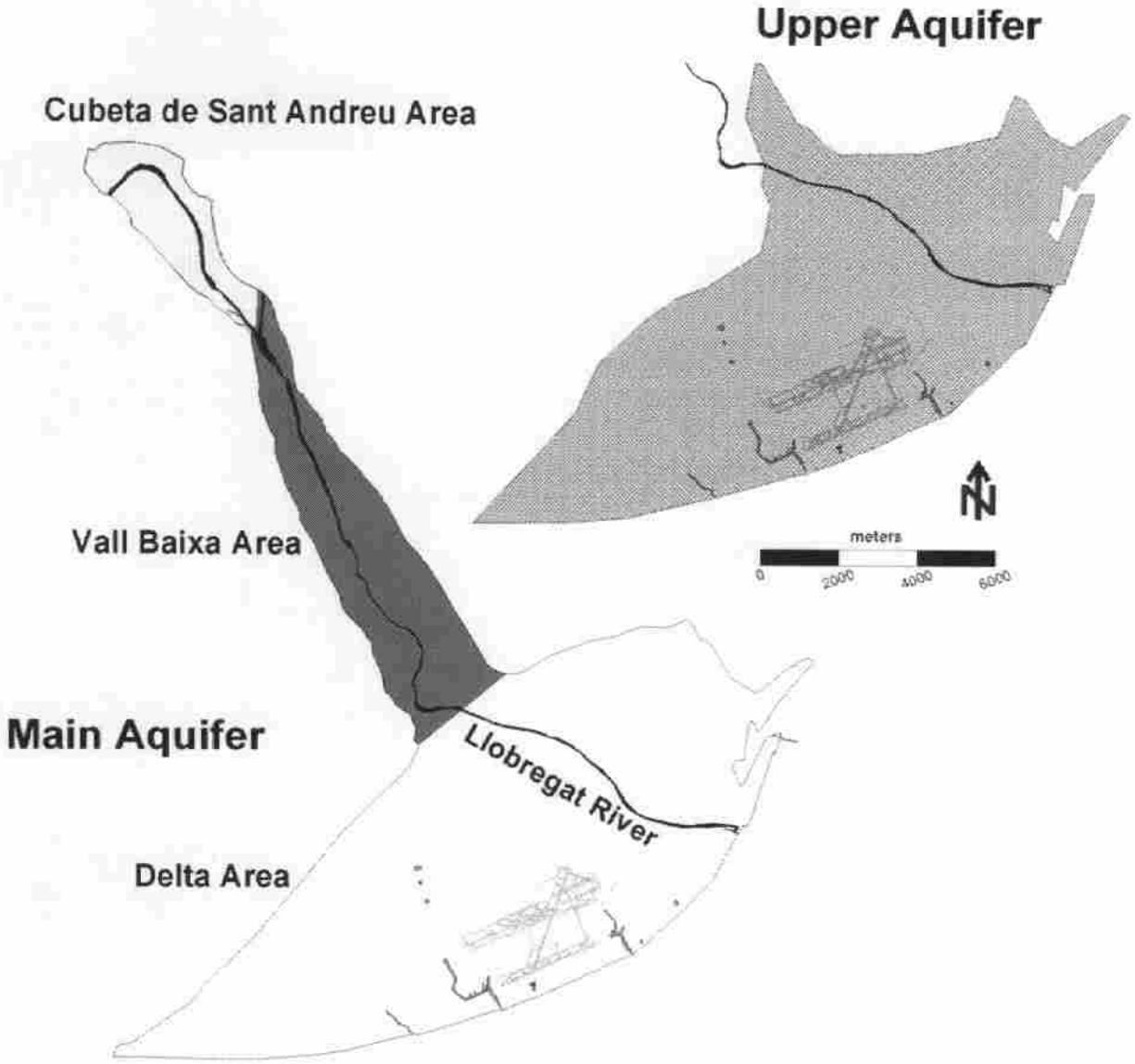
Upper Aquifer
Cubeta de Sant Andreu Area
Vall Baixa Area
Main Aquifer
Llobregat River
Delta Area
meters
0
2000
4000
6000

Figure 2.

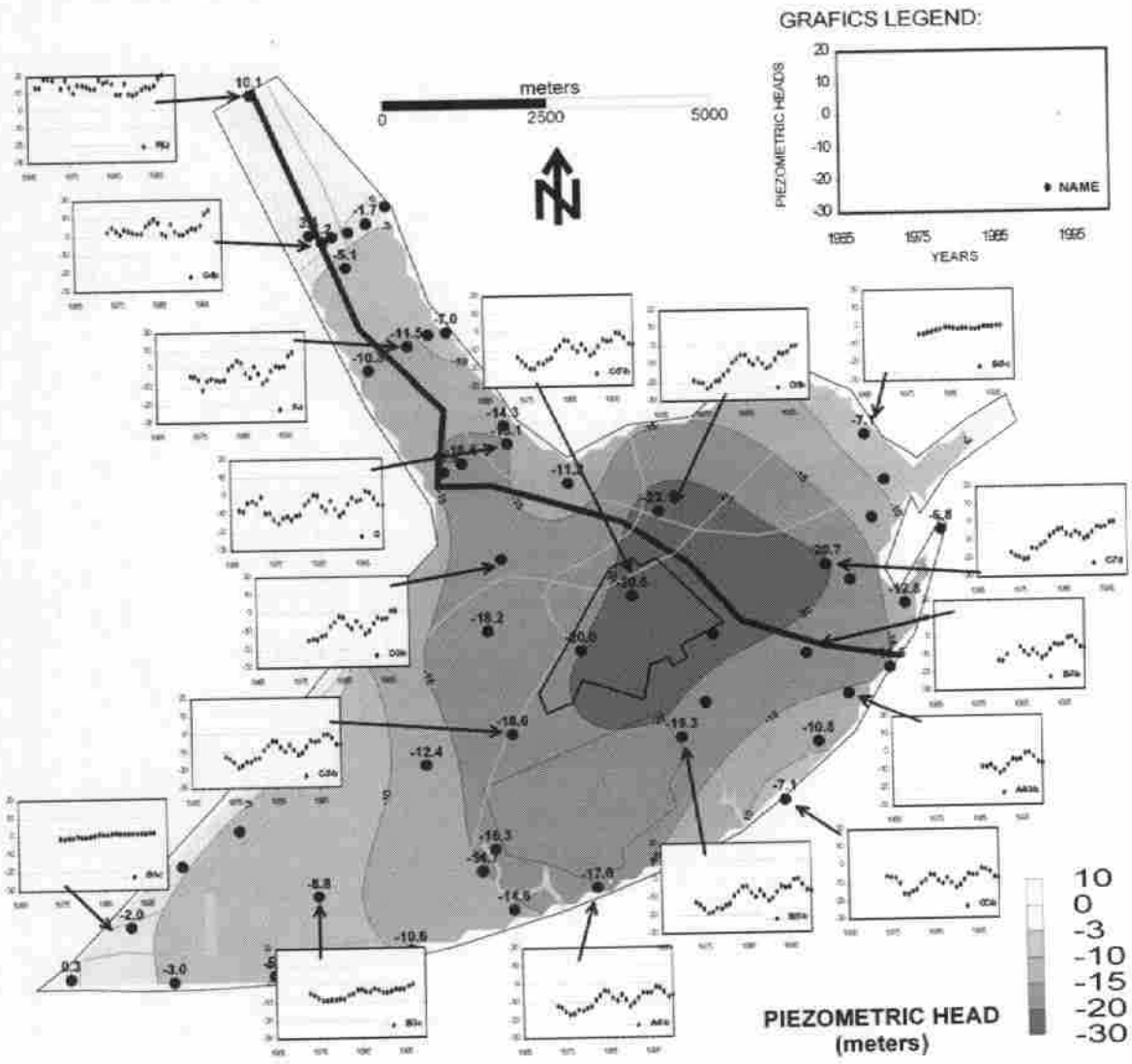
GRAFICS LEGEND:
PIEZOMETRIC HEADS
20
10
0
-10
-20
-30
NAME
1955
1975
1995
1995
YEARS
meters
0
2500
5000
N
10
0
-3
-10
-15
-20
-30
PIEZOMETRIC HEAD
(meters)

Figure 3.

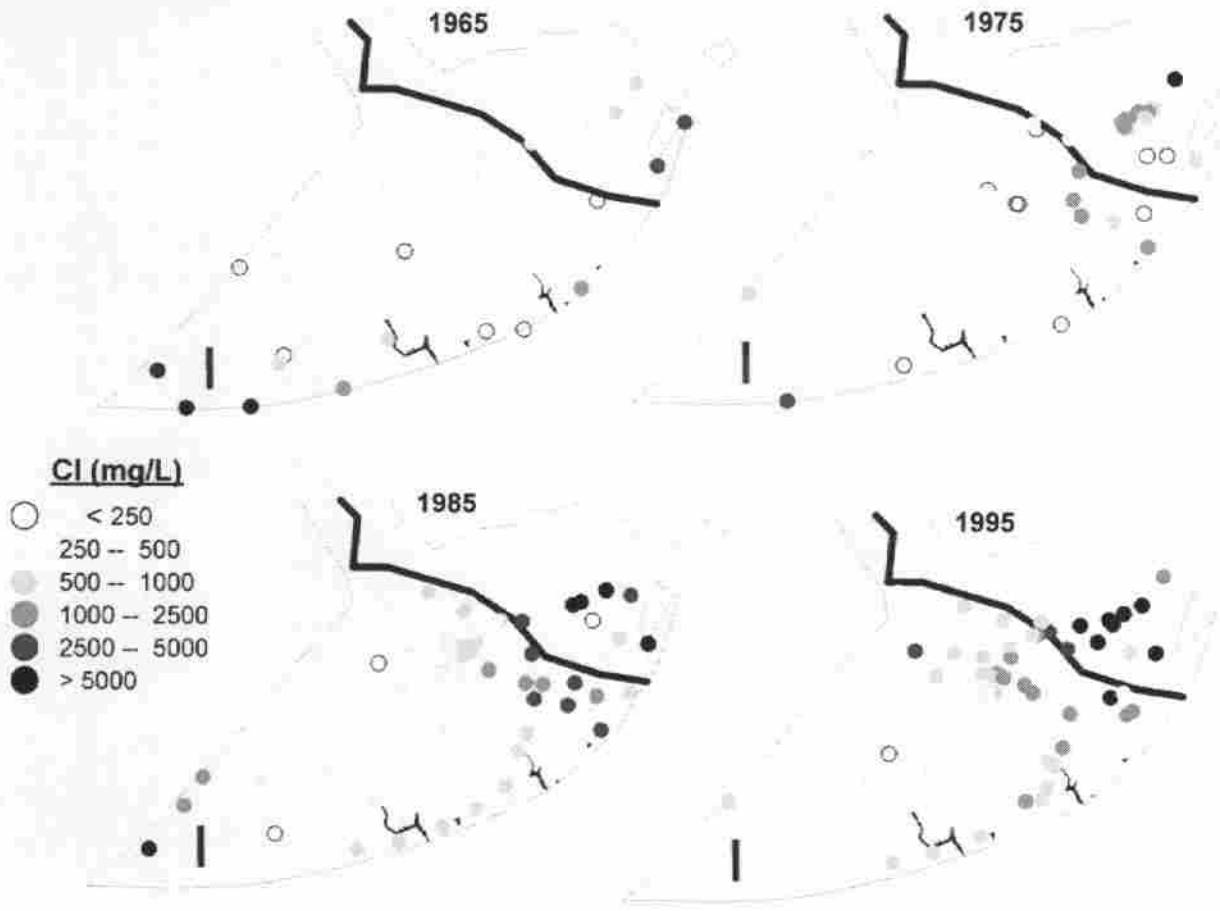
1965
1975
1985
1995
Cl (mg/L)
< 250
250 -- 500
500 -- 1000
1000 -- 2500
2500 -- 5000
> 5000

Figure 4.

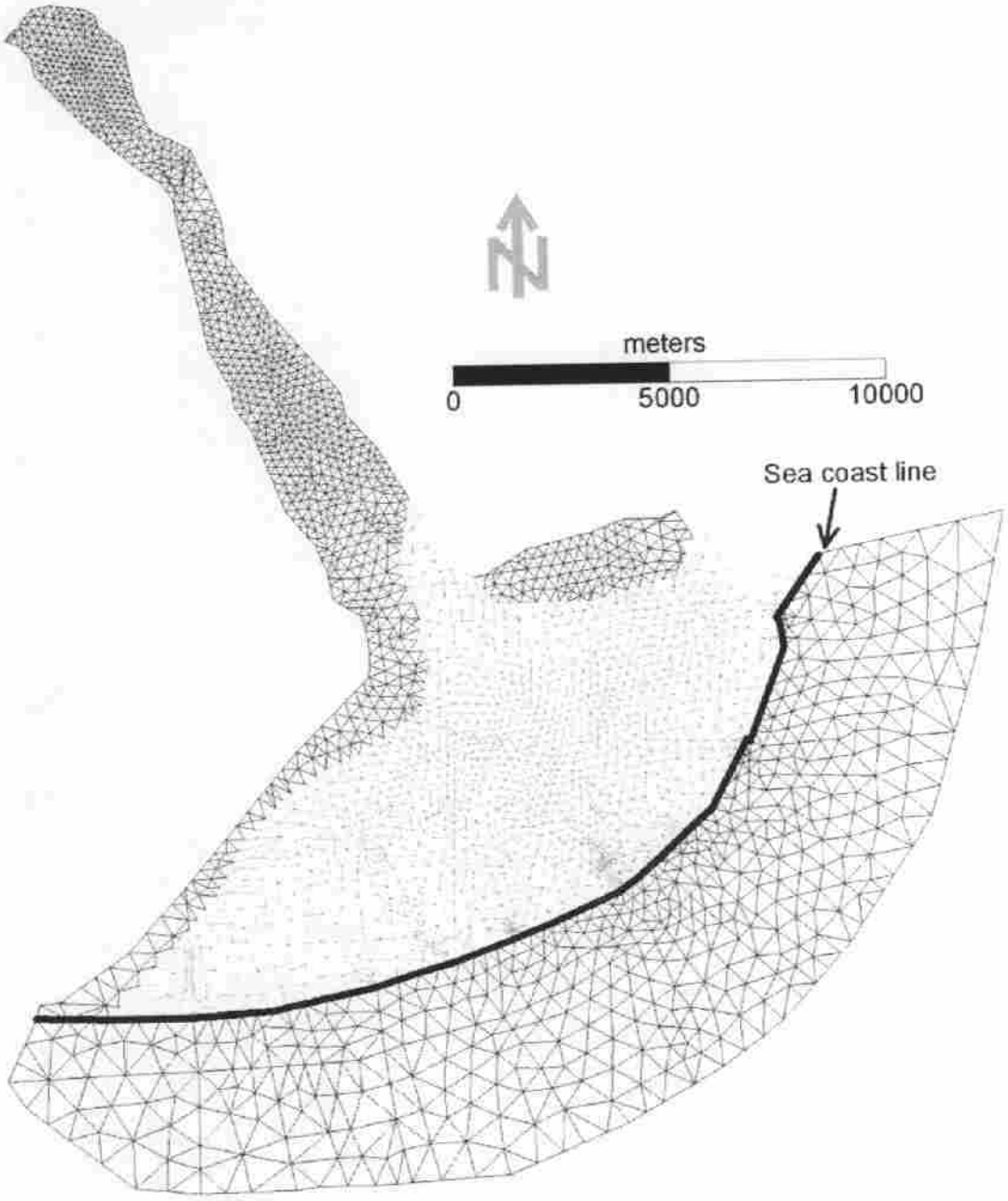

Figure 5.

Figure 6.

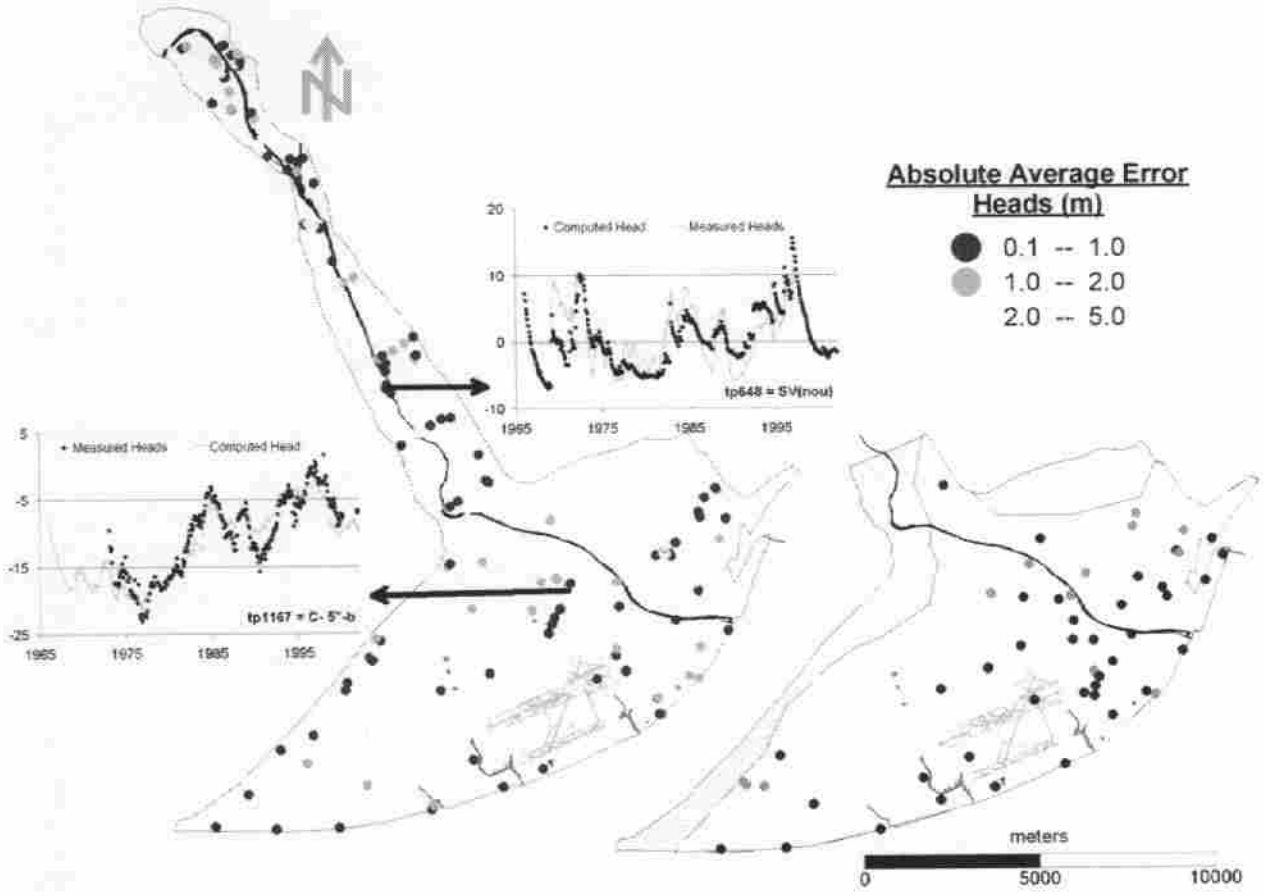
Absolute Average Error
Heads (m)
0.1 -- 1.0
1.0 -- 2.0
2.0 -- 5.0
Computed Head
Measured Heads
tp648 = SV(nou)
Measured Heads
Computed Head
tp1167 = C- 5"-b
meters
0
5000
10000

Figure 7.

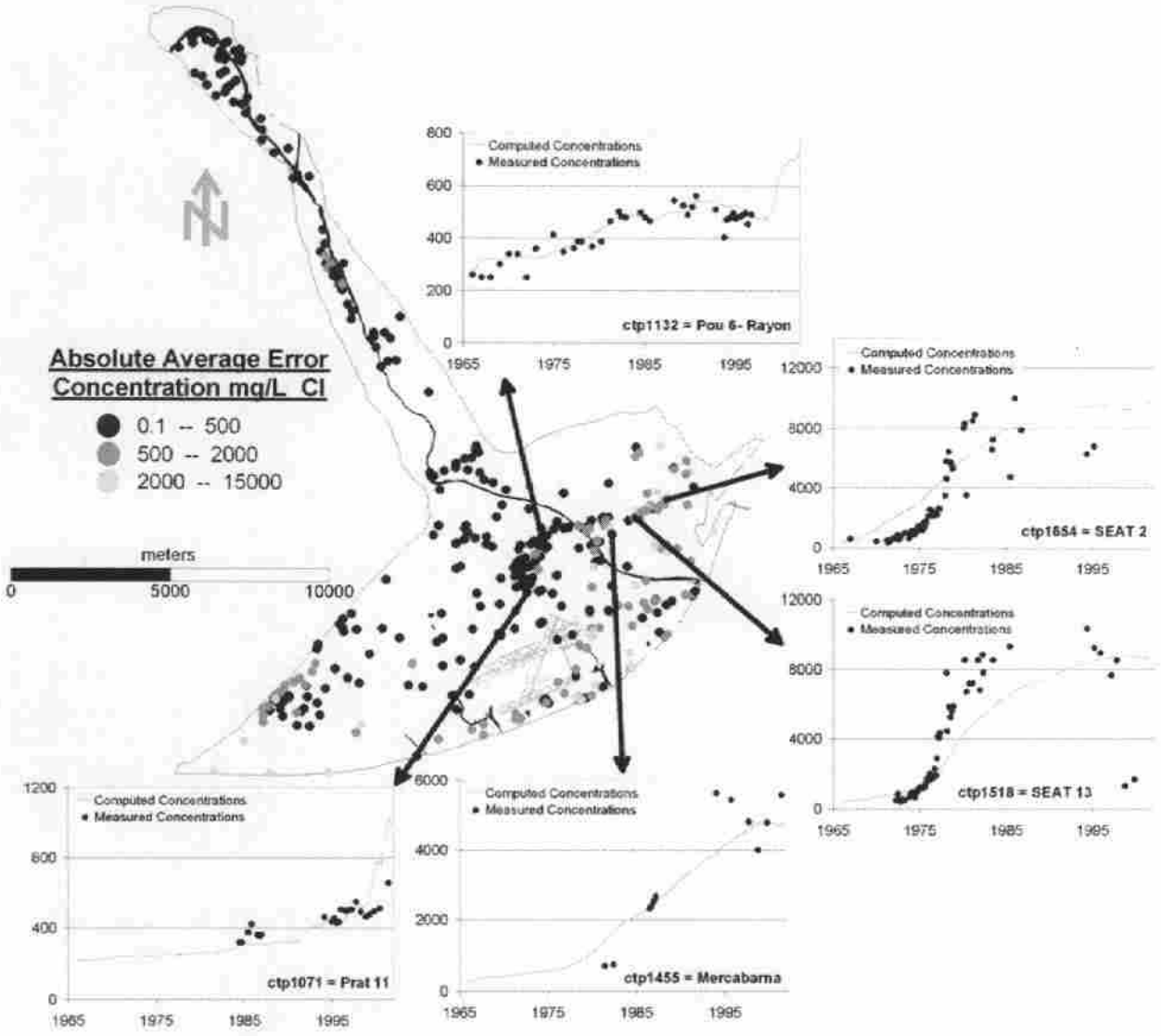
Absolute Average Error
Concentration mg/L Cl
0.1 -- 500
500 -- 2000
2000 -- 15000
meters
0
5000
10000
Computed Concentrations
Measured Concentrations
ctp1132 = Pou 6- Rayon
ctp1654 = SEAT 2
ctp1518 = SEAT 13
ctp1071 = Prat 11
ctp1455 = Mercabarna
1965
1975
1985
1995

Figure 8.

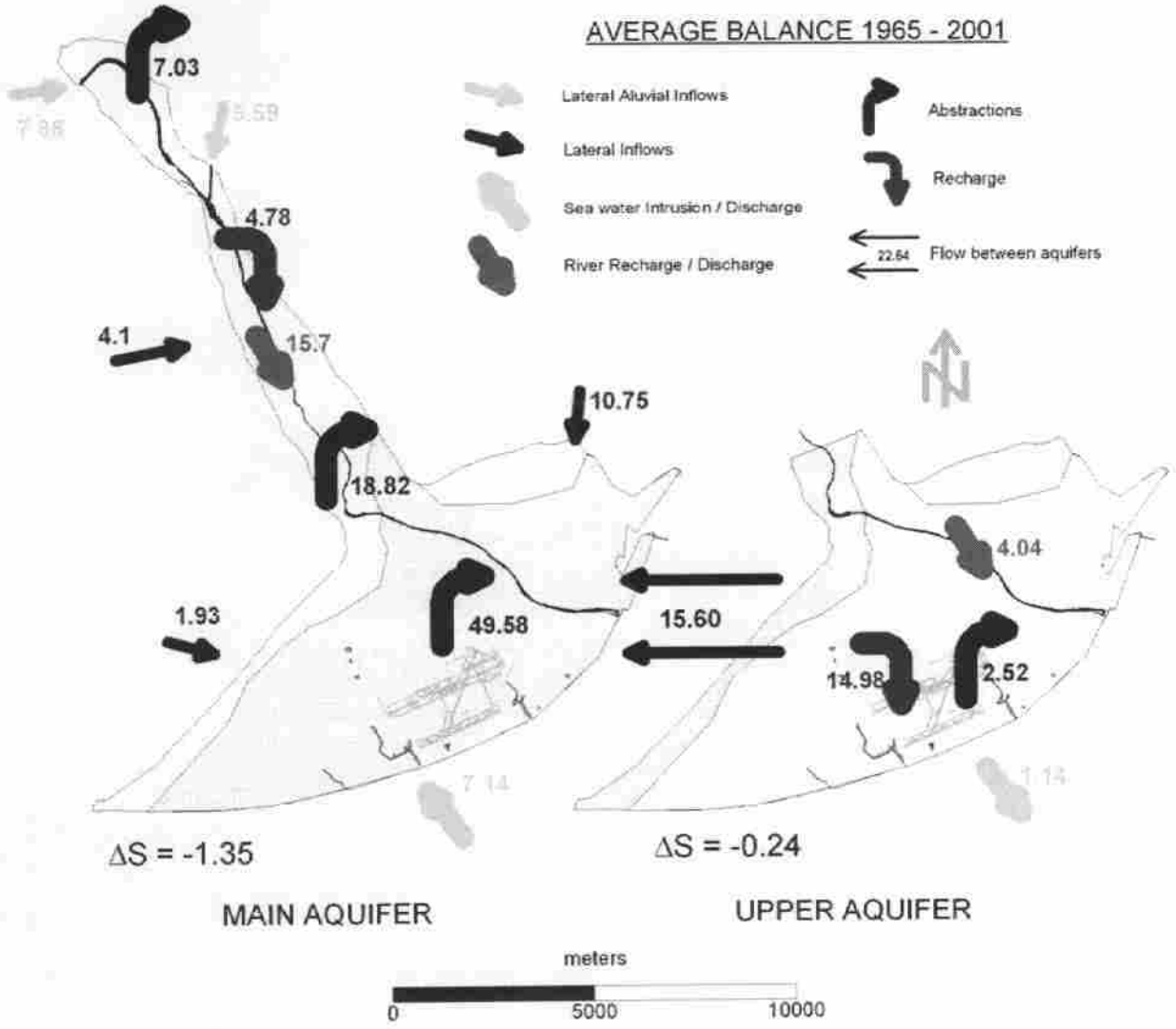
AVERAGE BALANCE 1965 - 2001
Lateral Aluvial Inflows
Lateral Inflows
Sea water Intrusion / Discharge
River Recharge / Discharge
Abstractions
Recharge
22.64
Flow between aquifers
7.03
4.78
4.1
15.7
10.75
18.82
1.93
49.58
15.60
4.04
14.98
2.52
ΔS = -1.35
ΔS = -0.24
MAIN AQUIFER
UPPER AQUIFER
meters
0
5000
10000

Figure 9.

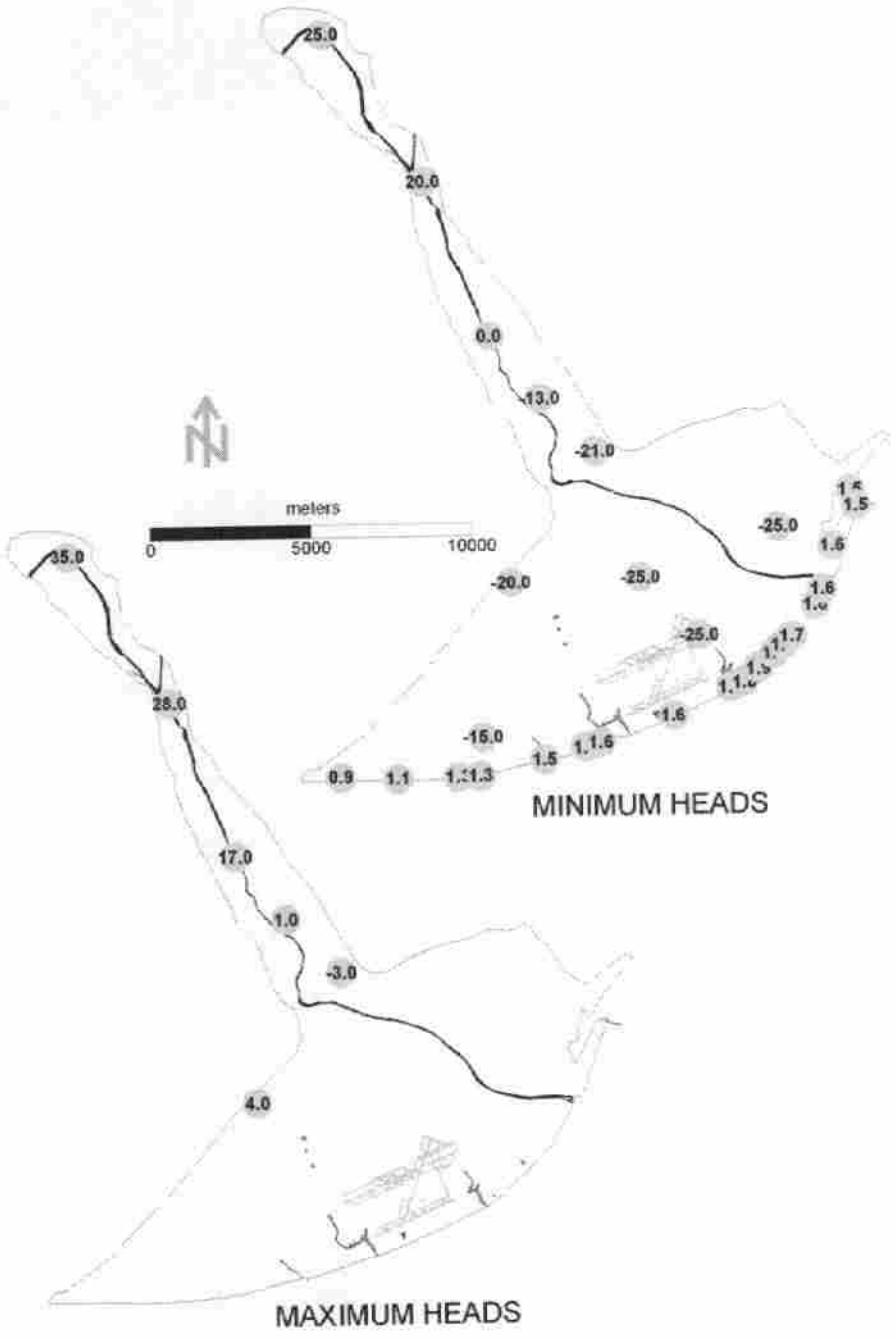
25.0
20.0
0.0
-13.0
-21.0
meters
0
5000
10000
-25.0
-20.0
-25.0
-25.0
35.0
28.0
-15.0
0.9
1.1
1.5
MINIMUM HEADS
17.0
1.0
-3.0
4.0
MAXIMUM HEADS

Figure 10.

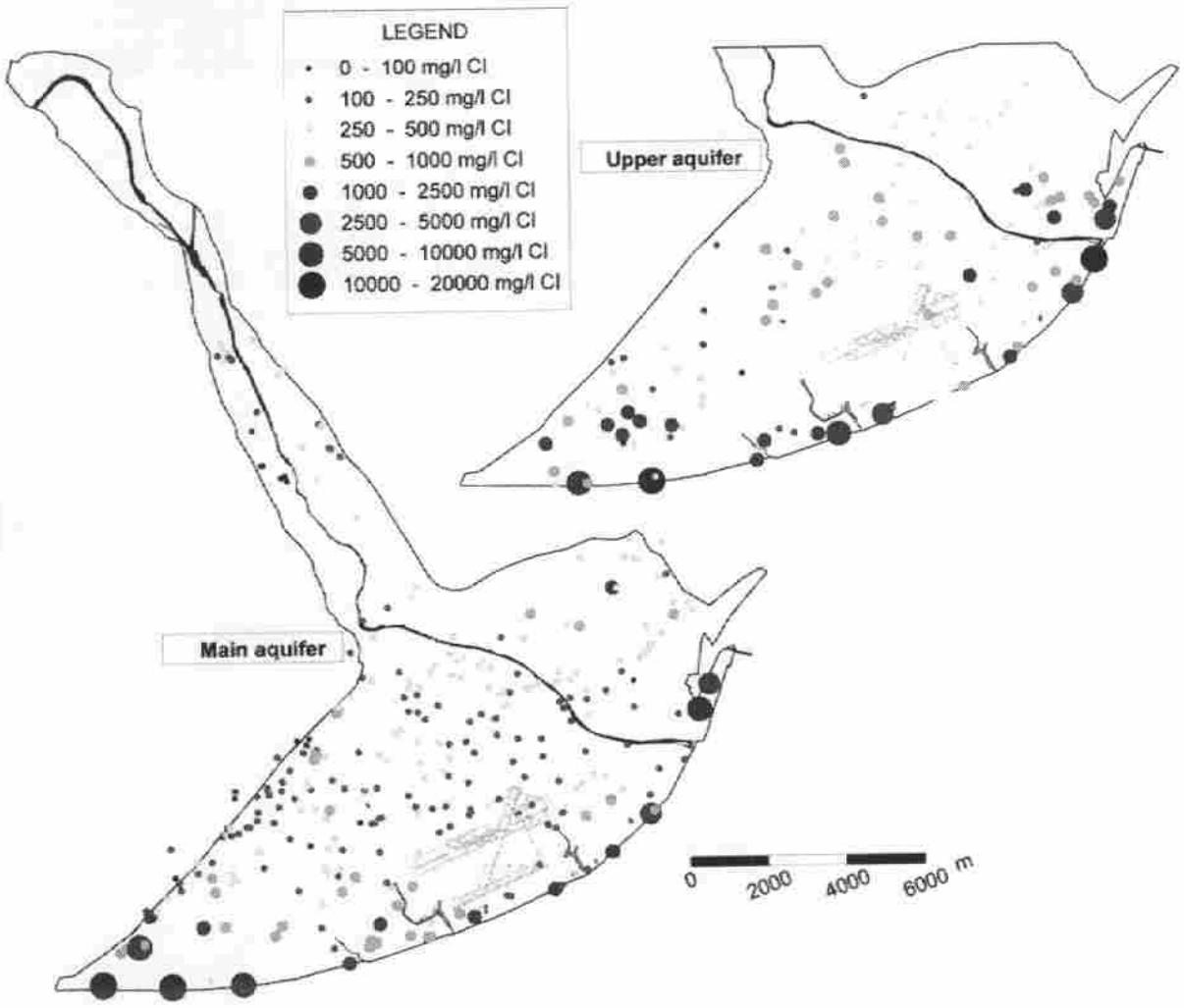
LEGEND
0 - 100 mg/l Cl
100 - 250 mg/l Cl
250 - 500 mg/l Cl
500 - 1000 mg/l Cl
1000 - 2500 mg/l Cl
2500 - 5000 mg/l Cl
5000 - 10000 mg/l Cl
10000 - 20000 mg/l Cl
Upper aquifer
Main aquifer
0
2000
4000
6000 m

Figure 11.

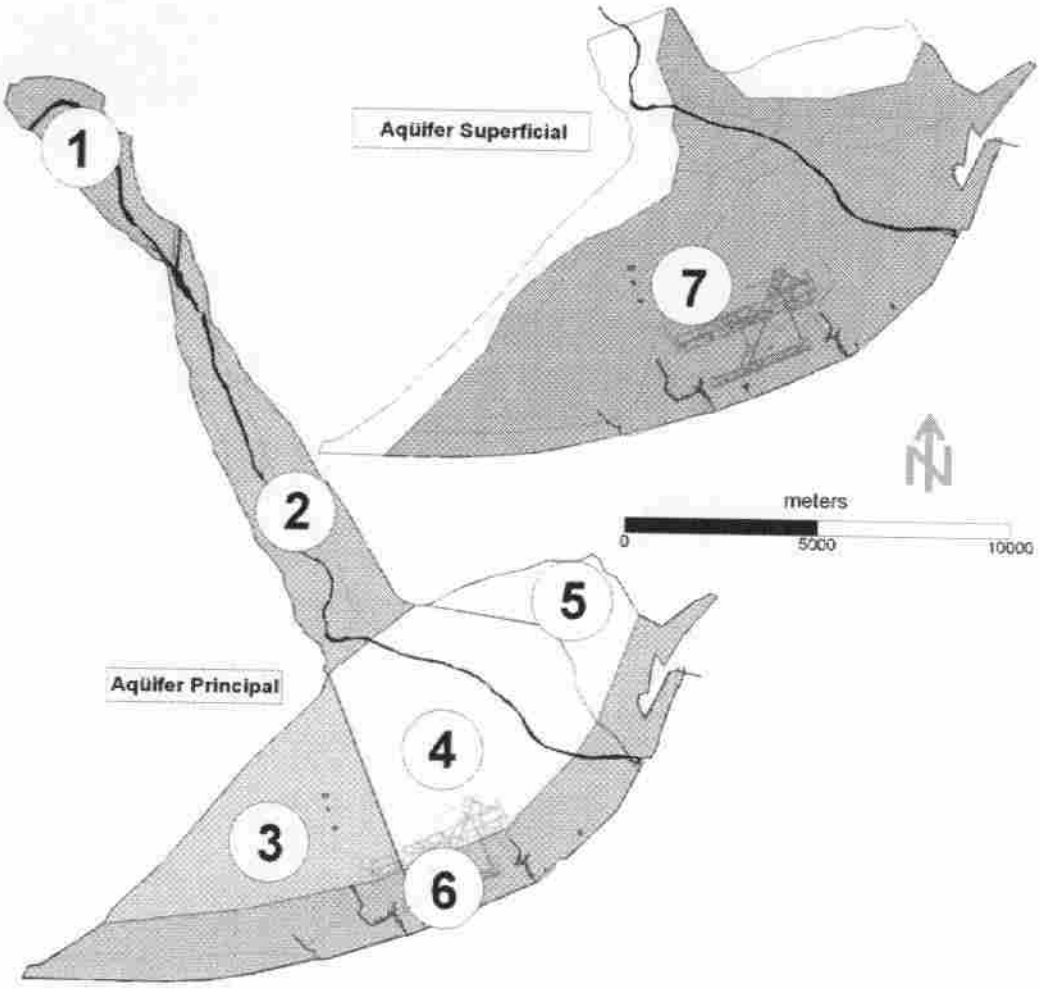
Aqüifer Superficial
Aqüifer Principal
1
2
3
4
5
6
7
meters
0
5000
10000

Figure 12.

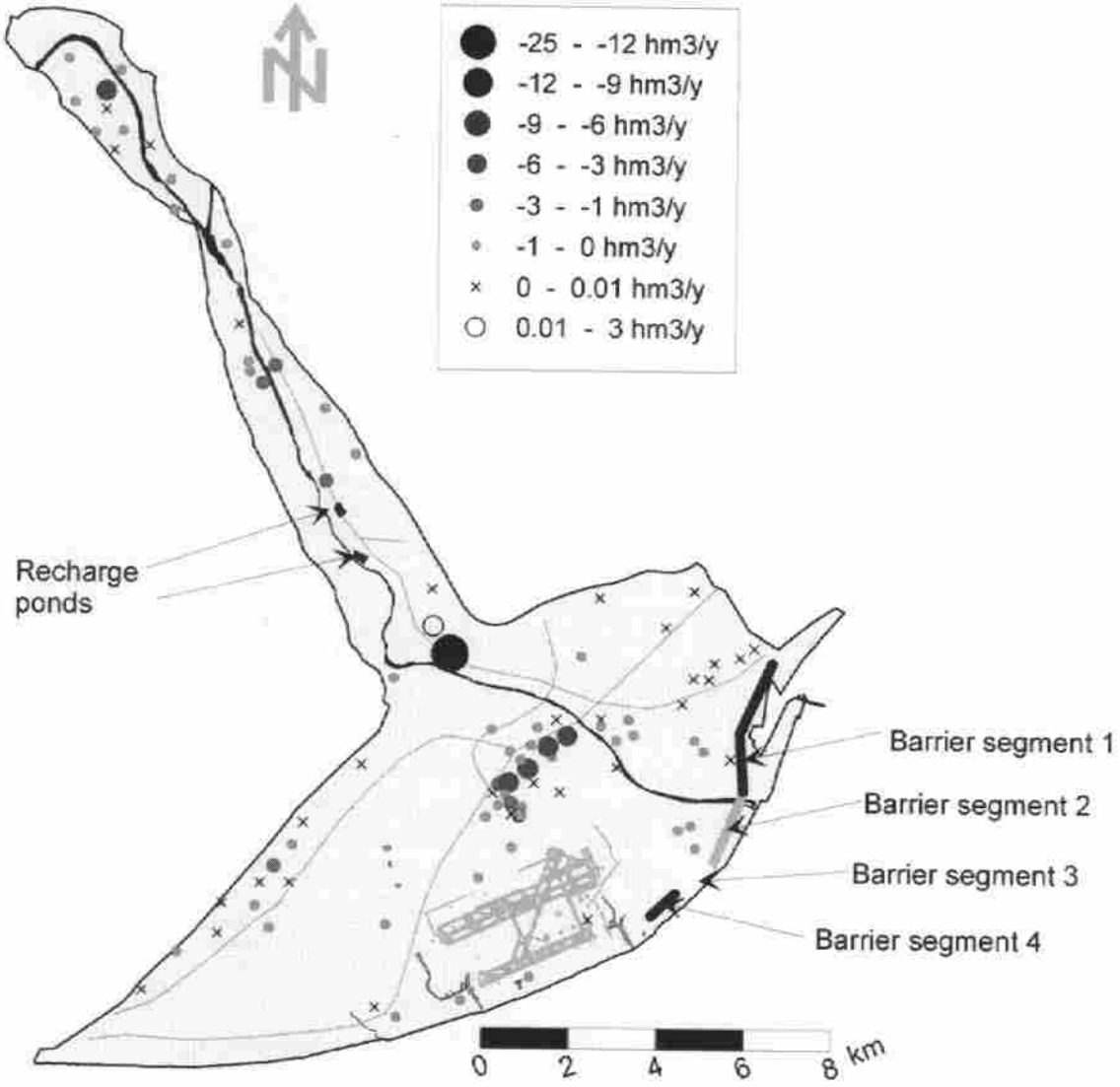
-25 - -12 hm3/y
-12 - -9 hm3/y
-9 - -6 hm3/y
-6 - -3 hm3/y
-3 - -1 hm3/y
-1 - 0 hm3/y
0 - 0.01 hm3/y
0.01 - 3 hm3/y
Recharge ponds
Barrier segment 1
Barrier segment 2
Barrier segment 3
Barrier segment 4
0 2 4 6 8 km

Figure 13.

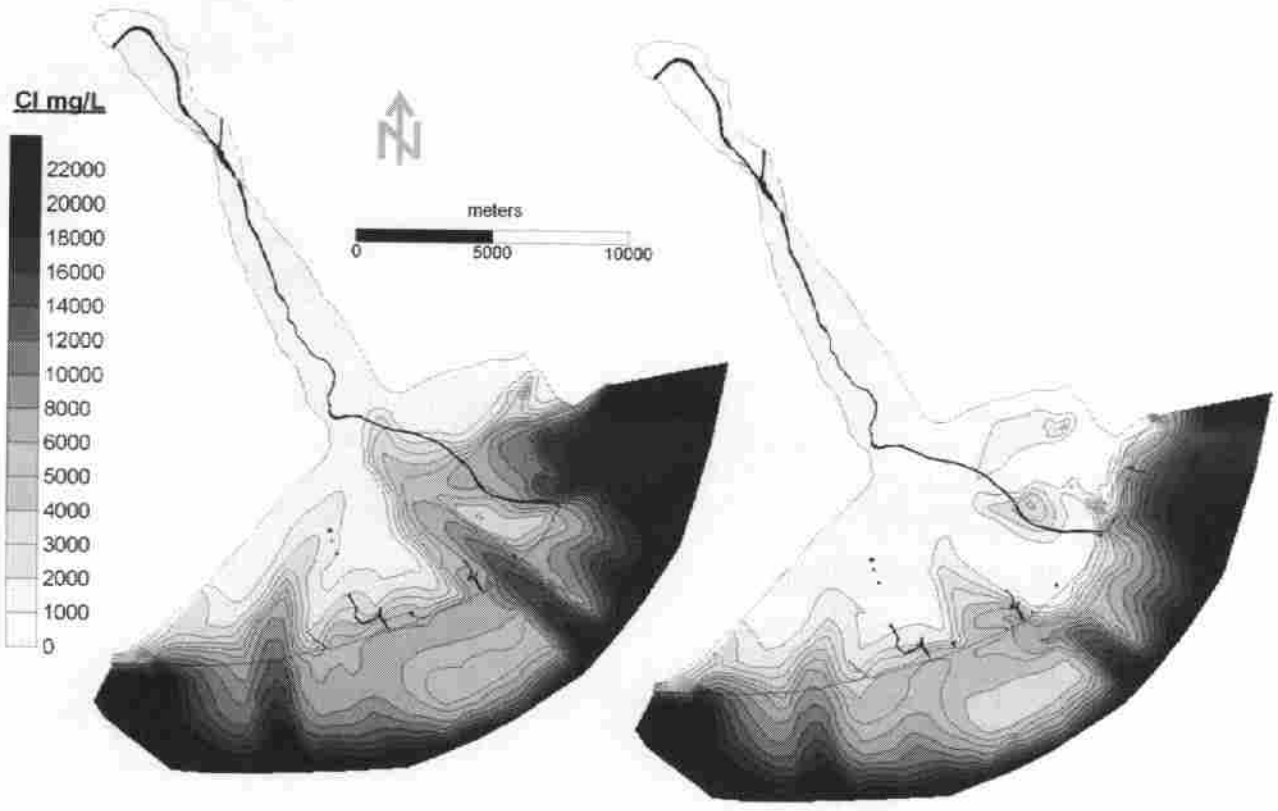
Cl mg/L
22000
20000
18000
16000
14000
12000
10000
8000
6000
5000
4000
3000
2000
1000
0
N
meters
0
5000
10000

Figure 14.

WATER RESOURCES RESEARCH, VOL. ???, XXXX, DOI:10.1029/,

Optimal design of measures to correct seawater intrusion

Elena Abarca, Enric Vázquez-Suñé, Jesús Carrera, Bernardo Capino, Desiré Gámez and Francisco Batlle

Dept. of Geotechnical Engineering & Geoscience, Technical University of Catalonia, Spain

---

Hydrogeology Group, Dept. of Geotechnical Engineering and Geoscience, School of Civil Engineering, Technical University of Catalonia, Build. D-2, Campus Nord, 08034 Barcelona, Spain (elena.abarca@upc.es)

Abstract.

Numerous studies have been devoted to optimization of groundwater management strategies in coastal aquifers. However, little has been done to address the problem of initially contaminated aquifers, which is the objective of this paper. To this end, we compare two optimization methods. The first one is linear and consists of maximizing pumping rates while constraining heads to prevent seawater inflow. The second one consists of minimizing the variation from current pumping rates, so as to preserve existing rights, while constraining concentrations, which leads to a non-linear programming problem. In both cases, corrective measures include potential reduction of pumping rates, inland artificial recharge and a coastal hydraulic barrier. Not surprisingly, the non-linear problem leads to a more efficient solution, both in terms of pumping rates and actual clean-up of the aquifer. Still, the linear formulation yields insights on the optimal allocation of pumping. More importantly, the linear formulation allows one to easily evaluate the hydraulic efficiency (gain in pumping rate per unit increase in recharge rate) of corrective measures. The fact that it is consistently larger than 1 proves that the hydraulic barrier acts not only by increasing resources but also by protecting the existing ones. Therefore, we conclude that both should be used.

1. Introduction

Seawater intrusion is a widespread contamination phenomenon affecting coastal semi-arid areas where groundwater becomes a critical factor for economical and demographic growth. High pumping rates cause groundwater heads to fall below sealevel inducing the inland flow of the denser saltwater. Many coastal aquifers are nowadays affected by seawater intrusion. They require corrective actions to restore groundwater quality or, at least, to reverse current negative trends. These can be grouped in actions over the demand (i.e. reduce pumping), actions aver the recharge (i.e. artificial recharge and territorial planning), relocation of pumping wells and additional engineering solutions (i.e. seawater intrusion barriers). The decision of the selected management policy is subject to a number of constraints including: strategic nature of the aquifer; existing infrastructures that may affect the relocation of pumping wells; and historical rights that require maintaining not only abstraction rates but also water quality as close as possible to the present ones. A compromise between groundwater needs and groundwater quality is needed. This compromise is hard to maintain when the final goal is to reverse the qualitative status of the already contaminated aquifer. Precautionary corrective measures are not applicable once a portion of the aquifer is affected by seawater intrusion. The recovery of groundwater quality is usually a very slow process as seawater intrusion is the result of a long term negative mass balance in the aquifer. Some actions to enhance the aquifer recovery are needed while helping to maintain pumping. An artificial increase on recharge or the construction of specific engineering measures such a seawater intrusion barrier are proposed to restore

groundwater quality in a coastal aquifer suffering from severe seawater intrusion problems.

Optimization is a classical tool to evaluate groundwater management alternatives. Optimization of groundwater resources has been subject of much research. Reviews of the topic are covered by *Gorelick* [1983], *Wagner* [1995] and *Ahlfeld and Heidari* [1994]. The latter contains a compilation of application to real cases.

Optimization problems are often aimed at maximizing overall pumping rate subject to some hydraulic or/and economic constraints, which leads to relatively easy formulations when heads depend linearly on flow rates. Unfortunately, this approach is not valid in coastal aquifers well connected to the sea, where the critical factor is the quality of the water. Application of quality constraints results in non-linear optimization problems since concentration is non-linearly related to the decision variables (groundwater abstraction). Still, optimization has been applied in the last decades to coastal aquifers using a broad range of formulations. Differential equations of groundwater flow and solute transport are solved using either analytical solutions [*Cheng et al.*, 2000; *Mantoglou*, 2003] or numerical simulation to represent the aquifer response. Numerical simulations of exclusively groundwater flow have been used [*Hallaji and Yazicigil*, 1996; *Zhou et al.*, 2003] using equivalent freshwater heads as constraints to prevent seawater intrusion. In other cases, seawater intrusion has been explicitly simulated using a sharp interface model [*Emch and Yeh*, 1998; *Rao et al.*, 2003; *Mantoglou*, 2003; *Mantoglou et al.*, 2004; *Park and Aral*, 2004] or chloride transport models [*Gordon et al.*, 2000]. Some of these used density dependent flow models [*Das and Datta*, 1999a, b]. However, computational cost restricted its application to relatively simple hypothetical cases. In fact, not only simulation cost, but also

optimization complexity increases when density variations are taken into account, which may lead to highly non-linear and non-convex problems [*Finney et al.*, 1992].

The choice of optimization method is ideally determined by nature of the decision variables (discrete or continuous), the linearity of the problem (degree of nonlinear dependence of objective function and constraints on decision variables), the continuity of the objective function, the availability of information for the derivatives and the potential existence of a local minima [*Cheng et al.*, 2000]. Therefore, it is not surprising that many different objective functions and sets of constraints have been applied. Some authors aim at maximizing the total pumping rate [*Shamir et al.*, 1984; *Hallaji and Yazicigil*, 1996; *Cheng et al.*, 2000; *Mantoglou*, 2003] while others aim at minimizing the salinity of the pumped water [*Das and Datta*, 1999a, b] or the volume of saltwater into the aquifer [*Finney et al.*, 1992; *Emch and Yeh*, 1998]. *Emch and Yeh* [1998] and *Gordon et al.* [2000] also include the pumping cost into the objective function. It is also possible to consider a multiobjective optimization problem [*Shamir et al.*, 1984; *Emch and Yeh*, 1998; *Das and Datta*, 1999a; *Park and Aral*, 2004]. Constraints applied in those studies include maximum and minimum pumping rates [*Hallaji and Yazicigil*, 1996; *Emch and Yeh*, 1998; *Das and Datta*, 1999a; *Cheng et al.*, 2000; *Zhou et al.*, 2003], toe location [*Cheng et al.*, 2000; *Mantoglou*, 2003; *Mantoglou et al.*, 2004; *Rao et al.*, 2004; *Park and Aral*, 2004] , groundwater heads [*Hallaji and Yazicigil*, 1996; *Emch and Yeh*, 1998; *Zhou et al.*, 2003], flow potential [*Mantoglou*, 2003; *Mantoglou et al.*, 2004] or salt concentration of the pumped water [*Gordon et al.*, 2000; *Das and Datta*, 1999a, b].

The above mentioned papers provide interesting methodological developments and often yield insights on how best pump coastal aquifers. Yet, actual application to real aquifers are scarce [*Shamir et al.*, 1984; *Willis and Finney*, 1988; *Finney et al.*, 1992; *Hallaji and Yazicigil*, 1996; *Zhou et al.*, 2003; *Mantoglou et al.*, 2004] This may reflect the complexity of coupling real aquifer dynamics and optimization methods. In fact, none of these applications deal with aquifers already affected by seawater intrusion. Instead, they typically aim at maximizing pumping while preventing seawater intrusion. They can hardly been applied to aquifers that are already salinized, such as the Llobregat delta's main aquifer, which motivates this work.

The objective of this work is to design optimal corrective measures to enhance a qualitative trend reversal in this aquifer. Reduction in current pumping rates along with the implementation of two additional corrective measures are considered (artificial recharge and a hydraulic barrier). Two classical optimization methodologies have been tested to asses groundwater management alternatives and design corrective measures in the main aquifer of the Llobregat delta.

2. Methodology

Two different methods are applied to asses the feasibility and to quantify the effectiveness of the proposed measures. A groundwater flow and chloride transport model is combined with two different optimization methods. In the first one heads constraints are used to ensure a gradient reversal along the coast line, which leads to a linear optimization problem. The second method consists of maximizing the amount of water pumped subject to quality constraints resulting in a non-linear optimization problem. The results

of both methodologies are compared and the drawbacks and advantages of each method are discussed. The basic steps to follow are:

1. Groundwater flow and transport model construction and calibration
2. Definition of the reference scenario
3. Optimization process
   (i) Problem formulation
   (ii) Solution of the optimization problem

The first two steps follow standard modelling approaches. Here, we focus on the description of the two optimization procedures:

2.1. Linear optimization problem

Our objective is to maximize the amount of water pumped subject to head constraints. The objective function is expressed as:

$$Q_{opt} = \sum Q_i \qquad i = 1, ..., M \tag{1}$$

where Q_i the pumping rates in each of the M pumping areas.

Constraints can be applied in a certain number (N) of control points at any time into the simulation period. Those control points can be divided into two groups: inland and coastal control points. Constraints applied to inland points control drawdowns produced by pumping, either to ensure that heads remain above a minimum (i.e., to prevent drying a wetland) or below a maximum (i.e., to prevent flooding a landfill). Constraints at coastal points aim at reversing the hydraulic gradient along the coast. Head is required to stay above the equivalent freshwater head of seawater at that particular location. The objective of these coastal control points is to try to reverse seawater intrusion only by

constraining heads (notice this concept is only valid in relatively thin aquifers, where vertical variations of salinity can be neglected). In our case, head constraints are applied at the end of the simulation period as

$$h_{j_{min}} \leq h_{j_0} - \Sigma Q_i \mathcal{A}_{ij} \leq h_{j_{max}} \tag{2}$$

where h_{j_0} is the groundwater head for the unstressed aquifer at the j^{th} control point, $h_{j_{max}}$ and $h_{j_{min}}$ are, respectively, the maximum and minimum allowed head at the j^{th} control point and $\mathcal{A}_{ij}$ is the response matrix, defined as the calculated drawdown at point j in response to a unit pumping in well i (actually, pumping will be grouped by zones).

Constraints in the maximum allowed pumping rate may also be applied:

$$Q_i \leq Q_{max_i} \tag{3}$$

where Q_{max_i} is the maximum allowed pumping rate at well i

The same type of constraints can be applied to any corrective measure implemented into the optimization process. To asses where freshwater injection is most efficient, the corrective measure (i.e., a barrier) can be divided into segments and the constraint applied is the total amount of water that is projected to be injected through the whole corrective measure by applying:

$$Q_{design_i} = \sum Q_{seg_i} \tag{4}$$

where Q_{design_i} is the projected pumping rate to be injected in a corrective measure i and Q_{seg_i} the injection rate in each of the segments in which the corrective measure has been divided.

Maximizing Equation 1 subject to constraints 2, 3 and 4 results in a linear problem. We have used IMSL [*IMSL MATH/LIBRARY*, 1997] routines to solve it.

One of the outputs of linear programming codes is the shadow price of each constraint. The shadow price is the Lagrange multiplier of the constraint. It represents the sensitivity of the objective function to the value imposed to the constraint, hence the term price. It expresses the marginal cost (in terms of objective function units) of a unit increase in the constraint. Thus, inactive constraints yield zero shadow price because the objective function is not sensitive to them. For management purposes, shadow prices may be as useful, if not more, as the actual optimal solution. They allow expressing, in terms of the objective function, the cost of any active constraints. We will use them to evaluate the hydraulic efficiency of corrective measures (i.e., the ratio between the increase in pumping rate per unit increase in recharge rate). As such, they will allow us to answer the question of weather or not a recharge barrier implies a net gain of resources or not.

2.2. Non-linear optimization problem

In coastal aquifers, groundwater abstraction is linked to groundwater quality, therefore, it may be necessary to evaluate whether the projected alternatives warrant a minimum groundwater quality. Considering that one of the goals is to protect existing water rights, the objective is to determine a pumping rate regime, as close as possible to the current one and the corrective measures needed to obtain a final good groundwater qualitative status. To achieve this goal, constraints in concentration can be imposed at some control points at any time into the simulation time. Since concentration is non linearly related to groundwater abstraction, the resulting optimization problem is non-linear. The problem

is somewhat simplified by considered that maximum pumping rates lead to generalized intrusion (in fact, this is the current situation along the Llobregat shores). Therefore, if concentration is constrained to be below a certain threshold at a point where intrusion is known to occur, such constraint will be active. Knowing which are the active constraints allows us to substitute the constraint by a penalty function in the objective function. We have used the penalty function of Courant [*Fletcher*, 1985]:

$$c_i \leq c_i^* \quad active \Rightarrow c_i = c_i^* \sim min \frac{c_i - {c_i^*}^2}{{\sigma_i}^2} \tag{5}$$

where c_i is the computed concentration at the i-th control point, c_i^* is the desired (maximum) concentration at such point and σ_i is the penalty's tolerance, which allows one to impose variable weights on each constraint (penalty). Actually c_i will tend to be slightly larger than c_i^*. However, they can be forced to be as close as possible as wished by reducing σ_i. Using Equation 5 together with the desired pumping and recharge rates allows us to substitute the general optimization problem by the minimization of the multiobjective function:

$$F = \lambda_c \sum_{i=1}^{N} \frac{(c_i^* - c_i)^2}{\sigma_{c_i}^2} + \lambda_Q \sum_{j=1}^{M} \frac{(Q_j^* - Q_j)^2}{\sigma_{Q_j}^2} + \lambda_R \sum_{k=1}^{L} \frac{(R_k^* - R_k)^2}{\sigma_{R_k}^2} \tag{6}$$

where N, M and L are the number of control points, pumping zones and additional corrective measures, respectively; Q_j^* the desirable pumping rate for the j flow zone; Q_j the calculated flow for the j flow zone; R_k^* the desirable injection rate in the k corrective measure; R_k the calculated injection for the k corrective measure; σ_{Q_j} and σ_{R_k} are tolerance parameters (analogous to σ_{c_i}) for the j-th flow zone and the k-th corrective measure; λ_c, λ_Q and λ_R are the weights of the objective function of concentration, pumping rates and corrective measures, respectively. The tolerance parameters allows varying

the importance assigned to each objective. Notice that for the concentration term, λ_c is equivalent to the σ parameter of *Fletcher* [1985]. The method calls for performing sequential optimization runs with increasing λ_c while dropping those control points whose concentrations do not satisfy Equation 5 (i.e., those for which c_i is strictly smaller than c_i^*). However, in practice, we performed some preliminary runs to find appropriate λ's and obtained satisfactory results.

With this formulation, the resulting problem is similar to that of parameter estimation. We have used the method of *Medina and Carrera* [1996] for minimizing Equation 6.

3. CASE STUDY: Application to the Llobregat Delta Main aquifer

3.1. Background and problem statement

The Llobregat's Delta is located South of Barcelona city (Spain) (Figure 1). It is a quaternary formation considered a classical example of a Mediterranean Delta controlled by fluvial and coastal processes (i.e., storms and long-shore drift). Geological studies [*Marqués*, 1984; *Simó et al.*, 2005] consider the Delta as formed by an Upper Complex (Q4 in Figure 2) and a Lower Complex (Q3, Q2 and Q1 in Figure 2). The Upper Complex is a typical stratigraphic delta sequence. The Lower Complex is formed by three fluvial systems associated to three currently submerged paleodeltas.

Hydraulically, the prodelta silts of Q4 act as a confining unit separating the permeable upper units from a very thin and basal very permeable layer of reworked gravels and beach's sands. This thin layer together with the upper gravels of Q3 constitute the Main aquifer of the Llobregat delta, object of this study. It is a horizontally large aquifer (around 100 km^2) of uniform thickness of 15-20 m and with higher transmissivity zones associated to the paleochannel systems of Q3 (Figure 3). The presence of this higher permeability

channels are of extreme importance for the optimal management of this aquifer.

The Llobregat delta is well-known since numerous studies have been carried out in this area since the 60's, among others, the hydrogeological synthesis works by *MOP* [1966]; *PHPO* [1985] and more recently *Iribar and Custodio* [1992]; *Iribar* [1992]. At the end of the 70's, when salinization problems became increasingly worrying, hydrochemistry works improved the knowledge of the aquifer systems and the mechanisms that cause seawater intrusion in the main aquifer of the Llobregat delta [*Custodio et al.*, 1976; *Custodio*, 1981; *Manzano et al.*, 1992; *Bayó et al.*, 1977; *Doménech et al.*, 1983], etc. Some groundwater flow models have been also developed for the Main Aquifer, named Lower Aquifer in previous works, [*Cuena and Custodio*, 1971; *PHPO*, 1985; *Custodio et al.*, 1989; *Iribar et al.*, 1997; *Vázquez-Suñé et al.*, 2005c]. Chloride distribution (Figure 5) shows how seawater intrusion affects large areas of the delta.

Our objective is to assess sustainable management alternatives in this aquifer as well as to correct the current salinization problem. The goal is to reverse the negative trends and recover the natural quality existing 35 years ago. Abstraction rates should remain as close as possible to current values. To achieve this goal two sets of corrective measures are considered: (1) to reduce current pumping rates, and (2) a coastal barrier and upland artificial recharge ponds. Designing the latter implies assessing where and which are most efficient as well as a quantification of the needed recharge/injection rates.

3.2. Groundwater flow and solute transport model construction and calibration

A two-layer areal model was built to simulate groundwater flow and chloride transport in the Llobregat delta aquifers. The fact that concentration are well mixed in the vertical direction and that the aquifer thickness is small compared to the horizontal extent, supports the use of a two-dimensional horizontal model. Two dimensional models can take into account the density differences by working with freshwater equivalent heads in points with high salinity as in the seaside boundary [*Iribar et al.*, 1997].

The flow and transport problem uses a finite element grid of 4354 nodes and 9698 elements, divided in two layers. The temporal variability of the main terms of the groundwater mass balance makes necessary to evaluate the management alternatives with a transient simulation model that takes into account the temporal variability in all sinks and source terms. The simulation time for the calibrated model corresponds to the period from 1965 to 2001. Model parameters are divided into zones representing the aquifer heterogeneity. The value of the parameters are considered constant in each zone. The main aquifer inputs are the recharge from rain infiltration along with the recharge from the river during flood events [*Vázquez-Suñé et al.*, 2005a, b] while the main output is groundwater abstraction. Inputs from surrounding aquifers is also considered as well as interaction with surface flow (rivers, drainage systems, lakes, etc.)

Parameter values were updated during the calibration process. Automatic adjustments were carried out with the code TRANSIN-IV [*Medina and Carrera*, 2003], starting from the prior information available of every parameter. The code minimizes an objective func-

tion that considers the differences between measured and calculated head and/or concentrations, as well as the likelihood of calculated parameters [*Medina and Carrera*, 1996]. Therefore, the code needs measured heads and concentrations at the defined observation points. The observation points provide a good coverage of the model domain. Head data at many observation points extends ever almost the whole calibration period (1965-2001). However, the concentration data are more disperse in time. Parameter values obtained from calibration are consistent with prior information. The obtained fit both in terms of heads (Figure 4) and chloride concentrations (Figure 5) are considered satisfactory. The calibrated model was validated with additional data (2002-2004) showing a reasonable fit between measured and calculated data (Figures 4 and 5)

3.3. Definition of a reference scenario

The model needs to be updated to be used as a management tool. As it will be applied to optimized future management strategies, some assumptions about the future behaviour of the main terms of the water balance are needed. These assumptions are subject of uncertainty. To evaluate this uncertainty some scenarios related to pumping rates, city growth and infrastructures have been considered. All of them showed that current abstractions are not sustainable in the sense that seawater intrusion progressed further inland in all the considered cases.

One of these scenarios was chosen as the reference to compare optimization results against. It considerers the following assumptions:

- For the simulation/optimization period (2002-2036) meteorology was taken equal to that of 1965-2001. It includes both long dry periods and long wet periods.

• Pumping history assumed for future years is the average of the last five years (1997-2001) for all wells except for the main pumping area (AGBAR) whose temporal variability of the last five years have been repeated along the simulation period.

• Location of the current pumping wells is maintained. The distribution of wells and the reference pumping rate used in this application are shown in Figure 6.

3.4. Management model

Optimization was applied to groups of existing wells defined as management polygons. Six polygons or management areas were defined in the main aquifer of the Llobregat Lower Valley. Five of them were defined according to geological, hydrological and management criteria. The sixth area, located along the coast, was defined for linear optimization requirements, as explained later. An equity principle was applied to the pumping wells located in the same management area, so that, if necessary, pumping rates are reduced in the same proportion at all pumping wells. Figure 7a shows the six management zones defined in this aquifer.

Two actions are considered, first to exclusively reduce the pumping rates and second, to increase the available resource by designing some additional corrective measures that help to maintain the current pumping rates. The considered additional measures are:

1. Recharge ponds to artificially increase the recharge. Two recharge ponds are proposed on the alluvial part of the main aquifer. The total area proposed is about 11 ha with a projected infiltration rate of 0.25 m/d., resulting in a total projected recharge of 11 hm^3/y. The location of the proposed ponds is indicated in Figure 6

2. A seawater intrusion barrier (hereinafter, referred as barrier). A freshwater injection barrier, divided in four sections according to the different transmissivity zones defined in the numerical model, is proposed in the eastern part of the coast. The four segments are located on the management Zone 6, however three of them are located in front of the management Zone 4 and one in the management Zone 5. Segment 1 is located over a preferential flowpath caused by the paleochannel C structure in Figure 3. The optimization problem allows one to optimally distribute the total amount of water injected into the four segments. This total projected injection rate is 3.65 hm^3/y.

3.5. Linear optimization problem

The objective is to maximize the total amount of water pumped so that, at the end of period of 35 years, heads are between a prescribed minimum and maximum head constraints. The constraints were applied to 30 control points spread all over the aquifer, 19 of them located along the coast (Figure 7b). Applied head constraints depend on the point location into the aquifer:

Minimum head constraints were applied to 25 control points. Minimum historic heads were applied to 6 inland control points located in the confined aquifer. h_{min} was set equal to the equivalent freshwater head of seawater at the other 19 points located along the coast, therefore, imposing a seawards hydraulic gradient.

Maximum and minimum head constraints were applied to 5 control points located in the unconfined portion of the aquifer. Maximum head was also constrained because of the risk of affecting underground structures in the urban area and of washing out some dangerous landfills buried along the fluvial valley. Minimum head constraint at that points was considered as 1/3 of the saturated thickness at that point.

As a starting point, no restriction were applied to pumping rates in the management areas. However, the total injection into the recharge ponds and the barrier was set equal to the projected values. In the case of the barrier, the total injected water is specified and the model optimizes the distribution of the total injection into the four defined segments. (11 hm^3/y for the ponds and 3.65 hm^3/y for the barrier).

Linear optimization results

Application of linear programming may lead to absurd results when the constraints are inappropriate. Therefore, care must be exercised to identify unrealistic solutions. Specifically, attention should be placed in Dirichlet and Cauchy boundary conditions. While these boundary conditions may be necessary for modelling, they can act as unrealistic source terms for management problem (e.g., pumping near a Dirichlet boundary may lead to huge pumping rates with small computed drawdowns). Eliminating these problems required careful scrutiny and motivated some of the constraints discussed earlier. In fact, we started the optimization process with five management zones. Results showed that the first division was not appropriated to linear programming. Originally, zones 3, 4 and 5 reached the coast. Since those zones contained pumping wells located close to the coast line and strict minimum head constraints, it was impossible to pump water from any of the three zones. Therefore, a long and thin additional management zone, the sixth in Figure 7a, was delineated parallel to the coast. This zone was defined to eventually be a dead zone in terms of pumping, since the constraints would not allow in any case to pump water from it.

Evolution towards more reasonable results was also achieved by adding lateral constraints (Equation 3) to the pumping rates allowed per management zone. The motivation of these additional constraints is to approach to the current pumping rates that should be, if possible, preserved due to the strong existing rights. The change in the results in terms of the obtained total abstraction and its distribution per management zones, compared to the current values (REF. Q), are presented in Figure 8 when no additional corrective measures are taken into account. If no lateral constraints are added (OPT1 in Figure 8) the total amount of water that can be pumped is above current values. However, the result is not acceptable in terms of the pumping distribution. According to this result most water should be abstracted from the management zone that is farther away from the coast. This is caused, first, by the higher density of control points and the most strict constraints applied and, second, by the presence of one Cauchy boundary condition (Figure 6 that act as an unrealistic source of freshwater. Therefore, this result can not be considered trustworthy. Moreover, insufficient water can be pumped from the critical management areas (Zone 2 and 4, actually, zero from zone 4)), where the main drinking supply companies are located. This solution is not socially acceptable, therefore additional lateral constraints in the maximum allowed pumping rate per zone are imposed *ad hoc*. Additional constraints cause a reduction in the total objective function (OPT2-OPT6 in Figure 8). Only in the last two optimization problems (OPT5 and OPT6) can water be pumped from Zone 4, the later being the most similar to the existing pumping distribution (REF. Q in Figure 8). A trade-off between Zone 2 and Zone 4 is clearly observed in OPT4-6. Constraining pumping in Zone 2 causes a pumping increase in Zone 4, together with a slight reduction in the total abstraction. Both zones are located over a high transmissivity zone (paleochan-

nel C in Figure 3) and this trade-off shows how those zones compete for the same resource.

The evolution of the total abstraction, the distribution of pumping and the shadow prices when additional corrective measures are implemented into the optimization process are presented in Figure 9. Total abstraction is larger than in 8 because water is injected in the recharge ponds (10.96 hm^3/y) and in the seawater intrusion barrier (3.65 hm^3/y). In fact, the first three optimization scenarios yield total pumping above the reference values. However, here also, the distribution of the pumping present problems of absurdity. According to optimization results, no water can be pumped from Zone 4 and most water should be pumped from Zone 5, where little water is currently pumped. This zone was added into the optimization process to be available for future management scenarios. However, an underground structure acts as a drainage in this zone. This drainage is implemented as a Cauchy boundary condition, that, in the extreme case that the piezometric head goes below the infrastructure base, could acts as a unrealistic source of water. To avoid this effect the abstraction in this management zone has constrained to 1.8 hm^3/y. Although total abstraction is significantly reduced, pumping from Zones 2 and 4 is, that way, possible. In OPT4-6, the trade-off between Zone 2 and 4 is also observed. The most appropriate solution seems to be the obtained in OPT5 as it is the most similar to the existent distribution of the total abstraction being the reduction in the pumping rates that should be applied to Zones 2 and 4 about the 25% of the current values.

The shadow prices obtained for the two additional corrective measures proposed are also shown in Figure 9. These shadow prices quantify the hydraulic efficiency of each corrective

measure for each optimization scenario. The hydraulic efficiency of the recharge ponds is, in all cases lower than 1. That means that some of the injected resource is lost before it arrives to the active wells. This resource probably goes to the river in the part that drains the aquifer and to the drainage underground structures located in management Zone 5. The latter is evidenced by the higher efficiency calculated when the maximum abstraction in Zone 5 is not constrained and most water is pumped from this area. The hydraulic efficiency calculated for the last three more realistic optimization cases (OPT4-6) is of 0.69, i.e., almost the 70% of the water recharged through the ponds can be pumped from the active wells. However, the calculated efficiency for the seawater intrusion barrier is higher than 1 in all cases. This is a really relevant result as a efficiency higher than one means that more water than what is injected can be pumped when applying this corrective measure. Usually freshwater injection barriers are criticized as corrective measures because part of the injected water flows seawards and therefore part of the new resource is lost. Our results point out that although part of the injected water is indeed lost, the protecting effect of the barrier against incoming seawater is highly efficient, thus preserving a high amount of freshwater from being contaminated and, therefore, increasing total available resources. The calculated hydraulic efficiency changes with the lateral constraints. As happened for the recharge ponds, the efficiency is higher in the cases in which the maximum pumping rate in Zone 5 is not constrained (OPT1-3). In fact, it is linearly related to the pumping rate in Zone 5. It has to be remarked that the barrier was divided into 4 segments depending on the different transmissivity zones defined in the numerical model. The four segments are located on the management Zone 6 (Figure 7), however three of them are located in front of the management Zone 4 and one in the management zone

3 over the paleochannel C in Figure 3. The optimization problem allows to optimally distribute the total amount of water injected into the four segments. In scenarios OPT1-3 water is injected in the three segments located in front of Zone 5. However, when the maximum pumping rate in zone 5 is constrained, an abrupt decrease of the hydraulic efficiency is observed together with the reduction of the total abstraction. Furthermore, it is accompanied by a change in the segments where water is injected into the barrier. In cases OPT4-6, the optimal injection takes place exclusively in the segment located in front of the management Zone 4, over a hydraulic preferential path (paleochannel C in Figure 3 that communicated the barrier with the main pumping areas in Zones 2 and 4.

Considering critical to maintain a distribution of the total pumping similar to the current values, the best solution are obtained for OPT6 when no additional measures are considered and OPT5 when the recharge pond and the injection barrier are added. In the first case a reduction of more than the 50% of the pumping rates should be applied to Zones 2 and 4. In the latter, when corrective measures are added the reduction is limited to a 25% in the same zones.

Those calculated optimal pumping rates guarantee that head objectives imposed as constraints are achieved after 35 years. Regarding seawater intrusion, head constraints at the coastal points ensure a reversal of the hydraulic gradient after 35 years. However, this reversal may be not be sufficient to clean the aquifer areas that are currently affected by seawater intrusion. To check this point a transport simulation starting form the present chloride distribution was carried out with the optimal pumping rates calculated in OPT5

along with additional corrective measures. The concentration distribution obtained after 35 years is shown in Figure 10b where it is compared with the chloride distribution calculated after 35 years of pumping according to the reference values (Figure 10a). An improvement in the quality is observed, but the existing salt is still moving towards the pumping or drainage areas. Although the pumping rates have been reduced and corrective measures imposed, the good qualitative status can not be reached by simply optimizing hydraulic variables.

3.6. Non-linear optimization problem

The above results obtained suggest that maximum salinity should be used as a constraint to guarantee the recovery of water quality. The resulting non-linear problem is presented next.

Pumping and injection rates are optimized so that a desired chloride concentration is reached after 35 years at control points. To ensure good water quality throughout the domain, control points were located along the coastline at the same 19 locations used in the linear optimization problem. Desired concentrations at the end of the 35 years management period, c^*, and tolerance, σ_{c_i}, (recall equation 5) were set to 1000 mg/l of chloride. Therefore, final concentrations at the control points should not exceed significantly 2000 mg/l. In addition to the recharge ponds and injection barrier, two wells (Figure 6) were specified to pump 2500 m^3/day each, during the first ten years, to clean the saltwater trapped inland of the barrier. Optimization parameters used are presented in Table 1.

Management areas are those of the linear problem, except for Zone 6, which is no longer needed and was distributed among Zones 3, 4 and 5, as originally planned.

Minimizing the objective function as presented in 6, yields the values of Q_{well} for each pumping area and Q_R for the recharging measures.

Non-linear optimization results

Results are summarized in Figure 11 by comparison to reference pumping rates and projected recharge values. It should be noticed that pumping can be maintained at current rates if corrective measures are applied with larger recharge rates than originally planned. In fact, recharge should increase by 50% at the ponds and by 200% at the seawater intrusion barrier.

These results were obtained with the values of λ presented in Table 1, being λ_Q a hundred times larger than λ_c. Placing a higher stress in the pumping rate function, the obtained pumping rates are forced to be close to the desired values while relaxing concentration objectives. In fact, concentration results in our case, are twice the desirable values at some of the control points, but being always inside the range of tolerance. A higher value of λ_c leads to better concentration results in detriment of the pumping rate objectives.

A transport simulation with the optimized pumping and recharge rates is shown in Figure 12b to asses the effectiveness of the methodology. The concentration distribution after 35 years is presented and compared with the chloride distribution calculated with the reference scenario, i.e., the current pumping rates (Figure 12a). The areas already contaminated, located at the left margin of the delta, are almost recovered with the optimized pumping and recharge rates. Some salty islands are still present, probably due to a poor election of the location of the two pumping wells to extract salt trapped inland

of the barrier or may be because the pumping period (ten years) was not long enough. A more specific work would be necessary to optimal design this pumping location and the pumping duration.

Other result that differs from the linear problem is the distribution of the injection water into the barrier segments. In the best linear results (OPT5 in Figure 9) optimal recharge at the barrier was concentrated into the segment 4 (Figure 6) because it coincides with a high permeability channel connected with inland pumping. However, in the non-linear problem the injection is almost equidistributed because to accomplish quality criteria is necessary to inject along the whole barrier

3.7. Comparison of the results

Considering critical to maintain a distribution of the total pumping similar to the current values, the best solutions obtained from both methods are presented in Table 2.

Two solutions are presented for the linear optimization method: with and without additional measures. When no additional measures are considered a reduction of more than the 50% of the pumping rates should be applied to Zones 2 and 4. If recharge ponds and the injection barrier are added the reduction is limited to a 25% in the same zones. Those values will be applicable for managing an uncontaminated or still unstressed aquifer. However, as the aquifer already suffers from seawater contamination, these reduction into the abstraction is not sufficient to recover a good quality of the aquifer. Still, this simple methodology gives important information to asses the hydraulic efficiency of each considered corrective measure. In this case, the hydraulic efficiency for the ponds is always lower than 1 while for the seawater intrusion barrier is about 1.5, resulting a much

more efficient corrective measure.

The non-linear problem quantifies how much water should be artificially recharged to maintain the total current abstraction as well as its current distribution guaranteeing a groundwater quality recovery. This method offers a good estimation of injection rate to design efficient corrective measures.

4. Conclusions

Linear and non-linear optimization methodologies can be used to design remediation measures for aquifers affected by seawater intrusion. Both provide different results and insights on coastal aquifers management.

Linear programming is easy and can effectively ensure that heads remain above sea level, thus ensuring that seawater will not penetrate. As such, it is appropriate for evaluating sustainable pumping rates and for evaluating the efficiency of hydraulic corrective measures (reduction of pumping rates, inland recharge through ponds and coastal injection barriers). However, as posed here, it is not appropriate for designing remediation measures.

Shadow prices remain an interesting subproduct of linear programming by allowing one to assess the effect of constraints. Here, we have used them to evaluate the hydraulic efficiency of recharge corrective measures (i.e. the net increase in total pumping per unit increase in recharge). We have found that coastal hydraulic barriers are more efficient

than inland recharge ponds.

This contradicts the widely extended belief that coastal injection is inefficient because it looses water to the sea. While this is true, the net gain obtained from protection of inland pumping more than compensates this loss. On the other hand, the hydraulic efficiency of inland recharge ponds was consistently less than one. This implies that, in a coastal aquifer, protecting existing freshwater from mixing is more efficient than just increasing freshwater resources. Optimization allows one to quantify this efficiency.

The non-linear optimization method with chloride concentration constraints is more complex, but provides a reliable assessment of the required corrective measures. In fact, as formulated here, where the objective was to keep existing pumping rather than maximizing it, the non-linear methods yields realistic solutions, while the linear method required numerous runs to sequentially constraint pumping rates that were too high. Moreover, the non-linear formulation is specially useful to design remediation measures for aquifers that are initially suffering seawater intrusion . Since corrective measures are usually analyzed well after the aquifer has been contaminated, we conclude that their design requires the nonlinear optimization problem.

The application of these methodologies to a real aquifer affected by seawater intrusion, and more specifically to a socially and hydraulically complex aquifer was a new challenge. In this case, the combined use of both methods was successfully applied to designing management alternatives in the main aquifer of the Llobregat delta.

Acknowledgments. This work was funded by the European Commission (SALTRANS project, contract EVK1-CT-2000-00062), the Catalonian Water Agency (ACA) and the Spanish Geological Survey (IGME). The first author was supported by the Catalonia Government with a FI doctoral scholarship and by the Technical University of Catalonia (UPC) with a scholarship to finish the PhD thesis. The authors would like to thank also to the community of end-users of the Llobregat delta aquifers (CUADLL) for their support and help.

References

Ahlfeld, D., and M. Heidari (1994), Applications of optimal hydraulic control to groundwater systems, *J. Water Resour. Plann. Manage.*, *120*(3), 350–365.

Bayó, A., E. Batista, and E. Custodio (1977), Sea water encroachment in Catalonia coastal aquifers, in *General Assembly IAH. Birmingham 1977*, vol. XIII, pp. F.1–14.

Cheng, A., D. Halhal, A. Naji, and D. Ouazar (2000), Pumping optimization in saltwater-intruded coastal aquifers, *Water Resour. Res.*, *36*(8), 2155–2165.

Cuena, S., and E. Custodio (1971), Construction and adjustment of a two layer mathematical model of the Llobregat Delta, Barcelona, Spain, in *Mathematical Models in Hydrology, Studies and Reports in Hydrology*, vol. 15, pp. 960–964, UNESCO, Paris.

Custodio, E. (1981), Sea water encroachment in the Llobregat delta and Besós areas, near Barcelona (Catalonia, Spain)., in *Sea Water Intrusion Meeting: Intruded and Fosil Groundwater of Marine Origin.*, vol. 27, edited by U. S. G. Undersökning, pp. 120–152.

Custodio, E., F. Cacho, and M. Peláez (1976), Problemática de la intrusión marina en los acuíferos del Delta del Llobregat., in *Segunda Asamblea Nacional de Geodesia y Geofísica, Barcelona.*, pp. 2069–2101, Instituto Geofísico y Catastral Madrid.

Custodio, E., L. Glorioso, M. Manzano, and E. Skupien (1989), Evolución y alternativas de un acuífero sobreexplotado: el Delta del Llobregat, in *Sobreexplotación de acuíferos*, pp. 207–227, International Association of Hydrologists (Spanish Group)-AEHS, Almeria.

Das, A., and B. Datta (1999a), Development of multiobjective management models for coastal aquifers, *J. Water Resour. Plann. Manage.*, *125*(2), 76–87.

Das, A., and B. Datta (1999b), Development of management models for sustainable use of coastal aquifers, *J. Irrigat. Drain.*, *125*(3), 112–121.

Doménech, J., E. Batista, A. Bayo, and E. Custodio (1983), Some aspects of sea water intrusion in Catalonia (Spain), in *8th SWIM. Bari.*, edited by I. di Geología Appicata e Geotecnia, p. 15, Bari.

Emch, P., and W. Yeh (1998), Management model for conjunctive use of coastal surface water and ground water, *J. Water Resour. Plann. Manage.*, *124*(3), 129–139.

Finney, B., Samsuhadi, and R. Willis (1992), Quasi-3-dimensional optimization model of jakarta basin, *J. Water Resour. Plann. Manage.*, *118*(1), 18–31.

Fletcher, R. (1985), *Practical Methods of optimization*, vol. II, John Wiley and sons, Chichester, England, 224 pp.

Gordon, E., U. Shamir, and J. Bensabat (2000), Optimal management of a regional aquifer under salinization conditions, *Water Resour. Res.*, *36*(11), 3193–3203.

Gorelick, S. (1983), A review of distributed parameter groundwater-management modeling methods, *Water Resour. Res.*, *19*(2), 305–319.

Hallaji, K., and H. Yazicigil (1996), Optimal management of a coastal aquifer in southern Turkey, *J. Water Resour. Plann. Manage.*, *122*(4), 233–244.

IMSL MATH/LIBRARY (1997), *FORTRAN Subroutine for Mathematical Applications*, Visual Numerics, Inc, Houston, Texas.

Iribar, V. (1992), Evolución hidroquímica e isotópica de los acuíferos del Baix Llobregat (Barcelona, España), Ph.D. thesis, Universitat de Barcelona (UB).

Iribar, V., and E. Custodio (1992), Advancement of seawater intrusion in the Llobregat delta aquifer, in *SWIM Study and Modelling of Saltwater Intrusion into Aquifers*, edited by E. Custodio and A. Galofre, pp. 35–50, CIMNE–UPC, Barcelona.

Iribar, V., J. Carrera, E. Custodio, and A. Medina (1997), Inverse modelling of sea water intrusion in the Llobregat delta deep aquifer, *J. of Hydrol.*, *198*(1–4), 226–244.

Mantoglou, A. (2003), Pumping management of coastal aquifers using analytical models of saltwater intrusion, *Water Resour. Res.*, *39*(12), 1335.

Mantoglou, A., M. Papantoniou, and P. Giannoulopoulos (2004), Management of coastal aquifers based on nonlinear optimization and evolutionary algorithms, *J. of Hydrol.*, *297*(1-4), 209–228.

Manzano, M., Custodio, E., and J. Carrera (1992), Fresh and salt water in the Llobregat delta aquifer: application of ion chromatography to the field data, in *SWIM Study and Modelling of Saltwater Intrusion into Aquifers*, edited by E. Custodio and A. Galofre, pp. 207–228, CIMNE–UPC, Barcelona.

Marqués, M. (1984), Les formacions quaternàries del delta del Llobregat., Ph.D. thesis, Universitat de Barcelona (UB). Institut d'Estudis Catalans, 208 pp., Barcelona.

Medina, A., and J. Carrera (1996), Coupled estimation of flow and solute transport parameters, *Water Resour. Res.*, *32*(10), 3063–3076.

Medina, A., and J. Carrera (2003), Geostatistical inversion of coupled problems: dealing with computational burden and different types of data, *J. of Hydrol.*, *281*(4), 251–264.

MOP (1966), Estudio de los recursos hidráulicos totales de las cuencas de los ríos Besós y Bajo Llobregat, *Tech. Rep. 4 vol*, CAPO-SGOP, Barcelona.

Park, C., and M. Aral (2004), Multi-objective optimization of pumping rates and well placement in coastal aquifers, *J. of Hydrol.*, *290*(1-2), 80–99.

PHPO (1985), Modelo de simulación de los acuíferos del delta del Bajo Llobregat. plan Hidrológico Nacional, *Tech. rep.*, Confederación Hidrográfica del Pirineo Oriental Comisaria de Aguas del Pirineo Oriental (PHPO).

Rao, S., B. Thandaveswara, S. Bhallamudi, and V. Srivivasulu (2003), Optimal groundwater management in deltaic regions using simulated annealing and neural networks, *J. Water Res. Manage.*, *17*(6), 409–428.

Rao, S., S. Bhallamudi, B. Thandaveswara, and G. Mishra (2004), Conjunctive use of surface and groundwater for coastal and deltaic systems, *J. Water Resour. Plann. Manage.*, *130*(3), 255–267.

Shamir, U., J. Bear, and A. Gamliel (1984), Optimal annual operation of a coastal aquifer, *Water Resour. Res.*, *20*(4), 435–444.

Simó, J., D. Gàmez, J. Salvany, E. Vàzquez-Suñé, J. Carrera, A. Barnolas, and F. Alcalà (2005), Arquitectura de facies de los deltas cuaternarios del río Llobregat, Barcelona, España, *Geogaceta*, *37*.

Vázquez-Suñé, E., J. Carrera, E. Abarca, and B. Capino (2005a), Estimation of recharge floods in disconnected sream-aquifers systems. Application to the Baix Llobregat aquifers, Barcelona, Spain., *Journal of Hydrology (submmited)*.

Vázquez-Suñé, E., et al. (2005b), Groundwater modelling as a tool for the European Water Framework Directive (WFD) application. The Llobregat case., *Phys. Chem. Earth, (submmited)*.

Vázquez-Suñé, E., et al. (2005c), Groundwater flow and saltwater intrusion modeling of the Low Valley and Llobregat Delta aquifers., in *Groundwater and saline intrusion. Selected papers from the 18th Salt Water Intrusion Meeting*, edited by L. Araguás, E. Custodio, and M. Manzano, pp. 693–705, IGME.

Wagner, B. (1995), Recent advances in simulation optimization groundwater-management modeling, *Reviews of Geophysics*, *33*, 1021–1028.

Willis, R., and B. Finney (1988), Planning-model for optimal-control of saltwater intrusion, *J. Water Resour. Plann. Manage.*, *114*(2), 163–178.

Zhou, X., M. Chen, and C. Liang (2003), Optimal schemes of groundwater exploitation for prevention of seawater intrusion in the Leizhou Peninsula in southern China, *Environ. Geol.*, *43*(8), 978–985.

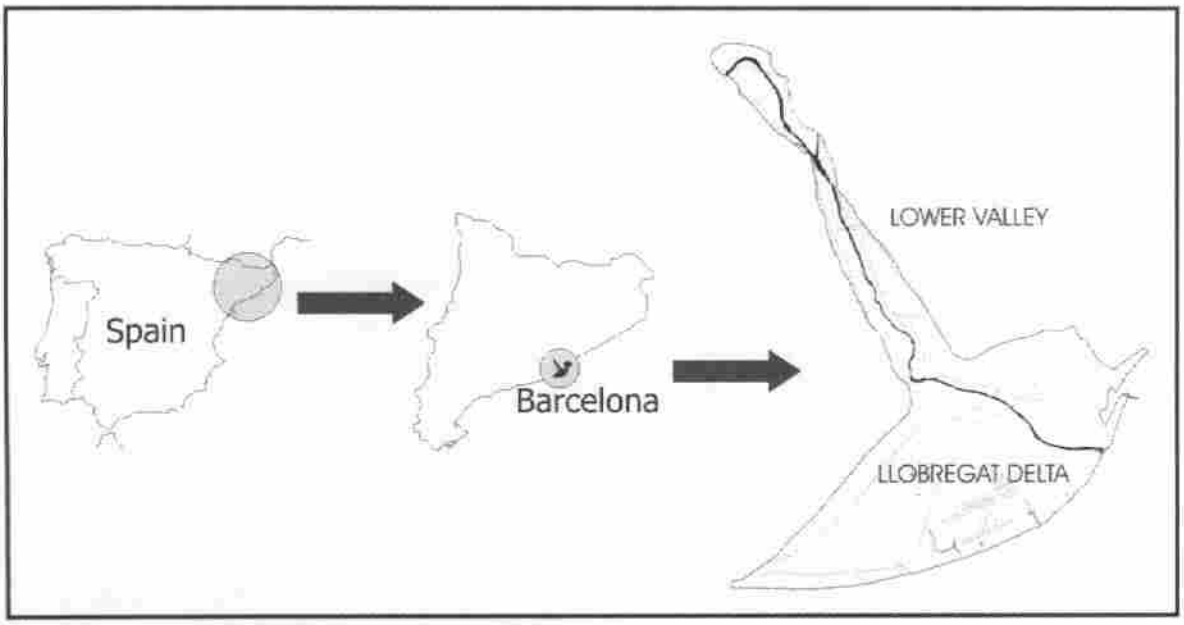

Figure 1. Location of the Llobregat delta and lower valley

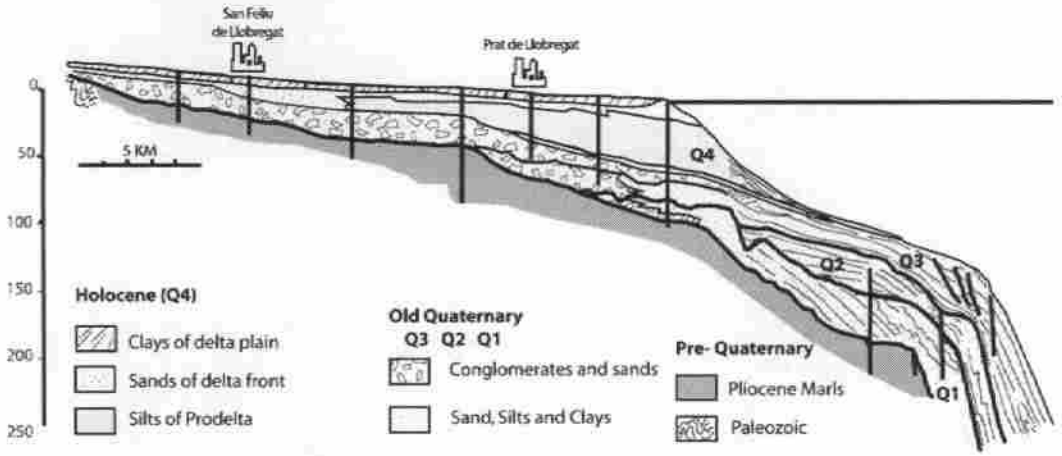

Figure 2. Modified from *Simó et al.* [2005]. Geological cross section perpendicular to the coast of the emerged and submerged Llobregat delta. The very thin layer below the silts off Q4 and the upper gravels of Q3 form the Main aquifer studied in this work. Notice that they are well separated from the shallow aquifer by the prodelta silts, so that the main aquifer is effectively confined and relatively thin.

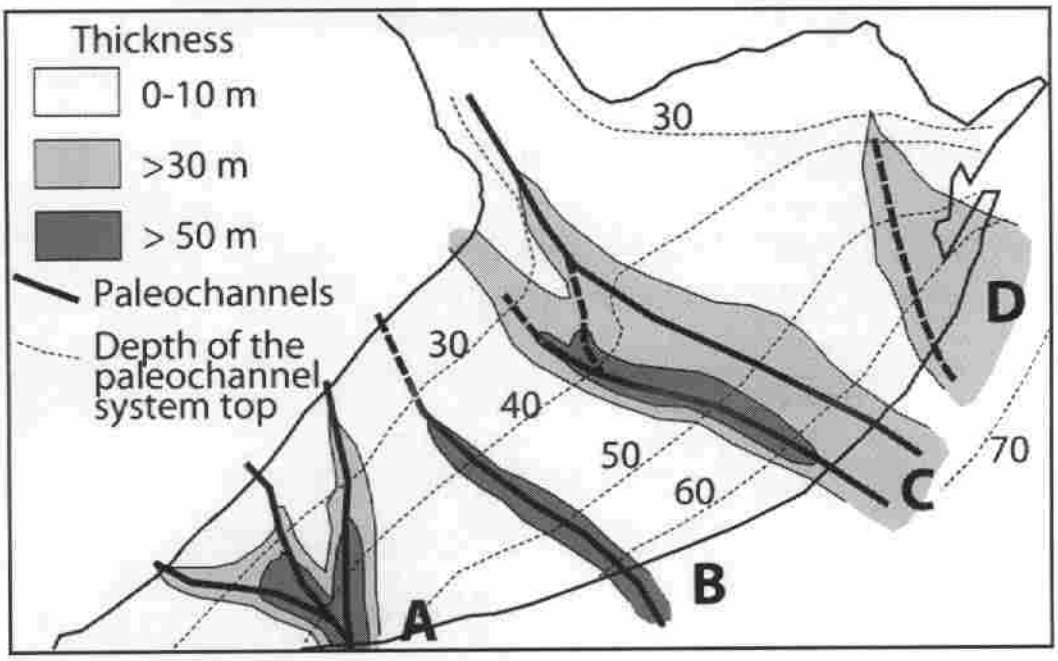

Figure 3. Modified from *Simó et al.* [2005]. Paleochannel systems (A, B, C) associated to the main aquifer of the Llobregat delta. Those paleochannels correspond to high permeability zones that may act as preferential seawater intrusion pathways and that make transmissivity distribution highly heterogeneous.

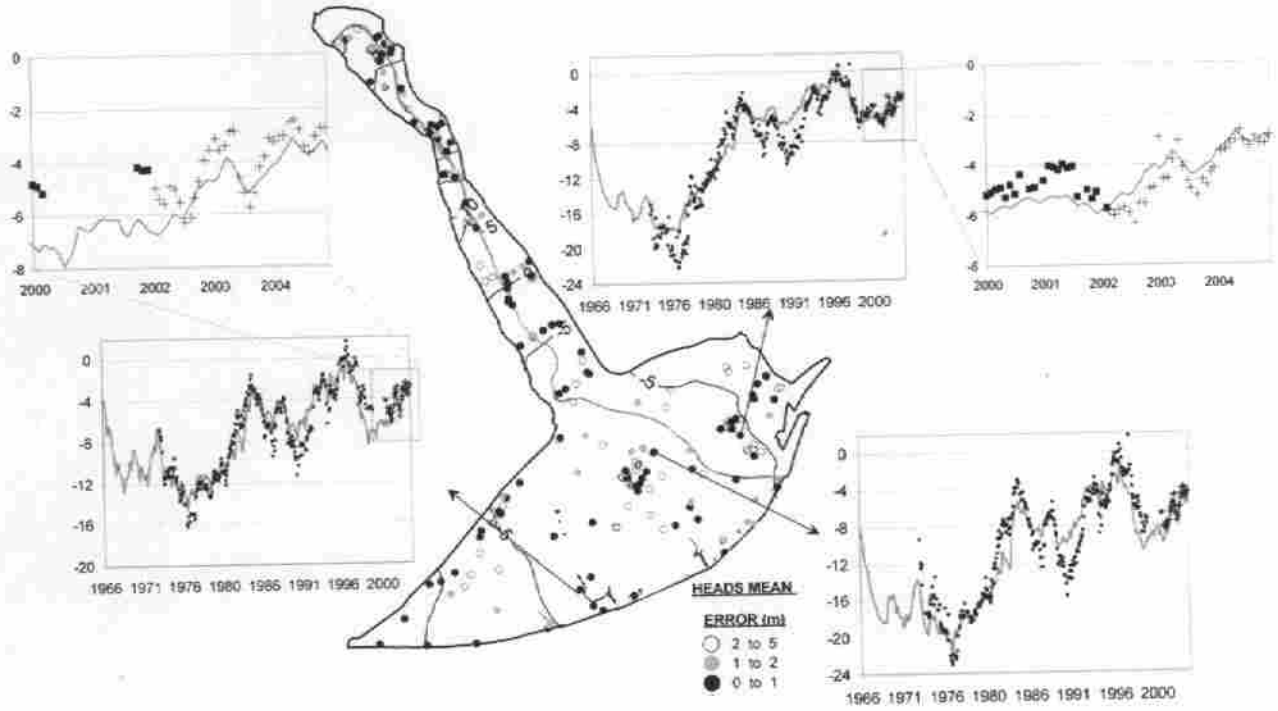

Figure 4. Piezometric map calculated for December 2001 together with the heads mean error and the calculated versus measured heads in four observation points. Calculated heads are plotted in a gray line, measured data used for calibration in black dots and data used for model validation in crosses.

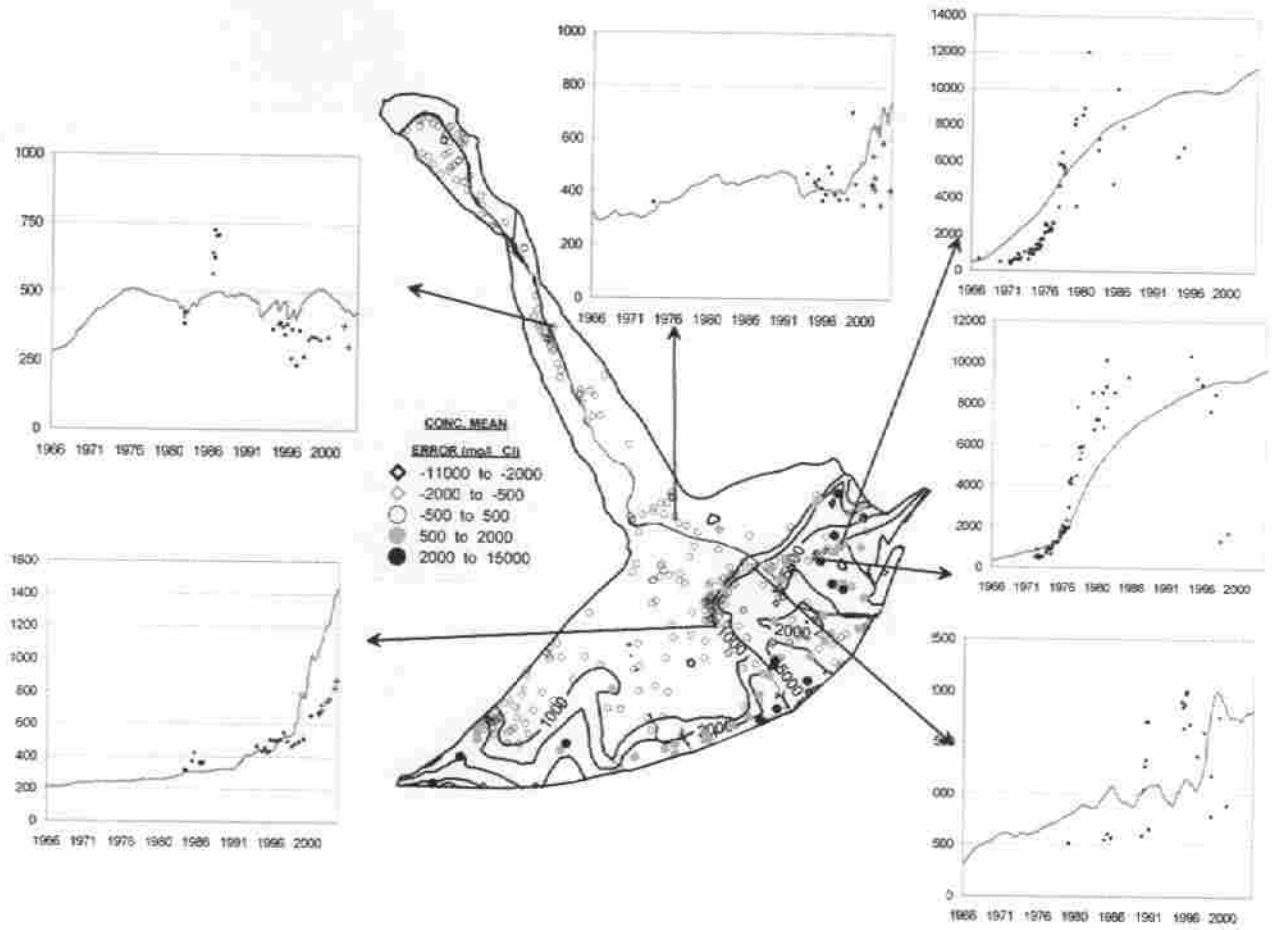

Figure 5. Chloride concentration map calculated for December 2001 together with the concentration mean error and the calculated versus measured heads in six observation points. Calculated heads are plotted in a gray line, measured data used for calibration in black dots and data used for model validation in crosses.

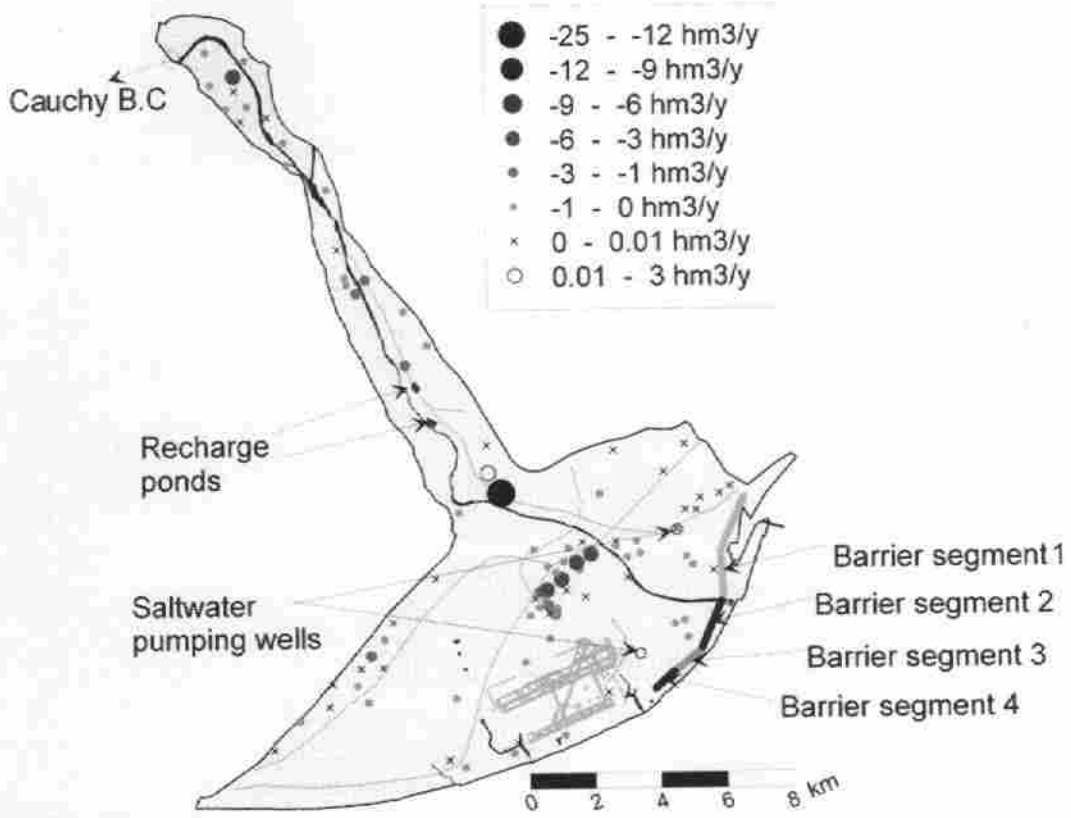

Figure 6. Location of the pumping wells and their average pumping rate in the period from 1997 to 2001 and location of the proposed corrective measures that are included in the optimization process

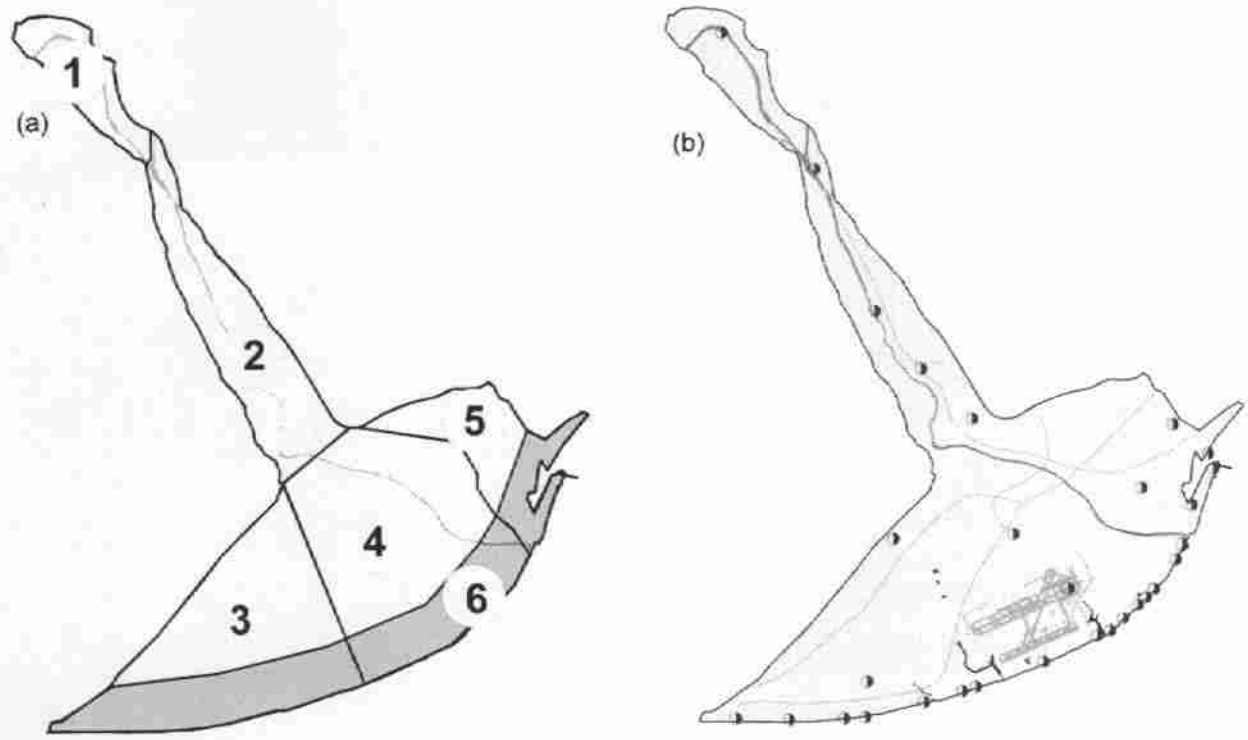

Figure 7. (a) Management areas defined in the aquifer according to geological, hydrological and management criteria and (b) location of the control points used for the optimization process

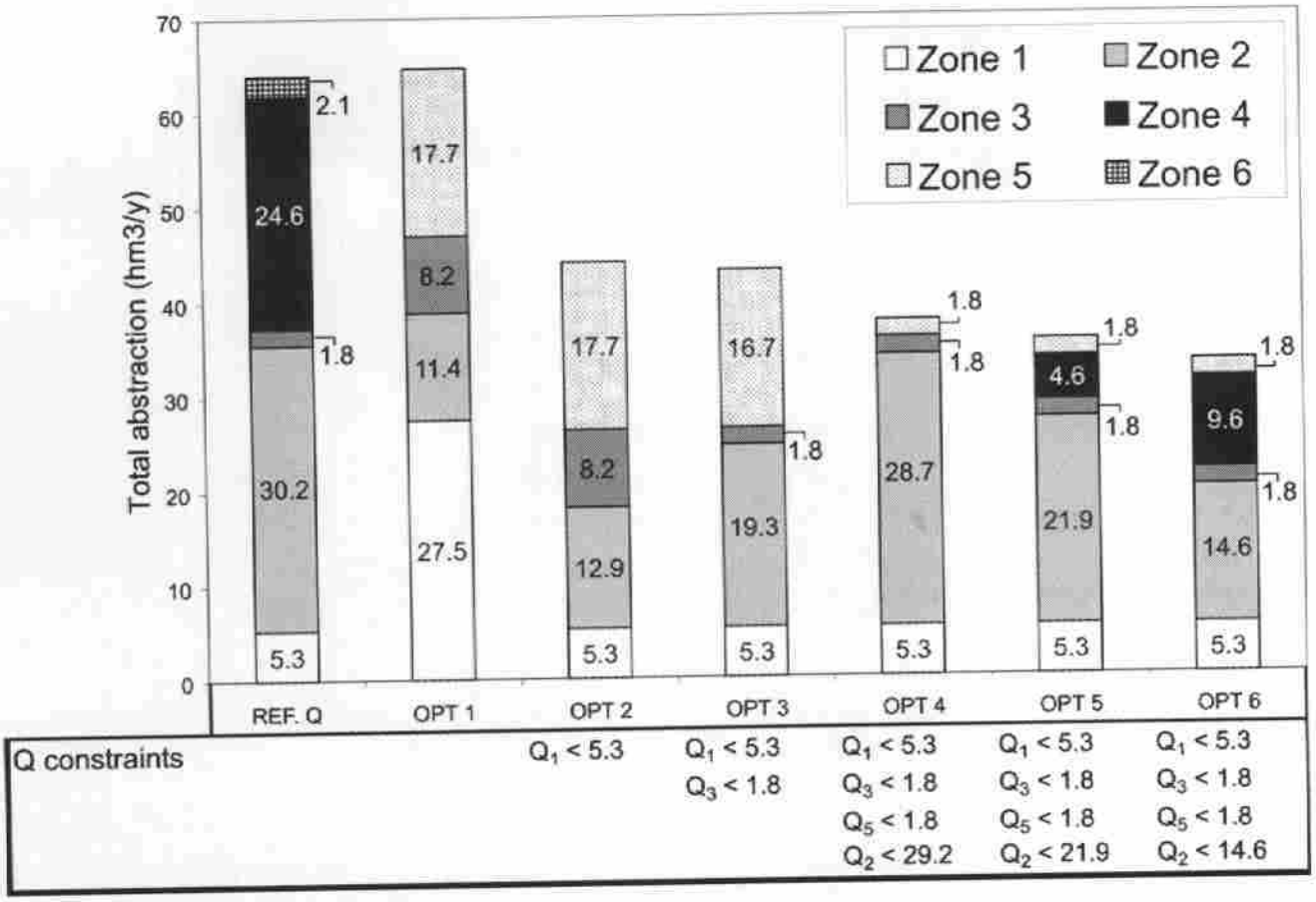

Figure 8. Results of the optimization of pumping rates for every management area and the total value of the objective function for different flow constraints applied. The reference values of the pumping rates are shown in the first bar.

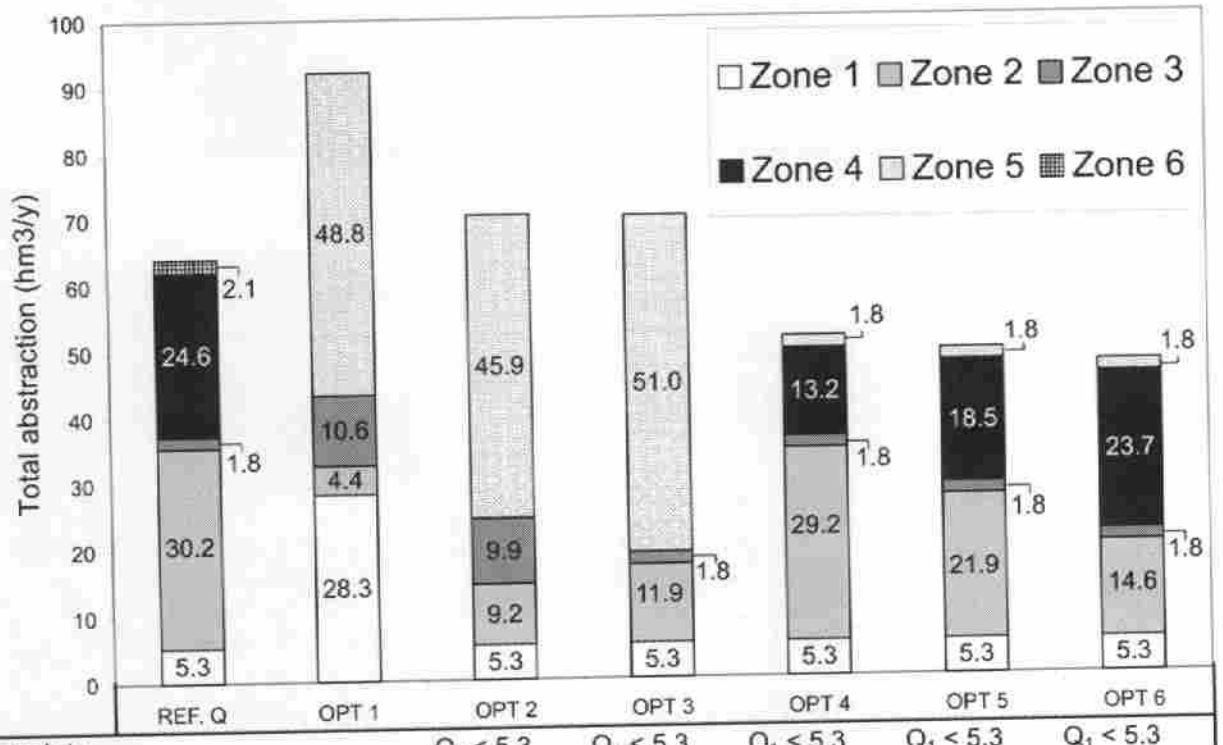

Q constraints		$Q_1 < 5.3$	$Q_1 < 5.3$ $Q_3 < 1.8$	$Q_1 < 5.3$ $Q_3 < 1.8$ $Q_5 < 1.8$ $Q_2 < 29.2$	$Q_1 < 5.3$ $Q_3 < 1.8$ $Q_5 < 1.8$ $Q_2 < 21.9$	$Q_1 < 5.3$ $Q_3 < 1.8$ $Q_5 < 1.8$ $Q_2 < 14.6$
Shadow prices						
Ponds	0.85	0.86	0.95	0.69	0.69	0.69
Barrier	3.83	2.83	4.47	1.43	1.46	1.46

Figure 9. Results of the optimization with additional corrective measures of pumping rates for every management area and the total value of the objective function for different flow constraints applied. The reference values of the pumping rates are shown in the first bar.

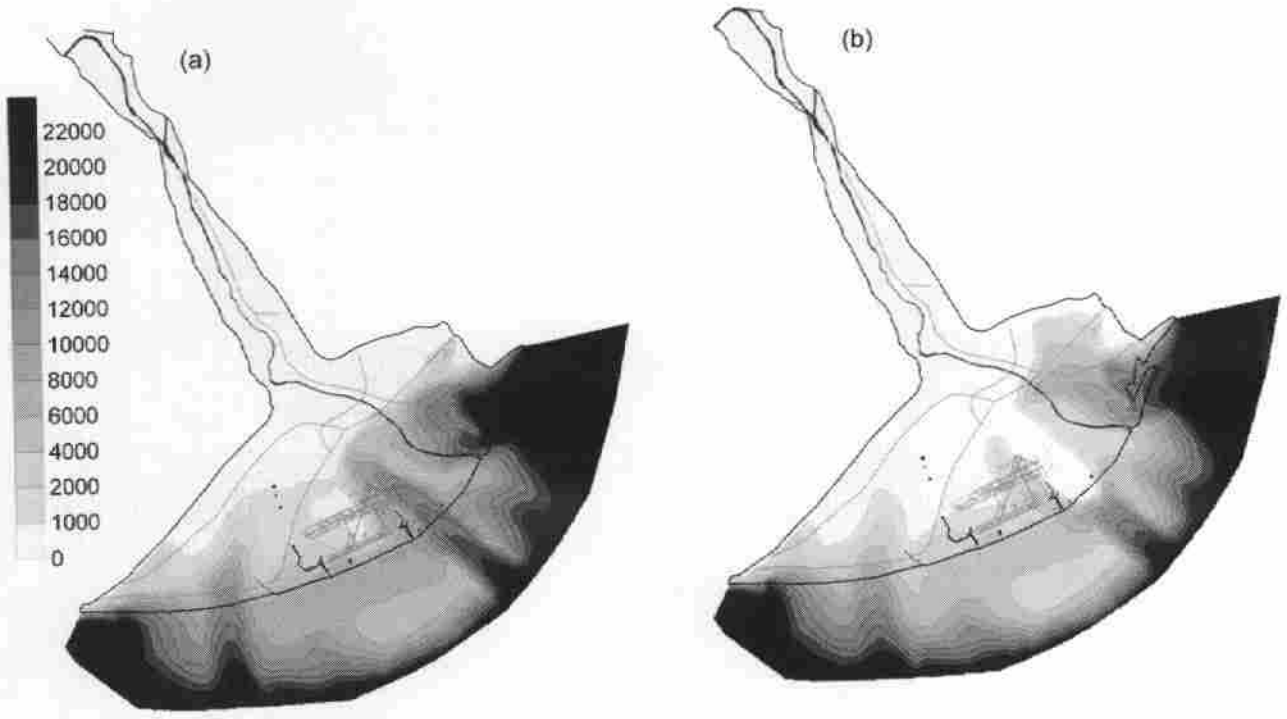

Figure 10. Chloride concentration map in the main aquifer of the Llobregat Lower Valley obtained (a) form the linearly optimized pumping rates and the implementation of corrective measures and (b) for the reference scenario

Table 1. Statistical parameters used in the simulations

Parameter	Value	Units
λ_c	1.	
λ_Q	100.	
σ_{c_i}	1000.	mg/l
$\sigma_{Q_{well}}$	$0.1 \cdot Q_i$	m^3/day
$\sigma_{Q_{pond}}$	0.25	m/day
$\sigma_{Q_{barrier}}$	10000.	m^3/day

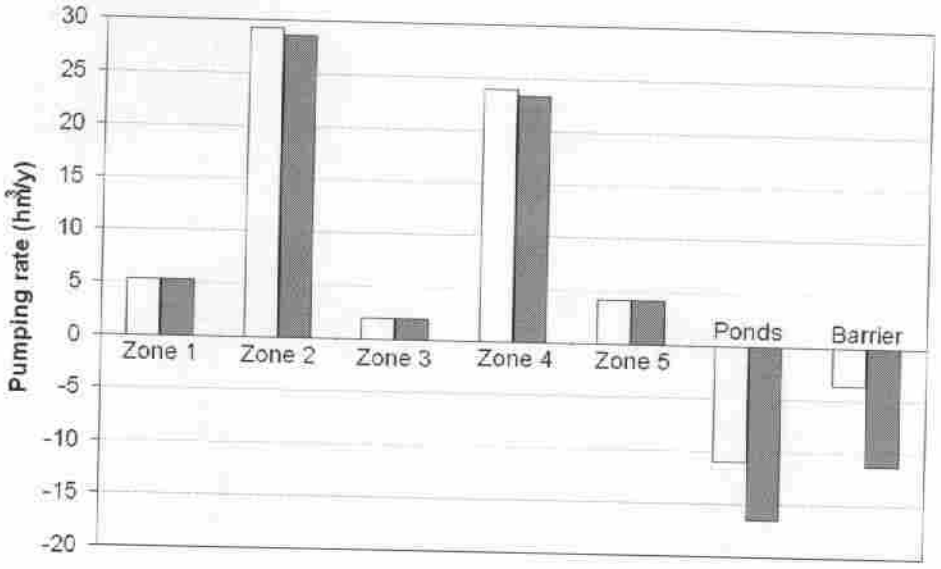

Figure 11. Results of the non-linear optimization problem. Obtained pumping rates per management zones and measures (gray bars) are compared to current values or projected values in the case of corrective measures (white bars).

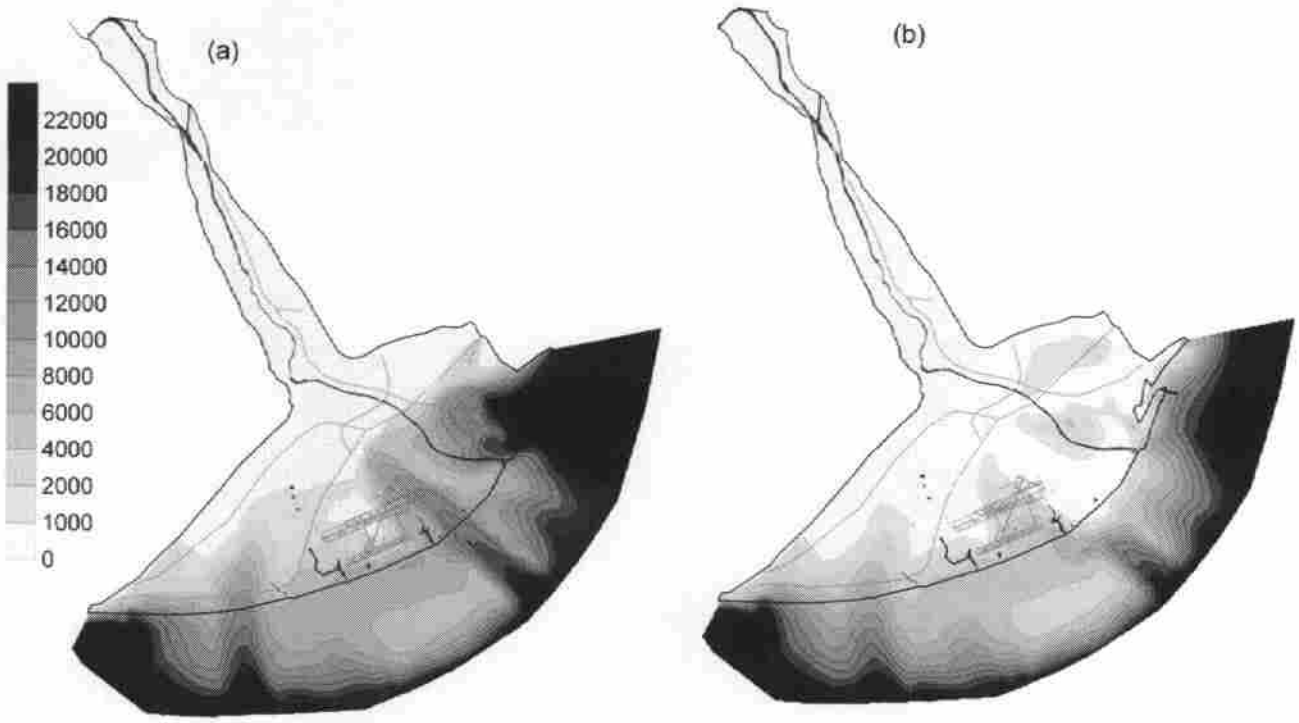

Figure 12. Chloride concentration map in the main aquifer of the Llobregat Lower Valley obtained (a) form the non-linearly optimized pumping rates and the implementation of corrective measures and (b) for the reference scenario

Table 2. Comparison of the results obtained with the linear and non-linear optimization process for the more realistic optimization scenarios (values in hm^3/y)

Management Zones	Average 1997-2001	Linear opt. (no additional measures)	Linear opt.	Non-linear opt.
Zone 1	5.29	5.28	5.28	5.29
Zone 2	30.23	21.92	21.92	28.62
Zone 3	1.77	1.83	1.83	1.98
Zone 4	24.59	4.64	18.49	23.38
Zone 5	0.00	1.83	1.83	4.16
Zone 6	2.14	0.00	0.0	–
Recharge ponds			-10.96	-16.45
Injection Barrier 1			-3.65	-2.68
Injection Barrier 2			0.00	-2.84
Injection Barrier 3			0.00	-1.27
Injection Barrier 4			0.00	-4.50
Total	64.02	35.48	49.35	63.41

ESTIMATION OF FLOODS RECHARGE IN DISCONNECTED STREAM-AQUIFER SYSTEMS. APPLICATION TO THE BAIX LLOBREGAT AQUIFERS, BARCELONA, SPAIN

Vázquez-Suñé, E.; B. Capino, E. Abarca and J. Carrera

Hydrogeology Group, Dept. of Geotechnical Engineering & Geoscience, School of Civil Engineering
Technical University of Catalonia. C/ Jordi Girona 1-3, Ed. D2, 08034, Barcelona, Spain

Corresponding author: enric.vazquez-sune@upc.edu, Fax: 34 934017251, Phone : 34 934011859

ABSTRACT

Stream-aquifer interaction has been the subject of much research for cases of good hydraulic connection (continuous saturated zone) between river and aquifer. Under these conditions, floods do not represent a very large net input to the aquifer because most of the water that enters the aquifer during the flood returns to the river when its stage recedes. The situation is different in disconnected stream-aquifer systems, where the stream bed lies above the aquifer water level, thus preventing return flow. Under these conditions, floods may represent large, but hard to quantify, water inputs. Here, we present a methodology to estimate recharge from floods for disconnected stream-aquifer systems. Recharge is estimated as the product of a floods time function (dependent on the streamflow) times an unknown factor, which is obtained from calibrating aquifer heads. This methodology is applied to the Baix Llobregat aquifers. Floods recharge is found to amount around 15 million m^3/year on the average, which represents 40% of total aquifer inputs. Floods recharge helps to explain major head recoveries.

KEY-WORDS: Llobregat Baix aquifers, Recharge, Inverse Modeling, Stream-aquifer interaction, Floods.

1. INTRODUCTION

The Llobregat Delta is a medium-size (approximately 100 km^2) quaternary formation located at the SW edge of the densely populated area of Barcelona, in the NE of Spain (Figure 1). The area, formerly devoted only to agricultural practice, now supports also important industrial settlements and city suburbs. Intense groundwater exploitation up to the late 70's caused an important seawater intrusion (Custodio et al., 1976). Pumping has been significantly reduced, but saline intrusion still affects large areas of the delta aquifers. In order to address this problem and respond to the requirements of the European Water Framework Directive, the Catalonian Water Agency (Agència Catalana de l'Aigua) is developing a groundwater management program (Abarca et al., 2005). This requires detailed aquifer characterization and identification of inputs. Recharge from the Llobregat River has been traditionally considered as one of them (REPO, 1965; FCIHS, 1997; UPC, 2004). As shown in Figure 2, well hydrographs react immediately to floods and lead to long term aquifer recovery. However, proper management requires quantifying this input. Unfortunately, no general method is available, which is the motivation of our work.

Stream-aquifer interaction has been the topic of much research since old (see reviews by Lerner et al., 1990; Winter, 1995, 1999; Sophocleous, 2002). Different interaction types can be defined depending on the stream stage, the groundwater table, and the saturation state between the streambed and the aquifer. According to these criteria two general types can be identified (Figure 3): first, the stream and the aquifer are hydraulically connected (Figure 3A y 3B) and, second, the zone between the streambed and the groundwater table is unsaturated and these are hydraulically disconnected (Figure 3C). In this context, stream aquifer interaction research has covered a wide range of topics, including bank storage (Cooper and Rorabaugh, 1963; Pinder and Sauer, 1971; Hunt, 1990; Barlow and Moench, 1998; Moench and Barlow, 2000), induced recharge (Glover and Balmer, 1954; Hantush, 1965; Jenkins, 1968; Hunt, 1999; others), hyporheic zone (Palmer, 1993; Boulton et al, 1998; Dahm et al, 1998; Cardenas et al., 2004; Salehin et al., 2004), aquifers characterization (Sophocleous et al, 1995, Sophocleous, 2005), etc. Nevertheless, recharge rate during flood events has not received as much attention.

The scant attention devoted to floods recharge probably reflects that most of the above studies assume connected stream-aquifer systems. Under these conditions, net recharge is usually low (Winter et al, 1998). During the flood period, when the flood stage rises (Figure 3B), stream water infiltrates into the aquifer and flows away from the stream, giving rise to bank storage. After the flood stage declines the previously infiltrated water flows back towards the stream (Chen and Chen, 2003) (Figure 3A). Thus, successive recharge and discharge of the aquifer has a buffering effect on the runoff regimes (Brunke and Gonser, 1997), but leads to small net recharge.

The physics of the problem is different, and quite complex, when the aquifer is disconnected. Infiltration water must pass through the hyporheic zone, and the unsaturated zone to finally arrive to the saturated zone. As a result, the actual recharge depends on a variety of factors (Sophocleous, 2002), such as the hydraulic gradient, hydraulics properties of the vadose zone, the available storage volume in the vadose zone, channel geometry and wet perimeter, flow duration and depth, antecedent soil moisture, clogging layers on the channel bottom, and water temperature. Unsaturated flow conditions usually occur where there is a relatively low-permeable clogging layer on the stream bottom (Sophocleous, 2002). This layers develops naturally through sedimentation of fine material and growth of biofilms during low discharge periods. Nevertheless, the low permeability layer is fully removed during the flood. Typically, the thickness of fully mobilised sediments is equal to about half of the stage of the river. As a result streambed leakage increases dramatically during floods. This together with the increase in wet perimeter and river head led to a sharp increase in recharge. Afterwards, recharge reminds high for a period of time but decreases slowly as the stream clogs again. Understanding and, much less, quantifying these processes is difficult.

Quantification of recharge from disconnected aquifers are usually evaluated with analytical solutions for ephemeral streams (Abdulrrazak and Morel-Seytoux, 1983; Sorman et al, 1997, and others). These analytical solutions are highly imprecise because they consider a pseudo steady state regime with a moderate recharge, while in reality flow varies rapidly. Therefore, the water-table fluctuation method (e.g. Healy and Cook, 2002) would be the method of

choice. Unfortunately, this method would require continuous and frequent monitoring, which is rarely the case.

Previous considerations about disconnected stream-aquifer system during floods (stream, groundwater, saturated and unsaturated zone, floods, bed-load capacity, etc.) make difficult to couple them in an analytical solution and therefore to be accurately quantified (De Vries and Simmers, 2002). For these reasons and due to the observations of how the water table rises as instantaneous response of floods, we propose to estimate the recharge from one or several flood events. The methodology is based on implementing historical series of floods data, piezometric heads (Figure 2) and river and groundwater Cl^- concentrations, into a numerical model. Calibration is carried out by means of the inverse problem fitting measured and computed heads and concentrations (Vázquez-Suñé et al., 2005).

2.- METHODOLOGY

The proposed method can be viewed as a variation of the water-table fluctuation mass balance method, applicable when groundwater head data are sparse. It consists of the following steps:

1. Definition of the conceptual model. This is achieved using conventional hydrogeological methods. It requires understanding geology, hydrogeology, meteorology, hydrology, soil uses, pumping rates, hydrochemistry, etc. Emphasis must be placed on evaluating not only total inputs and outputs, but also their time evolution.

2. Implementation into a numerical model. Once a conceptual model has been defined a numerical model is built. This requires specifying of all parameters, the spatial and temporal discretization and boundary conditions, (lateral inputs, recharge, pumping rates, etc).

3. Parameterization of flood recharge. Recharge during floods is implemented as a prescribed inflow along the river as:

$$Q_R(x,t) = \sum \beta_i \cdot f_{Ri}(x,t) \qquad (1)$$

Where $Q_R(x,t)$ is the recharge rate (here expressed per unit length of river), βi is an unknown parameters and $f_{Ri}(x,t)$ are functions representing the time variation of recharge. Ideally, these functions represent the modes of river recharge. The fact that they are left in terms of the unknown factor βi ought to simplify their definition, which must be prescribed by the modeller prior to proceeding. As mentioned in the introduction, a detailed account of all processes involved can be quite difficult. Factors affecting these include:

- Qpeak, peak flow rate, which controls the erosion capacity of the river, its stage and its wetted perimeter.
- Volume of flood, which can be quantified by the monthly maximum flow rate ($Q_{max}i$) or monthly averaged flow rate (Qi) and controls the total amount of water available for recharge.
- Morphological characteristics of the river bed, such as slope, channel width and river bed deposits.
- Sediment and nutrients load, which controls the rate at which the river bed clogs after a flood event.

These factors are not independent and, in turn, depend on the whole basin morphology and type of flood. Therefore, we argue for using simplified functions that capture the essence of the above, yet can be easy to define without the need of complex models. Some possible functions are defined below:

1. $f_{R1}(x,t)=1$, to represent recharge during low flow periods.
2. $f_{R2}(x,t)=Q^{\gamma}(z)$, where $\gamma > 1$ is an exponent to be estimated by trial-and-error. This function reflects the more than linear recharge with flow rate.
3. $f_{R3}(x,t)=\int Q(z)\cdot f_D(t-z)dz$, where f_D is a decay function representing clogging of the river bed after a flood: for example, $f_D(t)=\exp(t/T)$ with T being the characteristic clogging time.

4. Calibration

Three main points have to be taken into account while calibrating the model: first, consistency between a priori information and calibrated parameters must be pursued; second, good fit between measured and computed data, both in terms of piezometric heads and concentrations;

and third, the water and chloride mass balances must be consistent with the conceptual model and previous calculations. This can be achieved with inversion codes. Here we use the Maximum Likelihood Method (Carrera and Neuman, 1986; Medina and Carrera, 1996), which leads to minimizing an objective function (F).

$$F = \sum \lambda_h F_h + \sum \lambda_c F_c + \sum \lambda_p F_p \qquad (2)$$

Where F_h, F_c and F_p are the objective function of heads, concentrations and parameters, respectively; and λ_h, λ_c and λ_p are weighting coefficient for flow and transport parameters.

5. Iteration

The two last steps need to be repeated until finding the best fit. Results will be obtained choosing the run in which flood recharge function adjusts best. The resulting recharge is obtained from the mass balance of the numerical model of the aquifer.

3.- APPLICATION TO THE BAIX LLOBREGAT AQUIFERS

3.1.- Definition of the conceptual model

Hydrology

The Llobregat River extends from NW to SE along 156.5 km; its basin has an area of 4948.4 km^2. The study area corresponds to the final part of the basin (250.6 km^2) and it is divided in three parts: Sant Andreu Basin, Lower Valley Basin and the Llobregat Delta (Figure 1). Main tributaries are the Anoia river and the Rubí river. The climate is typically Mediterranean, with extreme temperatures in January and August, and a yearly average temperature of 15 °C. The cold and warm seasons are separated by two unstable climate seasons. The rainfall average is around 600 mm/year. The river basin is characterized by a fluvial regime with an average streamflow of 16.8 m^3/s in the Martorell gauging station (Figure 1).

The Llobregat River is a good example of a Mediterranean fluvial system, with low streamflow, marked ebb flood, strong floods and very irregular flow patterns (Marqués, 1984).

One of the most important phenomena to consider is the instantaneous maximum streamflow or peak, because of its direct implications on the formation of the Llobregat delta. Instantaneous maximum streamflow has always corresponded to intense rain storms, like those of the years 1962, 1971 or 1994, to mention some. Very intense and short term rain storms result in peak flows of short duration and big volumes.

Hydrogeology

Detailed characterization is necessary to define the conceptual model. The most difficult data to obtain are the recharge history, that depends on soil uses and is time dependent, and the groundwater extraction history. Maximum groundwater exploitation occurred in the 70's reaching values greater than 130 hm^3/y. This period corresponds to the maximum groundwater drawdown ever reached (25 m.b.s.l. in the central part of the delta). In the 70 s and 80s, due to this drawdown and some anthropic modifications (inland dock's enlargement) marine intrusion quickly progressed towards the central part of the delta, where some of the water supply main pumping areas were located.

The general guidelines of the Lower Valley and Llobregat Delta geology were established by Almera (1891), Llopis (1942, 1946), Solé-Sabaris et al. (1957) and Solé-Sabaris (1963). The cross-sections proposed in the late 60's and early 70's in the framework of an important project for hydrogeological resources characterization (MOP, 1966; Llamas y Molist, 1967) and some other reports published at that time, are still used today for hydrogeological purposes. Since then, new geological information has arisen because of the continuous construction related to civil works that are carried out in the delta area. This new information helped defining a more accurate geological model. A thorough sedimentological study was carried out to define in detail the three dimensional geological structure. It has been possible to redefine aquifer units, its geometries, and the lateral connections both between units and the sea. The synthetic geological model is presented in figures 4a and 4b.

Lower Valley and Llobregat Delta are formed by materials of Quaternary age (Pleistocene to Holocene) that rest discordantly on top of materials that range from the Paleozoic to the Pliocene. Sant Andreu and Lower Valley basins are constituted by the accumulation of alluvial sand and gravels. At the end of lower Valley begins a deltaic area that is built by the accumulation of four deltaic sedimentary cycles. The youngest cycle present wedge geometry with silts and clays separating two packages of sands and gravel (Figure 4a).

Different hydrogeological units can be identified from these geometries: 1) Shallow Aquifer: within the Superior Deltaic Complex (CDS, Figure 4a) an aquifer formed by sands. This aquifer has a unconfined behaviour. 2) Main aquifer: this is made up of the Deep aquifer (CDI, Figure 4a), aquifers of the Sant Andreu Basin and Lower Valley. 3) Silt wedge (Aquitard): the shallow and deep aquifers are separated by an intermediate level of highly heterogeneous materials (CDS a, Figure 4a) formed mainly by finer sediments that act as a confining layer. And 4) Inferior Aquifers: towards the base of the Inferior Deltaic Complex (CDI) two stratigraphic levels of coarse sediments (CDIa and CDIc, Figure 4a) also host aquifer units.

3.2.- Modelling

The **VisualTransin** code was used for calibration of the numerical model. This code solves the flow and transport equations using the finite element method. The model is divided in two layers corresponding to the shallow aquifer and main aquifers respectively. The domain was divided in 4411 nodes and 9848 elements, specially refined near the main pumping areas and the mesh was adapted to the main hydrogeological features. Elements are triangular and average size is about 200 m. Simulation time steps are set monthly from 1965 to 2002.

Prior hydraulic parameters of the model were based on data integration and geological review. This led to 101 transmissivity zones conditioned by aquifer thickness, lithofacies description, hydraulic test values, etc. The same procedure was applied to other parameters like storage coefficient, recharge, boundary conditions (boundary flows, interaction of the aquifer with stream, channels and linear works, pumping rates), porosity, diffusion and dispersivity.

Streams, channels and underground linear works can interact with present aquifers. If they are hydraulically connected inputs or outputs of water to the aquifer are a function of the heads difference between the mass of superficial water and the aquifer. In order to apply the Cauchy boundary condition it is necessary to define the external water heads (stream, channel or linear work reference heads) and a leakage parameter.

If they are disconnected, the input flow could be a function of the stream flow or flood magnitude. Along Sant Andreu basin and Lower Valley area the Llobregat river and its tributaries (Rubí river) are mostly disconnected (Figure 1).

As a result of calibration, the model displayed a good consistency between a *priori* information and calibrated parameters; second, a good fit between measured and computed data, both in terms of piezometric heads and concentrations, and third, the mass water and chloride balances consistent with the conceptual model and previous calculations have been obtained.

3.3.- Simulation of flood recharge events

A priori it is possible to define several functions but we don't know which one is the best. We have considered several alternatives that are described below.

Available data included daily streamflow rates (Qd) for the period between 1966 to 2001 in the Martorell and Sant Joan Despí gauging stations located in the Llobregat River. The average streamflow (Qb) of 15 m^3/s is considered the reference streamflow. These data were integrated monthly because of the time discretization we used in the model. This leads to our flood recharge function which is aimed at representing monthly averages. We used two types of functions: linear and power law.

Power law functions

This function represents that floods causes both the stage and the wetted surface to increases and also erodes the streambed eliminating the natural clogging thus allowing an exponential increase of recharge:

$$f_R^{\gamma}(Q(t)) = Q\exp\gamma = \begin{cases} Q_{\max i}^{\gamma} & \text{if} \quad Q_{\max i} > 50\ \text{m}^3/\text{s} \\ 0 & \text{if} \quad Q_{\max i} < 50\ \text{m}^3/\text{s} \end{cases} \tag{3}$$

where γ is an arbitrary exponent, which will be selected by trial-and-error. Here, we chose values between 1.0 to 1.6 ($Q_{exp}^{1.0}$,..... , $Q_{exp}^{1.6}$). Furthermore, the value 50 m^3/s was chose as "minimum flood value".

Linear functions

This kind of function represents both the floods and the base streamflows. It is considered that the base streamflow can induce recharge to the aquifer. This function defines two components of the river recharge to the aquifer: 1) it recharges during the flood events ($\alpha \cdot Q_{max\,i}$), and 2) it recharges from a base streamflow ($(1-\alpha) \cdot Q_i$). The resulting function is defined next:

$$f_R^{L}(Q(t)) = Qave\alpha = \begin{cases} \alpha \cdot Q_{\max i} + (1-\alpha)\cdot Q_i & \text{if} \quad Q_{maxi} > 50\ \text{m}^3/\text{s} \\ 0 & \text{if} \quad Q_{maxi} < 50\ \text{m}^3/\text{s} \end{cases} \tag{4}$$

where α is an arbitrary factor, that will be selected by comparing the performance of several values. Here, we chose values between 0.5 to 0.9 ($Q_{ave}^{0.5}$,....., $Q_{ave}^{0.9}$).

Constant flow rate

This function (Qcte) is defined as a constant streamflow. This constant value is computed as a proportion of the average streamflow (Qb).

$$f_Q = \beta \cdot Q_b \qquad (5)$$

where β is the proportion factor that will be obtained from calibration process.

This function disregards temporal variability of streamflow, therefore if temporal variability of river recharge is related to the evolution of piezomètric heads, this function can not be appropriate.

3.4.- Calibration and iterative process

To find the best fitting function it is necessary to calibrate the model for each of the 14 stream recharge functions obtained. All model parameters (transmisivities, recharges, "p" factor of the recharge functions from floods, boundary conditions, flow rate, leakage, etc.) have been calibrated.

The value of the objective function, good fit on measured and computed heads and concentrations, and the mass balance consistency, allows us to evaluate which is the best model and find the appropriate stream recharge functions for it.

4.- Results and discussion

Figure 8 contains the results in terms of the calibration objective functions and net recharges from floods for each recharge function. Power law functions lead to better fits than linear functions. It is observed that the best total fit (total objective function) was obtained for the exponent $\gamma = 1.4$ ($Q_{exp}^{1.4}$). Nevertheless there is little difference with other functions except for the constant flow function (Qcte), which led to a very poor fit. However, each component of the objective function was minimum for a different recharge function. In fact, the best fit for heads was obtained for the exponent $\gamma = 1.6$ ($Q_{exp}^{1.6}$) because it fits better the tips of the heads that occur after flood events. The best fit of parameters was also obtained for the $Q_{exp}^{1.6}$, although it was not so different from the rest of exponential functions. However, the best fit for concentrations was obtained for Qcte. This is due to the fact that the variability in aquifer concentration is low. Water recharged from floods is mixed with groundwater, therefore

floods concentration variability is diluted and the average concentration in groundwater is almost constant. The point is that the calibration leaves some room for uncertainty in the choice of recharge function. Therefore, more complex functions were not considered.

Figures 9 and 10 display measured and computed head and concentration fits from power law function with $Q_{exp}^{1.4}$. We consider them satisfactory. Some points of interest in the area of the model have been selected to show the space and temporary distribution of heads. It is observed how the model has been able to reproduce the spatial distributions of heads. Time variability and amplitude in the oscillations is also reproduced. Salinity trends in the aquifer of the Lower Valley and Llobregat delta are also reproduced satisfactorily (Figure 10).

Average mass balance calculations bring, among others terms, net aquifer recharge from the river. Most of the runs tend to a recharge rate values above 14 hm^3/year. The run that presents a best fit ($Q_{exp}^{1.4}$) gave a value of total river recharge of 14.7 hm^3/year (Figure 11). The exception is constant function (Qcte) run that gave very low values of recharge rate (0.97 hm^3/year), this value probably represents base streamflow recharge.

The most remarkable inputs into the aquifers mass balance are: total infiltration recharge (21.6 hm^3/year from both shallow and main aquifers) and Llobregat river recharge from floods with 14.7 hm^3/year (including the Llobregat river through the Sant Andreu Basin and the Lower Valley, and a portion of the tributary Rubí river). Moreover sea water inputs in the main aquifer are quite significant with a value of 6.8 hm^3/year. The opposite occurs at the shallow aquifer which discharges about 0.5 hm^3/year to the sea. The main output is pumping in the main aquifer with 71.8 hm^3/year. Flow from shallow to main aquifer is determined by the balance for each aquifer that is 19.6 hm^3/year.

Figure 12 contains the annual evolution of the net aquifer recharge from the river. In some years important recharge values are obtained in wet years (up to 70 hm^3/year). But those contributions are extremely low during dry years. The variation in the aquifer storage is mainly controlled by the contributions of the Llobregat river at flood events and by groundwater abstractions.

Figure 13 shows the relationship between the flood streamflow and the net recharge from the river to the aquifer, for several power law functions. A fundamental tool for the management of the water resources is obtained, since it allows considering the amount of water recharged to aquifers by a certain flood. The estimation of recharge from floods is quite robust and is not much sensitive to selected power law function because net quantified recharge is not so different. Obviously, sensitivity increases for higher river floods. Still, it is apparent that periodic flows, which are beneficial for may other river processes, also cause a sizeable amount of recharge.

5.- CONCLUSIONS

A transient (1965-2001) groundwater flow and solute transport model of the aquifers of the S. Andreu Basin, Lower Valley and Delta of the Llobregat River has been carried out. This model has been calibrated automatically against heads and concentration data obtaining very satisfactory fits for both variables. Mass balance and hydraulic parameters were also coherent with previous calculations. This case study reflects the importance to flood events in the aquifers mass balance, since they are one of the important inputs in a disconnected aquifer.

Disconnected stream-aquifer systems during floods are difficult to be accurately quantified. We propose to estimate the recharge from one or several flood events. The proposed method can be viewed as a variation of the water-table fluctuation mass balance method, applicable when groundwater head data are sparse. It consists in (1) definition of the conceptual model; (2) implementation into a numerical model; (3) parameterization of flood recharge (recharge during floods is implemented as a prescribed inflow along the river); (4) calibration and (5) iteration. The two last steps need to be repeated until finding the best fit. Results will be obtained choosing the run in which the flood recharge function fits best. The resulting recharge is obtained from the mass balance of the numerical model of the aquifer.

This methodology is applicable to very complex systems taking into account temporal variability of all water sources. Its application allowed us to quantify the recharge rates in the Llobregat aquifers due to river flood events. In order to accurately evaluate this recharge, different temporal functions based on river streamflow data were used to simulate recharge

from the Llobregat River during floods events. Two types of time varying functions (linear and power law function) and a constant function were considered.

The best results in terms of total objective function are obtained for power law functions representing better the river-aquifer interaction during floods events. Amongst them, the 1.4 exponent function produced the best result. The constant function was the worst model used in terms of heads fitting reflecting the critical importance of time variability to accurately represent the interaction between the Llobregat River and its aquifers.

For power law functions, the recharge value obtained in this process is about 15 hm^3/year, which becomes the second more significant input into the aquifer system in terms of annual volume.

A streamflow versus recharge graph results in a new tool for aquifer management. Groundwater managers are able to estimate the amount of water that can be recharged and design artificially generated flood events by controlled floodgate opening upstream.

ACKNOWLEDGEMENTS:

This work has been done in the framework of project funded and supported by the Catalonian Water Agency (Agència Catalana de l'Aigua); Comunitat d'Usuaris d'Aigües del Llobregat (CUADLL) and Spanish Geological Survey (IGME).

REFERENCES

Abarca E., Vázquez-Suñé E., Carrera J., Capino, B., Gámez D., Batlle F (2005) Optimal design of measures to correct seawater intrusion. Submitted to Water Resources Research.

Abdulrazzak MJ, Morel-Seytoux HJ (1983) Recharge from an ephemeral stream following wetting front arrival to water-table. Water Resources Research 19 (1) 194-200.

Almera J. (1891). Mapa geológico-topográfico de la provincia de Barcelona. Región I o de contornos de la capital, con la explicaciónsomera en la misma hoja. Esc. 1:40.000. 1ª edic. Barcelona. 1891, 2ª edic. Barcelona 1900.

Barlow PM, Moench AF (1998) Analytical solutions and computer programs for hydraulic interaction of stream-aquifer systems. US Geological Survey Open-File Report 98-415A, pp. 85.

Boulton AJ; Finlay S; Marmonier P, Stanley EH; Valett HM (1998) The functional significance of the hyporheic zone in streams and rivers. Annu Rev. Ecol Syst. 29:59-81.

Brunke M, Gonser T (1997) The ecological significance of exchange processes between rivers and ground-water. Fresh-water Biol 37: 1-33.

Cardenas MB, Wilson JL, Zlotnik VA (2004) Impact of heterogeneity, bed forms, and stream curvature on subchannel hyporheic exchange. Water Resources Research 40 (8): Art. No. W08307

Carrera J, Neuman SP (1986) Estimation of aquifer parameters under steady state and transient conditions: Maximum Likelihood Method Incorporating Prior Information. Water Resources Research 22 (2): 199-210.

Cooper HH; Rorabaugh MJ (1963) Groundwater movements and bank storage due to flood stages in surface streams. U.S. Geol. Surv. Water Supply Paper 1536-J, 343-366.

Chen X, Chen XH (2003) Stream water infiltration, bank storage, and storage zone changes due to stream-stage fluctuations. Journal of Hydrology 280(2003) 246-264.

Custodio E., Cacho F, Peláez MD (1976). Problemática de la intrusión marina en los acuíferos del Delta del Llobregat. Actas de la II Asamblea Nacional de Geodesia y Geofísica. Instituto Geográfico y Catastral. Madrid: 2069-2101.

Dahm CN; Grimm NB; Marmonier P; Valett MH; Vervier P (1998) Nutients dynamics at the interface between surface waters and groundwaters. Freshwater Biol 40: 427-451.

De Vries JJ, Simmers I (2002) Groundwater recharge: an overview of processes and challenges. Hydrogeology Journal 10(1):5-17.

FCIHS (1997) Estimació de la recàrrega del Llobregat als aqüífers del Delta del Llobregat. Consorci d'Aigües Ter-Llobregat. Unpublished Report.

Glover RE; Balmer CG (1954) River depletion resulting from pumping a well near a river. American Geophysical Union Transactions. V.35. Nº 3, pp. 468-470.

Hantush MS (1965) Wells near streams with semipervious beds. J. Geoph. Res. V. 70, Nº 12, pp. 2829-2838.

Healy RW; Cook PG (2002) Using groundwater levels to stimate recharge. Hydrogeology Journal, 10 (1) 91-109.

Hunt B (1990) An approximation for the bank storage effect. Water Resources Research, v. 26, Nº 11, pp. 2769-2765.

Hunt B (1999) Unsteady stream depletion from ground water pumping. Ground Water 37 (1): 98-102.

Jenkins CT (1968) Techniques for computing rate and volume of stream depletion by wells. Groundwater. V. 6. Nº 2, pp. 37-46.

Lerner, DN., AS. Issar and I. Simmer (1990) Groundwater rechrage. A guide to understanding and estimating natural recharge. IAH Int Contrib Hydrogeol 8. Heinz Heise, Hannover, 345 pp.

Llamas, M.R., J. Molist (1967). Hidrologia de los deltas de los ríos Besós y Llobregat. Documentos de Investigación Hidrològica, nº 2. Centro de Estudios, Aplicaciones e Investigaciones del Agua. Barcelona.

Llopis i Lladó, Noel (1942). Los Terrenos cuaternarios del llano de Barcelona. Publ. Inst. Geol. Dip. Prov. de Barcelona, VI, 52 pp. 8 figs.

Llopis i Lladó, Noel (1946). Los movimientos corticales intracuaternarios del NE. de España. Estudios Geológicos (Madrid). 3; 181-236.

Marquès MA (1984). Les formacions quaternàries del delta del Llobregat. Institut d'Estudis Catalans.

Medina A, Carrera J (1996) Coupled estimation of flow and solute transport parameters. Water Resources Research 32 (10): 3063-3076.

Moench AF, Barlow PM (2000) Aquifer response to stream-stage and recharge variations. I. Analytical step-response functions. Journal of Hydrology 230, 192-210.

MOP (1966). Estudio de los recursos hidráulicos totales de las cuencas de los ríos Besós y Bajo Llobregat. CAPO-SGOP. 4 vol. Barcelona.

Palmer MA (1993) Experimentation in the hyporheic zone: challenges and prospectus. J. N. Am.Benthol. Soc. 12:84-93.

Pinder GF, Sauer SP (1971) Numerical simulation of flood wave modification due to bank storage effects. Water Resources Research 7(1): 63-70.

Salehin M, Packman AI, Paradis M (2004) Hyporheic exchange with heterogeneous streambeds: Laboratory experiments and modeling. Water Resources Research 40 (11): Art. No. W11504

Solé-Sabaris, L., C. Virgili, I. Zamarreno (1957). "Livret guide d'excursions: Environs de Barcelona et Montserrat". V Congress. Inter.

Solé-Sabaris, L (1963).Ensayo de interpretación del Cuaternario Barcelonés. Miscelánea Barcinonensia, t. II, pp. 7-58, 8 figs., Barcelona.

Sophocleous M. (2002) Interactions between groundwater and surface water: the state of the science. Hydrogeology Journal, 10 (1) 52-67.

Sophocleous M. (2005) Groundwater recharge and sustainability in the high plains aquifer in Kansas, USA Hydrogeology Journal 13 (2): 351-365

Sophocleous M, Koussis A, Martin JL, Perkins SP (1995) Evaluation of simplified stream-aquifer depletion models for water rights administration. Groundwater Vol 33, 4. p.579.

Sorman AU., Abdulrazzak MJ. and. Morel-Seytoux HJ (1997) Groundwater recharge estimation from ephemeral streams. Case study: Wadi Tabalah, Saudi Arabia. Hydrological Processes, Vol. 11, 1607-1619.

UPC, 2004. Programa de gestió dels aqüífers de la cubeta de Sant Andreu, Vall baixa i Delta del Llobregat, Universitat Politècnica de Catalunya. Barcelona. Agència Catalana de l'Aigua. Unpublished Report.

Vázquez-Suñé E., Abarca E., Carrera J., Capino, B., Gámez D., Pool M., Simó T., Batlle F., Niñerola JM., Ibáñez X. (2005) Groundwater modelling as a tool for the European Water Framework Directive (WFD) application. The Llobregat case. Submitted to Physics and Chemistry of the Earth.

Winter TC (1995) Recent advances in understanding the interaction of groundwater and surface-water. Reviews of Geophysics 33:985-994.

Winter TC, Harvey JW, Franke OL (1998) Groundwater and surface water a single resource. US Geological Survey Circular, 1139.

Winter TC (1999) Relation of streams, lakes, and wetlands to groundwater flow systems. Hydrogeology Journal 7(1):28-45.

FIGURE CAPTIONS

Figure 1.- Map of the study area, Lower Llobregat aquifer units, Catalonia, Spain (Adapted from UPC, 2004).

Figure 2.- Stream flow hydrograph (thin line, right scale) and groundwater hydrographs (bold lines, left scale) at several piezometers of the Llobregat aquifers. Arrows shows river bed level near each piezometer. Fast recoveries of water levels are typically associated to floods while declines often coincide with floodless periods (pumping, not shown here, has also changed significantly, with maximum values at 70's.

Figure 3.- Types of stream-aquifer interactions: A) Connected gaining stream; B) Connected losing stream C) Disconnected stream (Adapted from Winter et al, 1998). Notice that the A and B types can be transient and occur during flood. As the stream-stage rises, the river recharges the aquifer. The flow direction may reverse when the stage recedes, leading to the situation depicted in B, so that net recharge is small. On the other hand, floods in disconnected streams (C) may cause larger net recharge, both because (1) return flow does not occur, and (2) the low permeability layer at the stream bed is removed.

Figure 4: Geological cross-section of the emerged and submerged delta based on old MOP data and from a reflexion seismic survey performed by IGME. The silt wedge separates the upper and main aquifers. Other Old Quaternary deltas (Q1-Q3) are part of a hidrologically unknown lower aquifer system. The modern delta (Q4) was formed 18000 years ago, although its progradation took place during the last 6000 years. Conceptual model of the incised systems of the called Lower Detritic Complex. Gravels and conglomerates are painted in orange and represent the different incised systems. Between the coarse sediments there are silts and sands. The lower grey area represents the Pliocene Blue Marls and the dark grey to the Miocene and pre-miocene basement.

Figure 5.- Daily stream flow hydrograph. Show are the average stream flow of 15 m^3/s (Qb) and minimum flood value of 50 m^3/s.

Figure 6.- Power law time functions for flood recharge. Show is the curves with exponents of 1.0, 1.4 and 1.6 for the period from 81 through 84.

Figure 7.- Linear time functions for flood recharge with weighting factors of 0.9 and 0.5 for the period from 81 through 84.

Figure 8.- Performance of the different types of flood recharge time functions. Vertical bars represent the objective function achieved with each time function. Notice that best fits are obtained with power law functions (optimum for 1.4 exponent) and that a constant recharge leads to a very poor fit. Also show is the average total floods recharge for the 1965-2001 model period. Notice that over all recharge estimate (around 15 million m^3/year) are not very sensitive to the exponent.

Figure 9: Spatial distribution of head calibration errors (average of the absolute value of the residual for each observation well). In general, largest errors correspond to wells with few head measurements. Also shown is the time evolution of measured and computed wells at several of the piezometers with longest measurement records.

Figure 10: Spatial distribution of concentration absolute. Also shown is the time evolution of measured (dots) and computed (continuous lines) concentrations at some of the wells with longest measurement records.

Figure 11. Schematic description of water balance for the Baix Llobregat aquifers expressed in million m^3/year. Mass balance for the main aquifer is shown on the left side and for the shallow aquifer on the right. Two parallel arrows show the flux from shallow to main aquifer.

Figure 12.- Yearly recharge from floods computed with Qexp1.4 time function.

Figure 13.- Fitted relationships between monthly recharge and flood stream flow. Notice that recharge is very similar for moderate floods.

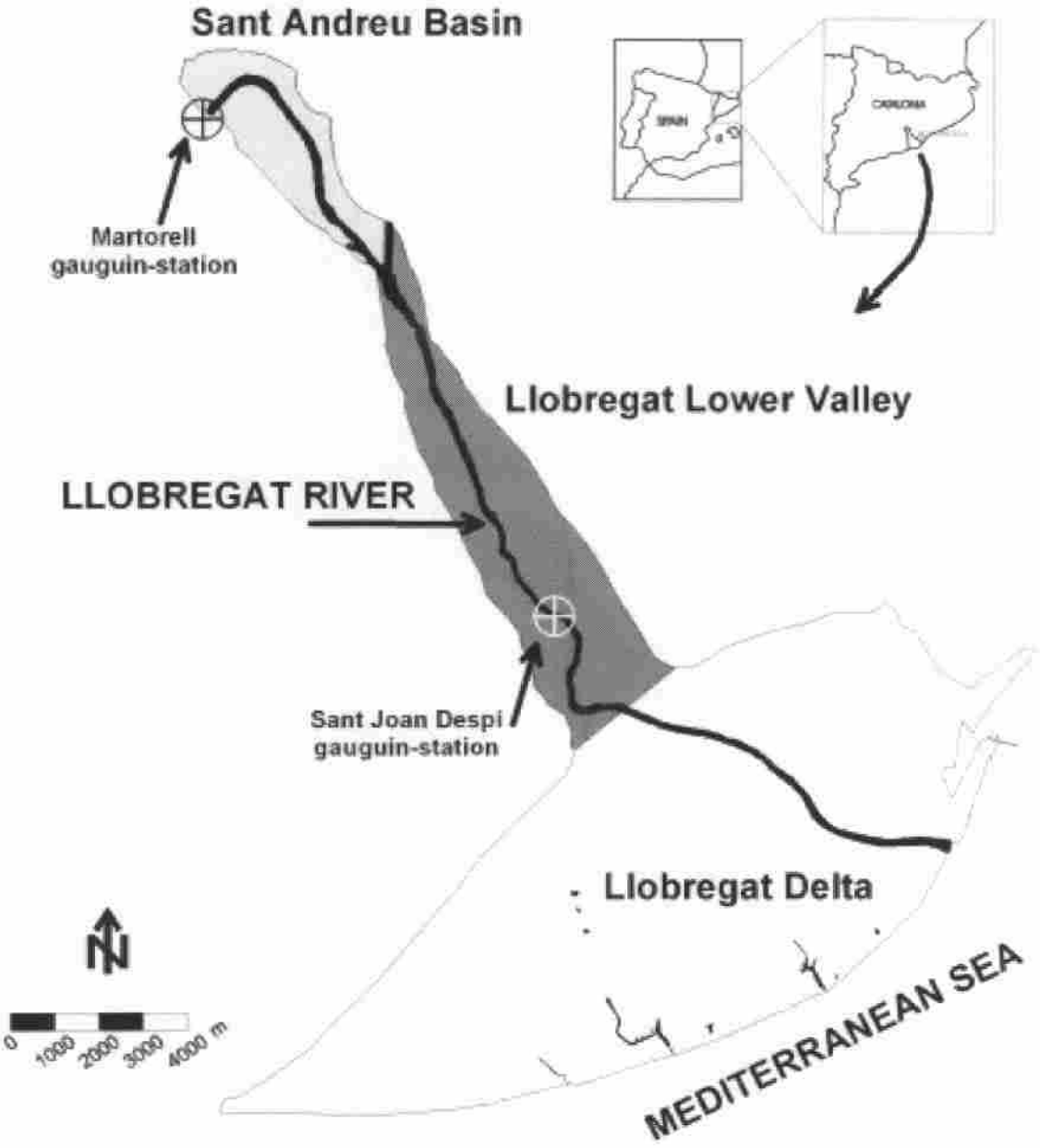
Sant Andreu Basin
Martorell
gauguin-station
Llobregat Lower Valley
LLOBREGAT RIVER
Sant Joan Despi
gauguin-station
Llobregat Delta
MEDITERRANEAN SEA
N
0
1000
2000
3000
4000 m

Figure 1

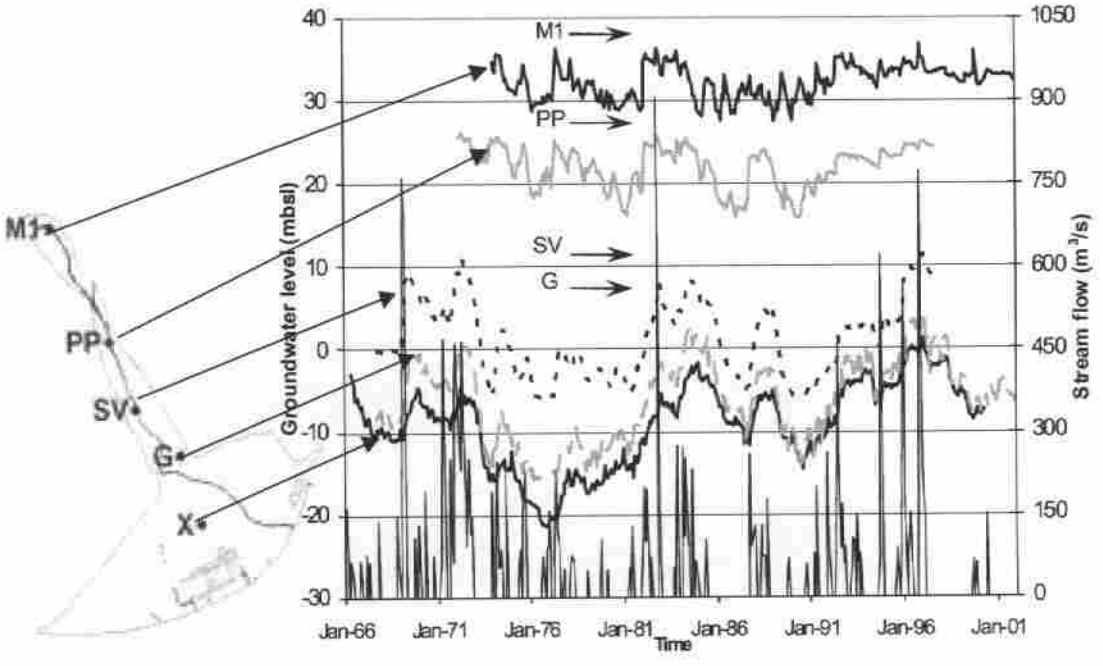
M1
PP
SV
G
X
40
30
20
10
0
-10
-20
-30
1050
900
750
600
450
300
150
0
Groundwater level (mbsl)
Stream flow (m³/s)
Jan-66
Jan-71
Jan-76
Jan-81
Jan-86
Jan-91
Jan-96
Jan-01
Time

Figure 2

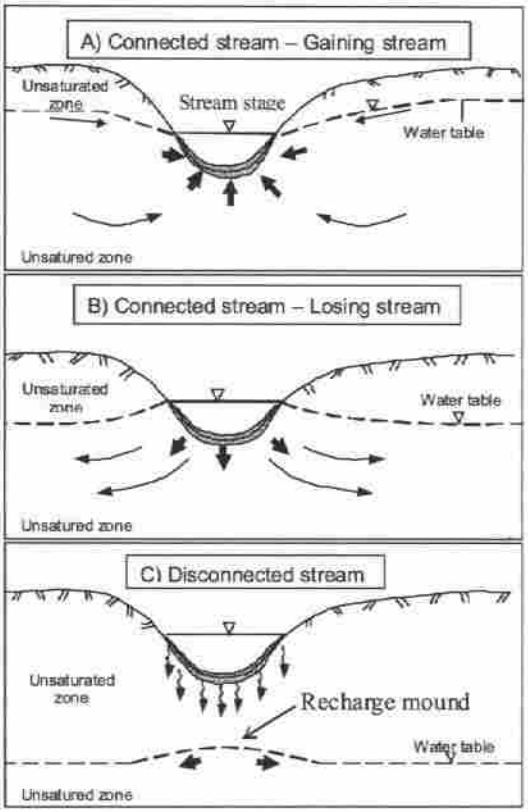
A) Connected stream – Gaining stream
Unsaturated zone
Stream stage
Water table
Unsatured zone
B) Connected stream – Losing stream
Unsaturated zone
Water table
Unsatured zone
C) Disconnected stream
Unsaturated zone
Recharge mound
Water table
Unsatured zone

Figure 3

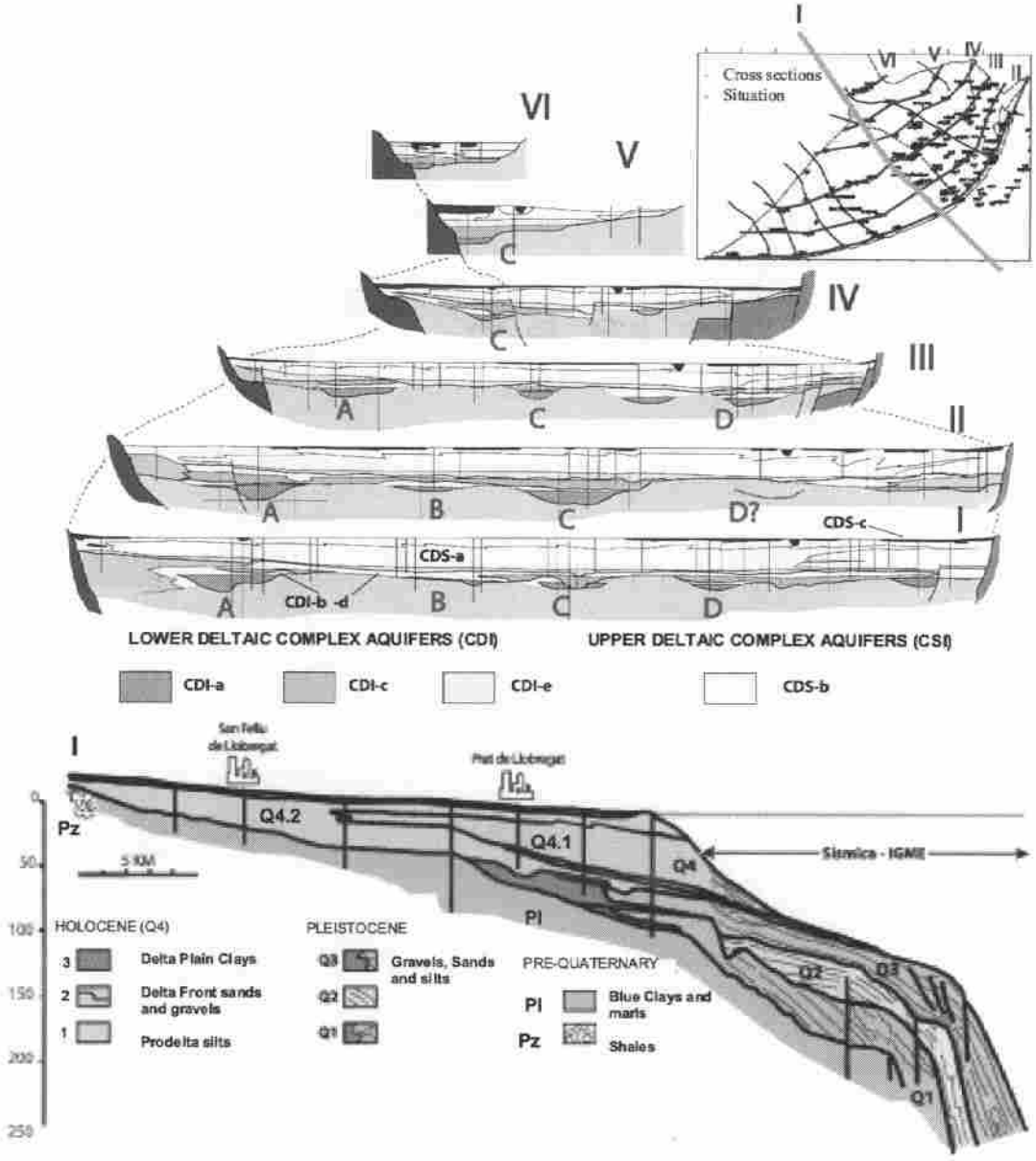
I
VI
V
IV
III
II
Cross sections
Situation
C
A
B
D
D?
CDS-c
CDS-a
CDI-b -d
LOWER DELTAIC COMPLEX AQUIFERS (CDI)
UPPER DELTAIC COMPLEX AQUIFERS (CSI)
CDI-a
CDI-c
CDI-e
CDS-b
Pz
Q4.2
Q4.1
Q4
Pl
Sísmica - IGME
5 KM
HOLOCENE (Q4)
3 Delta Plain Clays
2 Delta Front sands and gravels
1 Prodelta silts
PLEISTOCENE
Q3 Gravels, Sands and silts
Q2
Q1
PRE-QUATERNARY
Pl Blue Clays and marls
Pz Shales
0
50
100
150
200
250

Figure 4

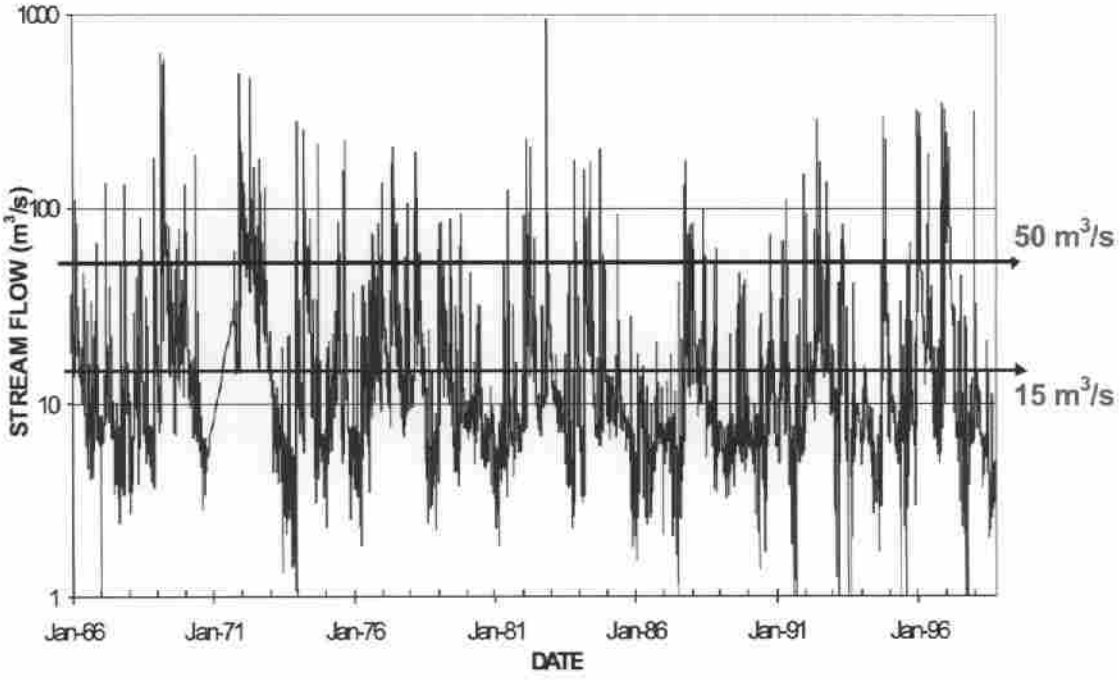
1000
100
10
1
STREAM FLOW (m3/s)
50 m3/s
15 m3/s
Jan-66
Jan-71
Jan-76
Jan-81
Jan-86
Jan-91
Jan-96
DATE

Figure 5

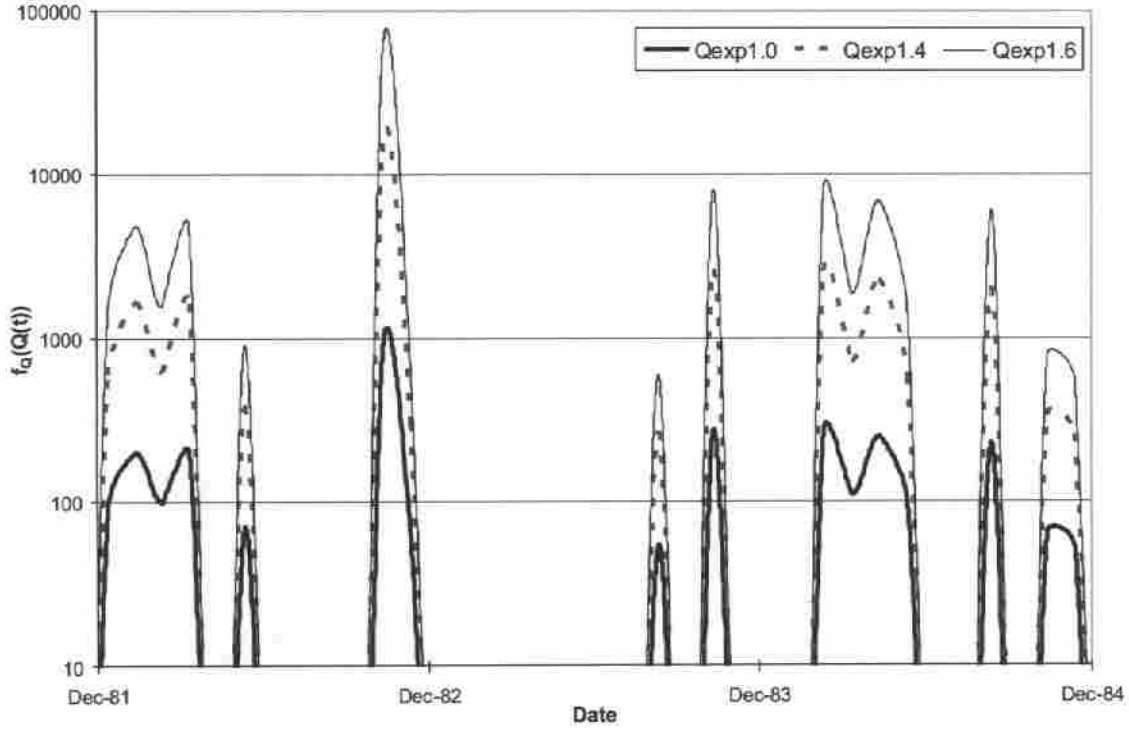
100000
10000
1000
100
10
$f_Q(Q(t))$
Qexp1.0
Qexp1.4
Qexp1.6
Dec-81
Dec-82
Dec-83
Dec-84
Date

Figure 6

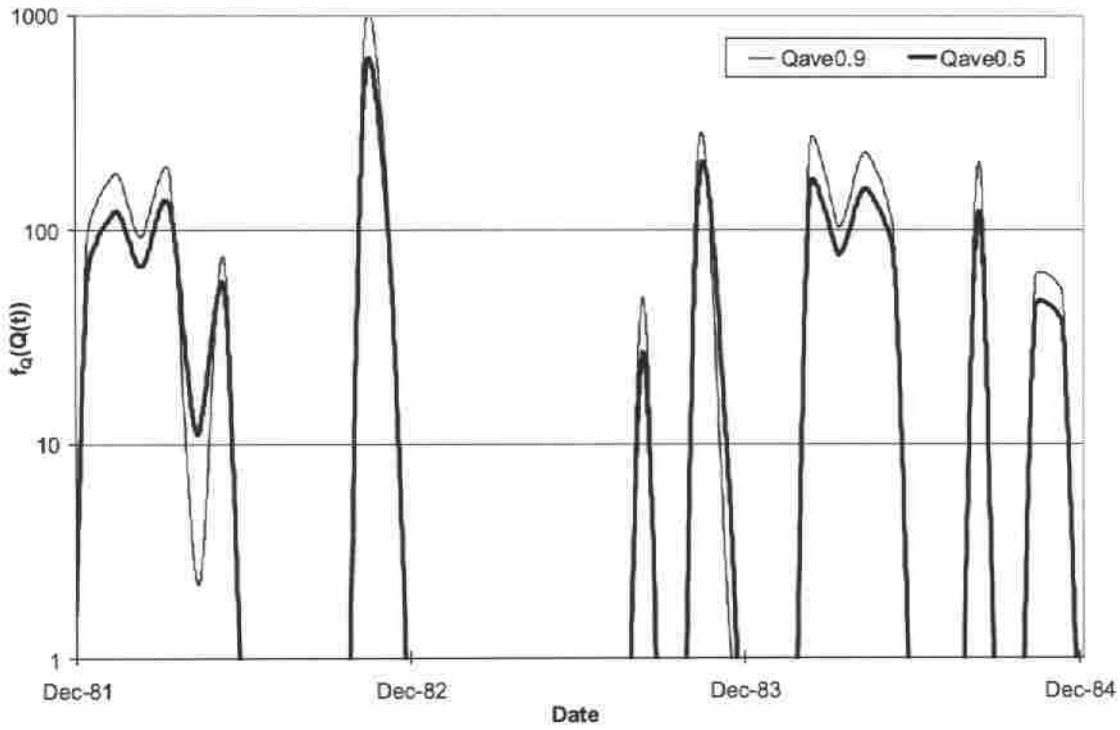
1000
100
10
1
$f_Q(Q(t))$
Qave0.9
Qave0.5
Dec-81
Dec-82
Dec-83
Dec-84
Date

Figure 7

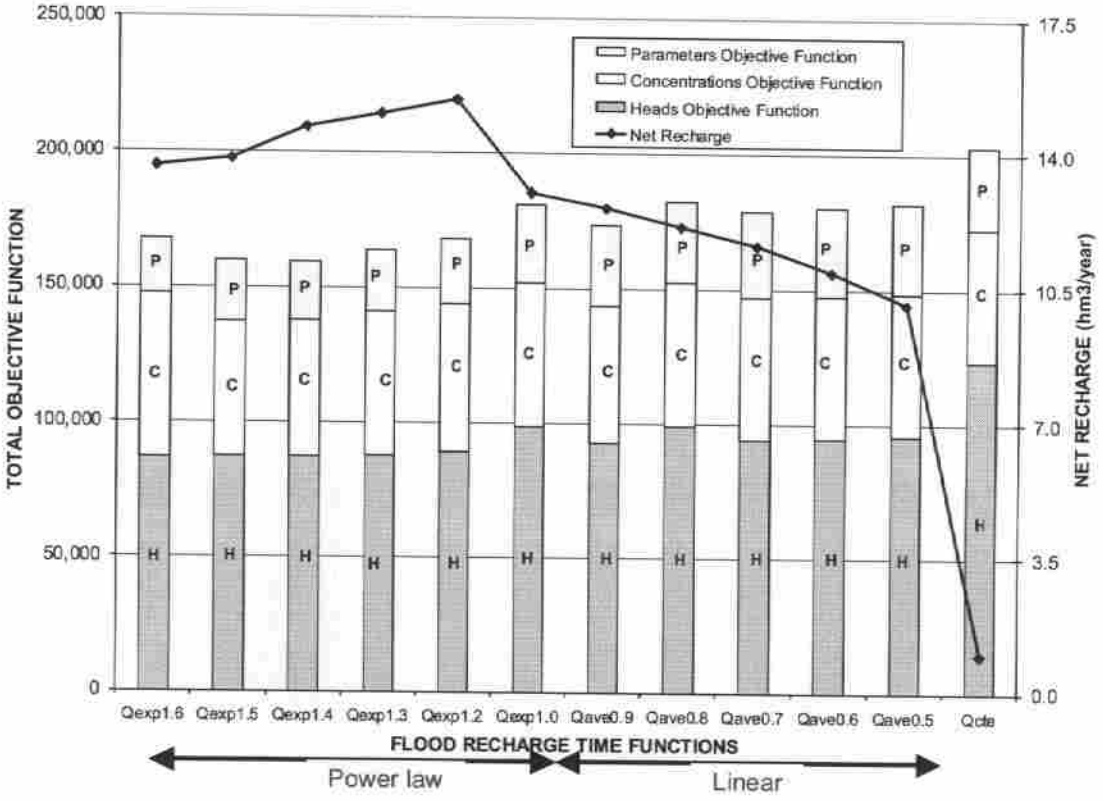
Parameters Objective Function
Concentrations Objective Function
Heads Objective Function
Net Recharge
TOTAL OBJECTIVE FUNCTION
NET RECHARGE (hm3/year)
250,000
200,000
150,000
100,000
50,000
0
17.5
14.0
10.5
7.0
3.5
0.0
P
C
H
Qexp1.6
Qexp1.5
Qexp1.4
Qexp1.3
Qexp1.2
Qexp1.0
Qave0.9
Qave0.8
Qave0.7
Qave0.6
Qave0.5
Qcte
FLOOD RECHARGE TIME FUNCTIONS
Power law
Linear

Figure 8

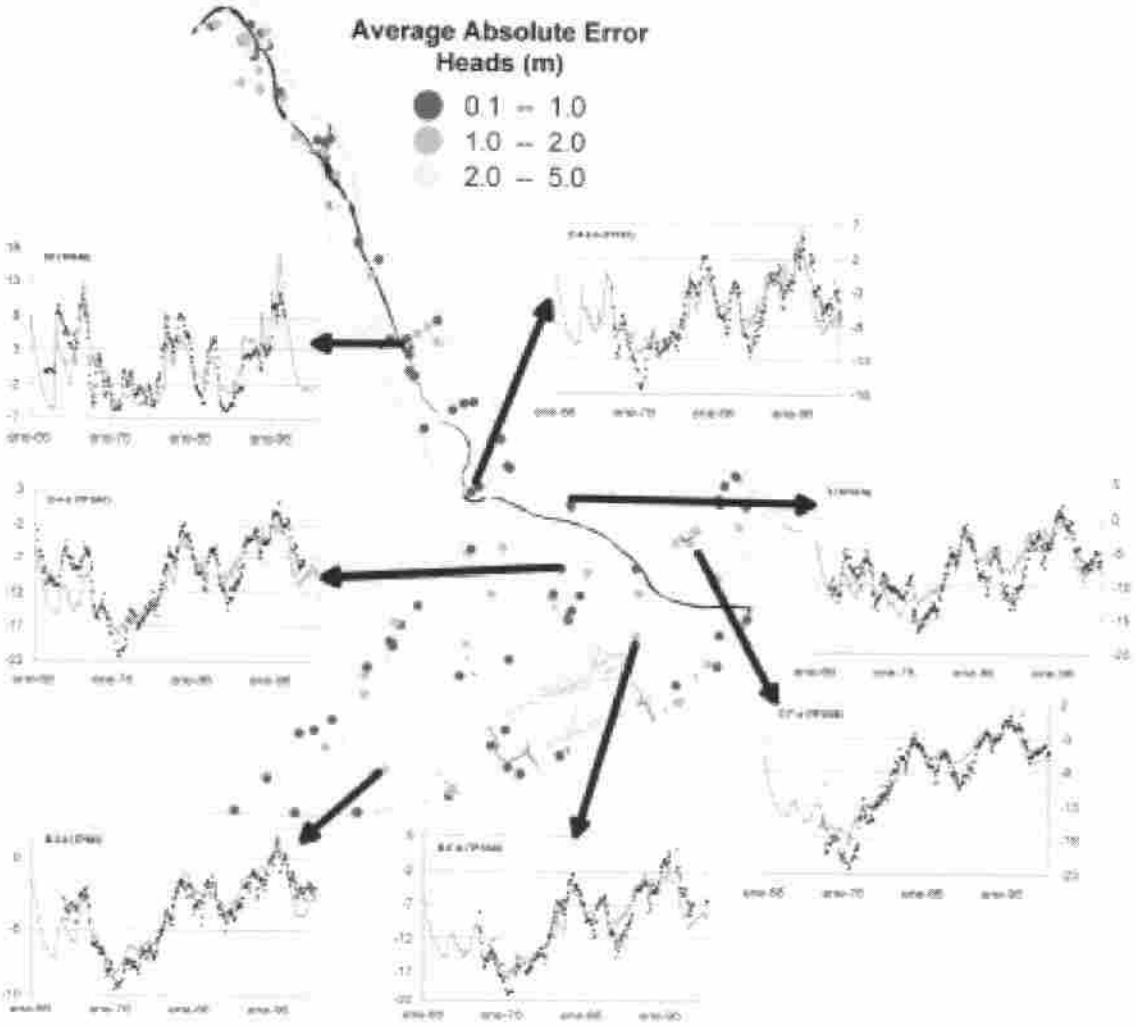

Figure 9

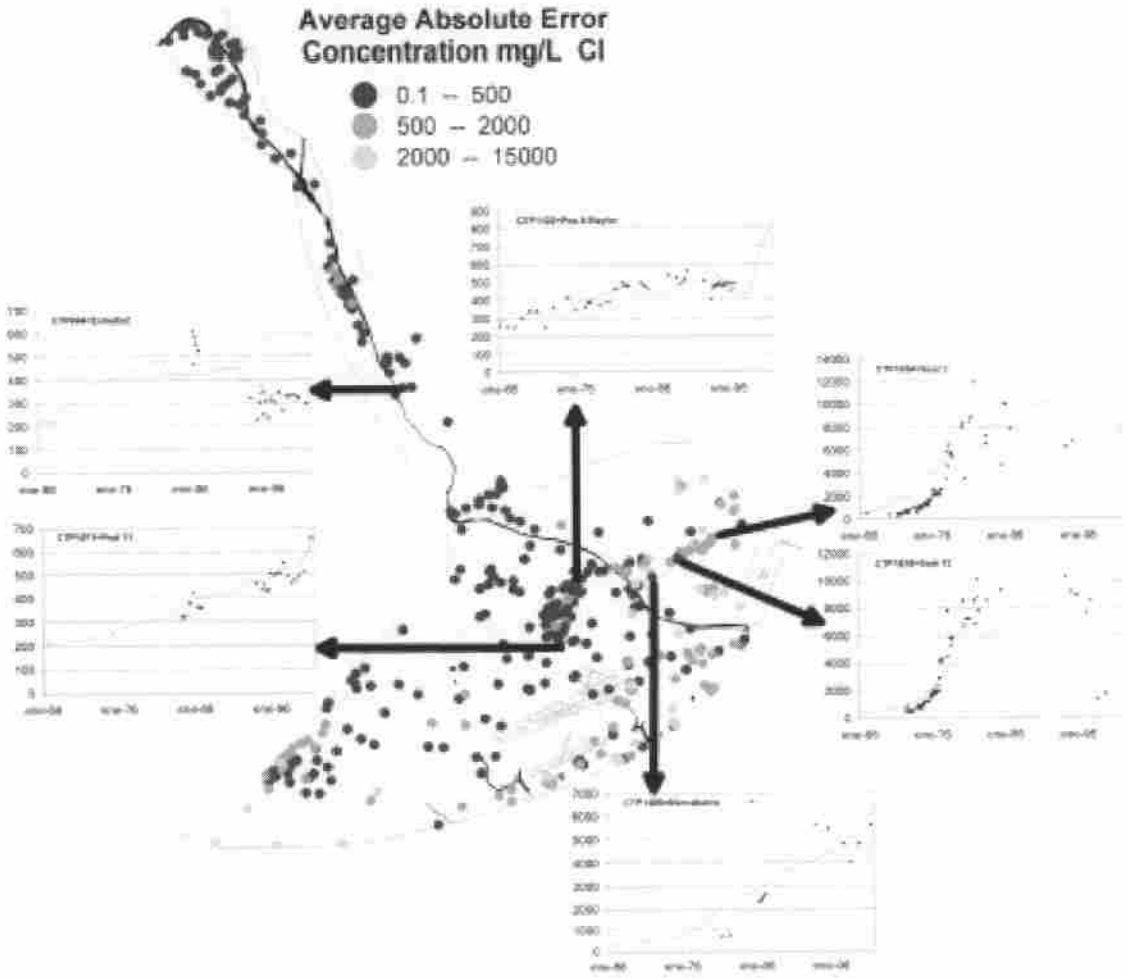
Average Absolute Error
Concentration mg/L Cl
0.1 -- 500
500 -- 2000
2000 -- 15000

Figure 10

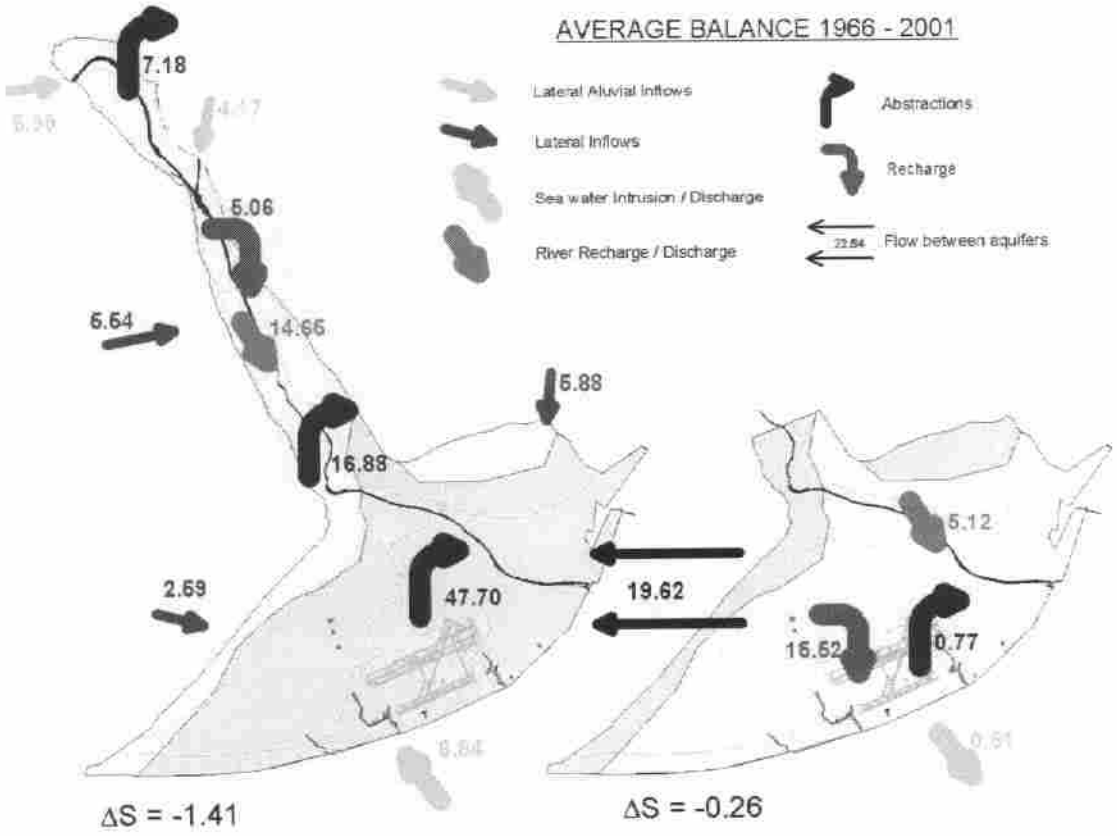
AVERAGE BALANCE 1966 - 2001
Lateral Alluvial Inflows
Lateral Inflows
Sea water Intrusion / Discharge
River Recharge / Discharge
Abstractions
Recharge
22.64 Flow between aquifers
7.18
5.30
4.17
5.06
6.64
14.66
5.88
16.88
5.12
2.69
47.70
19.62
16.52
0.77
6.84
0.61
ΔS = -1.41
ΔS = -0.26

Figure 11

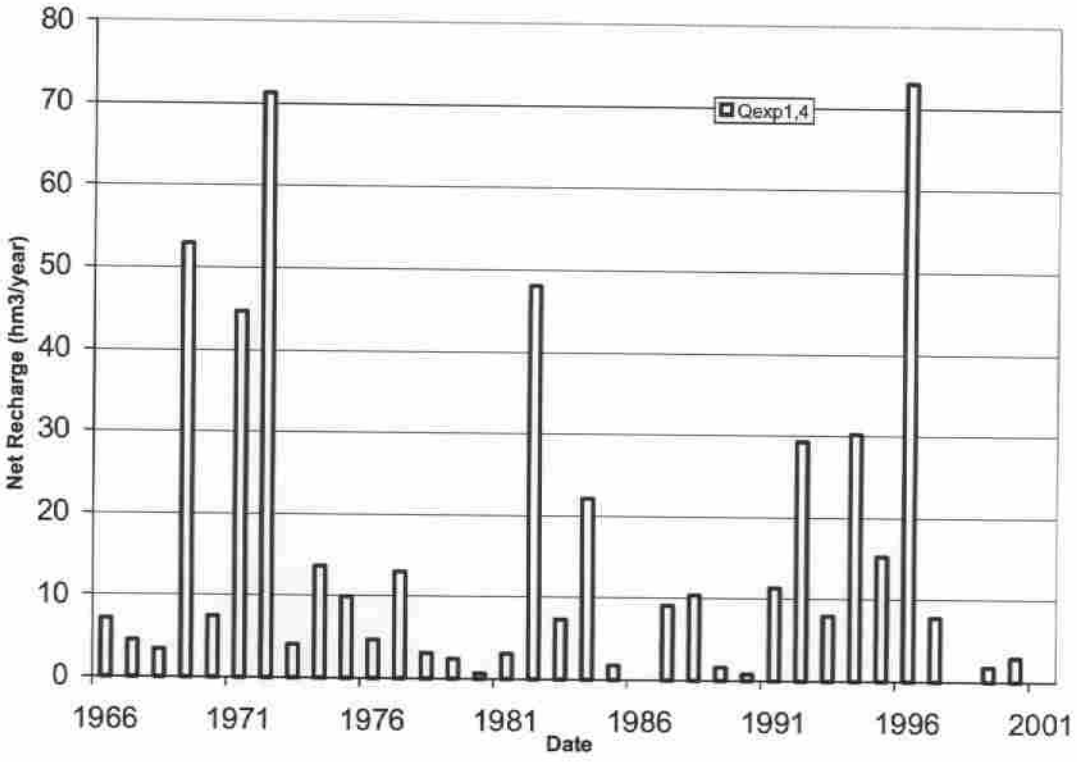
80
70
60
50
40
30
20
10
0
Net Recharge (hm3/year)
Qexp1,4
1966
1971
1976
1981
1986
1991
1996
2001
Date

Figure 12

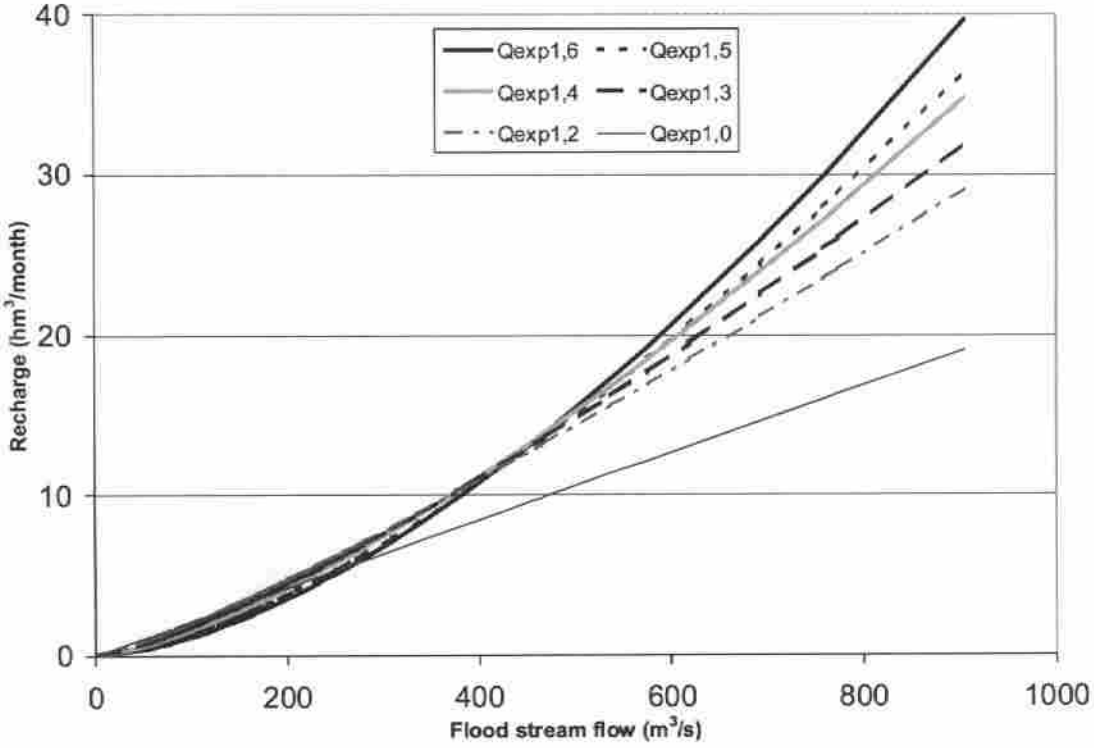
Qexp1,6
Qexp1,5
Qexp1,4
Qexp1,3
Qexp1,2
Qexp1,0
Recharge (hm³/month)
Flood stream flow (m³/s)
0
10
20
30
40
0
200
400
600
800
1000

Figure 13